

(NASA-CR-168189) ENERGY EFFICIENT ENGINE
HIGH-PRESSURE TURBINE COMPONENT RIG
PERFORMANCE TEST EFFORT (Pratt and Whitney
Aircraft Group) 249 P HC A11/MF A01

W85-29955

Unclas

CSCL 21E G3/07 16011

NASA-CR-168189
PWA-5594-243



ENERGY EFFICIENT ENGINE
HIGH-PRESSURE TURBINE COMPONENT RIG PERFORMANCE TEST REPORT



by

K. P. Leach

UNITED TECHNOLOGIES CORPORATION
Pratt & Whitney Aircraft Group
Engineering Division



Prepared for

NATIONAL AERONAUTICS AND SPACE ADMINISTRATION
Lewis Research Center
Cleveland, Ohio 44135

Contract NAS3-20646

1. REPORT NO. NASA CR-168189	2. GOVERNMENT AGENCY	3. RECIPIENT'S CATALOG NO.	
4. TITLE AND SUBTITLE Energy Efficient Engine High-Pressure Turbine Component Rig Performance Test Report		5. REPORT DATE May 1983	
		6. PERFORMING ORG. CODE	
7. AUTHOR(S) K. P. Leach		8. PERFORMING ORG. REPT. NO. PWA-559A-243	
9. PERFORMING ORG. NAME AND ADDRESS UNITED TECHNOLOGIES CORPORATION Pratt & Whitney Aircraft Group Engineering Division		10. WORK UNIT NO.	
		11. CONTRACT OR GRANT NO. NAS3-20646	
12. SPONSORING AGENCY NAME AND ADDRESS National Aeronautics and Space Administration Lewis Research Center 21000 Brookpark Road, Cleveland, Ohio 44135		13. TYPE REPT./PERIOD COVERED Technology Report	
		14. SPONSORING AGENCY CODE	
15. SUPPLEMENTARY NOTES Turbine Program Manager, Michael R. Vanco, NASA Lewis Research Center			
16. ABSTRACT Pratt & Whitney Aircraft successfully completed a rig test of the cooled high-pressure turbine component for the Energy Efficient Engine. The principal objective of this test was to substantiate the turbine design point performance as well as determine off-design performance with the interaction of the secondary flow system. The measured efficiency of the cooled turbine component was 88.5 percent, which surpassed the rig design goal of 86.5 percent. The secondary flow system in the turbine performed according to the design intent. Characterization studies showed that secondary flow system performance is insensitive to flow and pressure variations. Overall, this test has demonstrated that a highly-loaded, transonic, single-stage turbine can achieve a high level of operating efficiency.			
17. KEY WORDS (SUGGESTED BY AUTHOR(S)) Single Stage High-Pressure Turbine Energy Efficient Engine Highly-Loaded, Transonic Turbine Air-Cooled Turbine			
19. SECURITY CLASS THIS (REPT) UNCLASSIFIED	20. SECURITY CLASS THIS (PAGE) UNCLASSIFIED	21. NO. PGS	22. PRICE *

FOREWORD

The Energy Efficient Engine Component Development and Integration Program is being conducted under parallel National Aeronautics and Space Administration contracts to the Pratt & Whitney Aircraft Group, Engineering Division and the General Electric Company. The overall project is under the direction of Mr. Carl C. Ciepluch. The Pratt & Whitney Aircraft effort is under Contract NAS3-20646, and Mr. M. Vanco is the NASA Project Engineer responsible for the portion of the program described in this report. Mr. William B. Gardner is the Pratt & Whitney Aircraft Program Manager for the Energy Efficient Engine Program. This report was prepared by Mr. K. P. Leach of Pratt & Whitney Aircraft.

TABLE OF CONTENTS

Section	Title	Page
1.0	SUMMARY	1
2.0	INTRODUCTION	2
3.0	HIGH-PRESSURE TURBINE RIG DESIGN	4
3.1	Design Goals and Requirements	4
3.2	High-Pressure Turbine Component Design	4
3.2.1	Overview	4
3.2.2	Aerodynamic Design	6
3.2.3	Mechanical Design	9
3.3	High-Pressure Turbine Component Rig Design	14
3.4	Rig Fabrication and Assembly	15
3.5	Test Instrumentation	18
3.5.1	Performance Instrumentation	18
3.5.2	Structural Integrity Instrumentation	24
3.5.3	Instrumentation Calibration and Accuracy	24
3.5.4	Data Acquisition System	28
4.0	TEST PROGRAM AND TEST FACILITIES	29
4.1	Test Program	29
4.1.1	Full Stage Turbine Test	29
4.1.2	Vane Cascade Test	32
4.2	Test Facility	33
4.3	Data Reduction and Analysis	33
4.3.1	Analysis of Full Stage Data	35
4.3.2	Analysis of Cascade Data	36
5.0	TEST RESULTS AND ANALYSIS	37
5.1	Introduction	37
5.2	Mechanical Performance	37
5.3	Aerodynamic Performance	38
5.3.1	Turbine Stage Performance Assessment	38
5.3.2	Vane Cascade Performance Assessment	55
5.3.3	Turbine Blade Performance Analysis	69
5.3.4	Secondary Flow System Performance Characterization Studies	77
5.4	Post-Test Inspection Results	86
5.5	Summary of Results	86
6.0	CONCLUDING REMARKS	90
	APPENDIX A	91
	APPENDIX B	94
	LIST OF SYMBOLS	235
	REFERENCES	236
	DISTRIBUTION LIST	237

LIST OF ILLUSTRATIONS

<u>Number</u>	<u>Title</u>	<u>Page</u>
2-1	Overall Program Schedule	3
3.2.1-1	High-Pressure Turbine Component for the Flight Propulsion System	5
3.2.2-1	High-Pressure Turbine Flowpath	7
3.2.2-2	Vane Mean Section Aerodynamic Contour and Pressure Distribution	7
3.2.2-3	Blade Mean Section Aerodynamic Contour and Pressure Distribution	8
3.2.3-1	High-Pressure Turbine Rotor Assembly	10
3.2.3-2	Turbine Blade Cooling System	11
3.2.3-3	Vane and Inner Case Assembly	11
3.2.3-4	Turbine Vane Cooling Design	12
3.2.3-5	Turbine Blade Tip Seal Assembly	13
3.3-1	High-Pressure Turbine Component Test Rig	14
3.3-2	Turbine Secondary Flow System Air Supply Lines	15
3.4-1	Completed Turbine Rig Static Structure with PWA 1422 Directionally-Solidified Turbine Vanes	16
3.4-2	Completed Turbine Rotor Assembly Single Crystal (PWA 1480) Blades	16
3.4-3	Assembled Turbine Test Rig	17
3.5-1	Instrumentation Map of High-Pressure Turbine Component Rig	19
3.5.1-1	Circumferential Traverse Rake with Instrumentation Locations and Traverse Path	21
4.1-1	Test Envelope for Full Stage Turbine Test Program	31
4.2-1	Pratt & Whitney Aircraft X-203 Test Facility	34

LIST OF ILLUSTRATIONS (Continued)

<u>Number</u>	<u>Title</u>	<u>Page</u>
5.3.1-1	Turbine Stage Efficiency Trends as a Function of Pressure Ratio and Speed Parameter	40
5.3.1-2	Turbine Stage Efficiency	40
5.3.1-3	Turbine Reaction Characteristics	41
5.3.1-4	Turbine Secondary Flow System Map Showing Predicted and Measured Flow Rates and Pressures	43
5.3.1-5	Turbine Inlet Spanwise Total Pressure	45
5.3.1-6	Turbine Inlet Spanwise Total Temperature	46
5.3.1-7	Instrumentation and Circumferential Measurement Locations	47
5.3.1-8	Exit Spanwise Efficiency by Quadrant	48
5.3.1-9	Average Spanwise Efficiency	48
5.3.1-10	Efficiency Contour Plot of One Vane Gap in First Quadrant, Showing Maximum Efficiency Near the Midspan Region	49
5.3.1-11	Spanwise Profile of Turbine Exit Total Pressure	50
5.3.1-12	Turbine Exit Total Pressure Contour Plot	50
5.3.1-13	Spanwise Profile of Turbine Exit Total Temperature	51
5.3.1-14	Turbine Exit Total Temperature Contour Plot	51
5.3.1-15	Blade Air Exit Angle Characteristics	52
5.3.1-16	Air Angle Contour Plot	53
5.3.1-17	Average Spanwise Air Angle Trends Compared to the Design Prediction and Preceding Uncooled Rig Test Results	53
5.3.1-18	Blade Exit Mach Number Characteristics	54
5.3.2-1	Vane Loss Trends	56
5.3.2-2	Flow Capacity Characteristics	57

LIST OF ILLUSTRATIONS (Continued)

<u>Number</u>	<u>Title</u>	<u>Page</u>
5.3.2-3	Vane Deviation Versus Mach Number	57
5.3.2-4	Vane Cascade Inlet Total Pressure	58
5.3.2-5	Vane Cascade Inlet Total Temperature	58
5.3.2-6	Circumferential Vane Exit Pressure Characteristics	59
5.3.2-7	Spanwise Vane Exit Pressure Profile	60
5.3.2-8	Spanwise Vane Loss Characteristics	60
5.3.2-9	Vane Loss Profile Showing the Influence of Cooling on Performance	61
5.3.2-10	Contour Plot of Vane Loss Characteristics	62
5.3.2-11	Circumferential Trends of Vane Exit Temperature	63
5.3.2-12	Spanwise Profile of Vane Exit Temperature	64
5.3.2-13	Contour Plot of Vane Exit Temperature	64
5.3.2-14	Spanwise Vane Exit Air Angle Trends	66
5.3.2-15	Contour Plot of Vane Exit Air Angle	66
5.3.2-16	Comparison of Air Angle Trends	67
5.3.2-17	Spanwise Profile of Vane Exit Mach Number	67
5.3.2-18	Vane Root Section (11 Percent Span) Pressure Distribution	68
5.3.2-19	Vane Midspan (50 Percent Span) Pressure Distribution	68
5.3.2-20	Vane Tip Section (89 Percent Span) Pressure Distribution	69
5.3.2-21	Vane Suction Surface Film Cooling Effectiveness	70
5.3.3-1	Calculated Blade Pressure Loss as a Function of Exit Mach Number	71
5.3.3-2	Blade Deviation Versus Mach Number	71

LIST OF ILLUSTRATIONS (Continued)

<u>Number</u>	<u>Title</u>	<u>Page</u>
5.3.3-3	Spanwise Blade Exit Air Angle	73
5.3.3-4	Spanwise Blade Exit Mach Number	73
5.3.3-5	Spanwise Profile of Vane Inlet Air Angle	75
5.3.3-6	Blade Spanwise Efficiency	76
5.3.3-7	Blade Turning Characteristics	76
5.3.4-1	Tangential On-Board Injection System Rig Geometry	78
5.3.4-2	Tangential On-Board Injection Rig Instrumentation Locations	78
5.3.4-3	Tangential On-Board Injection Rig Radial Pressures	79
5.3.4-4	Front Rim Cavity Sensitivity to Tangential On-Board Injection Flow Rate Variations	81
5.3.4-5	Rim Cavity Pressures with Blade Tangential On-Board Injection Flow Rate Variations	81
5.3.4-6	Rim Cavity Temperatures with Blade Tangential On-Board Injection Flow Rate Variations	82
5.3.4-7	Rim Cavity Pressures with Mini Tangential On-Board Injection Flow Rate Variations	83
5.3.4-8	Rim Cavity Temperatures with Mini Tangential On-Board Injection Flow Rate Variations	83
5.3.4-9	Front Rim Cavity Sensitivity to Swirl Level Differences	84
5.3.4-10	Front Rim Cavity Sensitivity to Pressure Variations	84
5.3.4-11	High-Pressure Compressor Discharge Seal Leakage Study Results	85
5.4-1	High-Pressure Turbine Rotating Disk Assembly	87
5.4-2	Post-Test Condition of Turbine Vanes	87

LIST OF ILLUSTRATIONS (Continued)

<u>Number</u>	<u>Title</u>	<u>Page</u>
5.4-3	High-Pressure Turbine Outer Air Seal Segments	88
5.4-4	High-Pressure Turbine Full Stage Rig Exit Probe Instrumentation Ring Showing Galling and Metal Pickup	89

LIST OF TABLES

Number	Title	Page
3.1-I	High-Pressure Turbine Efficiency	4
3.2.1-I	High-Pressure Turbine Technology Features	5
3.2.2-I	General Aerodynamic Parameters	6
3.2.2-II	Design Gas Triangles	8
3.2.2-III	High-Pressure Turbine Aerodynamics After Restaggering	9
3.5.1-I	Flowpath Instrumentation	20
3.5.1-II	Secondary Flow System Instrumentation	22
3.5.1-III	Flow Measurement Instrumentation	25
3.5.1-IV	Speed, Humidity and Vibration Instrumentation	24
3.5.2-I	Rig Safety System X-203 Stand	26
3.5.2-II	Turbine Component Structural Integrity Instrumentation	27
3.5.3-I	Instrumentation Accuracy	27
3.5.3-II	Measurement Uncertainty of Turbine Parameters	28
4.1-I	Test Matrix for Full Stage Test	30
4.1-II	Turbine Vane Annular Cascade Test Conditions	32
5.2-I	Turbine Blade Tip Clearances	37
5.3.1-I	Comparison of Performance Parameters	38
5.3.1-II	Full Stage Turbine Warm Rig Test Results	39
5.3.1-III	Clearance Adjustment	42
5.3.1-IV	Secondary Flow System Flow Sensitivity Test Results	42
5.3.1-V	Full Stage Turbine Warm Rig Secondary System Coolant Flow Test Results	44
5.3.1-VI	Design Point Efficiency	47

LIST OF TABLES (Continued)

Number	Title	Page
5.3.2-I	High-Pressure Turbine Annular Cascade Test Conditions and Results	55
5.3.2-II	Cascade Loss by Quadrant	62
5.3.3-I	Wall Static Pressure	72
5.3.3-II	Internal Aerodynamics	74
5.3.4-I	Energy Efficient Engine Front Rim Cavity Data	80
5.3.4-II	Attachment Leakage for Vane	85
A-I	Test Rig Program	93
B-I	Full Stage Turbine Warm Rig Test Results	95
B-II	High-Pressure Turbine Cascade Test Results	171

SECTION 1.0
SUMMARY

As part of the NASA-sponsored Energy Efficient Engine program, Pratt & Whitney Aircraft successfully completed a rig test of the cooled high-pressure turbine component. The principal objective of this test was to substantiate the turbine design point performance as well as determine off-design performance with the interaction of the secondary flow system. The program was organized into both full stage and vane cascade tests. A total of 216 hours of testing was accomplished, and there were no major difficulties that prevented the acquisition of performance data. Performance data were acquired at 13 principal conditions during full stage testing, covering the intermediate and high power operating range of the integrated core/low spool.

The measured efficiency of the turbine component was 88.5 percent. This surpassed the rig design goal of 86.5 percent, the estimated component efficiency for the integrated core/low spool of 87.1 percent and the goal for the flight propulsion system of 88.2 percent. The measured efficiency was repeatable, indicating that no performance deterioration occurred during the test.

Cascade testing with the rotor removed showed that vane performance was generally in good agreement with the design prediction. In addition, these series of tests verified the effectiveness of the film cooling design.

Blade performance, on the basis of analysis, exceeded expectations. Performance trends showed that low loss design concepts, in conjunction with the introduction of trailing edge cooling, are effective in reducing losses at high exit Mach numbers. Results also showed that there is a slight compromise in rig performance when using engine hardware in a rig environment.

The secondary flow system in the turbine performed according to the design intent. Characterization studies showed that system performance, in particular the pressure-balanced tangential on-board injection system, is insensitive to flow and pressure variations.

Overall, this test demonstrated that a highly-loaded, transonic, single-stage turbine can achieve a high level of operating efficiency. In addition, it provides the confidence that the component is suitable for testing in the integrated core/low spool.

SECTION 2.0 INTRODUCTION

The Energy Efficient Engine Component Development and Integration Program, sponsored by the National Aeronautics and Space Administration (NASA), is directed toward demonstrating the technology to improve fuel efficiency and to reduce operating economics of future commercial gas-turbine engines. The program goals include a reduction in fuel consumption by at least 12 percent and a reduction in direct operating cost by at least 5 percent relative to a base Pratt & Whitney JT9D-7 turbofan engine. To demonstrate the technology to accomplish these goals, the program is organized into two main technical tasks:

- Task 1 Flight Propulsion System Analysis, Design and Integration
- Task 2 Component Analysis, Design and Development

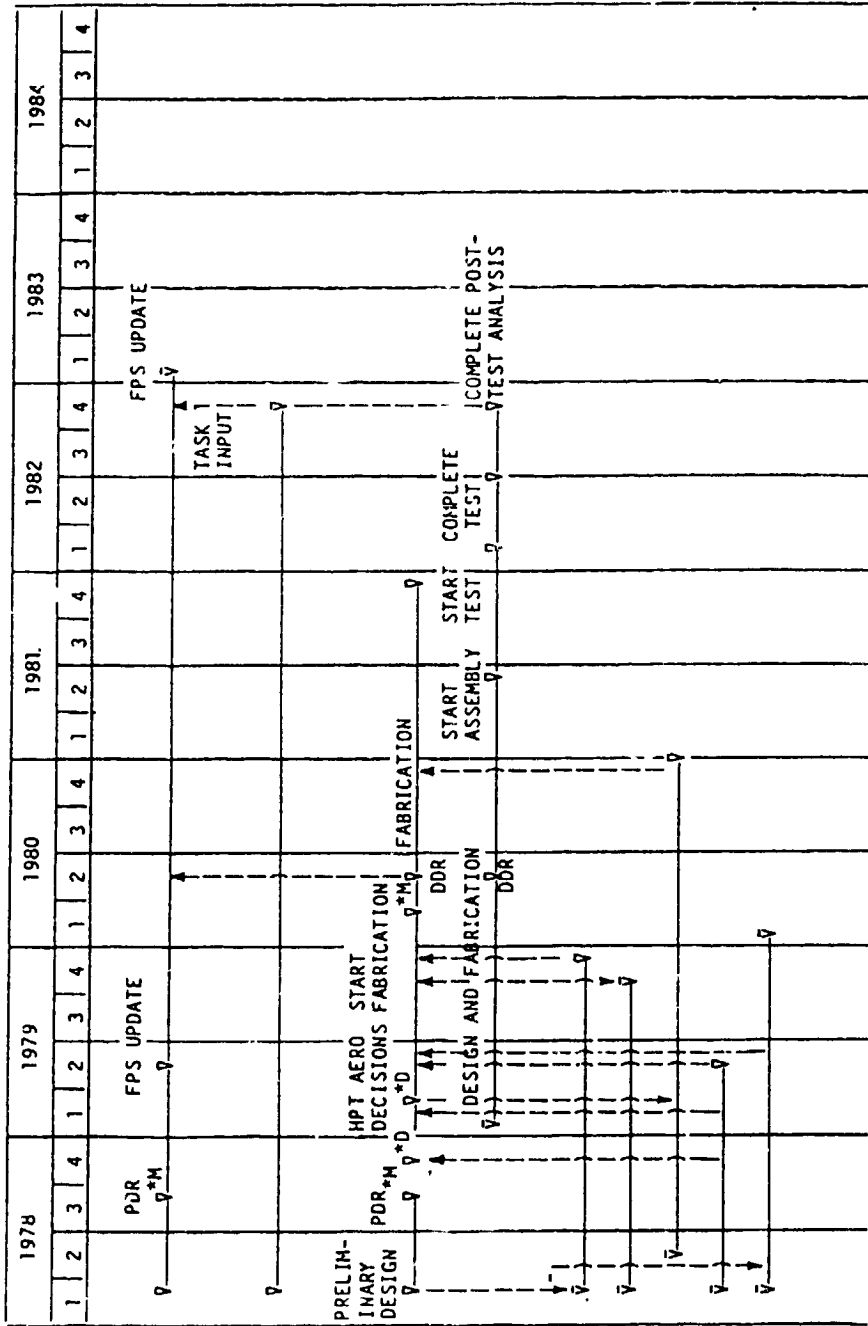
Under Task 2, an advanced high-pressure turbine component was designed for the Energy Efficient Engine. This turbine is a single-stage configuration and has various technology features in the areas of aerodynamics, structures and materials/cooling.

Substantiation of this turbine design involved two component rig test programs. The first, as shown in Figure 2-1, was a test of the uncooled turbine rig and was conducted as part of the Uncooled Rig Supporting Technology Program (Ref. 1). The results from this effort corroborated the aerodynamic design assumptions and established the uncooled efficiency base for the turbine component detailed design. The second test, which is the subject of this report, verified the performance of the cooled turbine component. This program involved both full stage and annular cascade testing, and it was directed toward demonstrating design and off-design performance as well as assessing performance sensitivity to the secondary flow system. With some exceptions, the turbine component used in this test is the same as designed for both the flight propulsion system -- the analytical study engine in the Energy Efficient Engine program -- and the integrated core/low spool test vehicle.

The results of the Cooled High-Pressure turbine Component Rig Test program are summarized in this report. The following section, Section 3, presents a description of the turbine component as designed for the integrated core/low spool and the design similarities and differences in the turbine rig. Section 4 outlines the test program and describes the test facility and data reduction method. Section 5 presents the results of both the full stage and annular cascade tests, in addition to an analysis of these results. This section also contains results from a related test on the blade tangential on-board injection system. Concluding remarks are presented in Section 6.

Two appendixes are included in this report. Appendix A contains additional information on the supporting blade tangential on-board injection rig test. Appendix B contains a presentation of performance data from both the full stage test and the annular cascade test.

HIGH-PRESSURE TURBINE PROGRAM LOGIC DIAGRAM



ORIGINAL BASED ON OF POOR QUALITY

ACTIVITIES/MILESTONES

TASK 1

FPS ANALYSIS, DESIGN AND INTEGRATION, DESIGN UPDATES

TASK 2

TOTAL HIGH PRESSURE TURBINE TIMING

COMPONENT ANALYSIS, DESIGN, AND FABRICATION

COOLED RIG PROGRAM

SUPPORTING TECHNOLOGY

LEAKAGE TESTS

SUPERSONIC CASCADE TESTS

COOLING MODEL TESTS

UNCOOLED RIG TESTS

FABRICATION DEVELOPMENT

*M DENOTES MAJOR MILESTONE *D DENOTES KEY DECISION POINT

Figure 2-1 Overall Program Schedule

SECTION 3.0
HIGH-PRESSURE TURBINE RIG DESIGN

3.1 DESIGN GOALS AND REQUIREMENTS

The high-pressure turbine component efficiency estimates and goals for the rig are summarized in Table 3.1-I. The estimate for the integrated core/low spool was based largely upon the results obtained from the earlier Uncooled Rig Test Program and then updated to reflect refinements in the design as the component definition evolved.

TABLE 3.1-I
HIGH-PRESSURE TURBINE EFFICIENCY STATUS
Aerodynamic Design Point -- 10,668 m (35,000 ft),
0.8 Mn Standard Day Condition

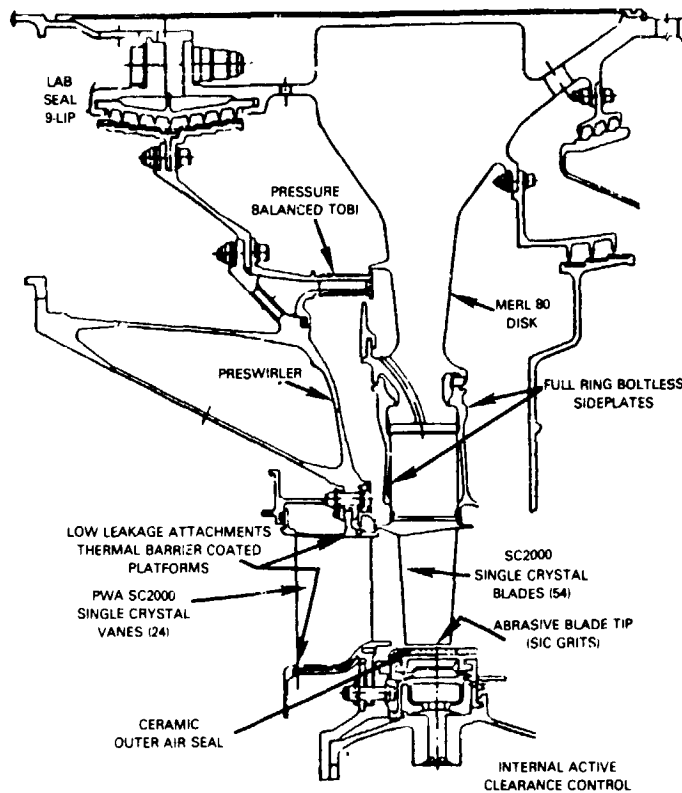
<u>Flight Propulsion System Goal (%)</u>	<u>Integrated Core/Low Spool Component Status (%)</u>	<u>Test Rig Goal (%)</u>
88.2	87.1	86.5

The goal for the test rig was defined at the beginning of the Energy Efficient Engine Program. Other key design parameters include a specific work output of 448,000 J/kgm (192.96 Btu/lbm), an expansion ratio of 4.0, a combined turbine cooling/leakage flow rate of 13.2 percent of core engine flow, and a rim speed of 527 m/sec (1730 ft/sec).

3.2 HIGH-PRESSURE TURBINE COMPONENT DESIGN

3.2.1 Overview

The high-pressure turbine component is shown in Figure 3.2.1-1 as defined for the Energy Efficient Engine flight propulsion system. It is a single-stage configuration designed to operate at a high velocity ratio and low ratio of throughflow to wheel speed (C_x/U). The design is based on advances in aerodynamics, structures and materials/cooling management. Some of the advanced design features are listed in Table 3.2.1-I. Details of the design are contained in Reference 2.



OPTIMIZED DESIGN
OF FOUR QUALITY

Figure 3.2.1-1 High-Pressure Turbine Component for the Flight Propulsion System

TABLE 3.2.1-1

HIGH-PRESSURE TURBINE TECHNOLOGY FEATURES

REDUCED COST CONCEPTS:

- Single-Stage Turbine
- Reduced Number of Airfoils

INCREASED AERODYNAMIC EFFICIENCY CONCEPTS:

- High AN^2 /High Rim Speed
- Contoured Vane End Walls
- Low Loss Airfoils
- Reduced Tip Loss Configuration
- Active Clearance Control
- High Airfoil Loadings

REDUCED LEAKAGE CONCEPTS:

- Reduced Leakage Length
- Improved Gap Sealing
- Improved Rim Sealing
- W-Seals

REDUCED COOLANT FLOW CONCEPTS:

- Single-Stage Turbine
- Improved Airfoil Cooling Effectiveness
- Single Crystal Airfoil Materials
- Thermal Barrier Coatings
- Efficient Coolant Supply System
- Low Windage

3.2.2 Aerodynamic Design

The general parameters governing the aerodynamic design of the turbine component are listed in Table 3.2.2-I.

TABLE 3.2.2-I

GENERAL AERODYNAMIC PARAMETERS

(Aerodynamic Design Point - Mn 0.8;
10,668 m (35,000 ft))

P_{TIN} , MPa (psia)	1.324 (192.1)
CET, K (°R)	1633 (2940)
RIT, K (°R)	1561 (2811)
N (RPM)	13232
ΔH , (Btu/sec)	13384
FP_{in} , ($W \sqrt{T_T/P_T}$)	16.98
W_C/A , (% W_{ae})	14.10
PR	4.0
Reaction	43.0 percent
Velocity Ratio, $\sqrt{U^2/2gJ\Delta h}$	0.556
NASA Work Factor, ($\Delta h/U^2$)	1.62
C_x/U	0.351
AN^2 , ($IN^2 RPM^2$)	4.06×10^{10}
U_{RIM} , m/sec (ft/sec)	481 (1580)
Clearance, cm (in)	0.0469 (0.0185)

The turbine flowpath is shown in Figure 3.2.2-1. In the single-stage configuration, there is a total of 24 vanes and 54 blades. The vane is characterized by aerodynamic sections having a blunt leading edge and a long chord with the maximum airfoil thickness near the leading edge. The inner vane endwall is cylindrical, while the outer wall is contoured in an "S" shape. The blades are highly tapered with a conical inner wall.

Figure 3.2.2-2 shows the aerodynamic definition of the vane mean section and corresponding predicted pressure distribution. Similar information for the mean section of the blade is shown in Figure 3.2.2-3. Velocity triangle data for both the vane and blade are contained in Table 3.2.2-II.

To achieve the desired low-pressure turbine inlet aerodynamic conditions in the integrated core/low spool test hardware, the turbine blade was restaggered opened 0.25 degree from its aerodynamic definition. The effect of restaggering is shown in Table 3.2.2-III

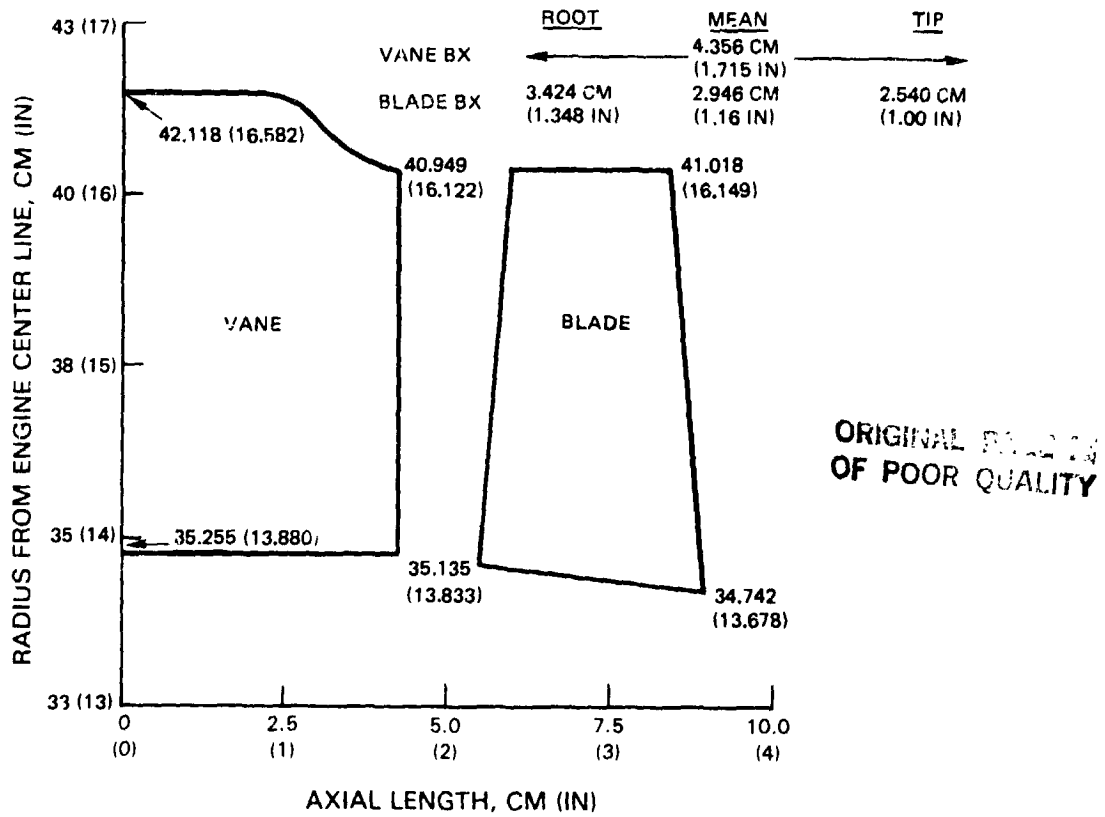


Figure 3.2.2-1 High-Pressure Turbine Flowpath

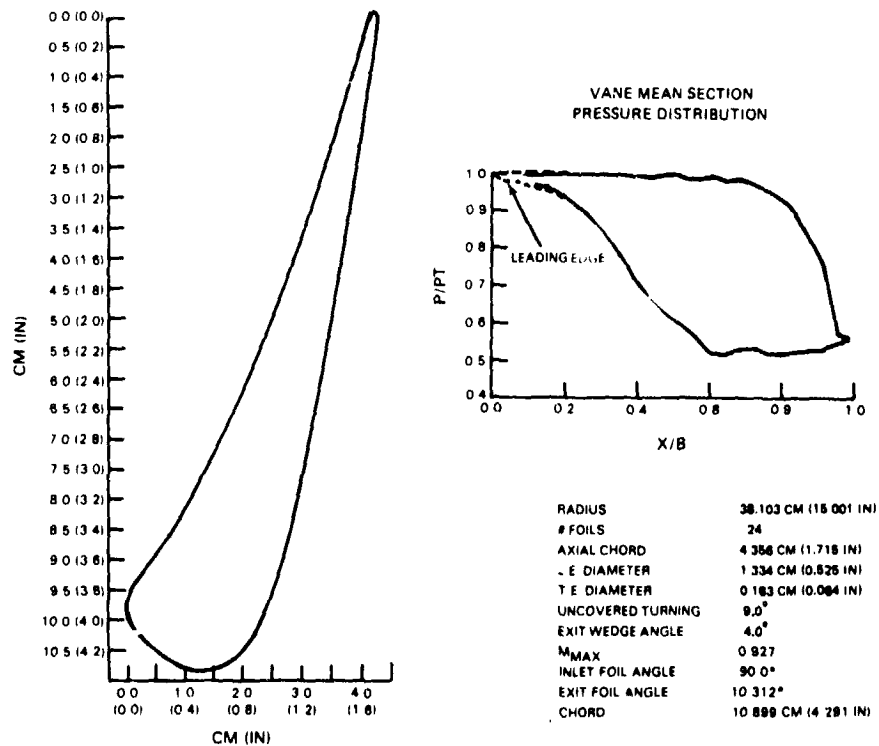


Figure 3.2.2-2 Vane Mean Section Aerodynamic Contour and Pressure Distribution

ORIGINAL PAGE IS
OF POOR QUALITY

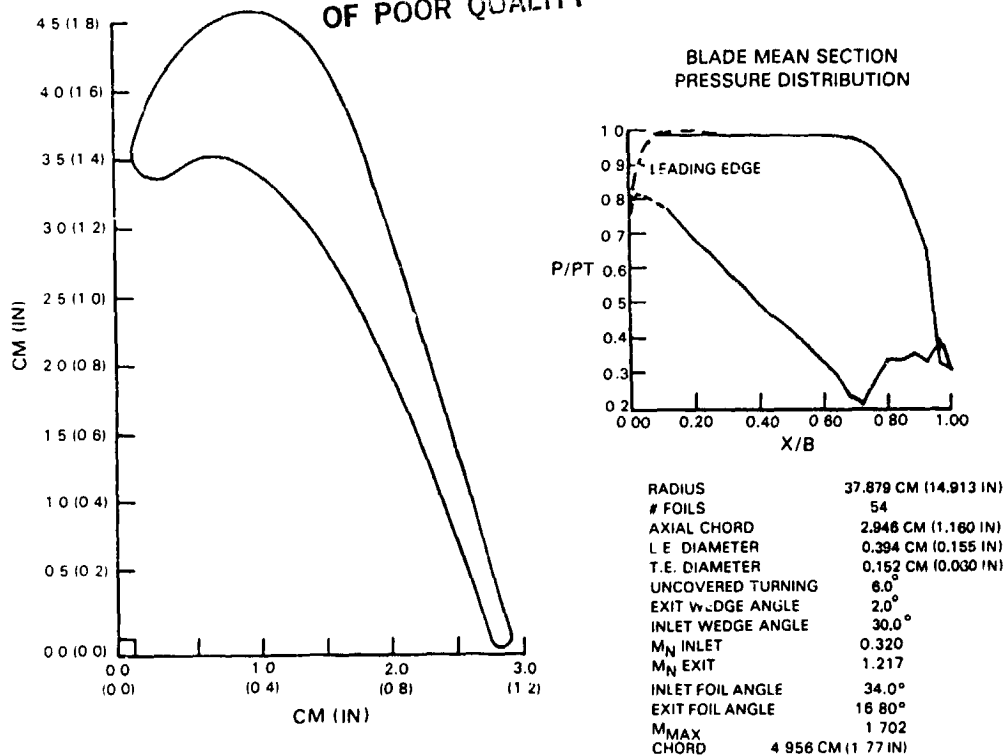


Figure 3.2.2-3 Blade Mean Section Aerodynamic Contour and Pressure Distribution

TABLE 3.2.2-II

DESIGN GAS TRIANGLES

	<u>Root</u>	<u>Mean</u>	<u>Tip</u>
VANE			
Inlet Air Angle (deg)	90	90	90
Exit Air Angle (deg)	11.6	10.3	9.1
Inlet Mach No.	0.09	0.08	0.07
Exit Mach No.	1.0	0.92	0.85
Gas Turning (deg)	78.4	79.7	80.9
BLADE			
Inlet Air Angle (deg)*	38.5	34.0	74.0
Inlet Air Angle (deg)**	33.5	42.7	63.6
Exit Air Angle (deg)	15.9	16.9	17.7
Inlet Mach No.	0.36	0.25	0.14
Exit Mach No.	1.22	1.24	1.28
Gas Turning (deg)	130.6	120.4	98.7
Exit Abs Air Angle (deg)	38.0	43.8	48.4
Exit Abs Mach No.	0.54	0.52	0.52

* With inlet temperature and vane loss profile

** Flat inlet temperature and flat vane loss profile

TABLE 3.2.2-III

HIGH-PRESSURE TURBINE AERODYNAMICS AFTER RESTAGGERING

	HPT Designed (Initial IC/LS)	HPT Run At LPT FP	Restaggered HPT Run at LPT FP (Final IC/LS)
FP HPT IN	16.983	16.983	17.023
FP HPT OUT	66.562	68.165	68.165
PR HPT	3.98	4.093	4.084
Reaction (%)	43.0	43.8	42.4
$\Delta\eta$ HPT (%)	BASE	0 to -0.3	0 to -0.15
Mn HPT OUT	0.523	0.554	0.539
α HPT OUT (deg)	43.8	43.0	44.0
LPT Convergence			
VI Root	1.4	1.35	1.4
BI Root	1.3	1.25	1.3

The secondary flow system in the high-pressure turbine is designed to maximize the use of secondary air for cooling and thrust balance as well as minimize parasitic leakage and the attendant performance penalty. The primary design features that enhance leakage control include:

- o A tangential on-board injection (TOBI) system for positive blade coolant flow supply
- o A front rim cavity mini tangential on-board injection (TOBI) system
- o Boltless and full ring rotor sideplates
- o A multi knife-edge, stepped high-pressure compressor discharge seal.

3.2.3 Mechanical Design

The major subsystems in the turbine component are the rotor system, vane and inner case assembly, and outer air seal.

Turbine Rotor Assembly

The Energy Efficient Engine high-pressure rotor construction is different from most previous Pratt & Whitney Aircraft designs in that the rotor is straddle mounted. This arrangement eliminates the bearing compartment forward of the high-pressure turbine disk and places it after the disk. The turbine rotor assembly is illustrated in Figure 3.2.3-1. Because of high rim speeds, the design is characterized by a thick bore region. The rim has a firtree attachment to hold the blades, shelves to support the front and rear sideplates, and a flange to support the vortex plate. The vortex plate is used to contain blade cooling air and provide a passage for free-vortex pressure rise to augment the pressure of the flow exiting the tangential on-board injection nozzle. The curved elliptical cooling air holes supply coolant from the vortex plate to the blade root. Pumping action through the curved elliptical hole also increases the pressure before the flow enters the blade root cavity.

The air-cooled turbine blades are retained in the disk by boltless sideplates. The full ring sideplates perform a dual function of blade retention and sealing in the rim areas.

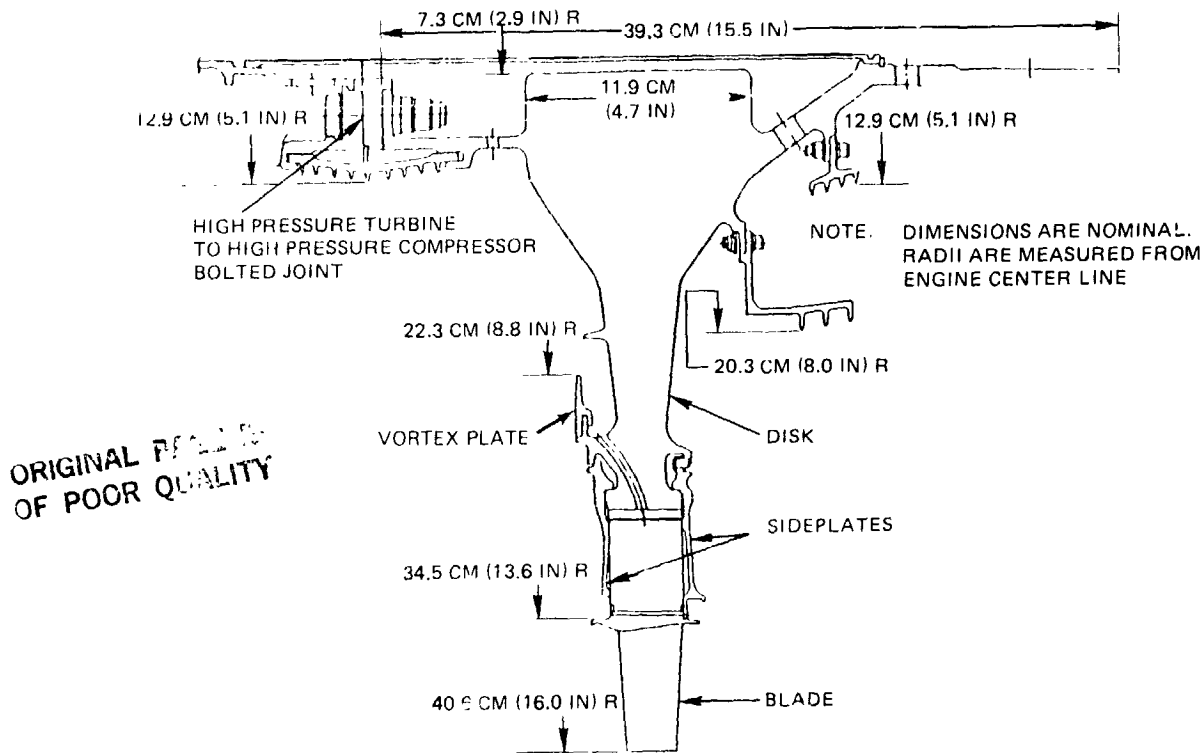


Figure 3.2.3-1 High-Pressure Turbine Rotor Assembly

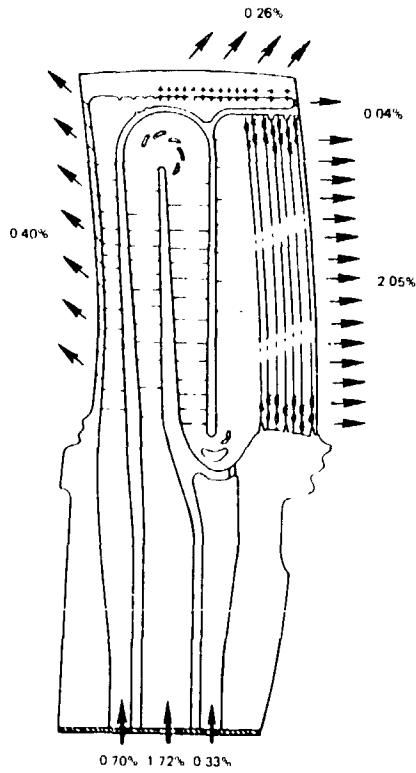
A schematic of the cooling design is shown in Figure 3.2.3-2. The blades require only 2.75 percent of the core engine inlet flow for cooling. They are cooled by a combination of internal convection and local film cooling. The internal geometry is designed to enhance cooling convection while external surfaces are locally film cooled from the leading edge showerhead holes and tip pressure side holes. There are no film cooling holes on either the pressure or suction surfaces of the airfoil.

Vane and Inner Case Assembly

The vane and inner case assembly is illustrated in Figure 3.2.3-3. The primary elements are the vanes, the tangential on-board injection (TOBI) system and the high-pressure compressor discharge seal.

The turbine vanes are also an advanced air-cooled design. Excluding the inner and outer platform surfaces, the vanes require only 6.41 percent of the core engine inlet flow for cooling. A schematic of the vane cooling system is presented in Figure 3.2.3-4. Effective internal cooling of the vane is achieved by cross flow impingement, augmented by strategically placed external film cooling holes. Cooling air enters the vane at both the tip and root and is distributed within the three internal cavities. The showerhead holes are angled to provide maximum heat transfer in the thick leading edge region. The pressure surface is film cooled by two sets of double row holes. The suction surface has three rows of holes. The platform cooling scheme consists of a combination of impingement cooling under the platform and convection cooling on the platform gas path surface.

BLADE COOLING FLOWS (TOTAL 2.75%)



ORIGINAL FIGURE OF POOR QUALITY

Figure 3.2.3-2 Turbine Blade Cooling System

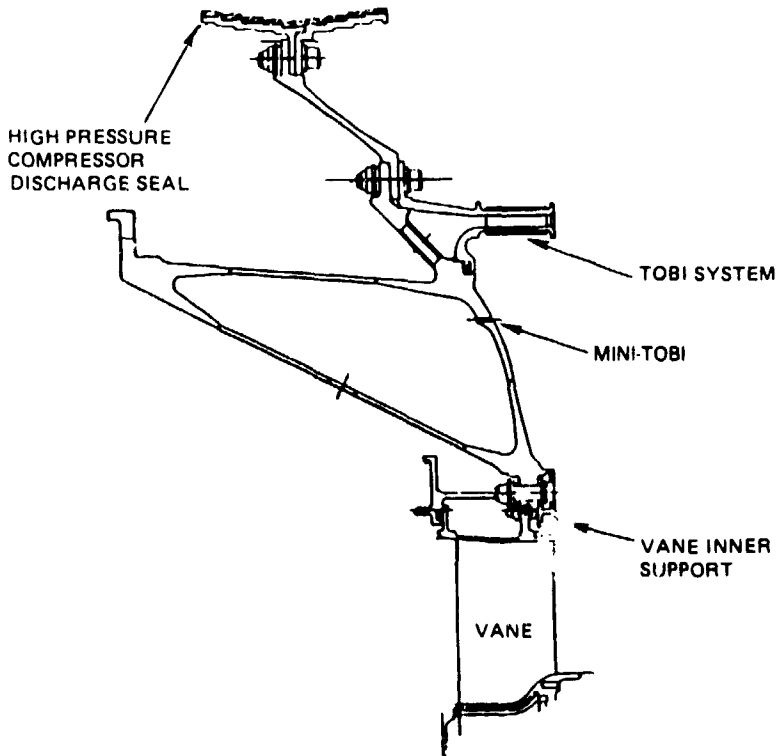


Figure 3.2.3-3 Vane and Inner Case Assembly

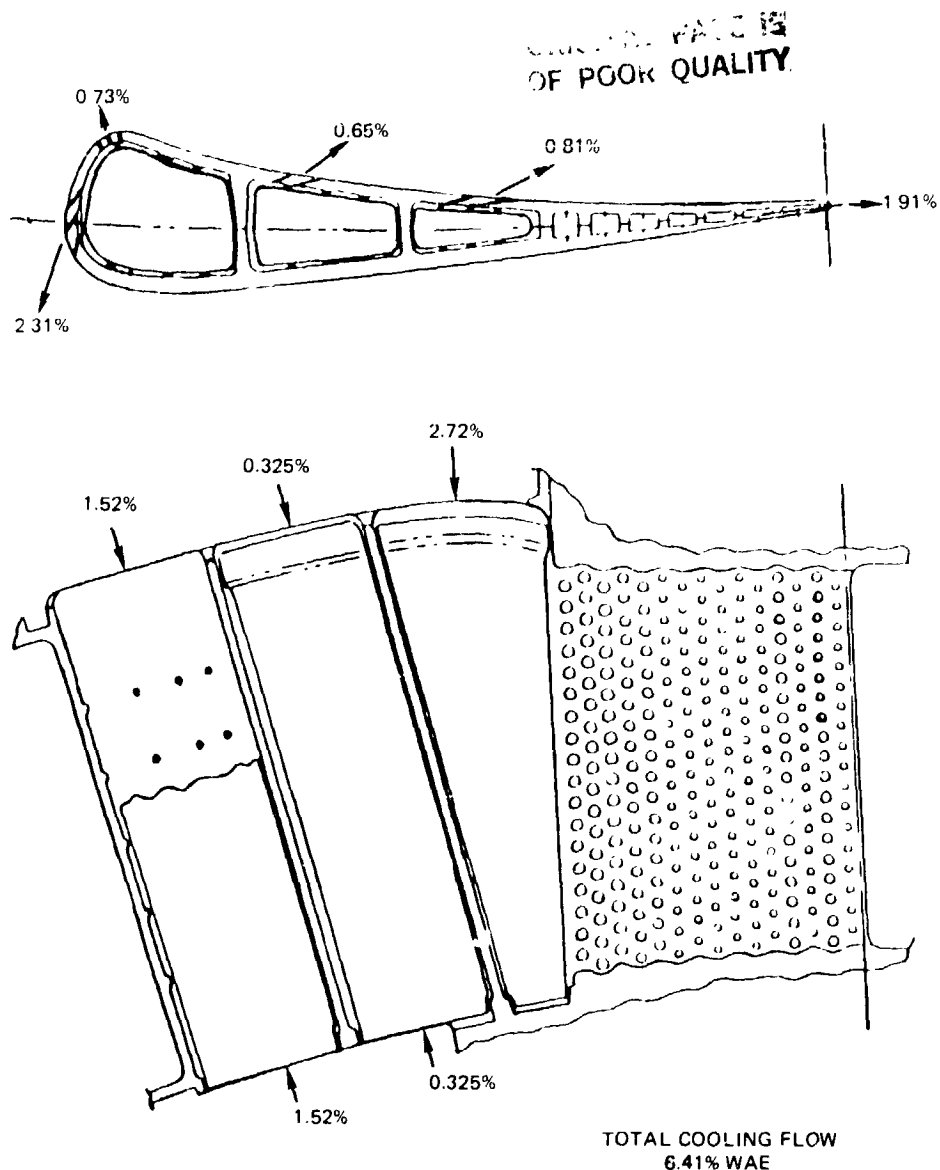


Figure 3.2.3-4 Turbine Vane Cooling Design

To minimize leakage caused by vane twisting, both the inner and outer surfaces are clamped along a chordal cut. By having a chordal cut, axial tilting of the vane, introduced by differential axial growth between the inner case and outer combustor case, is allowed to occur without binding up or opening a leak path. The vane platforms are sealed by feather seals to prevent leakage of compressor discharge air into the turbine flowpath.

The main or blade tangential on-board injection nozzle is a cascade design that provides cooling flow at a positive supply pressure to the disk rim and blade. A secondary or mini tangential on-board injection nozzle is used to swirl the coolant flow to the front side of the turbine disk to reduce disk heat-up caused by windage shear effects on the front sideplate.

The high-pressure compressor discharge seal is a knife-edge labyrinth configuration designed to maintain minimum clearance at all operating conditions.

Turbine Outer Case and Airseal

The turbine blade tip seal is part of the internal active clearance control system. The turbine outer case and seal design are shown in Figure 3.2.3-5. The major components include the front and rear outer airseal support rails, outer air seal shoe and impingement ring. To minimize cooling air leakage, "W" seals are used on the front and rear hooks of the shoe, and feather seals are used at the circumferential ship lap joint between shoes. The seal assembly is supported by the high-pressure turbine outer case which incorporates the manifold for the active clearance control system.

The active clearance control system maintains close blade tip clearances at all operating conditions by impinging controlled temperature air from the high-pressure compressor on the outer air seal support rails. The cooler temperature air reduces the rate of thermal expansion to control the radial movement of the seal shoes towards the blade tip. The blade tip clearance at the cruise condition (the aerodynamic design point) is 0.047 cm (0.0186 in).

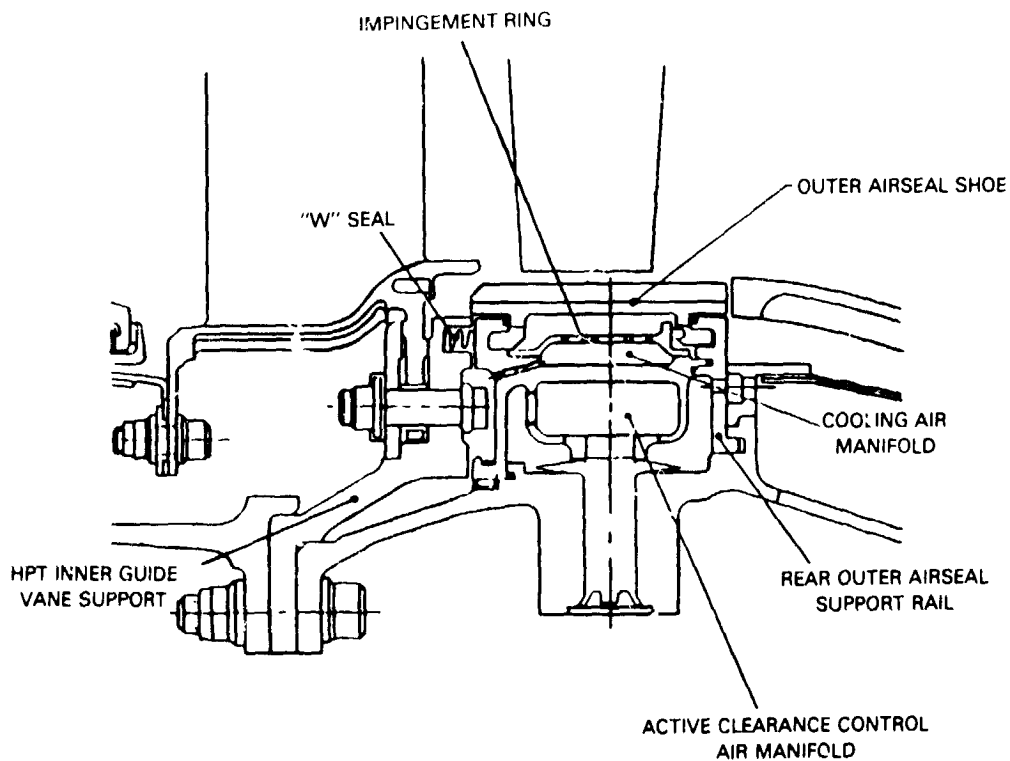


Figure 3.2.3-5 Turbine Blade Tip Seal Assembly

3.3 HIGH-PRESSURE TURBINE COMPONENT RIG DESIGN

The high-pressure turbine component rig was designed to confirm the aerodynamic performance of actual engine-type hardware prior to testing in the integrated core/low spool. A cross-sectional view of the rig is shown in Figure 3.3-1. Basically, it consists of an inlet section, test section and exhaust section. The inlet, exhaust and outer case sections are rig hardware. In contrast, the components in the test section are suitable for use in the integrated core/low spool. These components have been designed to meet the structural requirements of the integrated core/low spool and contain nearly all the technology features of the Energy Efficient Engine high-pressure turbine component described in the preceding section. The main exceptions are the use of a directionally solidified material for the vanes instead of a single crystal material and a metallic blade tip seal instead of ceramic material. In addition, since the rig was run at relatively low temperatures the airfoils were not coated. They were, however, restaggered closed 0.3-degree to account for the coating thickness.

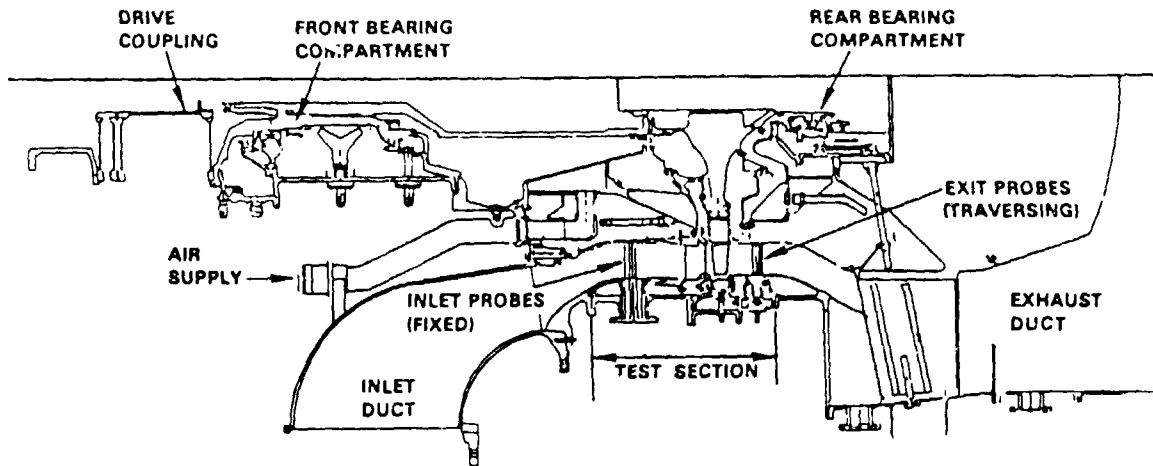


Figure 3.3-1 High-Pressure Turbine Component Test Rig

The rig secondary flow system was designed to simulate the Energy Efficient Engine requirements. Air supply lines, as shown in Figure 3.3-2, supply metered cooling air to the vane, tangential on-board injection (TOBI) system, bore cavity, mini tangential on-board injection system, and active clearance control system. For each metered flow, specific coolant and leakage flow splits were calculated using pretest flow calibrations of rig hardware. In addition, a separate cooling supply system was provided for the active clearance control system. This permits the air temperature to be varied over an approximate 167°C (300°F) temperature range to facilitate clearance change.

Special consideration was given to the type of material used in certain areas of the rig. For example, rig hardware exposed to main and secondary airflow was fabricated of stainless steel or comparable rust resistant alloy to prevent contamination of coolant passages. High strength materials were used in high temperature regions of the rig, while less expensive low carbon steel was used for external rig hardware.

ORIGINAL DESIGN
OF POOR QUALITY

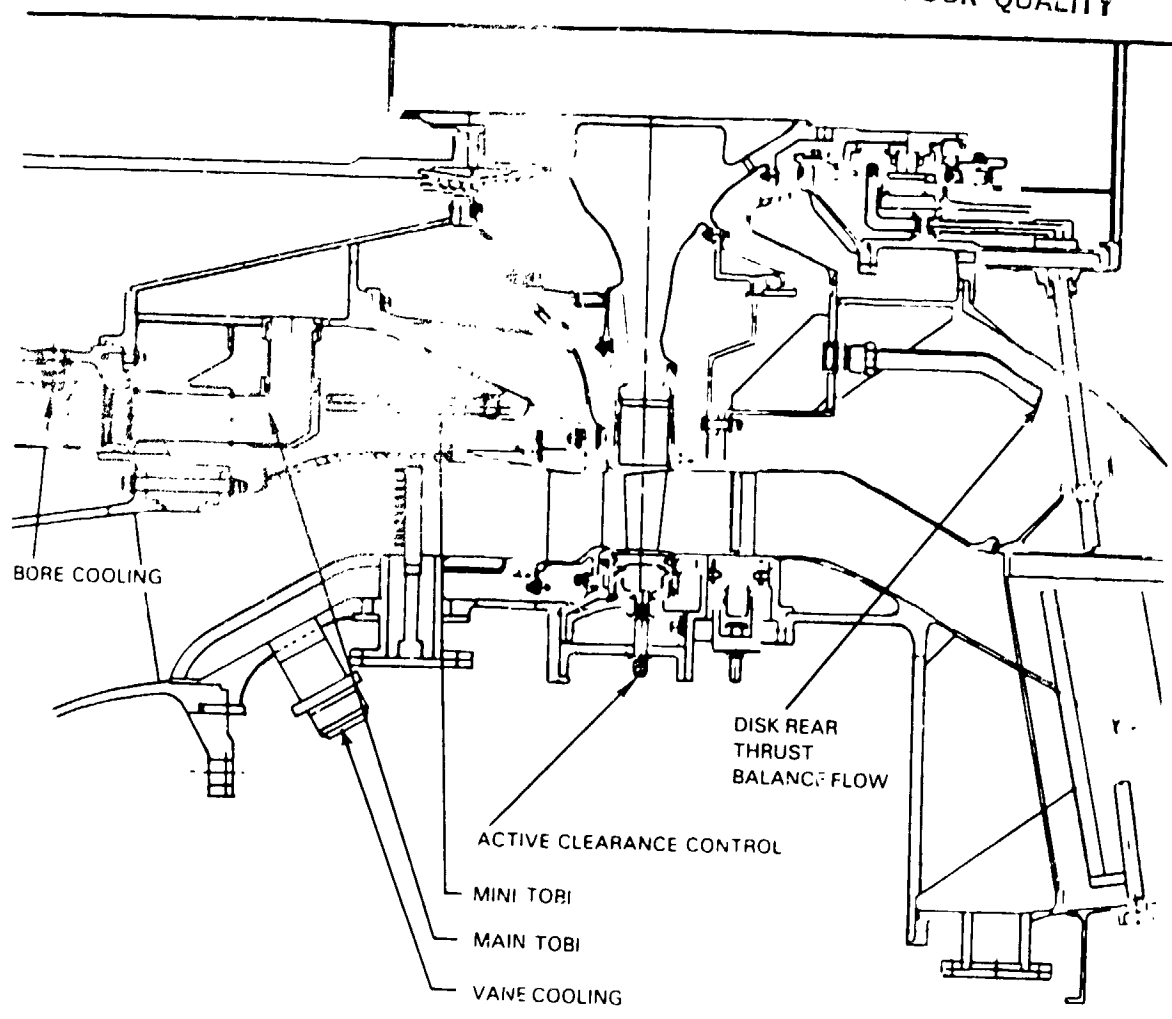


Figure 3.3-2 Turbine Secondary Flow System Air Supply Lines

The rig has two main safety systems. The first is a dump valve, which bypasses the rig airflow upon detection of an overspeed condition or loss of bearing oil. The second safety system is an alarm that is actuated when pre-established rig operating parameters are exceeded.

3.4 RIG FABRICATION AND ASSEMBLY

Components for the test rig were manufactured according to Pratt & Whitney Aircraft's standards for experimental test hardware. Figures 3.4-1 through -3 show some of the major components in the various phases of fabrication. Figure 3.4-1 shows the finished turbine vane and case subassembly. The completed rotor subassembly, including the installation of the full ring, boltless side-plates, is shown in Figure 3.4-2.

Okta.
OF POOR QUALITY

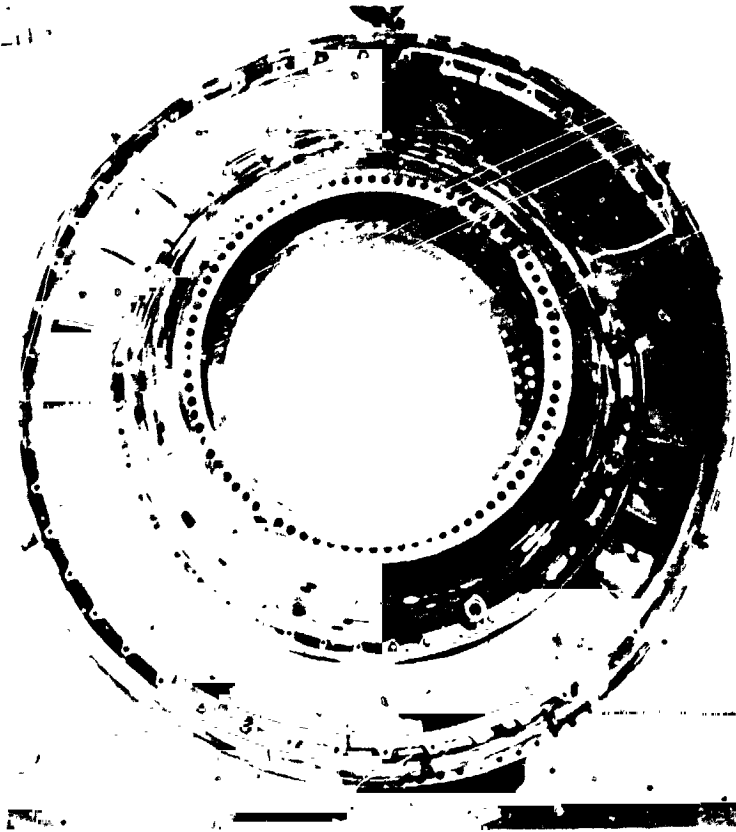


Figure 3.4-1 Completed Turbine Rig Static Structure with PWA 1422 Directionally-Solidified Turbine Vanes

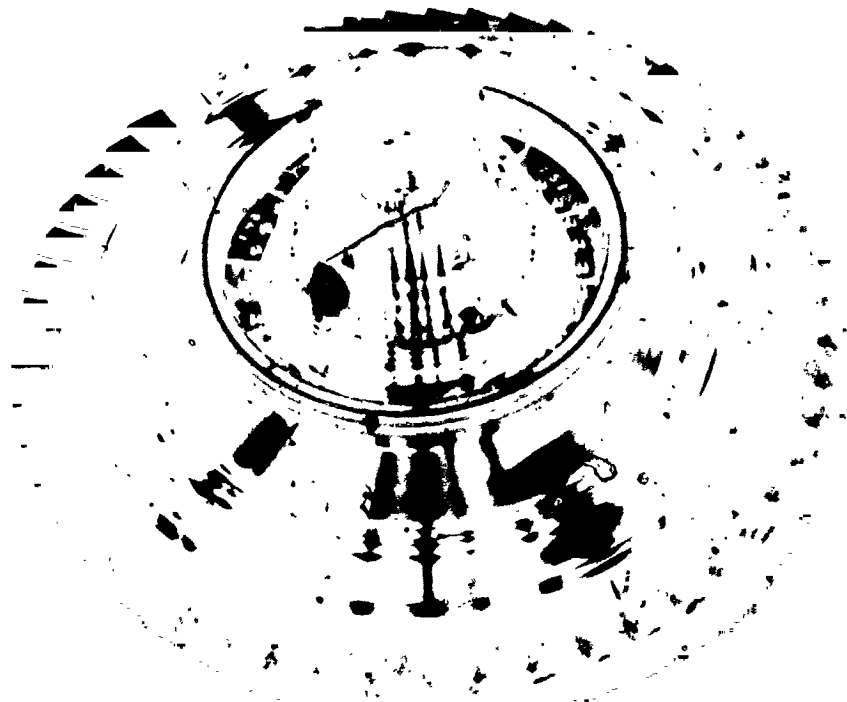


Figure 3.4-2 Completed Turbine Rotor Assembly Single Crystal (PWA 1480) Blades



ORIGINAL COPY
OF POOR QUALITY

Figure 3.4-3 Assembled Turbine Test Rig

Following fabrication, all parts were inspected to ensure conformity to blueprint dimensions. Also, gas path and secondary flow system components were individually flow checked. Test hardware was generally in good agreement with the design specifications. A dimensional check of the blades showed that the throat flow area was 4 percent less than the design. Measurements of the vane throat area showed the area to be 2 percent higher than desired.

An airflow check of the individual vanes showed that the cooling passage average flow rate was 14 percent less than the design requirement, resulting from slightly smaller than intended holes in both the impingement insert and airfoil walls. The vanes were considered acceptable for rig testing since the inlet temperature would not exceed 426°C (800°F) and the cooling air exit velocity was close to the design level. A flow check of the blade showed that the average cooling passage flow was within 1 percent of the design intent.

A cold flow calibration was conducted during assembly of the major rig components to ascertain specific secondary flow system coolant and leakage rates as well as provide baseline data for subsequent comparison of test results. The vane inner platform area leakage was approximately two times the predicted flow, while the outer platform area overflowed by approximately 1.5 times the predicted level. The vane subassembly cooling airflow was 15 percent under prediction, which confirmed results of airflow tests of individual vanes.

The active clearance control system showed a 20 percent higher flow rate at a 2.0 pressure ratio. The blade outer air seal cooling air supply holes overflown by 15 percent at a pressure ratio of 1.5. Four of these holes were plugged to reduce flow to the design intent.

The blade tangential on-board injection nozzle had a 4 percent higher than predicted flow, but was judged to be acceptable for testing. The mini tangential on-board injection nozzle, which swirls air in front of the turbine disk, had a flow rate 18 percent higher than the design intent. As a result, eight holes were plugged to reduce the flow rate.

Cooling airflow to the blades was only slightly underflowing the prediction and was in good agreement with the bench cooling flow results. Leakage past the attachment area of the blade was two times higher than the prediction. However, this result was expected since the rotor was stationary and, therefore, not encountering the normal centrifugal loads that would effectively seal the sideplates and damper seals.

The assembled test rig is shown in Figure 3.4-3 prior to shipment to the test stand. The rig was delivered to the Pratt & Whitney Aircraft Andrew Willgoos Laboratory in East Hartford, Connecticut in mid-February 1982.

At the test facility, all flows and clearances were rechecked. Flow ratios were in excellent agreement with the preceding calibration results. This information provided baseline data for subsequent comparison of test results.

3.5 TEST INSTRUMENTATION

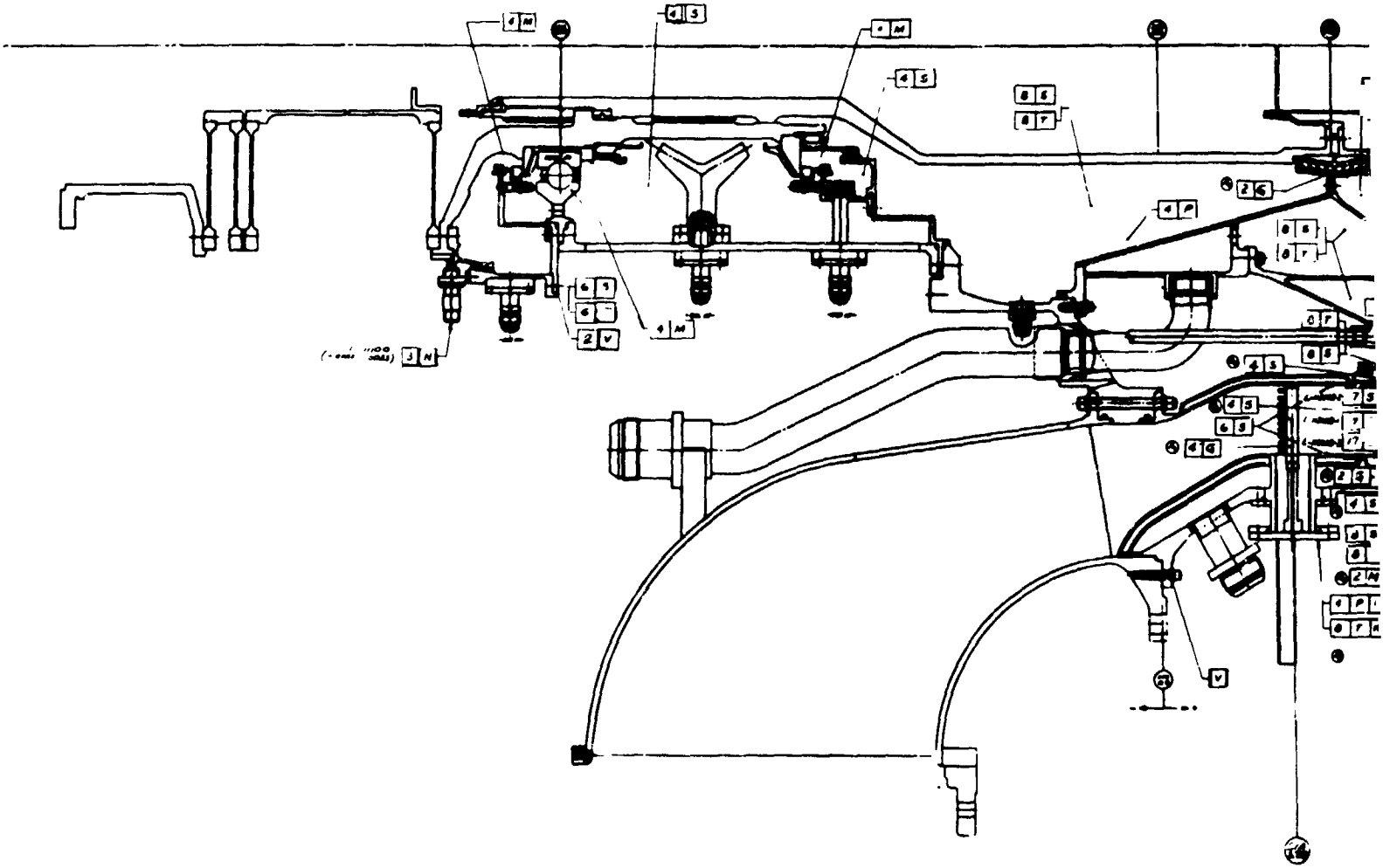
Test instrumentation, including type of sensor, quantity and location, was determined on the basis of analyses and previous turbine test experience. As shown by the instrumentation map in Figure 3.5-1, the rig was equipped with sufficient instrumentation to monitor and record turbine aerodynamic behavior. In certain areas, instrumentation was provided for redundant measurements to enable supervisory control of test conditions, establish data validity, enhance measurement precision, and minimize down time resulting from sensor failures.

3.5.1 Performance Instrumentation

A complete list of the flowpath instrumentation used in both the full stage and cascade tests is contained in Table 3.5.1-1. The inlet was instrumented with stationary pressure and temperature instrumentation rakes to properly establish rig inlet conditions. Three vanes were instrumented at the locations identified in Table 3.5.1-1 for the purpose of determining pressure distributions and cooling film effectiveness.

Laser proximity probes were used at four circumferential locations to measure blade tip clearance at different operating conditions during testing of the full stage. This system consists of a helium-neon laser, fiber optics and readout reticle, video camera, and monitoring/recording equipment.

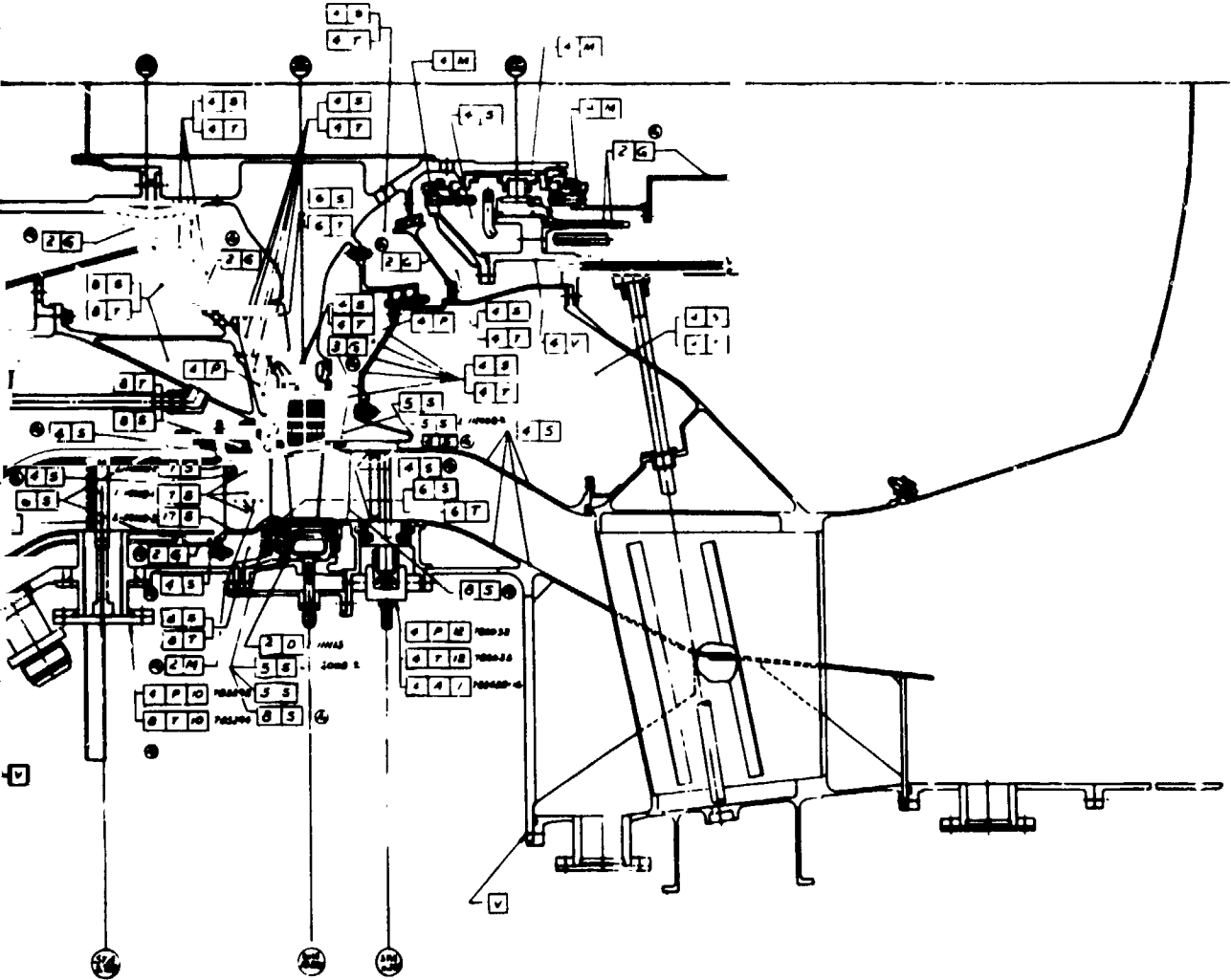
ORIGINAL PAID IN
OF POOR QUALITY



FOLDOUT FRAME

Figure

ORIGINAL OF
OF POOR QUALITY



Notes:

- 1 - All schematic views are looking forward
- 2 - Radial sensor locations numbered from outer diameter to inner diameter
- 3 - Angular locations are clockwise from top dead centerline (TDC)
- 4 - Scale: None

Instrumentation Identification

X Y N

- X** Number of probes (numerical)
- Y** Type of probe (alphabetic symbol)
- N** Number of sensors (numerical)

Y Type of Probe

- A - air angle
- B - acoustics
- D - measurement (blade tip, etc.)
- E - emissions
- F - airflow
- G - strain gage
- M - metal temperature

Z FOLDOUT FRAME

- N - rpm
- P - total pressure
- S - static pressure
- T - temperature
- V - vibration
- Z - miscellaneous

Figure 3.5-1 Instrumentation Map of High-Pressure Turbine Component Rig

TABLE 3.5.1-1

FLOWPATH INSTRUMENTATION

Location	Test		Measurement Type	Total Quantity	Purpose
	Cascade	Rotating			
Rig Inlet	X	X	TT-Temp. Rakes-10 Element	80	Establish Rig Inlet Conditions
	X	X	PT-Press. Rakes-10 Element	40	
	X	X	PS-ID Wall Static Taps	6	
	X	X	PS-OD Wall Static Taps	6	
Vane Assembly Shower Head Airfoil Suction Surface Lead Edge	X	X	PS-Cavity Static	4	Check Flow Injection Establish Cooling Scheme Effectiveness Establish LE Rad. Profile
	X	X	TM-Metal Temp.	8	
	X	X	PS-ID Cavity Static	4	
	X	X	PS-OD Cavity Static	4	
	X	X	PS-ID Endwall Axial Static Taps Gap 6	17	
	X	X	PS-ID Gapwise TE Static Taps Gap 6	5	
	X	X	PS-OD Endwall Axial Static Taps Gap 6	17	
	X	X	PS-OD Gapwise TE Static Taps Gap 6	5	
	X	X	PS-Root "S&P" Surface Static Taps Gap 6	17	
	X	X	PS-Mean "S&P" Surface Static Taps Gap 6	17	
Uncooled Foil Passage	X	X	PS-Tip "S&P" Surface Static Taps Gap 6	17	Establish Passage Flow Characteristics
	X	X	PS-ID Mid-Point Cooled Gaps 1-5	5	
	X	X	PS-ID Gapwise Cooled Gaps 2&3	8	
	X	X	PS-OD Mid-Point Cooled Gaps 1-5	5	
	X	X	PS-OD Gapwise Cooled Gaps 2&4	8	
	X	X	D-Tip Clearance (Laser Probe)	4	
Trail Edge Cooled Foil Passages	X	X	PS-ID Wall Static Taps	8	Establish TE Rad. Gap Profiles
	X	X	PS-OD Wall Static Taps	8	
	X	X	TI-Temp. Rakes (12 Element)	48	
Blade Tip Trail Edge	X	X	PT-Press Rakes (12 Element)	48	Establish Running Clearance Define Blade Exit Mach No.
	X	X	AA-Air Angle Wedge Traverse Probe	4	
	X	X	PS-OD Wall Static Taps	4	
	X	X	PS-ID Wall Static Taps	4	
Rig Exit Traverse Ring	X	X	PS-ID Wall Static Tap	4	Establish Exit Profiles: Temperature Pressure Air Angle Establish Mach No. @ Probe
	X	X	PS-OD Wall Static Tap	8	
Plane of Trav. Ring Exit Duct	X	X	PS-OD Wall Static Tap	8	Define Pressure Gradient
	X	X		8	

Circumferential traversing instrumentation was used to record turbine exit temperature, pressure and air angle. The traversing instrumentation ring contained four kiel-head total pressure pole rakes, four kiel-head total temperature rakes and four radially traversing air angle wedge probes. The locations of these probes are shown in Figure 3.5.1-1. The total range of the circumferential travel for the ring was 30 degrees, corresponding to two vane pitches. The circumferential positions of the rakes and wedge probes were selected to provide performance data in four quadrants of the rig to account for circumferential variations in vane hardware and to permit blade tip clearances to be properly documented.

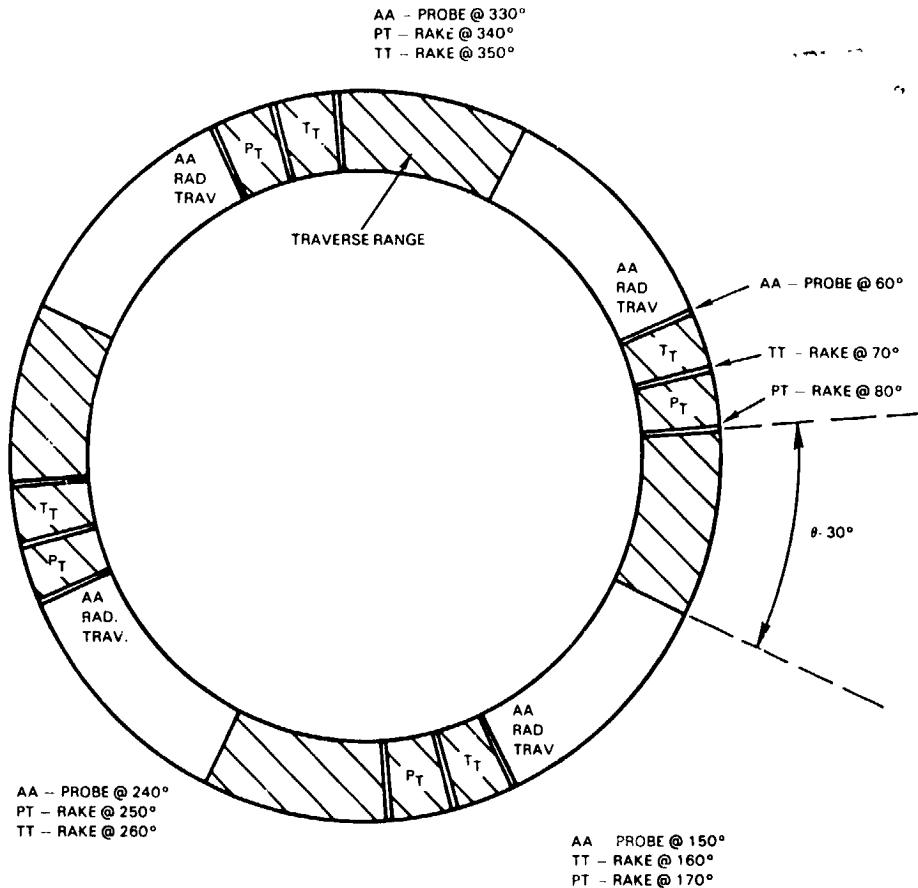


Figure 3.5.1-1 Circumferential Traverse Rake with Instrumentation Locations and Traverse Path

Static pressure taps were installed at three radial locations on selected vanes to determine the pressure distribution. Also, pressure taps were installed on the endwalls to provide information pertaining to blade and vane exit flow conditions.

A summary of instrumentation in the secondary flow system is contained in Table 3.5.1-II. A part of this instrumentation was used to record the thermodynamic states of the secondary flows in order to bookkeep turbine efficiency. The remaining instrumentation was used to record secondary system flows and thermal performance. For cascade testing, only pressure and temperature sensors in the vane inner and outer supply cavities were operative.

ORIGINAL FILED IN
OF POOR QUALITY

TABLE 3.5.1-I-II
SECONDARY FLOW SYSTEM INSTRUMENTATION

Location	Test		Measurement Type	Total Quantity	Purpose
	Cascade	Rotating			
Engine Thrust Balance		X	TT-Temperature in Cavity	4	Establish Flow Characteristics of Secondary Systems
Rear Rim Cavity		X	PS-Static Press. in Cavity	4	
No. 4 Bearing Buffer Cavity		X	TT-Temperature in Cavity	20	
		X	PS-Static Press. in Cavity	20	
Rear Bearing Front Seal Cavity		X	PT-Total Press. in Cavity	4	
Rear Seal Cavity		X	TT-Temperature in Cavity	4	
Rear Case ID Cavity		X	PS-Static Press. in Cavity	4	
Vane OD plus "BOAS" Supply Cavity		X	TM-Temperature of Bearing	4	
		X	TM-Temperature of Seal	4	
Trail Edge Cavity		X	PS-Static Press. in Cavity	4	
Blade Outer Air Seal Cavity Supply		X	TT-Temperature in Cavity	4	
Impingement Cavity		X	PS-Static Press. in Cavity	4	
		X	TT-Temperature in Cavity	4	
Cooling Cavity		X	PS-Static Press. in Cavity	8	
		X	TT-Temperature in Cavity	8	
Front Plate Rubstrip Shoe		X	TT-Temperature in Cavity	6	
Rear Plate		X	PS-Static Press. in Cavity	6	
Active Clearance Control Supply Cavity		X	TT-Temperature in Cavity	6	
		X	PS-Static Press. in Cavity	6	
Rail Cooling Cavity		X	TM-Temperature of Plate	12	
		X	TM-Temperature of Shoe	16	
		X	TM-Temperature of Plate	12	
		X	TT-Temperature in Cavity	4	
		X	PS-Static Press. in Cavity	4	
		X	TT-Temperature in Cavity	8	
		X	PS-Static Press. in Cavity	8	

TABLE 3.5.1-II

SECONDARY FLOW SYSTEM INSTRUMENTATION (Continued)

Location	Test		Measurement Type	Total Quantity	Purpose
	Cascade	Rotating			
Rig Thrust Balance		X	TI-Temperature in Cavity	6	Establish Flow Characteristics of Secondary Systems
Front Bearing		X	PS-Static Press. in Cavity	6	
Front Seal		X	TM-Temperature of Bearing	4	
Center Cavity		X	TM-Temperature of Seal	4	
Rear Seal		X	PS-Static Press. in Cavity	4	
Rear Cavity		X	TM-Temperature of Seal	4	
Bore Cooling Cavity		X	PS-Static Press. in Cavity	4	
		X	TI-Temperature @ 2 Radial Positions	8	
		X	PS-Static Press. @ 2 Radial Positions	8	
Vane ID Cavity	X	X	PI-Total Press. @ 1 Radial Position	4	
	X	X	TI-Temperature in Cavity	8	
Mini TOBI Cavity		X	PS-Static Pressure in Cavity	8	
Main TOBI Cavity		X	TI-Temperature in Cavity	8	
		X	PS-Static Pressure in Cavity	8	
Main TOBI Exit Cavity		X	TI-Temperature in Cavity	6	
ID TOBI Cavity		X	PS-Static Pressure in Cavity	12	
Front Rim Cavity		X	TI-Temperature @ 3 Radial Positions	12	
		X	PS-Static Press. @ 3 Radial Positions	20	
		X	TI-Temperature @ 5 Radial Positions	20	
		X	PS-Static Press. @ 5 Radial Positions	4	
Fishmouth Cavity		X	PI-Total Press. @ 1 Radial Position	4	
		X	TI-Temperature in Cavity	4	
		X	PS-Static Pressure in Cavity	4	

ORIGIN
OF POINT

Table 3.5.1-III presents a summary of the flow measurement instrumentation, and Table 3.5.1-IV identifies the location and type of instrumentation for recording rotor speed and humidity.

3.5.2 Structural Integrity Instrumentation

To ensure the structural integrity of the test rig, sensors were installed to record vibration as well as bearing temperature and oil pressure. This instrumentation is listed in Table 3.5.2-I.

In addition, several stationary components in the turbine test section were instrumented with strain gages as a precaution against a potential fatigue failure. The location and quantity of the strain gage instrumentation is contained in Table 3.5.2-II.

3.5.3 Instrumentation Calibration and Accuracy

Test instrumentation was calibrated, as appropriate, to ensure a high level of measurement accuracy. Five types of calibrations were conducted. These included:

- (1) Calibrator curves generated at Pratt & Whitney Aircraft and traceable to the National Bureau of Standards for voltage, pressure and ice point reference units.
- (2) Thermocouple wire electromotive force correction curves generated at Pratt & Whitney Aircraft and traceable to the National Bureau of Standards.
- (3) Aerodynamic recovery curves for flowpath mounted total temperature and total pressure rake kiel head sensors and wedge probes (established in the Pratt & Whitney Aircraft Free Air Jet Test Facility).
- (4) Choked venturi discharge flow coefficient curves established at the Colorado Experimental Engineering Station and traceable to the National Bureau of Standards.
- (5) Scanivalve pressure transducer curves which were updated during each performance acquisition by a secondary calibration employing dead weight tests traceable to the National Bureau of Standards.

TABLE 3.5.1-IV
SPEED, HUMIDITY AND VIBRATION INSTRUMENTATION

Location	Test		Measurement Type	Total Quantity	Purpose
	Cascade	Rotating			
Main Shaft Speed		X	N - Electromagnetic Pickup Dew Cell	3	Establish Rig Speed
Rig Inlet		X	TA-Dew Cell Air Temperature	1	Establish Inlet Humidity
		X	T _h -Dew Cell LiCl Temperature	1	
		X	PS-Dew Cell Static Pressure Dew Cell	1	
TOBI Supply		✓	T _h -Dew Cell Air Temperature	1	Establish TOBI Humidity
		X	T _h -Dew Cell LiCl Temperature	1	
		X	PS-Dew Cell Static Pressure	1	

TABLE 3.5.1-III
FLOW MEASUREMENT INSTRUMENTATION

Location	Test		Measurement Type	Total Quantity	Purpose
	Cascade	Rotating			
Upstream Rig Inlet	X	X	Sonic Venturi Meter's	3	Establish Inlet Air Flow
	X	X	TT-Temperature Upstream PS-Static Press. Up & Downstream	6	
Air Heater	X	X	Sonic Venturi Meter's	3	Establish Burner Fuel Flow
	X	X	TT-Temperature Upstream PS-Static Press. Up & Downstream	6	
Secondary System Bore Cooling Cavity	X	X	Sonic Venturi Meter's	3	Establish Coolant Flows
	X	X	TT-Temperature Upstream PS-Static Press. Up & Downstream	6	
Main TOBI	X	X	Sonic Venturi Meter's	3	
	X	X	TT-Temperature Upstream PS-Static Press. Up & Downstream	6	
Mini TOBI	X	X	Sonic Venturi Meter's	3	
	X	X	TT-Temperature Upstream PS-Static Press. Up & Downstream	6	
Trim Flow Rear Disk	X	X	Sonic Venturi Meter's	3	
	X	X	TT-Temperature Upstream PS-Static Press. Up & Downstream	6	
No.4 Bearing Buffer Cavity	X	X	Sonic Venturi Meter's	3	
	X	X	TT-Temperature Upstream PS-Static Press. Upstream & Throat	6	
Vane ID	X	X	Sonic Venturi Meter's	3	
	X	X	TT-Temperature Upstream PS-Static Press. Up & Downstream	6	
Blade Outer Air Seal	X	X	BOAS Orifice Metering Holes	8	
	X	X	TT-Temp. Vane OD Cavity Supply PS-Static Press. Upstream "VODCS"	8	
Vane OD Plus "BOAS"	X	X	PS-Static Press. Downstream "BOASCS"	6	
	X	X	Sonic Venturi Meter's	3	
Active Clearance Control	X	X	TT-Temperature Upstream PS-Static Press. Up & Downstream	6	
	X	X	Sonic Venturi Meter's	3	
			TT-Temperature Upstream PS-Static Press. Upstream & Throat	6	

ORIGINAL SOURCE IS
OF POOR QUALITY

TABLE 3.5.2-I

RIG SAFETY SYSTEM
X-203 STANDANNUNCIATOR AND WARNING LIGHT IN
CONTROL ROOM WHEN LIMIT EXCEEDED

Parameter	Quantity	
External Vibration		
Front Case Horizontal	1	0.005 cm (0.002 in)
Front Case Vertical	1	0.005 cm (0.002 in)
Rear Case Horizontal	1	0.005 cm (0.002 in)
Rear Case Vertical	1	0.005 cm (0.002 in)
Internal Vibration		
Front Bearing Horizontal	1	0.005 cm (0.002 in)
Front Bearing Vertical	1	0.005 cm (0.002 in)
Rear Bearing Horizontal	1	0.005 cm (0.002 in)
Rear Bearing Vertical	1	0.005 cm (0.002 in)
Rig Overspeed	1	9500 RPM*
Thrust Balance Cavity Pressure	1	206,844 Pa (30 psi)
Rig Low Oil Pressure Front*	1	241,318 Pa (35 psig)
Rig Low Oil Pressure Rear*	1	241,318 Pa (35 psig)
Rig Oil Out High Temperature	1	176°C (350°F)
Rig Oil In Low Temperature	1	71°C (160°F)
Rig Oil Filter Differential Pressure	1	34,474 Pa (5 psid)
Front Compartment	1	34,474 Pa (5 psid)
Rear Compartment	1	34,474 Pa (5 psid)
Rig Oil Tank Low Level	2	Low Level
Rig Oil Tank High Level	2	High Level
Rig Bearing Temperature		
Front Bearing	1	176°C (350°F)
Rear Bearing	1	176°C (350°F)
Loss of Rig Oil Scavenge	2	68,948 Pa (10 psia)
Main Stream Filter Differential		
Pressure	2	34,474 Pa (5 psid)
Low Bearing Differential Pressure Front	2	13,789 Pa (2 psid)
Low Bearing Differential Pressure Rear	2	13,789 Pa (2 psid)
Active Clearance Control Cal Rod Heat Exchanger	2	

* Overboard dump valve initiated at 9700 RPM

TABLE 3.5.2-II

TURBINE COMPONENT STRUCTURAL INTEGRITY INSTRUMENTATION

Location	Quantity
(1) Midpoint aft bearing center-line spring	Two sets of 0/45/90 degree rosettes 180-degree apart
(2) Carbon seal support ring close to aft fillet	Two gages with axial grids
(3) Inner aft turbine seal	Two radial grids
(4) Thrust balance seal	Three equally spaced circumferential grids on the seal land
(5) High-pressure compressor discharge seal	Two radial grids on forward portion of seal land
(6) High-pressure compressor discharge seal support cone	Two radial grids
(7) Inlet probes	Two radial grids at center of flat portion of inlet temperature probes close to the outer attachment and two grids on the pressure probes
(8) Inner vane outer spring seal	Two axial grids

Table 3.5.3-I presents the error/accuracy of the instrumentation in test stand X-203 that was used to conduct the test program. The analysis included the precision and bias associated with both the hardware and related calibrations used in establishing the engineering unit value for each parameter.

TABLE 3.5.3-I

INSTRUMENTATION ACCURACY
(95 Percent Confidence Level)

<u>Parameter</u>	<u>Bias*</u>	<u>Precision*</u>
Pressure, %	± 0.05	± 0.10 (% of transducer range)
Temperature, °C (°F)	± 0.23 (± 0.41)	± 0.21 (± 0.38)
Air Angle, deg	± 0.22	± 0.65
Tip Clearance, cm (in)	Negligible	± 0.002 (± 0.001)
Air Flow, %	± 0.20	± 0.30 (% of indicated flow)
Radial Position, cm (in)	± 0.0063 (± 0.0025)	± 0.0088 (± 0.0035)
Circumferential Position, deg	± 0.01	± 0.04
Speed, rpm	Negligible	± 5

* 2 standard deviations

A standard error propagation analysis for key performance parameters provided the absolute uncertainties (precision plus bias) shown in Table 3.5.3-II at the 95 percent confidence level (2 standard deviations).

TABLE 3.5.3-II
MEASUREMENT UNCERTAINTY OF TURBINE PARAMETERS
(95 Percent Confidence Level)

Efficiency, %	+ 0.38
Pressure Ratio	\pm 0.04
Speed Parameter, ($N/\sqrt{T_{in}}$)	\pm 0.16

3.5.4 Data Acquisition System

Test data were acquired with the Computerized High Accuracy Data (CHAD) system, located at the X-203 test stand. This system is designed to obtain pressure, temperature, speed, and spatial position data from both stationary and traversing instrumentation. Traversing instrumentation is regulated by a Computerized Automatic Traversing System (CATS) that controls probe movement through a digital feedback loop. Once the computer locates the probes, position data are acquired from radial and circumferential digital shaft encoders and yaw balance data from analog differential pressure transducers. The computer for the CHAD system acts as a master control station, issuing commands not only for its own internal acquisition hardware, but also to the automatic traversing system. Scan lists are incorporated into the data acquisition system to define the order in which rig instrumentation is sampled.

SECTION 4.0 TEST PROGRAM AND TEST FACILITIES

4.1 TEST PROGRAM

The principal objective of the High-Pressure Turbine Component Rig Test Program was to substantiate turbine design point performance as well as determine off-design performance. Other test objectives included evaluating performance sensitivity to blade tip clearances and defining secondary system sensitivity to tangential on-board injection (TOBI), mini TOBI and compressor discharge seal flow rate variations.

To accomplish these objectives, the test program was organized into two parts. The first part consisted of full stage testing for characterization of turbine and secondary flow system performance. The full stage test was structured into the five phases indicated by the test matrix in Table 4.1-I. Figure 4.1-1 shows an envelope of the test points along with the corresponding operating conditions of the test rig.

Vane cascade testing, the second part of the program, was directed toward evaluating turbine vane aerodynamic performance over a range of exit Mach numbers and Reynolds numbers for insight in the analysis of full stage performance. The test matrix is presented in Table 4.1-II.

The test program, consisting of rig installation, testing, and data analysis, was a nine-month effort. A total 216 hours of testing was conducted. Performance data were acquired for 13 principal test conditions during the full stage rig test, covering the high and intermediate power range of the integrated core/low spool.

4.1.1 Full Stage Turbine Test

Before actual testing was initiated, a series of pretest checks was conducted to (1) verify the proper operation of all test support systems and equipment and (2) demonstrate the mechanical integrity of the test rig. Checks of the instrumentation and data acquisition systems were performed both during rig assembly and after it was installed in the test facility to ensure proper operation. Also, a pretest shakedown of the facility was conducted to check out the rig supervisory control and each secondary flow system coolant line. Finally, a shakedown test of the turbine rig was accomplished to verify both the mechanical integrity of the rig and proper functioning of rig instrumentation.

The full stage test, as indicated by the test matrix in Table 4.1-I, consisted of five phases. The first was directed toward substantiating turbine design point performance as well as determining off-design performance. Secondary cooling flows were set at the values listed in Table 4.1-I, and an average blade tip clearance of 0.0472 cm (0.0186 in) was achieved by regulating the active clearance control air temperature.

In the next phase, an assessment of performance sensitivity to blade tip clearance was made by operating the turbine rig at the design condition and varying the blade tip clearance. The desired clearances were obtained by regulating the temperature of the active clearance control air. Clearances were measured by four laser proximity probes and traversing data provided a basis for identifying performance changes.

TABLE 4.1-1
TEST MATRIX FOR FULL STAGE TEST

Test Point	Pressure Ratio	Speed Parameter	SECONDARY FLOW SUPPLY PRESSURE RATIO*			Vane & BOAS	Blade Tip Clear.cm (in)	DATA ACQUIRED			TEST OBJECTIVES
			Main TOBI	Mini TOBI	Bore Cooling			HPT Perf	Sec Sys	ACC	
PHASE I -- Turbine Design and Off-Design Performance Assessment											
1	4.0	244	0.907	1.027	0.622	1.027	0.0472 (0.0186)	X	X		
2	4.0	234	0.907	1.027	0.622	1.027	0.0472 (0.0186)	X	X		
3	4.0	222	0.907	1.027	0.622	1.027	0.0472 (0.0186)	X	X		
4	4.0	260	0.907	1.027	0.622	1.027	0.0472 (0.0186)	X	X		
5	3.5	244	0.907	1.027	0.622	1.027	0.0472 (0.0186)	X	X		
6	3.5	234	0.907	1.027	0.622	1.027	0.0472 (0.0186)	X	X		
7	3.5	222	0.907	1.027	0.622	1.027	0.0472 (0.0186)	X	X		
8	3.2	244	0.907	1.027	0.622	1.027	0.0472 (0.0186)	X	X		
9	4.5	244	0.907	1.027	0.622	1.027	0.0472 (0.0186)	X	X		
10	4.0	244	0.907	1.027	0.622	1.027	0.0472 (0.0186)	X	X		Design Point Repeat
PHASE II -- Turbine Tip Clearance/Active Clearance Control Study											
11	4.0	244	0.907	1.027	0.622	1.027	0.088 (0.035)	X	X	X	Blade Tip Clearance Sensitivity
12	4.0	244	0.907	1.027	0.622	1.027	0.032 (0.0126)	X	X	X	
13	4.0	244	0.907	1.027	0.622	1.027	***	X	X	X	
14	4.0	244	0.907	1.027	0.622	1.027	0.0472 (0.0186)	X	X	X	Design Point Repeat
PHASE III -- Secondary Flow System Performance Characterization											
15	4.0	244	-20% **	1.027	0.622	1.027	0.0472 (0.0186)	--	X	--	Main TOBI Flow Sensitivity
16	4.0	244	-10% **	1.027	0.622	1.027	0.0472 (0.0186)	--	X	--	
17	4.0	244	+10% **	1.027	0.622	1.027	0.0472 (0.0186)	--	X	--	
18	4.0	244	+20% **	1.027	0.622	1.027	0.0472 (0.0186)	X	X	--	(Blade Coolant Increase Sensitivity)
19	4.0	244	No Flow	1.027	0.622	1.027	0.0472 (0.0186)	--	X	--	Mini TOBI Flow Sensitivity
20	4.0	244	-33% **	1.027	0.622	1.027	0.0472 (0.0186)	--	X	--	
21	4.0	244	+33% **	1.027	0.622	1.027	0.0472 (0.0186)	X	X	--	
PHASE IV -- Additional Off-Design Performance Investigation											
22	5.0	234	0.907	1.027	0.622	1.027	0.0472 (0.0186)	X	X	--	Additional Off-Design Perf. Sensitivity
23	3.5	260	0.907	1.027	0.622	1.027	0.0472 (0.0186)	X	X	--	
24	4.0	244	0.907	1.027	0.622	1.027	0.0472 (0.0186)	X	X	--	Design Point Repeat
PHASE V -- Compressor End Seal Study											
25	4.0	244	0.907	1.027	-25% **	1.027	0.0472 (0.0186)	--	X	--	Compressor End Seal Leakage Study
26	4.0	244	0.907	1.027	+25% **	1.027	0.0472 (0.0186)	--	X	--	
27	4.0	244	0.907	1.027	+50% **	1.027	0.0472 (0.0186)	--	X	--	

For All Test Conditions, Turbine Inlet Temperature = 426°C (800°F) and Secondary Flow Temperatures = 62°C (145°F).

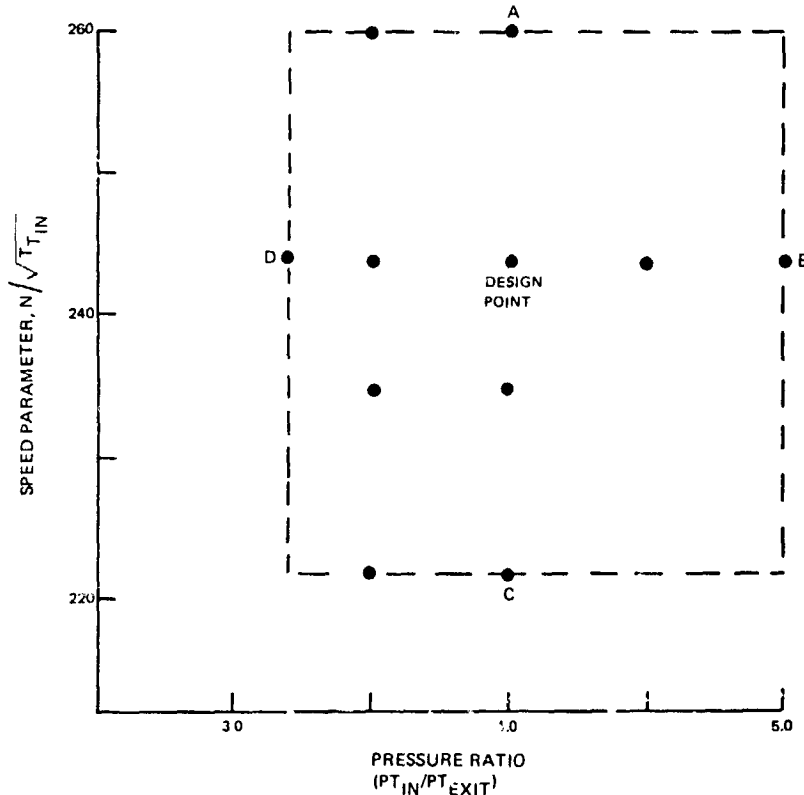
* Ratio of Secondary Flow Supply Pressure to Turbine Inlet Pressure

** Flow Measured for Test Point No. 1 Changed by Percentage Shown

*** Operation at a Value Below the Status Clearance of 0.0320 cm (0.0126 in.)

ORIGINAL PAGE IS
OF POOR QUALITY

Test Point	PT _{in} (MPa) (psia)	TT _{in} (K) (°R)	PT _{out} (MPa) (psia)	TT _{out} (K) (°R)	Turbine Inlet Flow (kg/sec) (lb/sec)	Speed (RPM)	Torque (FT-LB _f)	H.P.	Vane* and BOAS Coolant	TOBI*	Mini* TOBI	Bore* Coolant	Buffer* Brg. Cavity	Rear* Disk Trim	Active* Clearance Control (ACC)
D.P.	0.441 (64.0)	700 (1260)	110 (16.0)	472 (850)	14.2 (31.4)	8660	2550	4210	11.33	3.35	0.59	0.47	0.23	0.12	0.29
	0.441 (64.0)	700 (1260)	110 (16.0)	472 (850)	14.2 (31.4)	9230	2390	4210	↓	↓	↓	↓	↓	↓	↓
B	0.552 (80.0)	700 (1260)	110 (16.0)	450 (810)	17.8 (39.3)	8660	3590	5930	↓	↓	↓	↓	↓	↓	↓
C	0.441 (64.0)	700 (1260)	110 (16.0)	472 (850)	14.2 (31.4)	7850	2800	4210	↓	↓	↓	↓	↓	↓	↓
D	0.353 (51.2)	700 (1260)	110 (16.0)	497 (895)	11.3 (25.1)	8660	1750	2890	↓	↓	↓	↓	↓	↓	↓



*Metered Secondary Flows - % of HPT Inlet Flow

Figure 4.1-1 Test Envelope for Full Stage Turbine Test Program

The influence of both the blade and mini tangential on-board injection (TOBI) systems was evaluated during the third phase of the program as part of the overall performance characterization of the secondary flow system. An evaluation of the blade flow sensitivity provided pertinent information to assess the influence of blade off-design cooling flows on turbine performance as well as TOBI performance. Next, the sensitivity of the secondary cooling system to variations in the mini tangential on-board injection flow was investigated. Testing included operation with no mini tangential on-board injection flow.

The fourth phase of the program was aimed at providing additional mapping of turbine off-design performance. Testing was conducted at more exaggerated off-design conditions in comparison to those in the initial phase of the program.

TABLE 4.1-II

TURBINE VANE ANNULAR CASCADE TEST CONDITIONS

PHASE I - Mach Number Effects (Ambient Discharge)

Test Point	Exit Mach Number	T _{Tin} °C (°F)	Reynolds Number (10 ⁵)	Cooling	
				PR	TR
1	0.70	426 (800)	1.97	1.027	0.48
2	0.85	426 (800)	2.56	1.027	0.48
3	0.91	426 (800)	2.82	1.027	0.48
4	1.00	426 (800)	3.24	1.027	0.48
5	1.08	426 (800)	3.62	1.027	0.48
6	1.16	426 (800)	3.92	1.027	0.48
7	0.56	426 (800)	1.52	1.027	0.48

PHASE II - Reynolds Number Effects - High-Pressure Discharge

8	0.92	426 (800)	4.66	1.027	0.48
9	0.92	426 (800)	6.44	1.027	0.48

The final series of tests evaluated the influence of compressor discharge seal flow rates on the pressure distribution in the front disk cavity and blade TOBI supply plenum as well as the resultant effects on blade coolant flow.

4.1.2 Vane Cascade Test

The annular cascade rig essentially consists of all the components in the full stage rig, except that the turbine rotor was removed. With the removal of the rotor, the exit traversing instrumentation system was positioned behind the vane stage to obtain aerodynamic measurements at different circumferential locations.

Various pretest checks were conducted to verify the proper operation of the test rig and support systems. These checks followed the same format as those performed in the full stage rig program.

The vane cascade test consisted of two phases. The first phase of testing evaluated vane performance under varying exit Mach number conditions with an ambient discharge. The range of Mach numbers tested (0.56 - 1.18) bracketed the design point for the integrated core/low spool high-pressure turbine. Test point 3 (Table 4.1-II) corresponds to design point conditions or test point No. 1 in the full stage rig test matrix. Data acquired at this condition were used with the full stage data to assess stage gas path aerodynamics.

In the second phase, the rig was back pressured to evaluate vane performance at higher Reynolds numbers.

4.2 TEST FACILITY

Test stand X-203, located at the Pratt & Whitney Aircraft Andrew Willgoos Turbine Laboratory in East Hartford, Connecticut, was used for the Turbine Rig Test Program. The test facility is shown in Figure 4.2-1, and is designed for development testing of full scale turbine component rigs.

The test stand consists of a large enclosed test cell and an adjacent control room. The component is mounted on an open bedplate, sealed to the air supply and exhaust ducts, and connected to the dynamometers by a suitable drive shaft through a gearbox. Air can be supplied at a rate up to 56 kg/sec (125 lb/sec) at 635 cm (250 in) Hg absolute. High pressure air can be heated to 537°C (1000°F) by two natural gas-fired heaters. Through the controlled use of laboratory compressors, a refrigeration system, air heaters, and exhauster units, sea level and altitude operating conditions can be simulated over a wide range.

Two eddy-current dynamometers, each with a 10,000 horsepower absorption capacity, are connected to the component through a gearbox to reduce the output speed of the test unit to a level acceptable for the dynamometers. Only one dynamometer was used for this turbine rig test. Auxiliary equipment used to support testing included a remotely controlled lubrication system and a natural gas supply system. The stand is also equipped with an extensive safety and fire protection system.

Stand services available to operate equipment in support of testing include 689,480 and 2,413,180 Pa (100 and 350 psig) air supply, 120 and 480 volt, 60 cycle per second A.C. and 24 volt D.C. electrical power, 206,844 and 2,999,238 Pa (30 and 435 psig) steam supply, and city or river water supply.

All controls and instrumentation required to operate the test rig and monitor performance are located in the adjacent control room. The test operator has direct control of the test vehicle, inlet and discharge air valving associated with the test stand and the power absorbing dynamometers.

During the test, a Rig Supervisory Control system was used to aid in setting performance points, maintaining test parameters within preprogrammed limits, and monitoring rig and facility safety parameters for early detection of problems. The supervisory control is a digital computer control with appropriate input and output signal circuiting. In addition to the Rig Supervisory Control, certain additional monitoring systems were used to ensure both rig and facility safety.

4.3 DATA REDUCTION AND ANALYSIS

The analysis of data obtained from this program was accomplished in two steps. The first step assessed the validity of the data and executed preliminary calculations to obtain turbine performance information. This was conducted in near real time.

The second step consisted of more comprehensive calculations to obtain final turbine performance values. In addition, the test results were compared to Design System calculations. This work was completed shortly after the completion of testing.

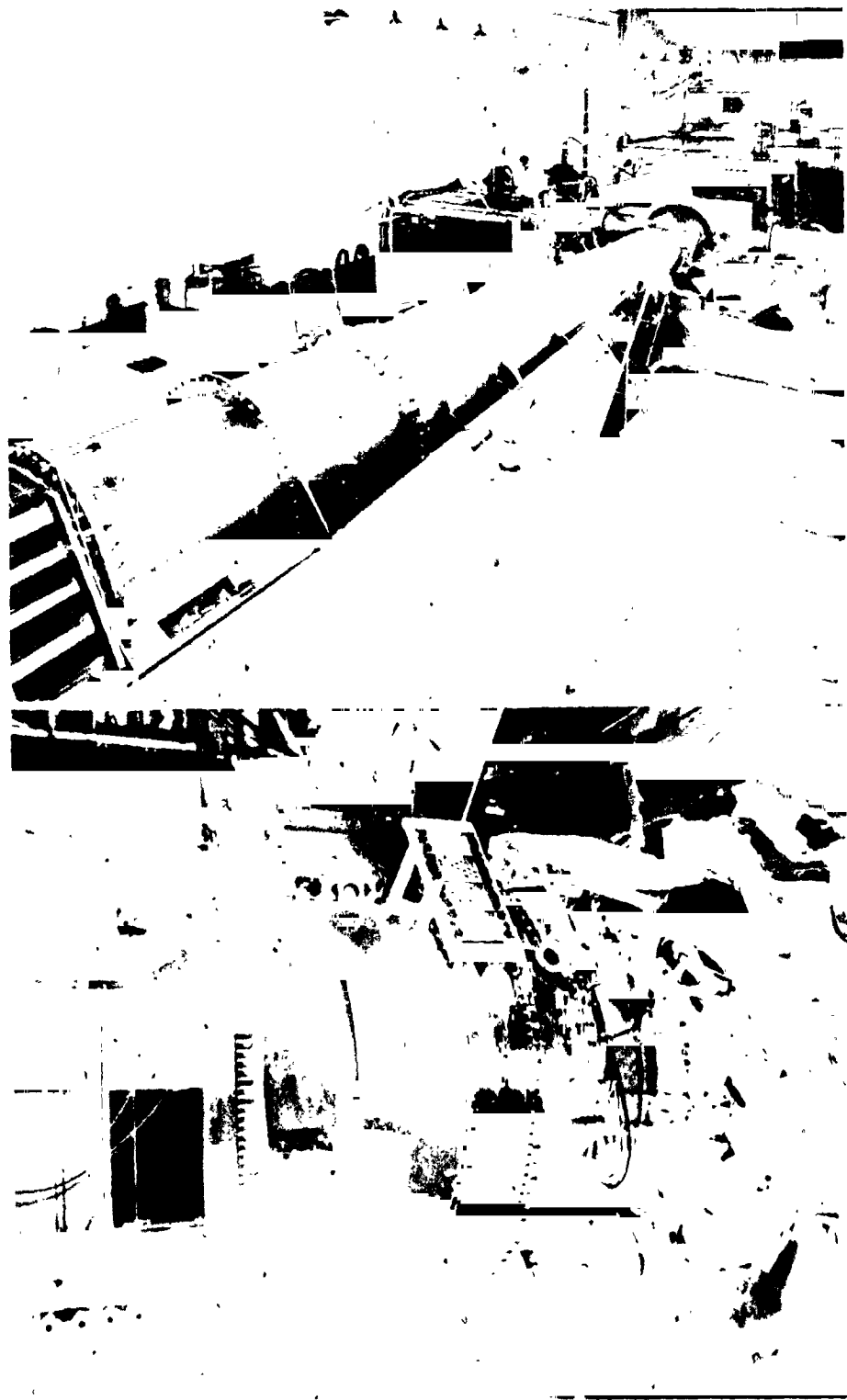


Figure 4.2-1 Pratt & Whitney Aircraft X-203 Test Facility. (The top photograph shows the internal ducting as well as the location of the test component. The bottom photograph shows a typical test component without the ducting installed.)



Data acquired at the test stand by a Honeywell 316 computer were sent to a Univac 1100 computer, which converted raw data (electrical voltages) to engineering units. The engineering unit data sets were then sent to the IBM computer network for review and analysis in near real time. The culmination of the near real time effort was the execution of preliminary turbine efficiency and secondary system performance calculations employing existing computer programs.

4.3.1 Analysis of Full Stage Data

Data obtained during testing were analyzed in detail to determine turbine and secondary system performance at design and off-design conditions. For each test point, the thermodynamic efficiency of the component was calculated in accordance with the following definition.

$$\text{turbine efficiency} = \frac{\sum_i m_i \Delta h_i}{\sum_i m_i \Delta h_i'}$$

m_i - mass flow of i^{th} stream

Δh_i - actual enthalpy change of i^{th} stream

$\Delta h_i'$ - ideal enthalpy change expanding flow to turbine exit pressure

Where the numerator and denominator are summed over the primary and all coolant and leakage flows.

Comparisons of test data with design system predictions were made in the following areas:

- turbine efficiency
- turbine flow capacity (flow parameter)
- stage reaction
- turbine exit air angle profile
- turbine Mach number profile
- secondary system performance (pressures and temperatures)
- active clearance control (ACC) response
- vane surface pressure distributions (design point only)
- vane suction surface cooling effectiveness (design point only)

4.3.2 Analysis of Cascade Data

For each test point, comparisons of data with design system predictions were made in the following areas:

- full passage total pressure loss
- exit air angle profile
- exit Mach number profile
- vane flow parameter
- vane surface pressure distributions (design point only)

SECTION 5.0 TEST RESULTS AND ANALYSIS

5.1 INTRODUCTION

This section presents the results of the turbine rig test program. The mechanical performance of the turbine rig is discussed in the following section, and Section 5.3 presents the results and analysis of turbine aerodynamic performance. The presentation of aerodynamic performance results is divided into three categories. First, stage performance is discussed. Second, vane cascade performance and supporting data are presented. Third, the results from the vane cascade testing are used with results from stage testing for a characterization of turbine blade performance. Finally, Section 5.4 presents the results of a post-test inspection of the turbine rig hardware.

5.2 MECHANICAL PERFORMANCE

The test rig was successfully operated over a range of conditions that simulated operation of the integrated core/low spool at both intermediate and high power levels. No major difficulties were encountered that prevented the acquisition of performance data. Throughout the test, the mechanical performance of the turbine test section components -- the turbine gas path and secondary flow system components -- was flawless. This was confirmed by a post-test inspection. Component stress levels were low, on the order of 13.8 MPa (2000 psi), with no significant change during the course of the test.

During the initial shakedown of the rig, excessive bearing compartment and facility dynametric coupling shaft vibrations were encountered at mechanical speeds above 8300 rpm. Also, the exit circumferential instrumentation traverse ring experienced binding at temperatures above 315°C (600°F). To account for this, the maximum rig operating temperature was reduced from 426 to 315°C (800 to 600°F), the speed parameter was held, and the air density ratio was increased from 0.48 to 0.52 at the design condition.

In addition, blade tip clearance measurements disclosed an eccentricity or displacement of the rotor/case assembly. As indicated in Table 5.2-I, clearances ranged from 0.020 cm (0.008 in) in quadrant 1 to as large as 0.078 cm (0.031 in) in quadrants 3 and 4. This condition, which was attributed in part to tolerance differences in the experimental hardware, somewhat restricted the blade clearance investigation planned in Phase II of the program. Selected clearance variations were achieved by regulating both the rig inlet temperature to reduce rotor growth and the active clearance control air temperature.

TABLE 5.2-I
TURBINE BLADE TIP CLEARANCES

<u>Location (Deg)</u>	<u>Clearance Reading cm (in)</u>
42	0.020 (0.008)
132	0.033 (0.013)
222	0.078 (0.031)
342	0.078 (0.031)

For the analysis of performance, an average tip clearance of 0.048 cm (0.019 in) is used, and efficiency measurements have been adjusted accordingly.

5.3 AERODYNAMIC PERFORMANCE

5.3.1 Turbine Stage Performance Assessment

The turbine rig overall performance parameters are listed in Table 5.3.1-I. These nondimensional parameters show a relatively close modeling of the integrated core/low spool design at the rig design point. At this point, rig performance exceeded all efficiency goals and closely matched the design level of flow capacity and reaction. As indicated in Table 5.3.1-I, the measured flow capacity was 17.2 compared to a design value of 17.0 and the stage pressure reaction was 43.1 percent compared to the design level of 42.4 percent.

The measured efficiency of 88.5 percent surpassed the rig efficiency goal of 86.5 percent. Moreover, it surpassed the expected test efficiency for the integrated core/low spool (87.1 percent) and the goal for the flight propulsion system (88.2 percent). It is also noteworthy to compare this efficiency to the level measured in the preceding Uncooled Turbine Rig Program, which was 91.1 percent. Thus, a deficit of 2.6 percent is imparted by the introduction of component cooling and the functional operation of the secondary flow system.

TABLE 5.3.1-I
COMPARISON OF PERFORMANCE PARAMETERS

	<u>INTEGRATED CORE/LOW SPOOL DESIGN</u>	<u>TURBINE RIG</u>
Mean Velocity Ratio	0.551	0.557
Work Factor	1.65	1.61
Cx/U	0.360	0.332
Expansion Ratio	4.084	4.014
Inlet Flow Parameter	17.023	17.191
Exit Flow Parameter	69.165	65.215
Cooling Flow, % Wae	14.56	12.36
Pressure Reaction, %	42.4	43.1
Exit Mach Number	0.539	0.519
Exit Angle, deg	44.0	49.8
$\Delta h/T_T$ RIT	0.685	0.675
T_T RIT, K (°R)	1550 (2791)	566 (1019)

5.3.1.1 Component Efficiency and Reaction

Test data were processed to determine the mass-averaged cooled turbine efficiency at design and off-design conditions evaluated in Phases I and IV of the program. The test conditions for these Phases are shown in Table 5.3.1-II along with the measured clearance, mass-averaged efficiency, mass-averaged efficiency adjusted to a clearance of 0.048 cm (0.019 in) and pressure reaction. The design point was repeated in Phase IV of the program, as shown in Table 5.3.1-II. Results are in excellent agreement with the first design point test and verify the level of efficiency. In addition, the results show that there was no performance deterioration during the test.

TABLE 5.3.1-11

FULL STAGE TURBINE WARM RIG TEST RESULTS

PHASE I - Turbine Design and Off-Design Performance Assessment

Test Point	Press Ratio	Speed Para.	Corrected Flow	Reaction Percent	PTIn MPa (psia)	TTIn °C (°F)	TTout °C (°F)	Efficiency Measured Mass Avg.	Avg. Clear. cm (in)	Efficiency @ 0.048 cm (0.019 in) Mass Avg.
1	4.01	244.8	17.19	43.1	0.454 (65.87)	315.4 (599.8)	128.2 (262.9)	88.37	0.053 (0.021)	88.54
2	4.03	234.1	17.05	43.7	0.475 (68.87)	367.2 (695.0)	163.2 (325.9)	87.45	0.053 (0.021)	87.62
3	3.91	222.3	17.07	42.9	0.462 (67.05)	366.6 (692.0)	167.9 (334.3)	86.64	0.058 (0.023)	86.98
4	3.98	253.1	17.18	42.5	0.446 (64.74)	309.7 (589.5)	125.0 (257.1)	88.88	0.048 (0.019)	88.88
5	3.49	244.4	17.13	39.2	0.465 (67.44)	316.1 (601.1)	142.8 (289.1)	88.03	0.050 (0.020)	88.12
6	3.48	235.5	17.20	39.4	0.474 (68.72)	311.1 (592.1)	141.5 (286.7)	87.35	0.053 (0.021)	87.52
7	3.49	223.0	17.15	39.8	0.477 (69.21)	327.8 (632.0)	142.4 (288.4)	86.50	0.060 (0.024)	86.93
9	4.43	245.3	17.22	45.0	0.541 (78.44)	311.9 (593.5)	117.1 (242.9)	88.29	0.050 (0.020)	88.38

PHASE II - Turbine Tip Clearance/Active Clearance Control Study

11	4.06	243.3	17.38	42.9	0.465 (67.39)	148.8 (300.0)			0.066 (0.026)	
14	4.05	243.9	17.37	43.8	0.463 (67.15)	148.8 (299.9)			0.048 (0.019)	

PHASE III - Secondary Flow System Performance Characterization

15	4.00	246.2	17.21	42.9	0.459 (66.56)	309.3 (588.9)			0.053 (0.021)	
18	4.03	244.6	17.15	43.7	0.458 (66.46)	315.7 (600.4)	127.1 (260.9)	88.06	0.055 (0.022)	88.32
19	4.00	244.1	17.17	42.7	0.458 (66.36)	316.3 (601.5)			0.053 (0.021)	
20	4.00	244.2	17.21	43.2	0.459 (66.26)	316.9 (602.5)			0.053 (0.021)	
21	4.02	244.2	17.18	43.4	0.457 (66.21)	316.2 (601.3)	127.6 (261.8)	88.27	0.053 (0.021)	88.44
28	4.01	244.8	17.28	43.1	0.454 (65.82)	314.1 (597.5)	129.2 (264.6)	88.31	0.050 (0.020)	88.40

PHASE IV - Additional Off-Design Performance Investigation

22	4.30	234.4	17.22	44.8	0.523 (75.84)	314.5 (598.1)	123.2 (253.9)	87.36	0.055 (0.022)	87.62
23	3.47	253.8	17.17	39.2	0.449 (65.18)	315.6 (600.1)	141.6 (287.0)	88.72	0.048 (0.019)	88.72
24	4.04	244.8	17.19	43.1	0.457 (66.26)	310.5 (591.0)	124.3 (255.9)	88.39	0.053 (0.021)	88.56
29	4.75	243.8	17.36	46.3	0.602 (87.38)	288.1 (550.6)	98.9 (210.1)	87.56	0.053 (0.021)	87.73

PHASE V - Compressor End Seal Study

25	4.00	244.2	17.19	43.1	0.454 (65.87)	316.1 (601.0)			0.053 (0.021)	
26	4.00	245.0	17.17	43.2	0.453 (65.77)	316.3 (601.5)			0.053 (0.021)	
27	4.00	244.5	17.19	43.2	0.453 (65.67)	316.6 (602.0)			0.053 (0.021)	

ORIGINAL PAGE IS OF POOR QUALITY

Figure 5.3.1-1 shows turbine efficiency trends as a function of pressure ratio and speed parameter ($N/\sqrt{T_T}$). These results show efficiency at the design speed parameter of 244 increasing with pressure ratio to the design level of 4.0 and then decreasing. Efficiency also increases with speed parameter at a given pressure ratio. This trend is more apparent in Figure 5.3.1-2, which is a cross plot of Figure 5.3.1-1 with speed parameter as the primary variable.

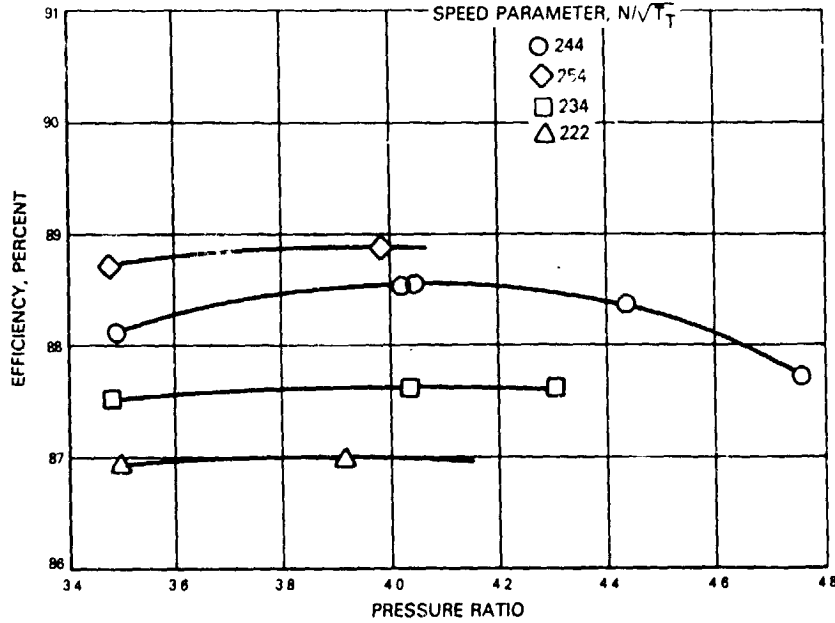


Figure 5.3.1-1 Turbine Stage Efficiency Trends as a Function of Pressure Ratio and Speed Parameter

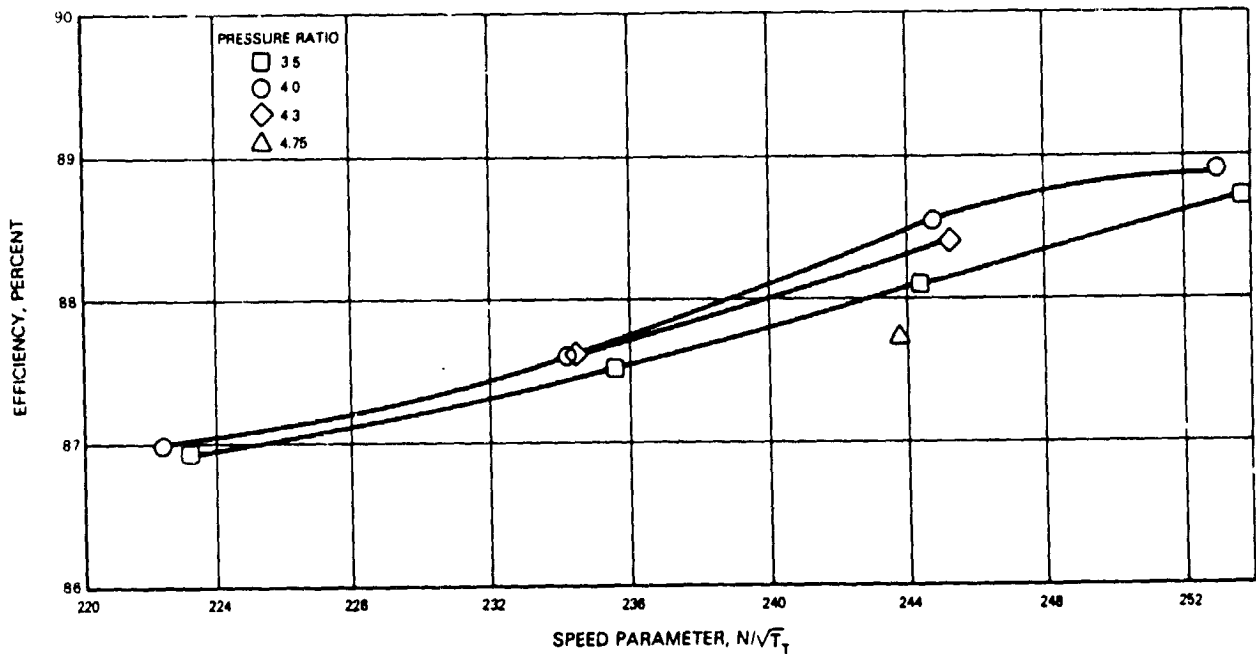
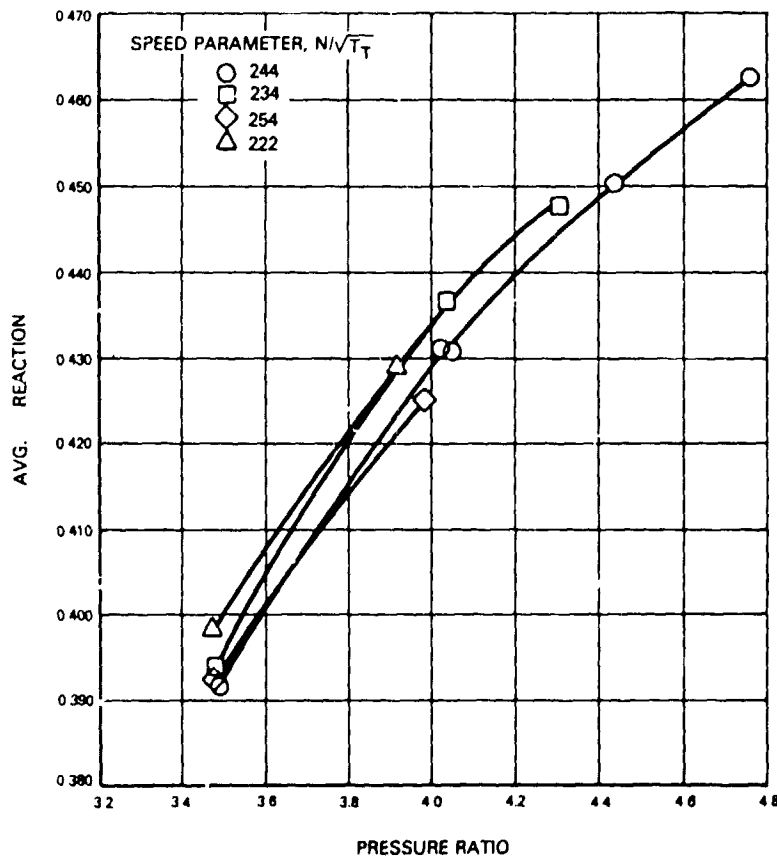


Figure 5.3.1-2 Turbine Stage Efficiency

Turbine reaction, which is defined as the ratio of the static pressure drop across the rotor to the static pressure drop across the stage, is presented in Figure 5.3.1-3. The static pressure reaction increases smoothly with pressure ratio through the design point level of 43.1 percent.



ORIGINAL PAGE IS
OF POOR QUALITY

Figure 5.3.1-3 Turbine Reaction Characteristics

5.3.1.1.1 Blade Tip Clearance Adjustment

As discussed earlier, blade tip clearances showed a variation at the measuring locations. Since efficiency was not measured at the same locations as the blade tip clearances (refer to Figure 5.3.1-7), the average clearance was used to correct the average efficiency. The sensitivity of turbine efficiency to tip clearance was determined on the basis of results of Phase II. This sensitivity was used to correct the efficiency at the measured clearance to the design clearance of 0.048 cm (0.019 in). During this test, two tip clearances were evaluated at the design point conditions using the active clearance control system. The results are presented in Table 5.3.1-III and show the clearance change with the attendant change in efficiency for quadrants one through three. (Data from the fourth quadrant were not used since that quadrant was partially affected by instrumented vanes and did not exhibit consistent results.) The clearance adjustment factor for correcting efficiency was the average of quadrants one through three. The average clearance adjustment factor is a 0.09 percent increase in efficiency for a 0.002 cm (0.001 in) decrease in clearance.

ORIGINAL COPY IS
OF POOR QUALITY

TABLE 5.3.1-III
CLEARANCE ADJUSTMENT

	Quadrant	Quadrant	Quadrant
	1	2	3
Δ Clearance, cm (in)	0.015 (0.006)	0.020 (0.008)	0.015 (0.006)
$\Delta \eta\%$	0.61	0.61	0.74

$$\Delta \eta / \Delta \text{clearance} = 0.09\% / \text{mil tip clearance}$$

Reference: $\Delta \eta / \Delta \text{clearance} = 0.08\% / \text{mil tip clearance uncooled rig}$

5.3.1.1.2 Secondary Flow System Performance

All major components in the secondary flow system, which include the blade and mini tangential on-board injection systems, blade outer air seal, and compressor discharge seal, performed according to the design intent. The map of the secondary flow system shown in Figure 5.3.1-4 compares measured flow rates and pressure levels with the prediction for the design condition. An excellent agreement between the prediction and test data is apparent. With this good data correlation, corrections to performance data are not necessary to adjust for anomalies in the secondary flow system.

In addition, as discussed in Section 5.3.4, results of characterization studies showed that, for this turbine design, system performance is relatively insensitive to variations in flow rates and pressures. Table 5.3.1-IV presents a summary of flow sensitivity tests, in which the effects of variations in flow rate to the main and mini tangential on-board injection nozzles and vane case were evaluated. These results indicate a relatively small potential error in efficiency for the cooling flow variable tolerance maintained during the test. The cooling flow parameters are listed in Table 5.3.1-V for each of the test points.

TABLE 5.3.1-IV
SECONDARY FLOW SYSTEM
FLOW SENSITIVITY TEST RESULTS

Test Point No.	Identification	Pressure Ratio			Efficiency
		Main Tobi	Mini Tobi	Vane Case	
	Design Intent	0.946	1.027	1.027	
1	Design Point	0.942	1.030	1.027	Base
18	+23% Main TOBI Air Flow	1.059	1.021	1.030	-0.22%
21	+19% Mini TOBI Air Flow	0.949	1.194	1.025	-0.10%
28	-9% Vane Case Air Flow	0.932	1.028	1.016	-0.14%
Design Point Error $\Delta \eta\%$		+0.008	-0.002	0.000	

ORIGINAL DRAWING
OF POOR QUALITY

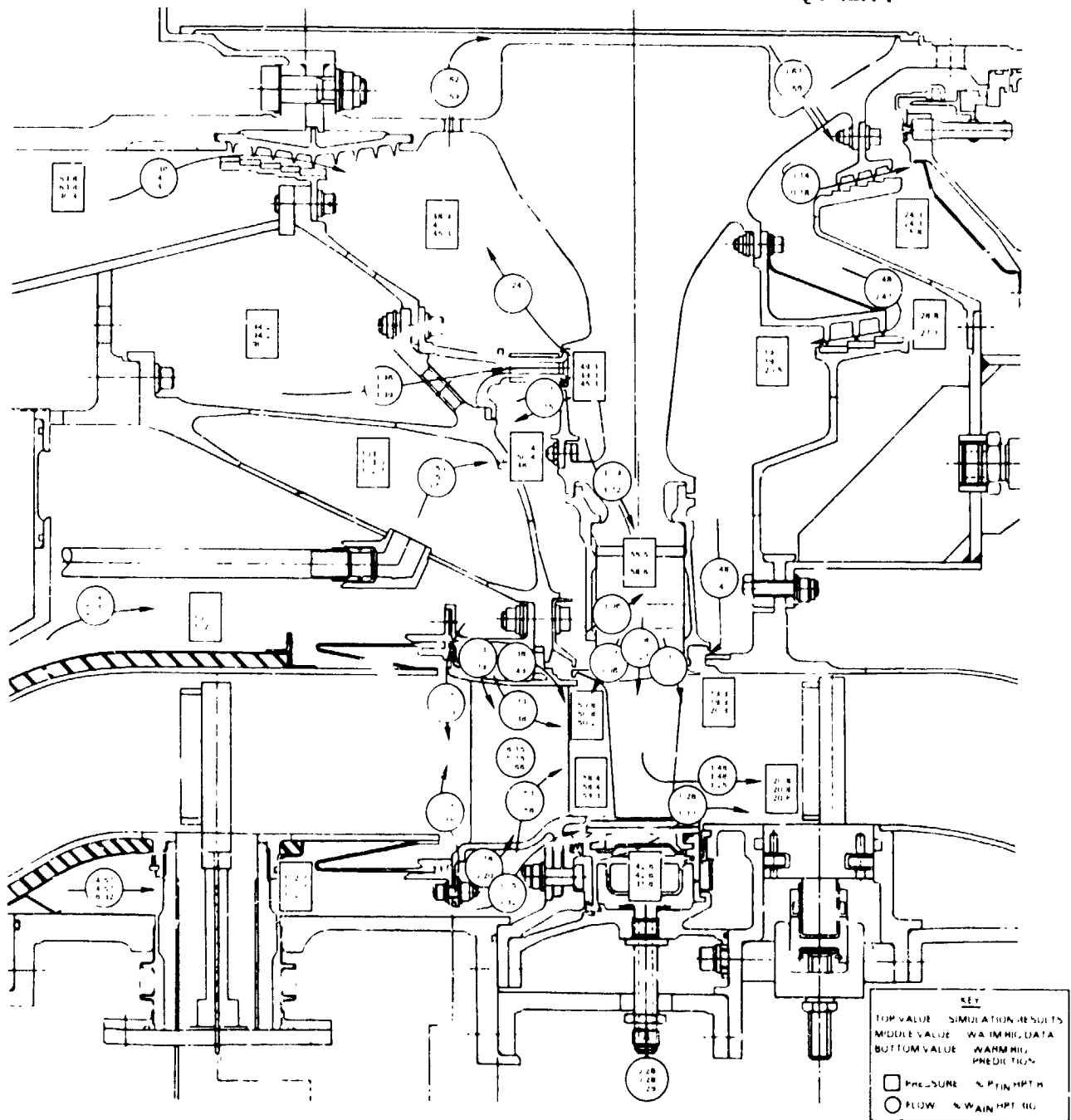


Figure 5.3.1-4 Turbine Secondary Flow System Map Showing Predicted and Measured Flow Rates and Pressures

TABLE 5.3.1-V

FULL STAGE TURBINE WARM RIG SECONDARY SYSTEM
COOLANT FLOW TEST RESULTS

PHASE I - Turbine Design and Off-Design Performance Assessment

Test Point	Main TOBI		w(%)		PR	Mini TOBI		w(%)		PR	Bore Cooling		Vane ID		Vane OD & BOAS	
	PR	TR	PR	TR		PR	TR	PR	TR		PR	TR	PR	TR	PR	TR
1	0.942	0.525	3.75	0.57	1.030	0.515	0.700	0.554	0.41	1.026	0.517	4.97	1.027	0.526	4.54	
2	0.946	0.493	3.98	0.60	1.033	0.478	0.747	0.510	0.48	1.030	0.485	4.43	1.032	0.484	5.95	
3	0.949	0.490	4.02	0.59	1.027	0.477	0.680	0.508	0.41	1.027	0.485	4.57	1.028	0.486	5.42	
4	0.966	0.534	3.89	0.56	1.020	0.523	0.683	0.560	0.39	1.023	0.528	4.22	1.024	0.529	5.11	
5	0.947	0.525	3.76	0.57	1.026	0.515	0.715	0.552	0.43	1.026	0.518	4.55	1.027	0.525	5.07	
6	0.945	0.530	3.75	0.56	1.022	0.518	0.729	0.554	0.45	1.022	0.522	4.37	1.023	0.528	4.76	
7	0.943	0.527	3.75	0.57	1.030	0.518	0.721	0.550	0.45	1.029	0.519	4.71	1.030	0.526	5.06	
9	0.943	0.530	3.72	0.56	1.014	0.518	0.693	0.554	0.41	1.028	0.522	4.51	1.029	0.522	5.28	

PHASE II - Turbine Tip Clearance/Active Clearance Control Study

11	0.939	0.716	3.03	0.48	1.027	0.702	0.709	0.740	0.39	1.024	0.695	3.93	1.025	0.701	4.51
14	0.940	0.717	3.04	0.48	1.027	0.703	0.716	0.743	0.39	1.027	0.696	3.94	1.025	0.709	4.51

PHASE III - Secondary Flow System Performance Characterization

15	0.806	0.530	2.99	0.56	1.020	0.521	0.695	0.558	0.41	1.021	0.521	4.96	1.023	0.530	4.52
18	1.059	0.525	4.60	0.56	1.021	0.516	0.700	0.551	0.41	1.029	0.515	4.96	1.030	0.525	4.52
19	0.952	0.523	3.81	0.00	0.495	0.521	0.709	0.551	0.42	1.024	0.514	5.07	1.026	0.524	4.53
20	0.952	0.522	3.82	0.38	0.761	0.519	0.703	0.551	0.41	1.022	0.514	4.98	1.024	0.524	4.53
21	0.949	0.521	3.81	0.68	1.194	0.512	0.694	0.551	0.40	1.024	0.515	4.93	1.026	0.525	4.52
28	0.932	0.529	3.69	0.56	1.028	0.519	0.701	0.555	0.41	1.015	0.525	3.99	1.016	0.529	4.65

PHASE IV - Additional Off-Design Performance Investigation

22	0.939	0.525	3.73	0.57	1.026	0.517	0.723	0.549	0.46	1.025	0.522	3.98	1.026	0.523	5.45
23	0.940	0.529	3.74	0.56	1.022	0.518	0.71	0.555	0.43	1.026	0.518	4.83	1.027	0.527	4.69
24	0.946	0.527	3.77	0.56	1.028	0.519	0.703	0.555	0.41	1.024	0.519	4.96	1.025	0.529	4.52
29	0.941	0.546	3.58	0.48	0.916	0.539	0.700	0.576	0.42	1.013	0.546	3.87	1.014	0.547	4.54

PHASE V - Compressor End Seal Study

25	0.949	0.524	3.80	0.56	1.022	0.515	0.652	0.553	0.33	1.024	0.518	4.96	1.025	0.527	4.51
26	0.953	0.523	3.82	0.56	1.020	0.51	0.790	0.549	0.51	1.026	0.517	4.95	1.027	0.525	4.52
27	0.946	0.523	3.79	0.56	1.019	0.514	0.884	0.547	0.62	1.023	0.518	4.91	1.025	0.526	4.51

5.3.1.2 Design Point Performance Characterization

The following sections present the turbine rig inlet pressure and temperature profiles; exit pressure, temperature, and air angle profiles; and calculated efficiency and Mach number profiles. Also, the rig exit Mach number and air angle profiles are compared to the design intent.

5.3.1.2.1 Inlet Profiles

The inlet total pressure and total temperature profiles are shown in Figures 5.3.1-5 and -6. Figure 5.3.1-5 presents the spanwise total pressure profile at four circumferential locations, and shows a spanwise variation of only 1.5 cm (0.6 in) of mercury and a circumferential variation of 0.2 cm (0.1 in) of mercury. The spanwise total temperature profile in Figure 5.3.1-6 shows the mid-span circumferential variation to be approximately 4°C (6°F). This figure also shows the lower temperature at the inner and outer walls resulting from heat transfer into the rig structure. These profiles show a consistent and well documented inlet for calculating turbine efficiency.

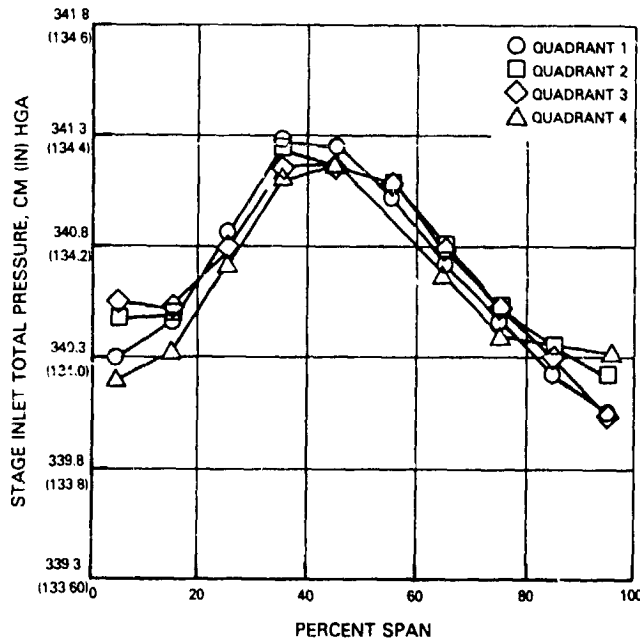


Figure 5.3.1-5 Turbine Inlet Spanwise Total Pressure

5.3.1.2.2 Turbine Efficiency

The design point turbine efficiency for the four quadrants defined in Figure 5.3.1-7 is presented in Table 5.3.1-VI and Figure 5.3.1-8 as a function of span. The efficiency level shown is based on the spanwise measured inlet and exit temperature and pressure measurements. The resulting profile was adjusted to reflect the bulk cooling air effects, i.e., the efficiency profile was lowered such that the integrated average agreed with the cooled efficiency definition. These profiles show the maximum efficiency to be consistently in the 30 to 50 percent span region.

ORIGINAL
OF PCD

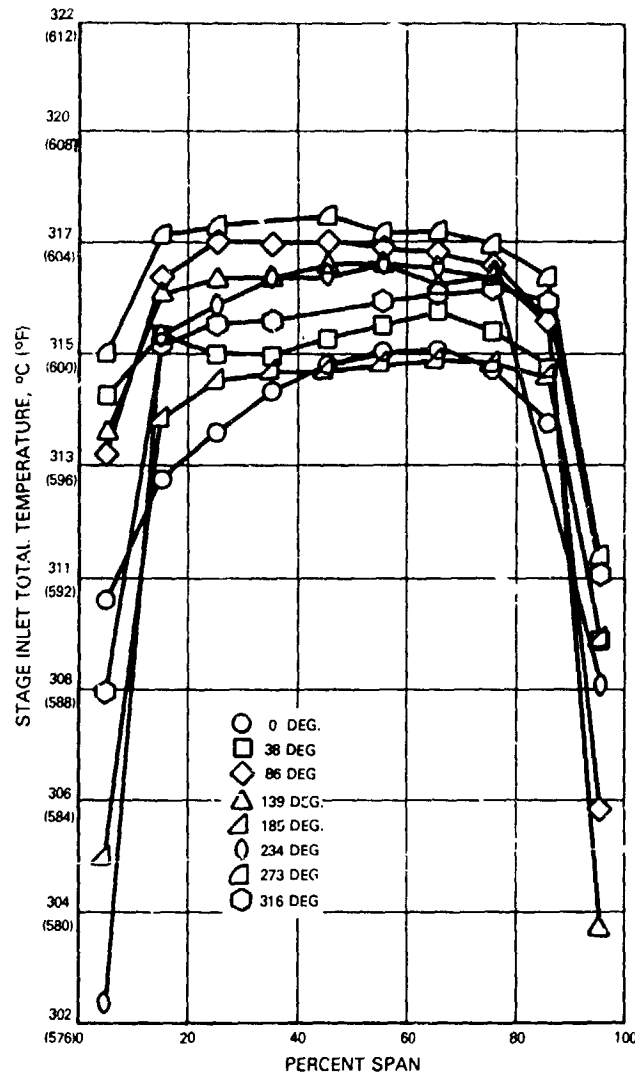


Figure 5.3.1-6 Turbine Inlet Spanwise Total Temperature

The profiles also show the efficiency change with circumference. The blade tip clearances in Table 5.2-I show that the first quadrant has the tightest clearance. This is reflected in Figure 5.3.1-8 by the highest level of efficiency in the tip region. Similarly, quadrant three, which has the most open clearance, has the lowest outer wall efficiency. This tip clearance effect appears to extend toward the inner wall to approximately 60 percent span where efficiency in all four quadrants is within 1 percent. The data from these four quadrants were averaged to produce the profile in Figure 5.3.1-9.

An efficiency contour of the first quadrant is shown in Figure 5.3.1-10. This contour, which shows one vane gap, indicates that the efficiency is relatively flat in the circumferential direction with the variation shown caused by the upstream vanes. Like the spanwise profile, the contour plot shows the maximum efficiency near midspan and lower efficiency at both the inner and outer walls.

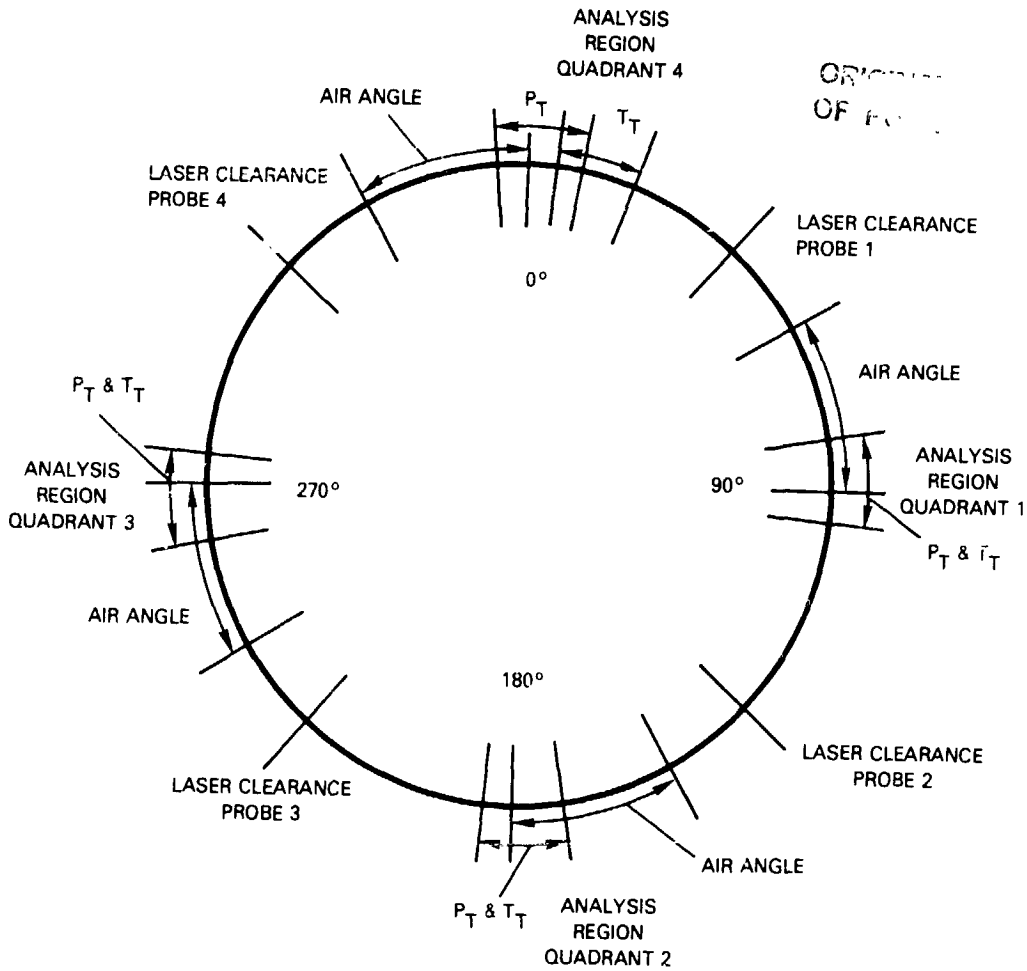


Figure 5.3.1-7 Instrumentation and Circumferential Measurement Locations (Looking forward at the rear of the rig)

TABLE 5.3.1-VI

DESIGN POINT EFFICIENCY

Quadrant	Circumferential Location, deg	Efficiency at Measurement Clearance, %	Measurement Clearance, cm (in)
1	42 80-95	89.13	0.020 (0.008)
2	132 170-185	89.17	0.033 (0.013)
3	222 260-275	87.04	0.081 (0.032)
4	312 355-20	88.12	0.078 (0.031)
	Average	88.37	0.053 (0.021)

ORIGINAL SOURCE OF POOR QUALITY

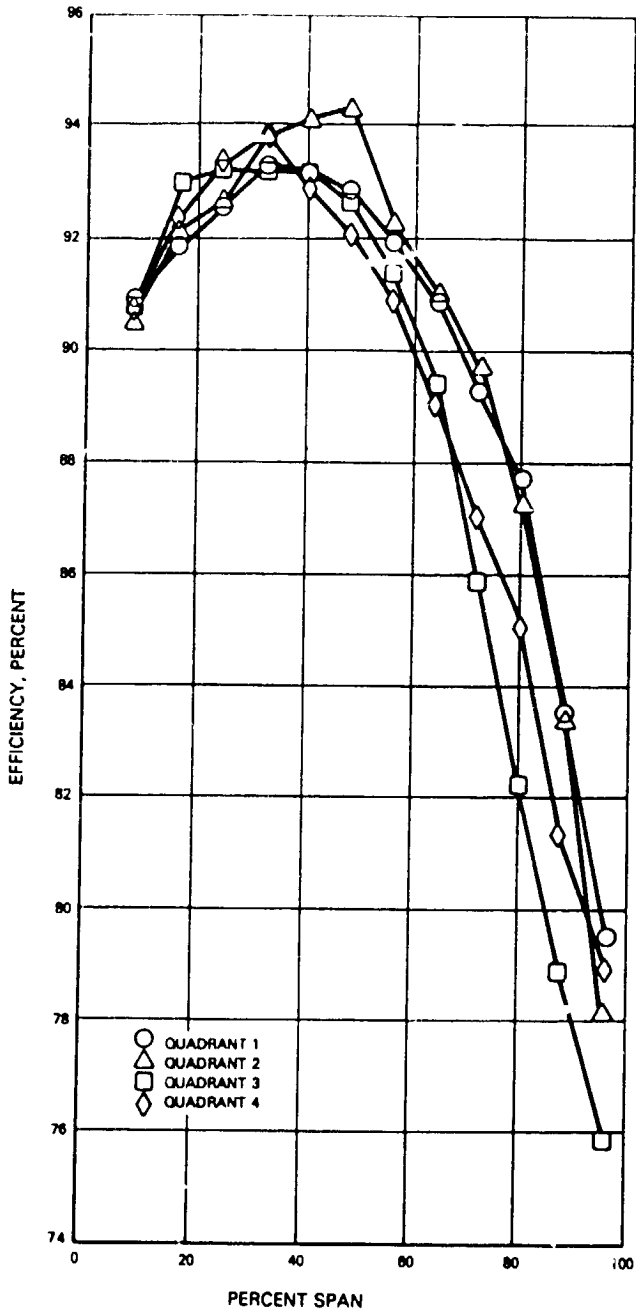


Figure 5.3.1-8 Exit Spanwise Efficiency by Quadrant

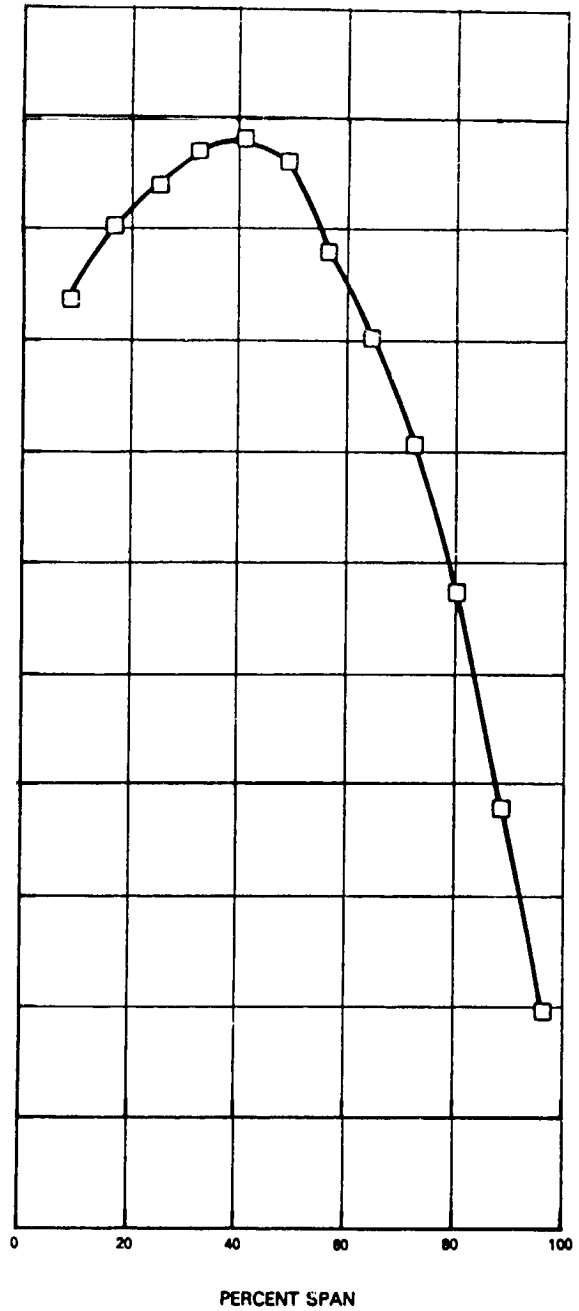


Figure 5.3.1-9 Average Spanwise Efficiency

ORIGINAL COPY
OF POOR QUALITY

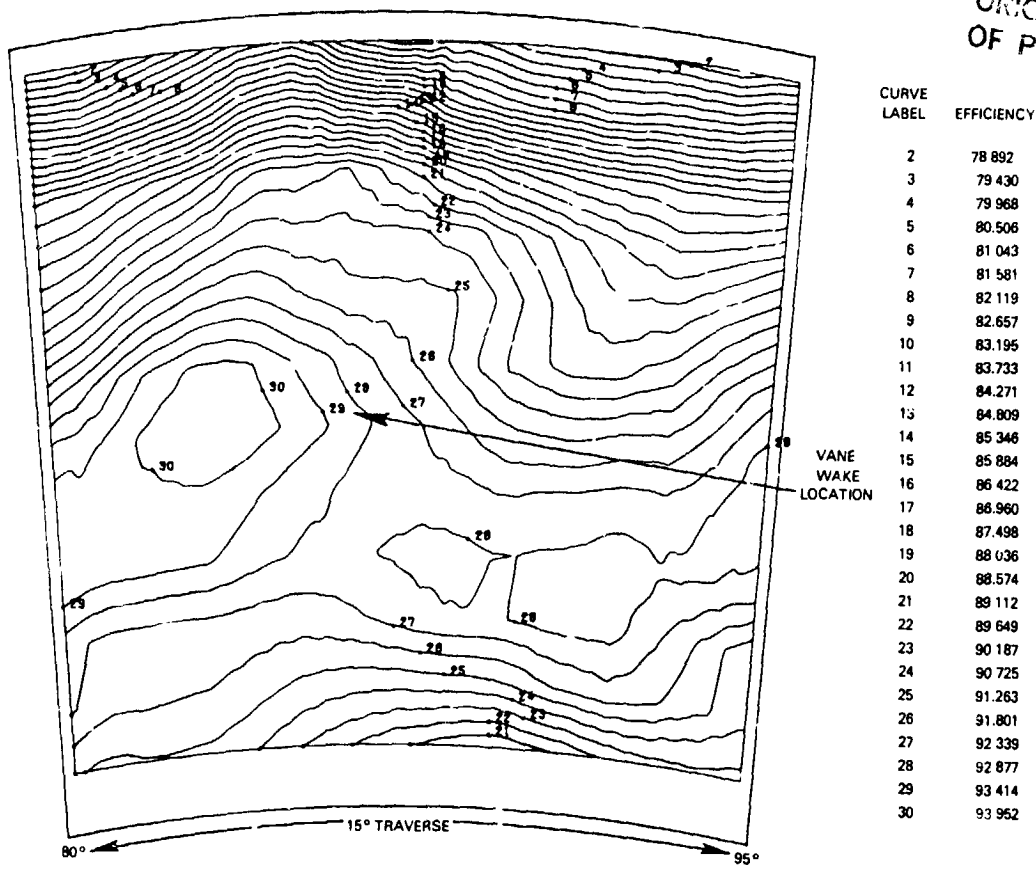


Figure 5.3.1-10 Efficiency Contour Plot of One Vane Gap in First Quadrant, Showing Maximum Efficiency Near the Midspan Region

5.3.1.2.3 Turbine Exit Aerodynamics

A spanwise profile of the turbine exit total pressure for all four quadrants is presented in Figure 5.3.1-11. All four quadrants have the same general shapes. The total pressure increases to approximately 70 percent span and then decreases to 90 percent span where the effect of tip clearance causes the total pressure to increase toward the tip. Figure 5.3.1-12 shows the total pressure contour over a 30-degree section of the circumference in the first quadrant. This figure exhibits the same spanwise profile seen in Figure 5.3.1-11 and also shows the effect of two upstream vane wakes which cause the circumferential pattern.

The turbine exit total temperature characteristics are presented as a spanwise profile of all four quadrants in Figure 5.3.1-13 and as a contour plot for quadrant one in Figure 5.3.1-14. As shown in Figure 5.3.1-13, all quadrants have consistent shapes with temperature increasing from the inner to the outer wall. As with the total pressure data, the temperature data show the effect of tip clearance. This is evident by the data from the third quadrant, where the largest clearance has allowed the most hot gas to bypass the rotor and produce the highest temperatures. The contour plot of these temperatures in Figure 5.3.1-14 shows the same increasing temperatures from the inner to the outer walls as the spanwise plots. The contour plot also shows the effect of the cooling air from the upstream vanes. This vane cooling air dilution causes the resulting circumferential pattern.

ORIGINAL
OF POOR

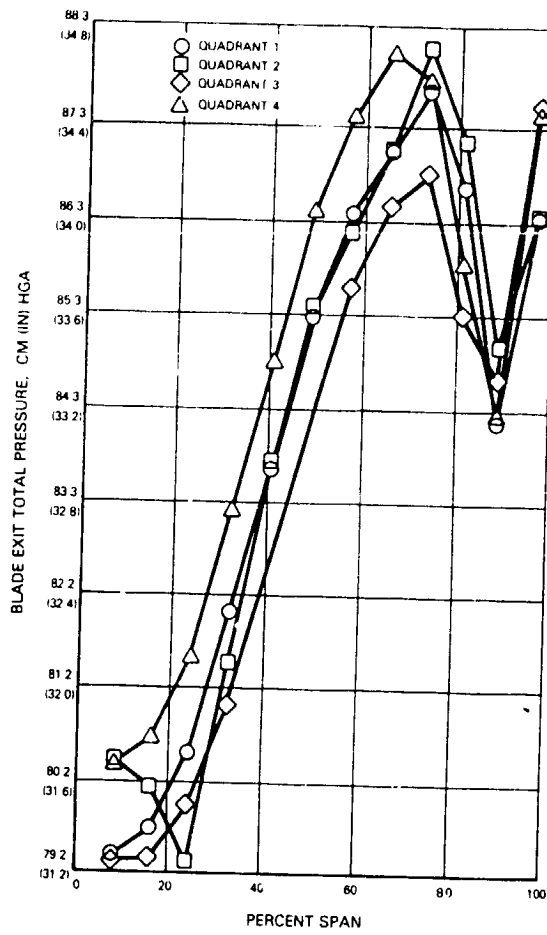


Figure 5.3.1-11 Spanwise Profile of Turbine Exit Total Pressure

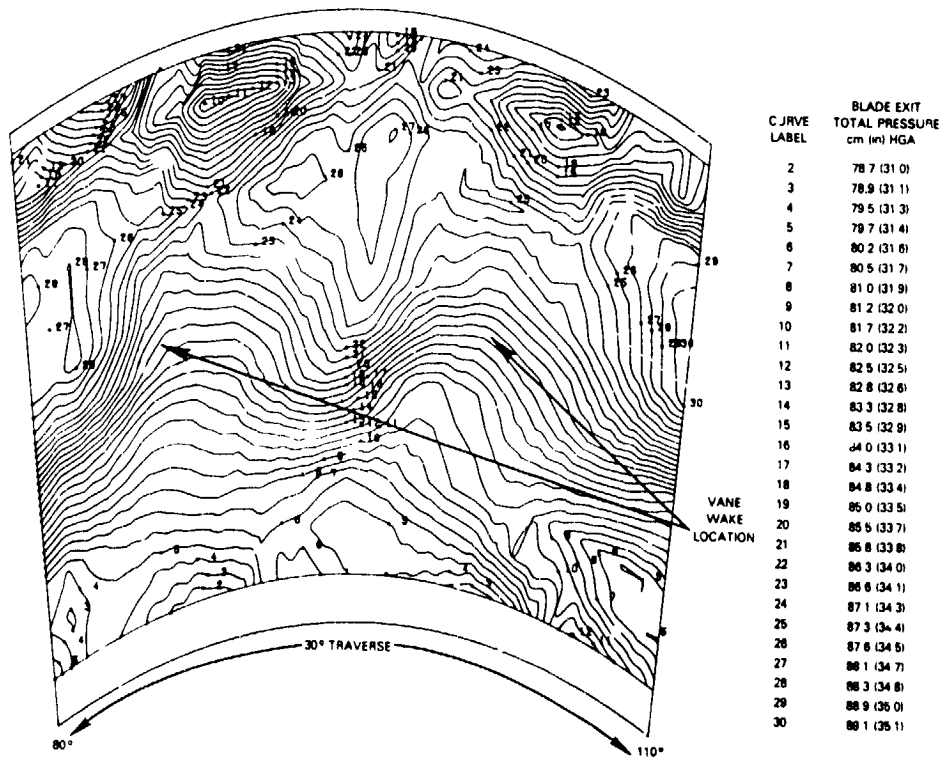
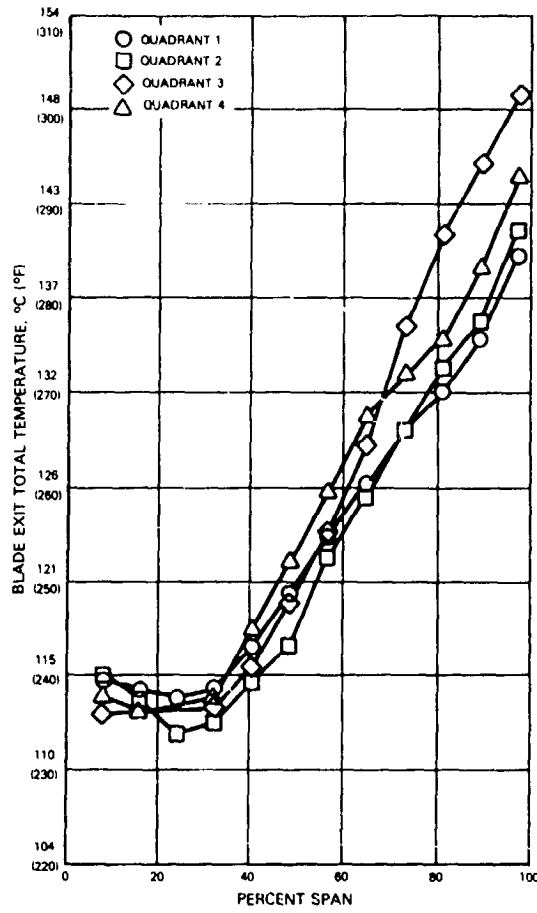


Figure 5.3.1-12 Turbine Exit Total Pressure Contour Plot



ORIGINAL SOURCE OF FLOW QUALITY

Figure 5.3.1-13 Spanwise Profile of Turbine Exit Total Temperature

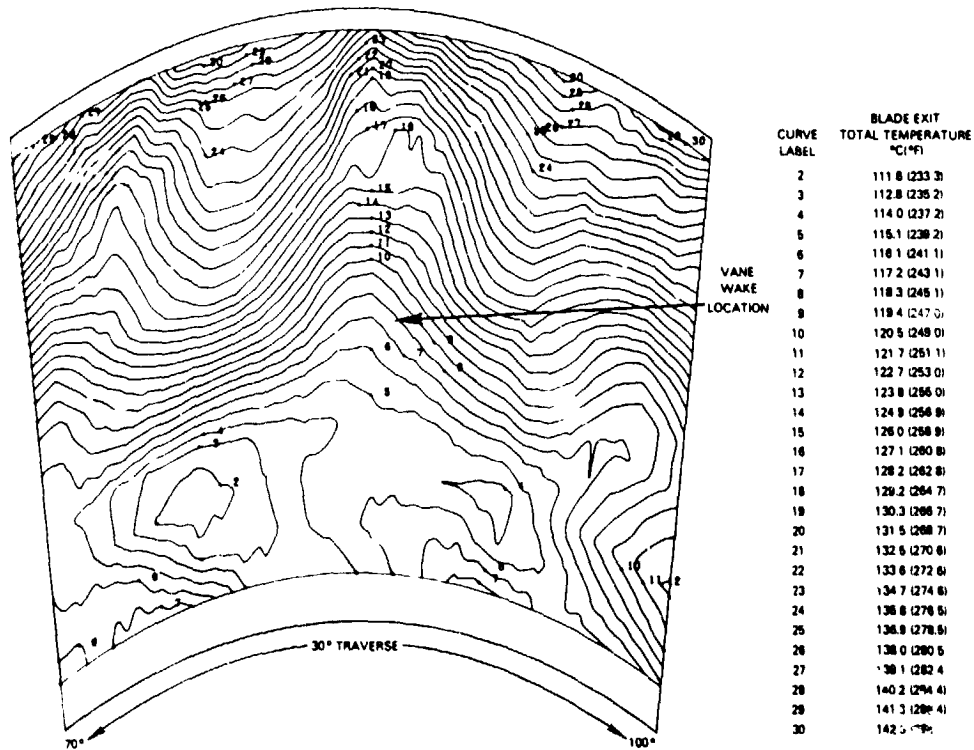


Figure 5.3.1-14 Turbine Exit Total Temperature Contour Plot

A summary of turbine exit air angle data is presented in Figures 5.3.1-15 through -17. Figure 5.3.1-15 shows a spanwise plot of the four quadrants. The data trends indicate that exit air angles in all quadrants are generally consistent, with the air angle becoming more axial toward the outer wall. As with the pressure and temperature data, the effect of tip clearance can be seen in the air angle data. The largest tip clearance would be expected to have the air angle closest to the vane exit conditions. This is shown by the data, since quadrant three has the most axial flow of the four quadrants and the largest tip clearance. The effect of tip clearance again can be seen to persist toward the inner wall to approximately 60 percent span as the air angle plots for the four quadrants agree within 4 degrees at this location.

The air angle contour plot in Figure 5.3.1-16, shows a 15-degree sector of air angle data from a circumferential traverse. It shows the same spanwise trend as in the preceding figure and a relatively flat contour in the circumferential direction.

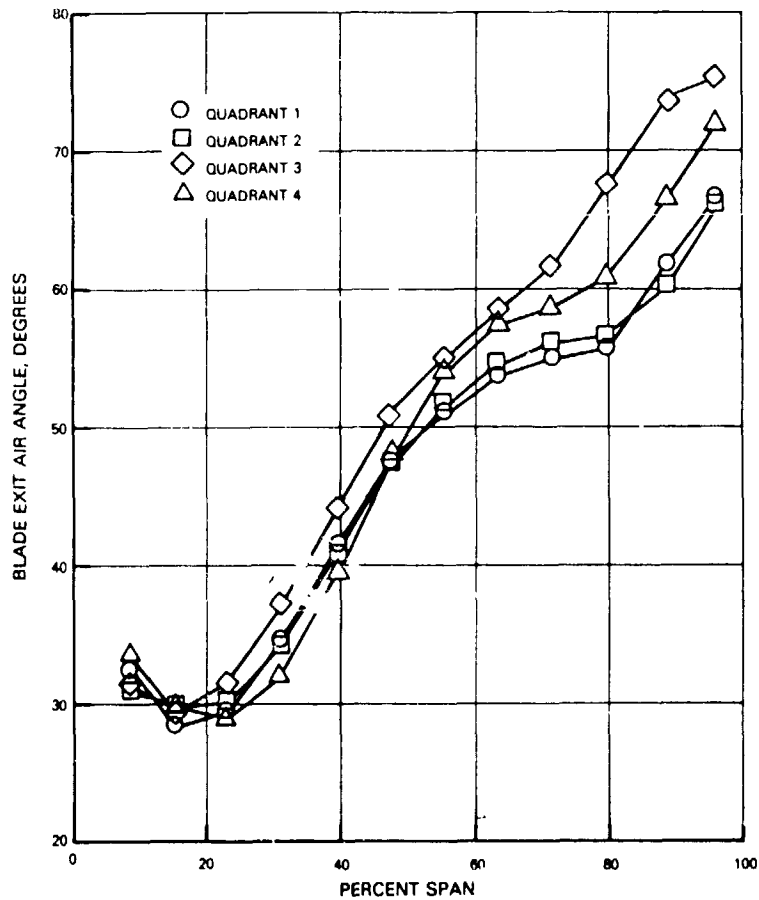


Figure 5.3.1-15 Blade Air Exit Angle Characteristics

ORIGINAL COPY
OF POOR QUALITY



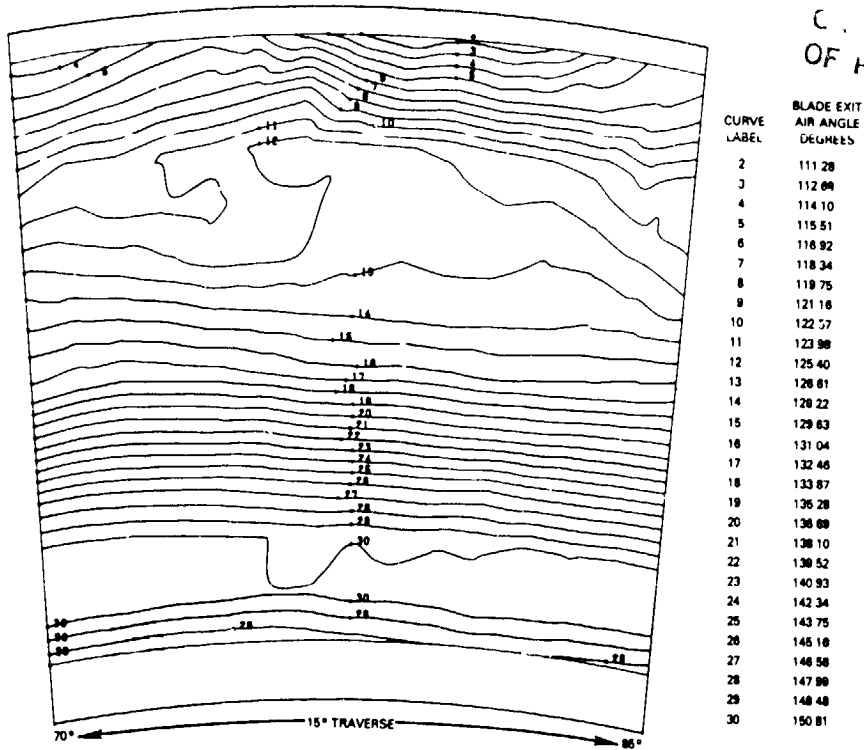


Figure 5.3.1-16 Air Angle Contour Plot

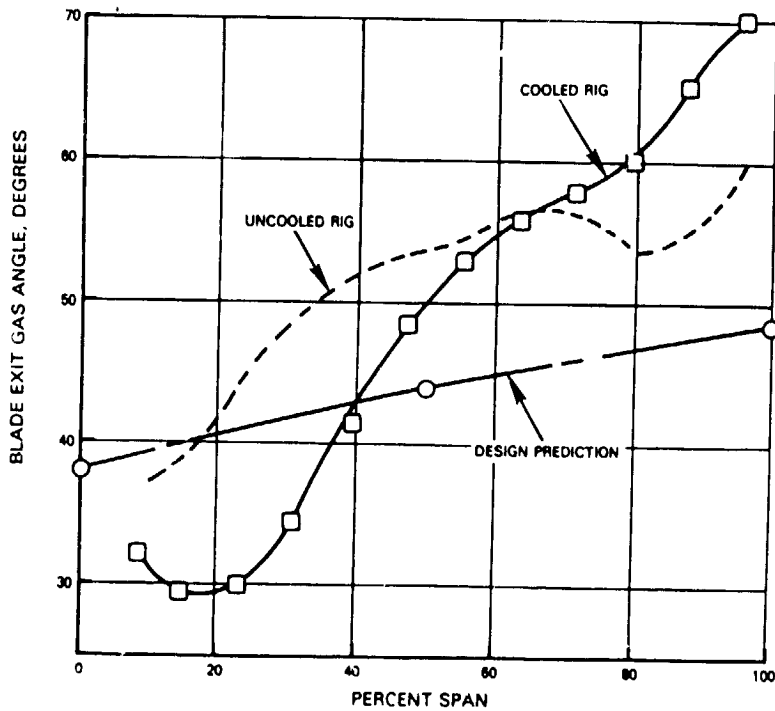


Figure 5.3.1-17 Average Spanwise Air Angle Trends Compared to the Design Prediction and Preceding Uncooled Rig Test Results

In Figure 5.3.1-17, the average spanwise air angle data are compared to the design prediction. As shown, the results differ considerably in slope from the prediction. In terms of the aerodynamic impact on the strut fairing in the transition duct, this type of flowfield would cause a more negative incidence from the root to approximately 40 percent span and a more positive incidence over the rest of the span. When comparing the design prediction to the results acquired from this test as well as the previous uncooled rig test (build 2), the slopes at the midspan region are similar. However, the root and tip regions show different slopes than the prediction. At the root, the uncooled rig results show a steeper slope resulting from viscous three-dimensional effects. The cooled rig results have a still steeper slope. This is attributed to the addition of cooling air, since the aerodynamics of the two rigs are similar. In the tip region, the uncooled rig air angle starts to show a fall off similar to the root region and then turns more axial because of the affect of the tip clearance. This trend is not duplicated by the results from the cooled rig test. The addition of cooling air and the tip clearance combine to cause the air to become progressively more axial from the midspan to the tip.

Figure 5.3.1-18 shows the turbine exit Mach number compared to the design prediction. Exit Mach number was calculated using the exit total pressure data and assuming a linear static pressure distribution between the inner and outer wall pressure taps at the instrumentation plane. The results, therefore, follow the exit total pressure distribution. The prediction has a considerably flatter profile, since it assumed a flat spanwise loss profile.

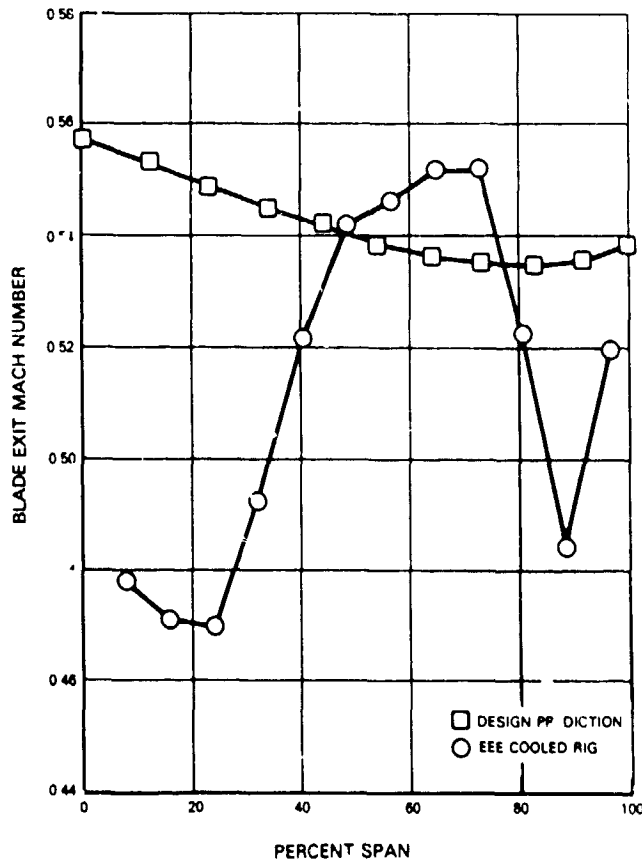


Figure 5.3.1-18 Blade Exit Mach Number Characteristics



5.3.2 Vane Cascade Performance Assessment

Vane cascade testing was conducted at a series of Mach numbers that bracketed the vane exit Mach number in the full stage test. In addition, the cascade design point was run at three Reynolds number levels, with the highest at the stage test level. The overall results from this testing showed that the vane loss was above the level for the uncooled vane cascade and at the pre-test predicted level.

5.3.2.1 Pressure Loss

Cascade data were acquired in two phases. The test conditions and results for both phases are presented in Table 5.3.2-I.

TABLE 5.3.2-I
HIGH-PRESSURE TURBINE ANNULAR CASCADE TEST CONDITIONS AND RESULTS

<u>PHASE I - Mach Number Effects</u>							
Test Point	Exit Mach Number	Corrected Flow	PTin MPa (psia)	TTin °C (°F)	Reynolds Number (10 ⁵)	Pressure Loss (%)	Mass Avg
1	0.70	15.58	0.146 (21.15)	316.0 (600.9)	1.97	3.06	
2	0.85	16.67	0.173 (25.15)	314.0 (597.3)	2.56	4.49	
3	0.91	16.94	0.187 (27.09)	314.6 (598.3)	2.82	5.16	
4	1.00	17.05	0.212 (30.74)	313.5 (596.3)	3.24	6.54	
5	1.08	17.22	0.237 (34.36)	314.5 (598.1)	3.62	7.80	
6	1.16	17.22	0.257 (37.25)	314.0 (597.2)	3.92	9.03	
7	0.56	13.78	0.129 (18.65)	316.1 (601.1)	1.52	2.06	
<u>PHASE II - Reynolds Number Effects</u>							
8	0.92	17.06	0.310 (44.90)	315.9 (600.7)	4.66	5.49	
9	0.92	16.94	0.427 (61.99)	316.2 (601.3)	6.44	5.40	

In the first phase, the cascade was tested at a series of vane exit Mach numbers that bracketed the full stage test. These tests were performed with an ambient discharge and, therefore, varying Reynolds numbers. Test data were processed to determine the mass averaged total pressure loss. The results presented in Figure 5.3.2-1 indicate the typical vane pressure loss increase with Mach number.

In the second phase of testing, the design point Reynolds number was elevated in two steps by backpressuring the test rig so a match could be made with the stage test Reynolds number. Results showed no effect on the loss level within the accuracy of the pressure measurements. Figure 5.3.2-1 also shows results from the uncooled cascade test (build 1). As expected, the uncooled vane loss is lower. However, adding the predicted cooling penalty to the uncooled cascade pressure loss results produced a pre-test level that is in a good agreement with the cooled rig results.

ORIGINAL
OF POOR QUALITY

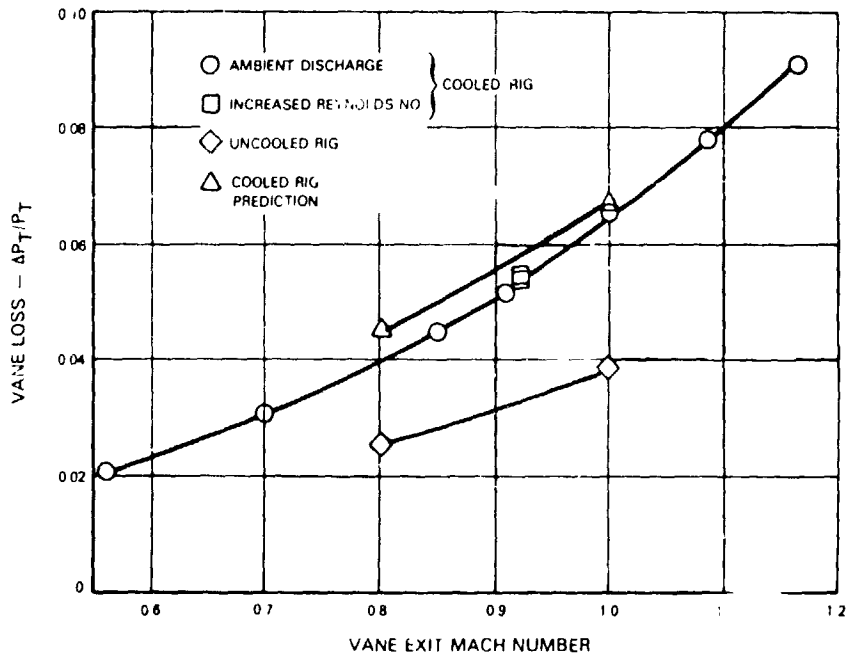


Figure 5.3.2-1 Vane Loss Trends

5.3.2.2 Flow Capacity and Vane Deviation

Vane cascade inlet flow parameter data are presented in Figure 5.3.2-2. Results show flow capacity increasing as a function of Mach number until the cascade becomes choked. The data also show an excellent agreement with the design predicted flow capacity.

Vane air angle deviation is presented in Figure 5.3.2-3 as a function of vane exit Mach number. For this presentation, deviation is defined as the exit air angle minus the gage angle, where air angle is measured from tangential. The exit air angle for this analysis was calculated from continuity. The results in Figure 5.3.2-3 show both the total deviation, which includes the affect of cooling air injection and aerodynamic deviation.

5.3.2.3 Design Point Performance Characterization

The following sections present the measured vane cascade rig inlet pressure and temperature profiles; the exit pressure, temperature, and air angle profiles; and the calculated total pressure loss and Mach number profiles. In addition, the total pressure loss profile is compared to the uncooled annular cascade results, and the exit air angle and Mach number profiles are compared to the design prediction.

5.3.2.3.1 Inlet Profiles

The cascade inlet total pressure and total temperature profiles are shown in Figures 5.3.2-4 and 5.3.2-5, respectively. Figure 5.3.2-4 presents the spanwise total pressure at three circumferential locations. These profiles show a spanwise variation of 0.7 cm (0.3 in) of mercury and a circumferential variation of 0.2 cm (0.1 in) of mercury.



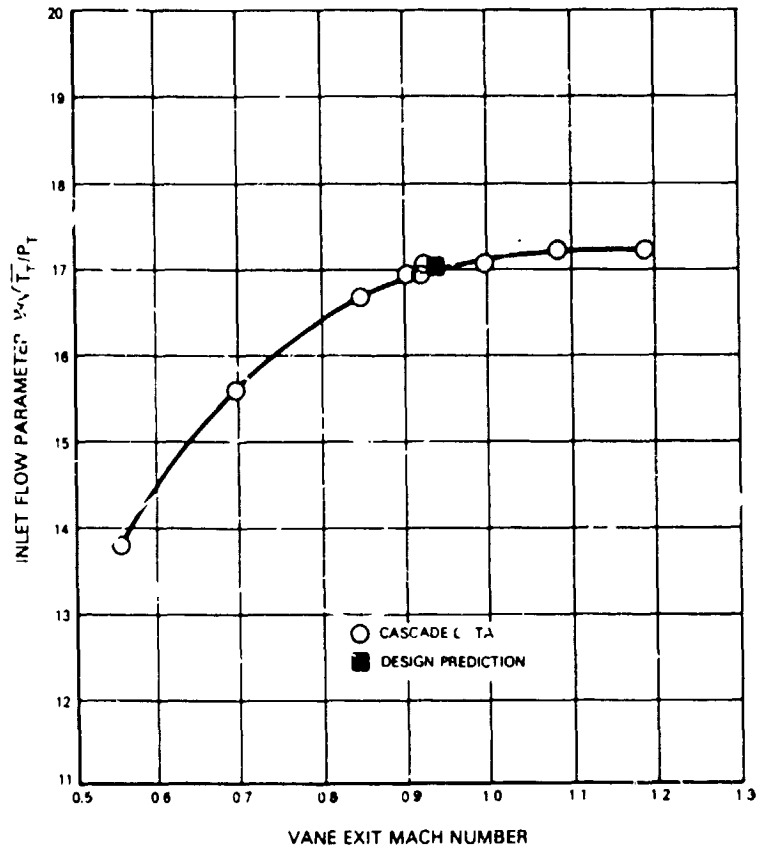


Figure 5.3.2-2 Flow Capacity Characteristics

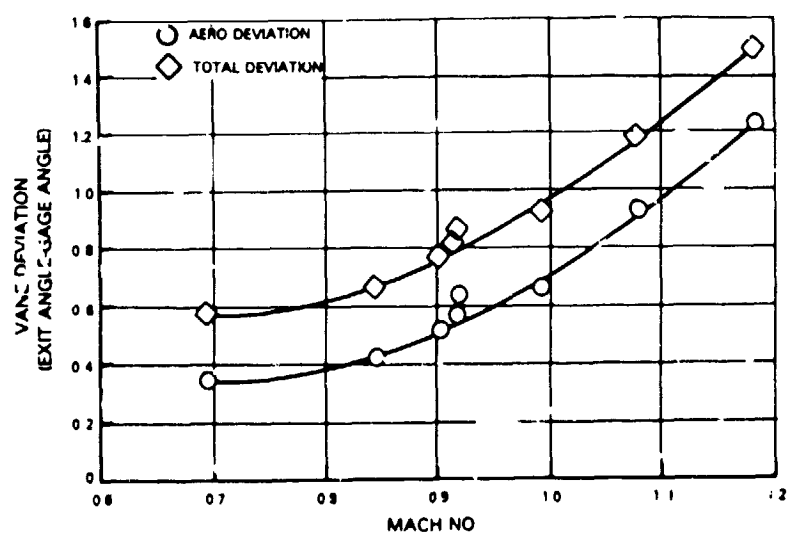


Figure 5.3.2-3 Vane Deviation Versus Mach Number



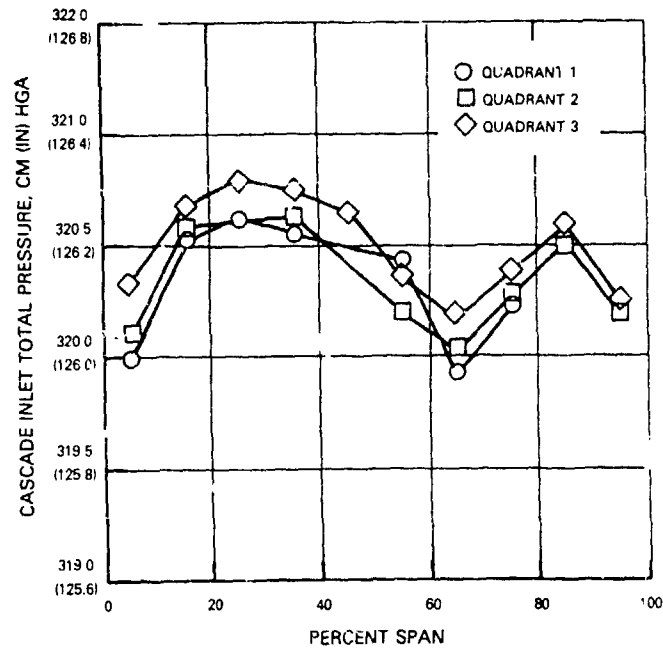


Figure 5.3.2-4 Vane Cascade Inlet Total Pressure

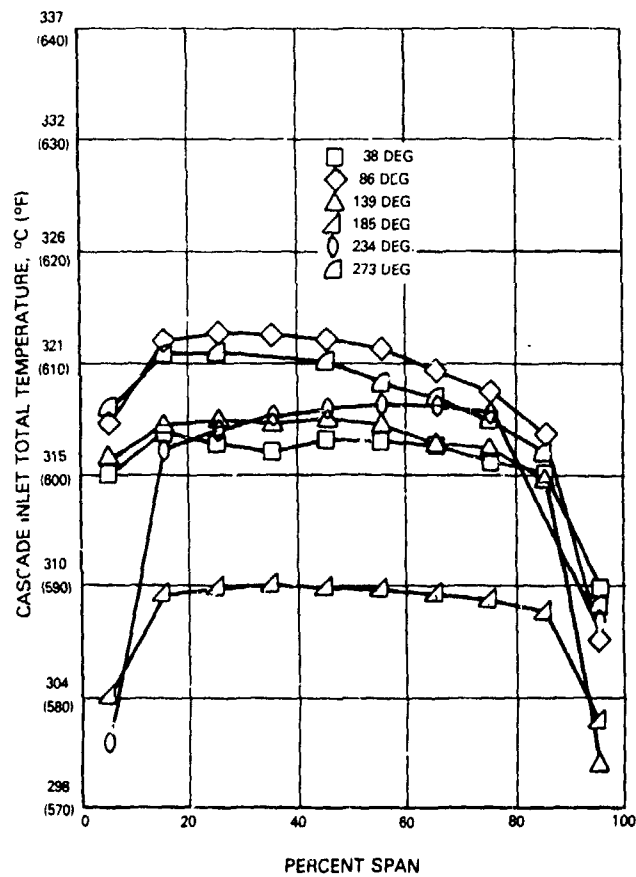


Figure 5.3.2-5 Vane Cascade Inlet Total Temperature

Figure 5.3.2-5 presents the spanwise total temperature profile at six circumferential locations. These results show a midspan circumferential variation at five locations to be within 10 degrees, with one location showing an additional 10 degrees of variation. The profiles also show the characteristic lower temperature at the inner and outer walls because of the heat transfer into the rig structure. Overall, these profiles show a well documented inlet with consistent pressure profiles for use in calculating the cascade total pressure loss.

5.3.2.3.2 Vane Exit Aerodynamics

Pressure Loss

Cascade exit total pressure characteristics are shown in Figures 5.3.2-6 and -7. Figure 5.3.2-6 shows the circumferential pressure variation as measured at twelve radial locations in the first quadrant. The profile shows two vane wakes with the lowest exit pressure, highest loss, at the inner and outer walls. A spanwise profile of the vane exit total pressure in quadrants one, two and three is presented in Figure 5.3.2-7. The profiles shown are a result of area averaging the circumferential data for each quadrant over one vane pitch, 15 degrees. Along with the inlet pressure profiles, these spanwise profiles were used to determine the spanwise vane loss characteristics shown in Figure 5.3.2-8.

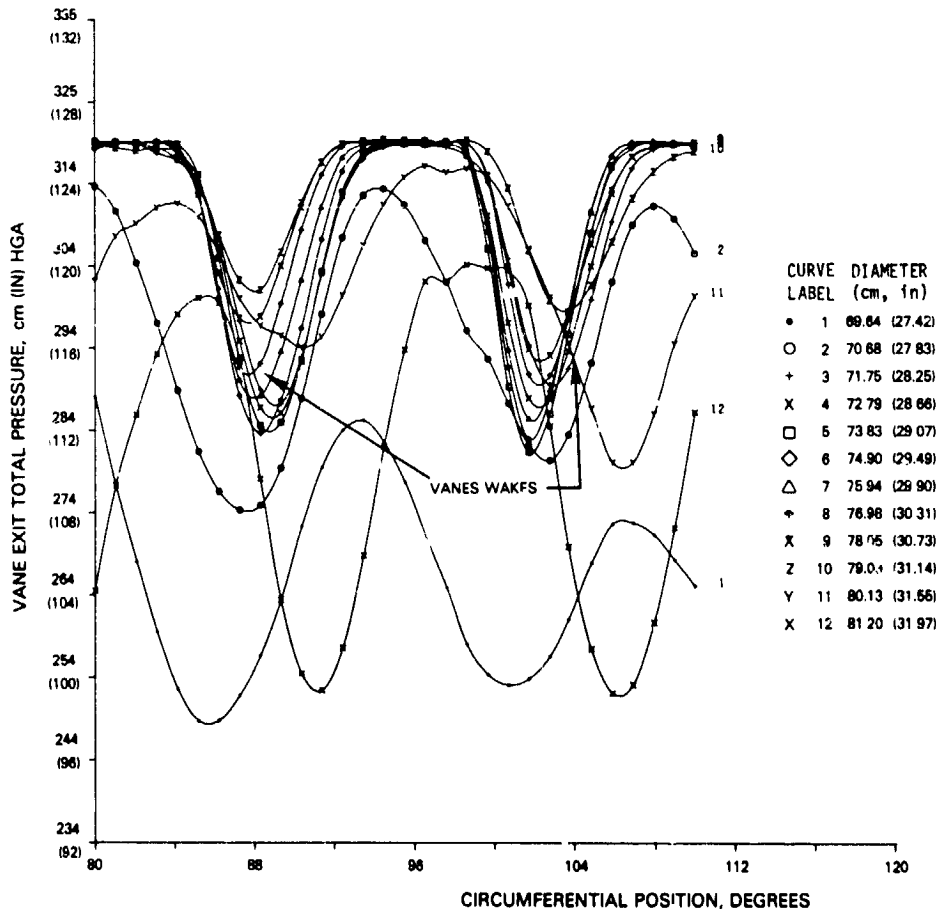


Figure 5.3.2-6 Circumferential Vane Exit Pressure Characteristics

ORIGINALLY
OF POOR QUALITY

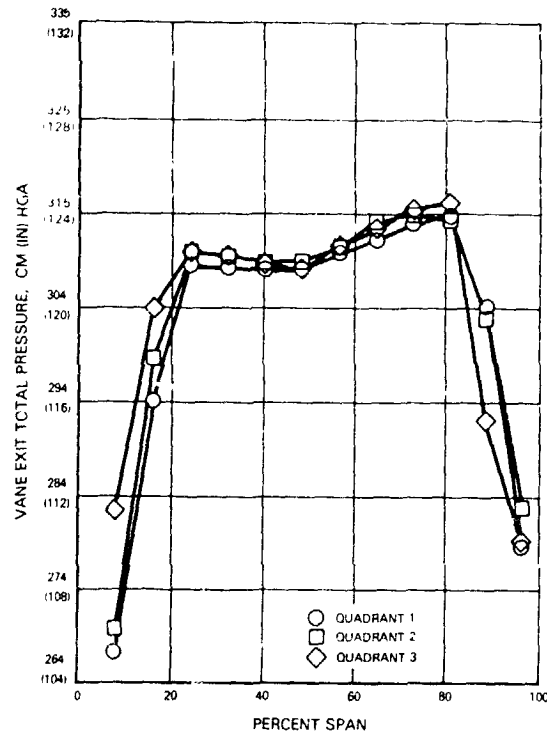


Figure 5.3.2-7 Spanwise Vane Exit Pressure Profile

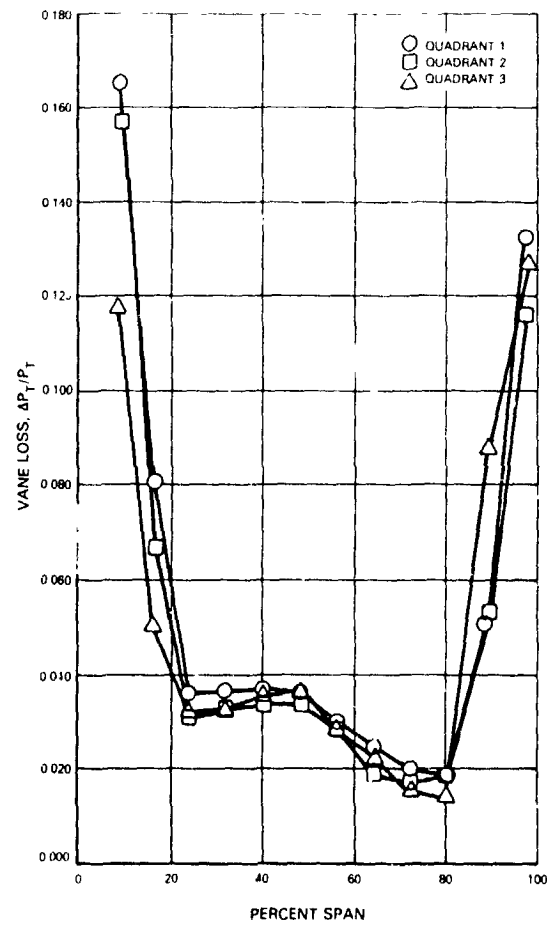
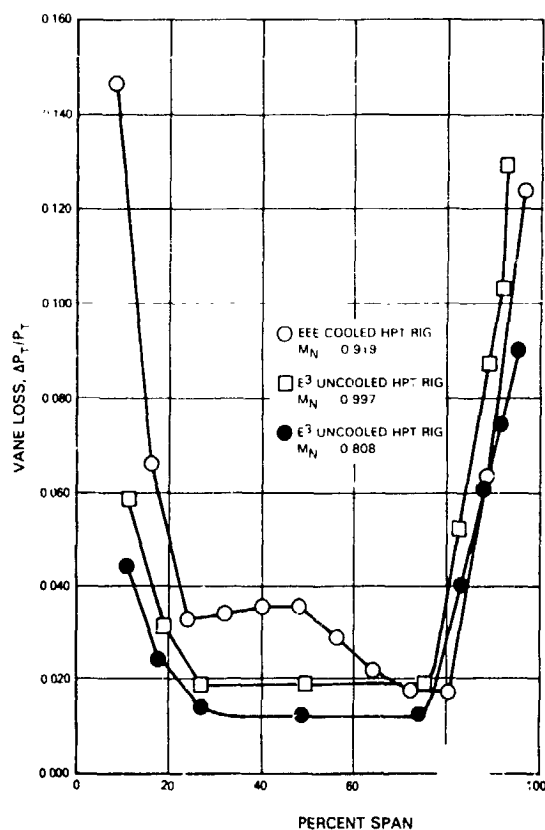


Figure 5.3.2-8 Spanwise Vane Loss Characteristics

The results in this figure show high endwall loss in the inner and outer 20 percent span regions and lower midspan loss from 20 to 80 percent span. These trends show good agreement for the three quadrants measured.

Figure 5.3.2-9 presents a comparison of average spanwise pressure loss for similar conditions tested in both the cooled and previous uncooled rig tests. The two test points shown for the uncooled rig bracket the cooled cascade test exit Mach number. Overall, the data trends are very similar. The three sets of data show the highest loss in the endwalls with comparatively lower losses in the midspan region. As expected, data from the Cooled Rig Test Program exhibit higher losses. Endwall losses are more pronounced because of platform cooling and leakage effects and midspan loss levels are increased over uncooled rig test data because of the losses encountered with the addition of cooling flow.



ORIGINATED BY
OF FOREIGN QUALITY

Figure 5.3.2-9 Vane Loss Profile Showing the Influence of Cooling on Performance

The contour plot in Figure 5.3.2-10 shows vane pressure loss measured in one quadrant. Typically, the areas of high loss are the endwalls and the vane wake, with the highest loss occurring at the endwalls. This profile also shows a nonsymmetrical pressure gradient emanating from the suction and pressure surfaces. This nonsymmetry is primarily a function of the measurement technique as opposed to airfoil aerodynamics. In addition, Figure 5.3.2-10 shows the zero loss core region occurring between the vanes. This flow region accounts for approximately 50 percent of the pitch and 60 percent of the span. Since the core region is expected to be loss free, this confirms the validity of the test measurements.

ORIGINAL OF POOR QUALITY

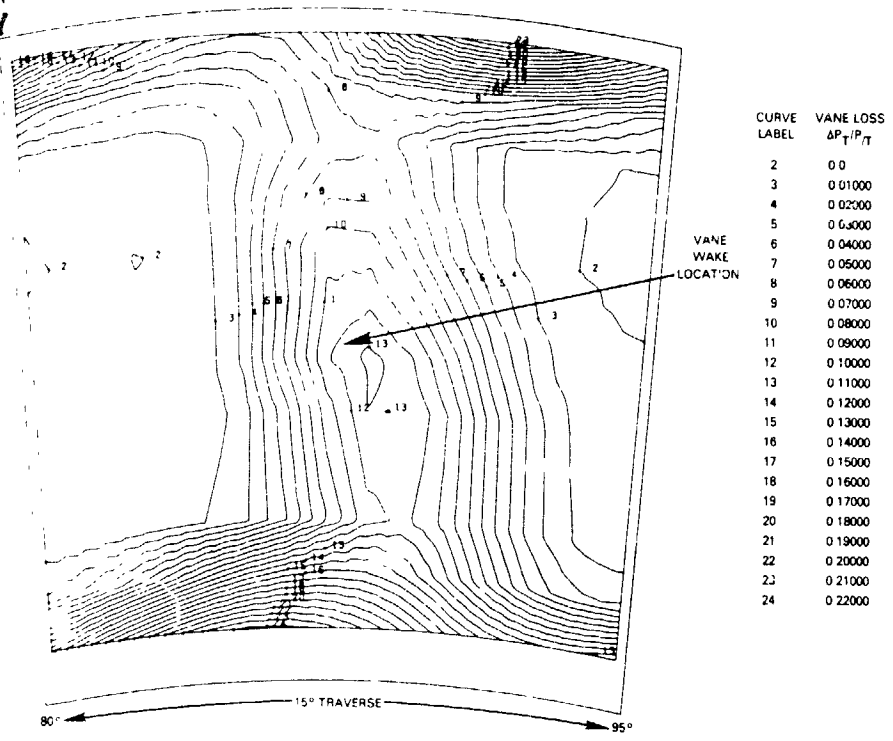


Figure 5.3.2-10 Contour Plot of Vane Loss Characteristics

A summary of vane cascade loss characteristics for each exit Mach number tested is presented in Table 5.3.2-II on a quadrant by quadrant basis. The results indicate a consistent difference in measured pressure levels in each quadrant, with the first quadrant having a higher level of loss. These differences are mostly attributed to circumferential tolerance variations in the experimental engine hardware and not measurement error.

TABLE 5.3.2-II
CASCADE LOSS BY QUADRANT

Test Point No.	Average Mach No.	Quadrant 1	Quadrant 2	Quadrant 3	Average $\Delta P_t/P_t$
1	0.70	3.41	2.97	2.81	3.06
2	0.85	4.97	4.40	4.08	4.49
3	0.91	5.76	4.95	4.75	5.16
4	1.00	7.06	6.33	6.21	6.53
5	1.08	8.27	7.59	7.52	7.80
6	1.16	9.50	8.91	8.64	9.03
7	0.56	2.23	1.99	1.94	2.06
8	0.92	5.92	5.40	5.11	5.49
9	0.92	5.83	5.36	4.99	5.40

Temperature Profiles

Vane cascade exit temperatures, as measured in the fourth quadrant of the rig, are presented in Figures 5.3.2-11 through -13. Figure 5.3.2-11 shows the circumferential temperature distribution and the influence of cooling flow across the vane gap. Results indicate that the coolant has mixed effectively with the main stream, spreading out to approximately 50 percent of the gap. Temperatures at the endwalls are consistently lower because of the influence of gas path leakage as well as platform cooling.

The integration of circumferential data into a spanwise profile of vane exit total temperature is presented in Figure 5.3.2-12. The effect of leakage and platform cooling on endwall temperature levels is prominent. Temperatures in these regions are approximately 28°C (50°F) lower in comparison to the average midspan temperature.

The contour profile in Figure 5.3.2-13 shows the circumferential temperature gradients as measured at the vane exit plane. The wake region, as expected, has the lowest temperature level, followed by the endwalls. The nonsymmetry of the gradients on the pressure and suction surfaces is primarily a result of the measurement technique.

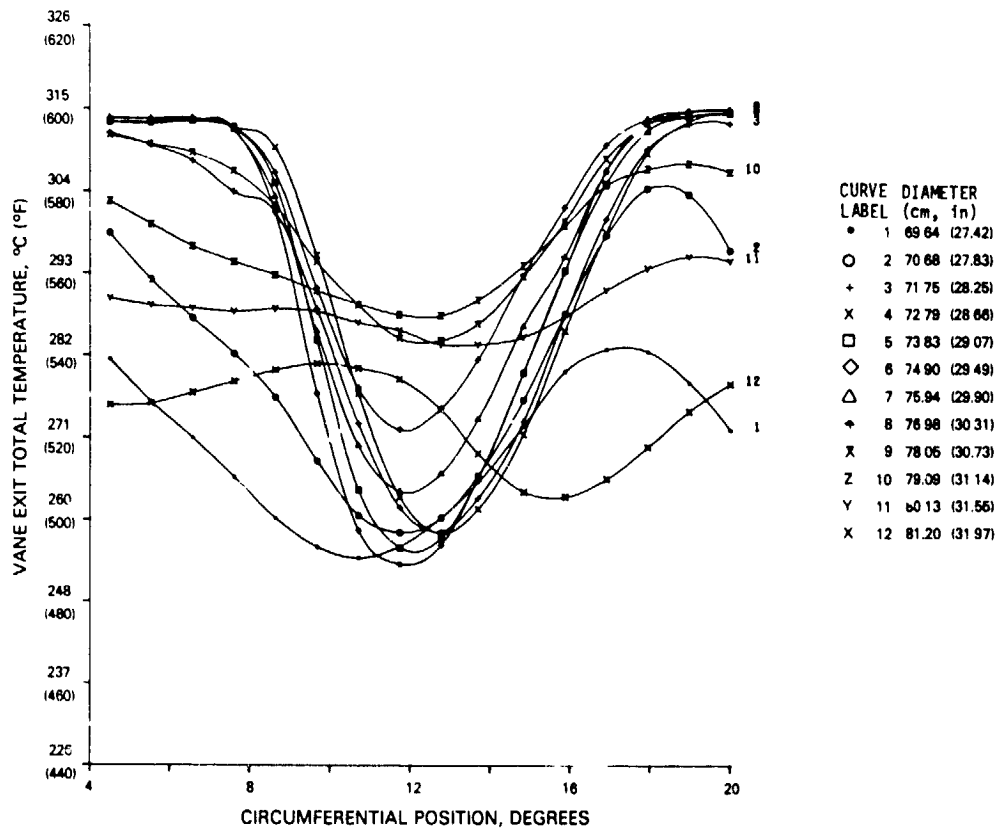


Figure 5.3.2-11 Circumferential Trends of Vane Exit Temperature

ORIGINAL COPY
 OF POOR QUALITY

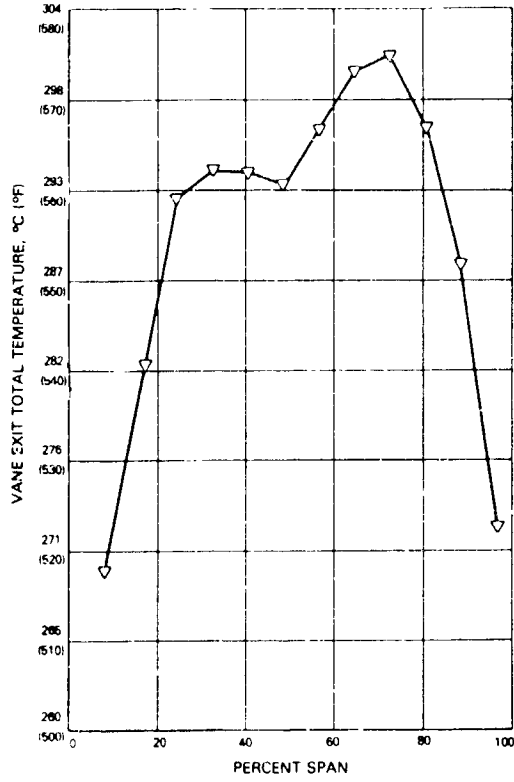


Figure 5.3.2-12 Spanwise Profile of Vane Exit Temperature

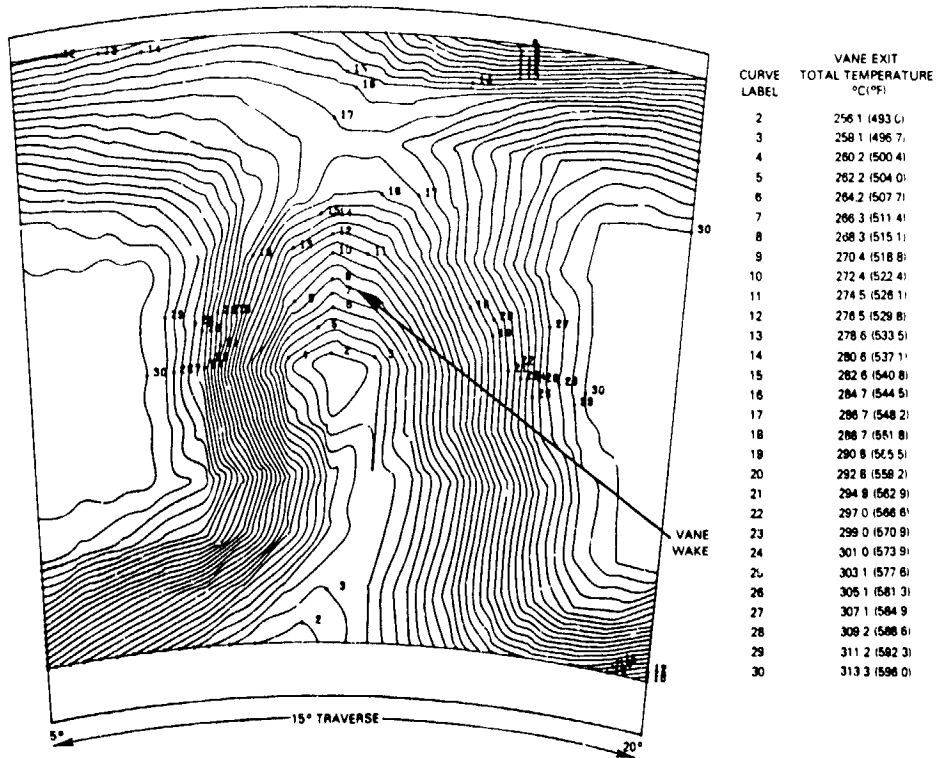


Figure 5.3.2-13 Contour Plot of Vane Exit Temperature

Exit Air Angle

A summary of vane exit air angle characteristics is presented in Figures 5.3.2-14 through -15. The data in Figure 5.3.2-14 show spanwise air angle trends, as integrated from a circumferential traverse of quadrants 1, 3 and 4. The general slopes of the curves are uniform, showing a high exit angle at the root and a low angle at the tip. The steep gradient in air angle is further indicated by the contour plot in Figure 5.3.2-15. This figure shows the circumferential angle variation over the vane gap with the discontinuity across the vane trailing edge.

A comparison of these results to data acquired during the preceding Uncooled Rig Program is presented in Figure 5.3.2-16. Overall, the data are in close agreement. When compared to the design prediction, however, there is considerable deviation, particularly at the root and tip locations. This is a result of the streamline analysis used in the prediction.

Exit Mach Number

A spanwise profile of vane exit Mach number, as calculated from the measured exit total pressure profile and a linear distribution of static pressure from the inner and outer wall pressure taps, is shown in Figure 5.3.2-17. The results essentially duplicate the vane exit spanwise pressure distribution shown previously in Figure 5.3.2-7.

Figure 5.3.2-17 also compares the measured data to the design prediction. In general, the prediction is in good agreement with test data throughout the 25 to 75 percent span region. Since the prediction does not account for viscous effects, Mach numbers in the endwall regions show an expected dissimilarity.

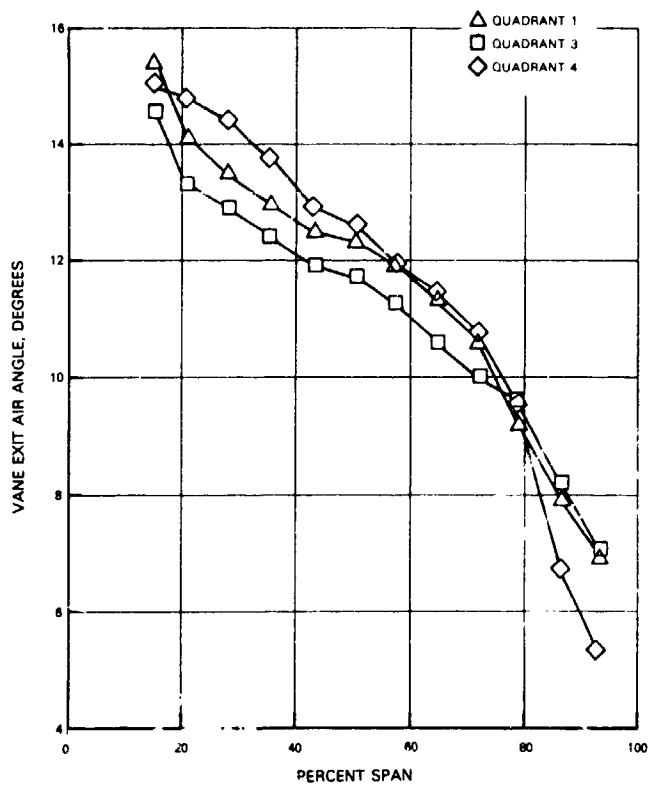
Vane Pressure Distributions

Vane pressure distributions were obtained by normalizing the airfoil static pressure, acquired from surface pressure taps, to the inlet total pressure at the respective radial locations. A comparison of test data to the design intent for the vane root, mean and tip sections is presented in Figures 5.3.2-18, -19 and -20, respectively. In the evaluation of these distributions, it is noteworthy to point out that the measured span location at the root is 11 percent as opposed to 0 percent for the prediction. Similarly, the measured tip location is 89 percent span as opposed to 100 percent for the prediction. Furthermore, the prediction is based on an inviscid flow analysis.

In taking these factors into consideration, there is good agreement between test data and the prediction for the root and tip sections (Figures 5.3.2-18 and -20). Data in the midspan region more closely match the prediction, as shown in Figure 5.3.2-19. This reflects the capability of the analysis to more accurately simulate the aerodynamic behavior in the 20 to 80 percent span region.

Vane Film Effectiveness

The entire suction surface of the vane is film cooled only by the air discharged through holes near the leading edge. This design assumes that the cooling film does not deteriorate over the long chord of the vane and maintains acceptable metal surface temperatures.



ORIGINAL OF FIGURE 5.3.2-14

Figure 5.3.2-14 Spanwise Vane Exit Air Angle Trends

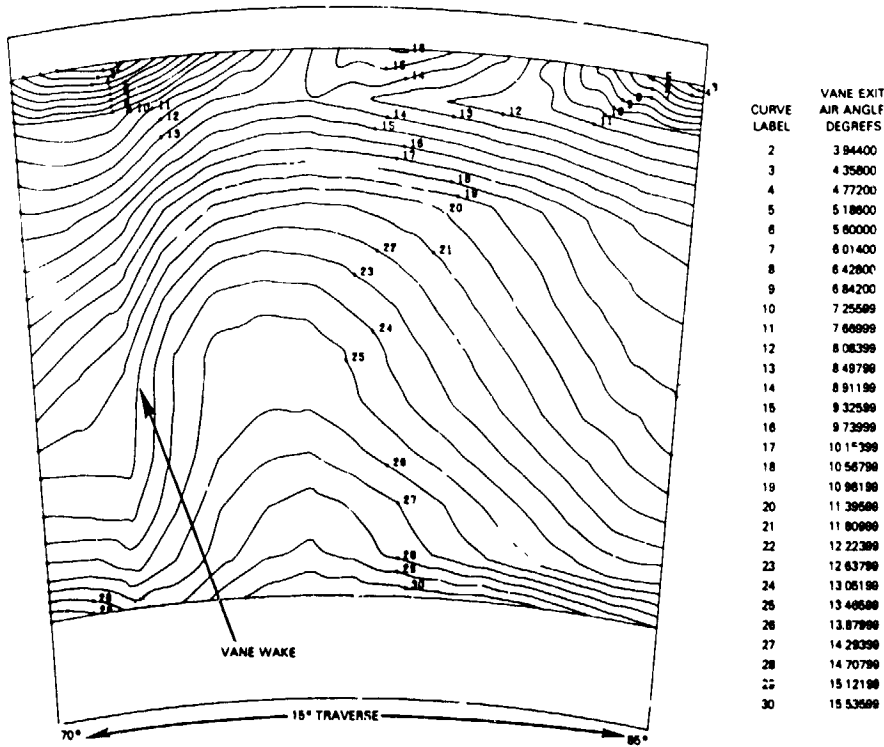


Figure 5.3.2-15 Contour Plot of Vane Exit Air Angle

ORIGIN OF PAGES

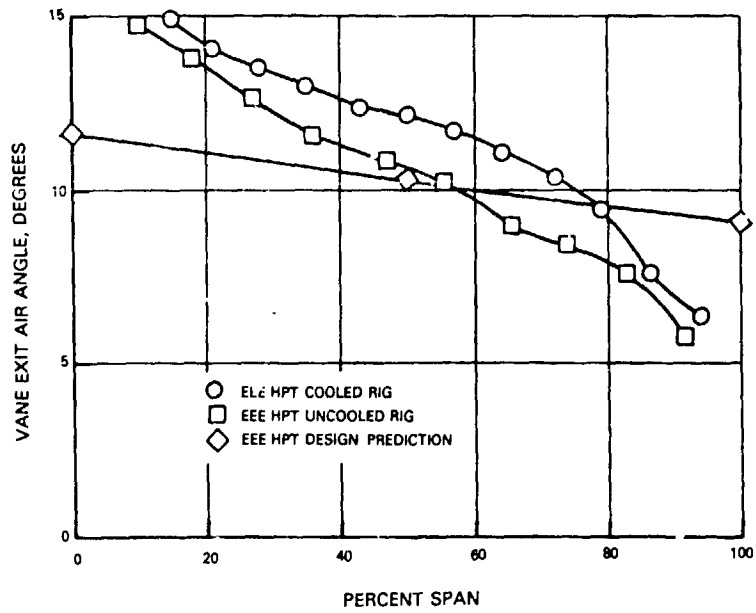


Figure 5.3.2-16 Comparison of Air Angle Trends

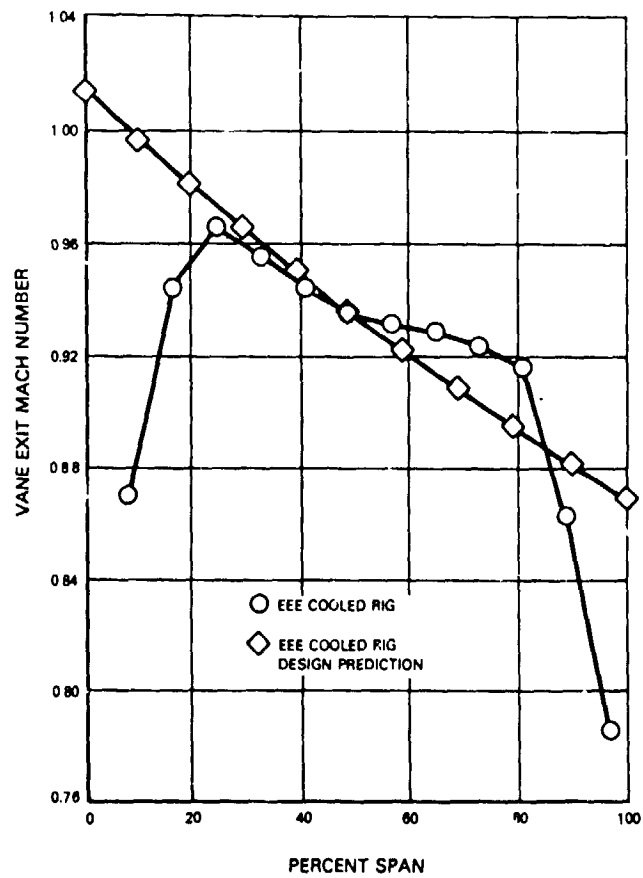


Figure 5.3.2-17 Spanwise Profile of Vane Exit Mach Number

ORIGINAL DRAWING
OF POOR QUALITY

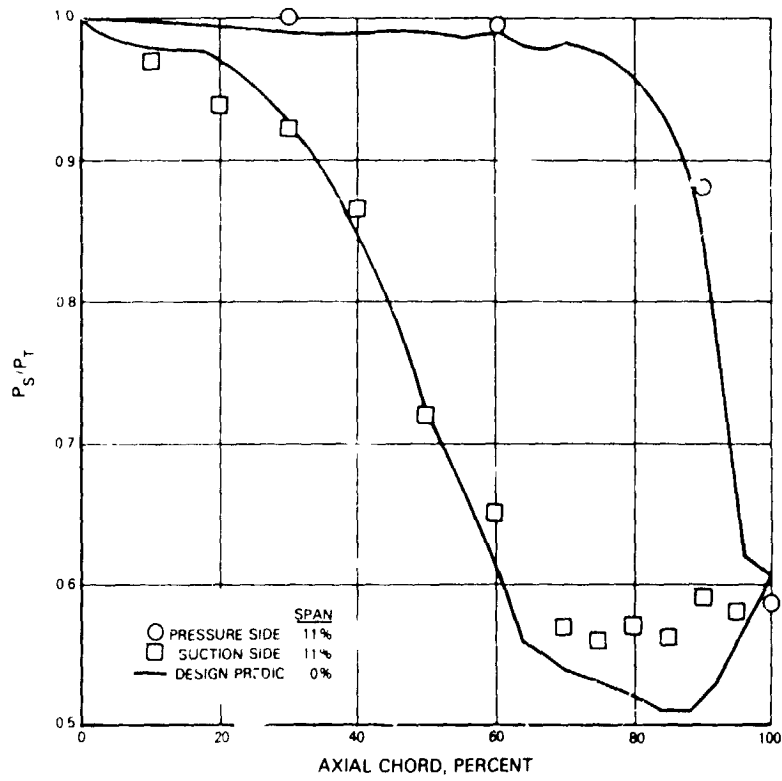


Figure 5.3.2-18 Vane Root Section (11 Percent Span) Pressure Distribution

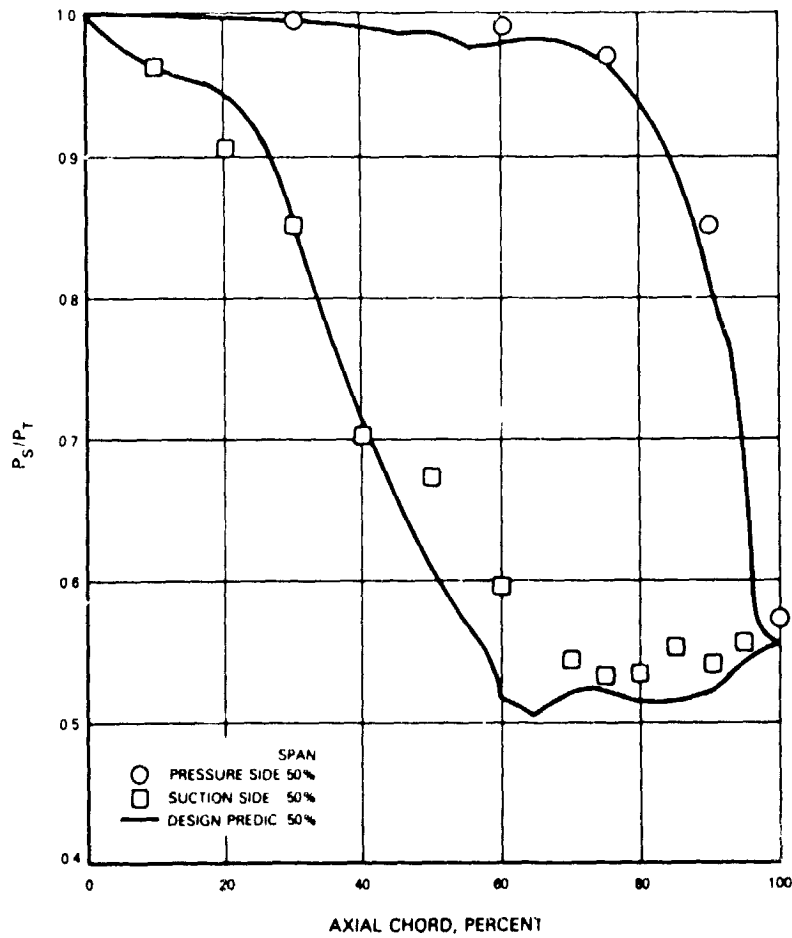
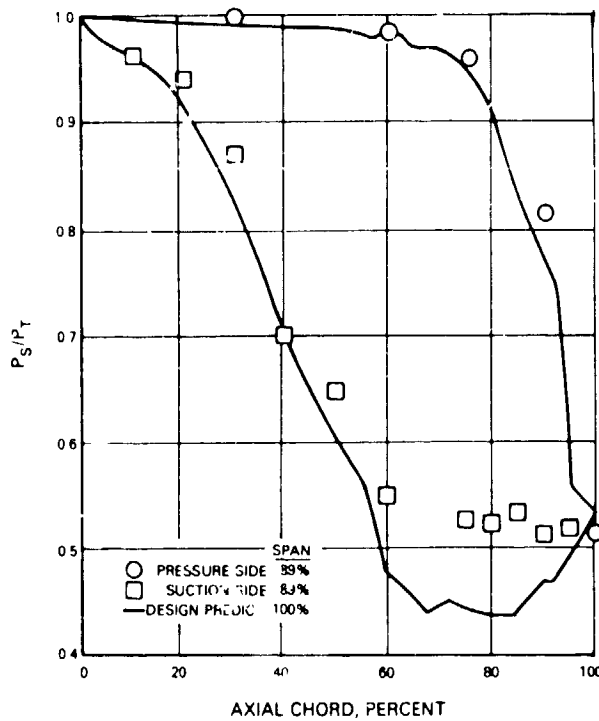


Figure 5.3.2-19 Vane Midspan (50 Percent Span) Pressure Distribution





ORIGIN
OF P...

Figure 5.3.2-20 Vane Tip Section (89 Percent Span) Pressure Distribution

To verify the effectiveness of the suction surface cooling, one vane was modified by plugging the last two cooling supply cavities, thereby allowing air to enter only the front cavity. (As shown in Figure 3.2.3-4, this cavity supplies cooling to the first three rows of spanwise injection holes near the leading edge and the second three rows of spanwise injection holes near the suction surface.) Temperatures were measured by thermocouples positioned at four axial locations and two radial locations on the suction side.

Results of the evaluation are presented in Figure 5.3.2-21. The measurements show that the film cooling effectiveness is far more superior than initially predicted during the vane design and in good agreement with a refinement of this prediction. Test results suggest that, because of the location of the stagnation point and the pressure distribution around the leading edge of the airfoil, the first three rows of cooling enhance the suction surface effectiveness. This suggests that it may be possible to design a second-generation vane for the same application with a smaller percentage of leading edge coolant flow.

5.3.3 Turbine Blade Performance Analysis

Data acquired from both the full stage and vane cascade tests were used in the analysis of blade performance. As part of the analysis, a streamline model was generated to evaluate blade incidence effects and turning. The following sections present a discussion of pressure loss, deviation and internal aerodynamics.

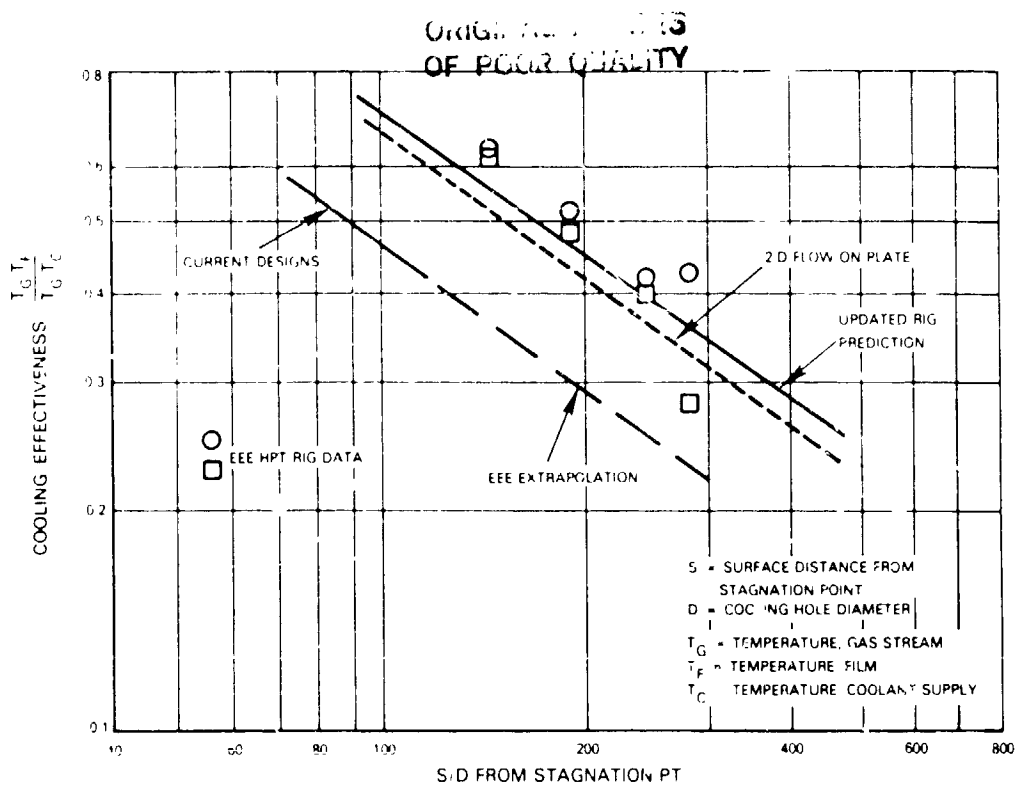


Figure 5.3.2-21 Vane Suction Surface Film Cooling Effectiveness

5.3.3.1 Blade Pressure Loss

Pressure loss is calculated from the measured stage efficiency and vane cascade pressure loss levels at Mach numbers evaluated during the stage test. A summary of blade performance trends is presented in Figure 5.3.3-1, showing the relative pressure loss as a function of exit Mach number.

The trends, which include tip clearance losses, show the expected relationship of increasing pressure loss as a function of Mach number. In addition, losses increase with positive incidence and decrease with negative incidence relative to the design incidence angle.

Of particular significance are the results at transonic Mach numbers. This blade was designed to minimize loss in the transonic region by the use of a refined curvature distribution on the suction side downstream of the throat, plus trailing edge coolant ejection to control the shock structure. These concepts, which were demonstrated in the High-Pressure Turbine Supersonic Cascade Supporting Technology program (Ref. 3), are shown to be effective in providing a more linear as opposed to a highly skewed loss trend in the transonic region.

5.3.3.2 Deviation

Blade deviation, as calculated from the air angle at the exit plane minus the throat plane air angle, is shown in Figure 5.3.3-2. The results in this figure show both the total deviation, which includes the affect of cooling air injection, and aerodynamic deviation. As expected, deviation increases with Mach number and the addition of cooling air.

QUALITY IS OF HIGH QUALITY

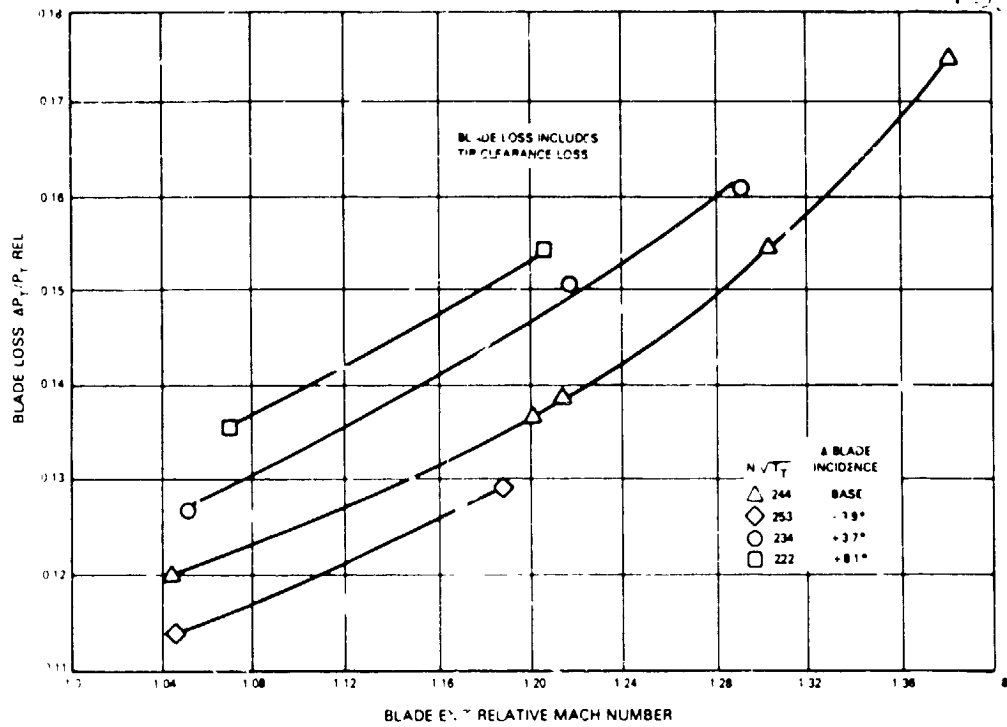


Figure 5.3.3-1 Calculated Blade Pressure Loss as a Function of Exit Mach Number

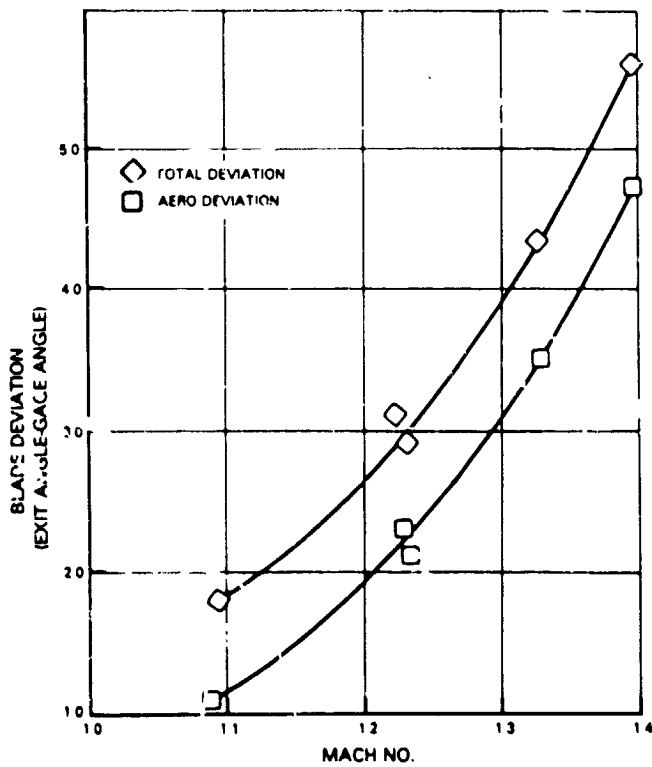


Figure 5.3.3-2 Blade Deviation Versus Mach Number



5.3.3.3 Internal Aerodynamics

A streamline simulation was generated and used to determine the stage internal aerodynamics, including incidence trends and blade turning characteristics. The simulation was made for the design point condition evaluated during the full stage test. The stage inlet and exit total temperature and pressure profiles were input values. Vane exit conditions for the design point were ascertained from the results of the cascade test. In specific, the vane total pressure loss profile was adjusted for stage exit Mach number level, the cascade exit total temperature profile was adjusted for stage inlet temperature level and the vane exit air angle profile was adjusted so that the streamline simulation matched the vane endwall static pressures in the stage test. Also, the simulation accounted for the measured stage inlet flow and cooling flows.

Table 5.3.3-I presents a comparison of the simulation predicted endwall static pressure to the test data. Again, there is a good correlation between the simulation and the measured data.

TABLE 5.3.3-I

WALL STATIC PRESSURE
MPa (psia)

	<u>Measured</u>	<u>Streamline</u>
Vane Leading Edge Inner Diameter	0.45 (65.5)	0.45 (65.6)
Vane Leading Edge Outer Diameter	0.45 (65.5)	0.45 (65.7)
Vane Trailing Edge Inner Diameter	0.23 (33.5)	0.23 (33.5)
Vane Trailing Edge Outer Diameter	0.27 (38.6)	0.27 (38.6)
Blade Trailing Edge Inner Diameter	0.09 (13.2)	0.09 (13.1)
Blade Trailing Edge Outer Diameter	0.10 (14.0)	0.10 (14.5)

Simulation-predicted blade exit air angle and exit Mach number profiles are presented in Figures 5.3.3-3 and -4, respectively, and compared to measured data. In both cases, the simulation results are in good correlation to the measured data, verifying the validity of the simulation.

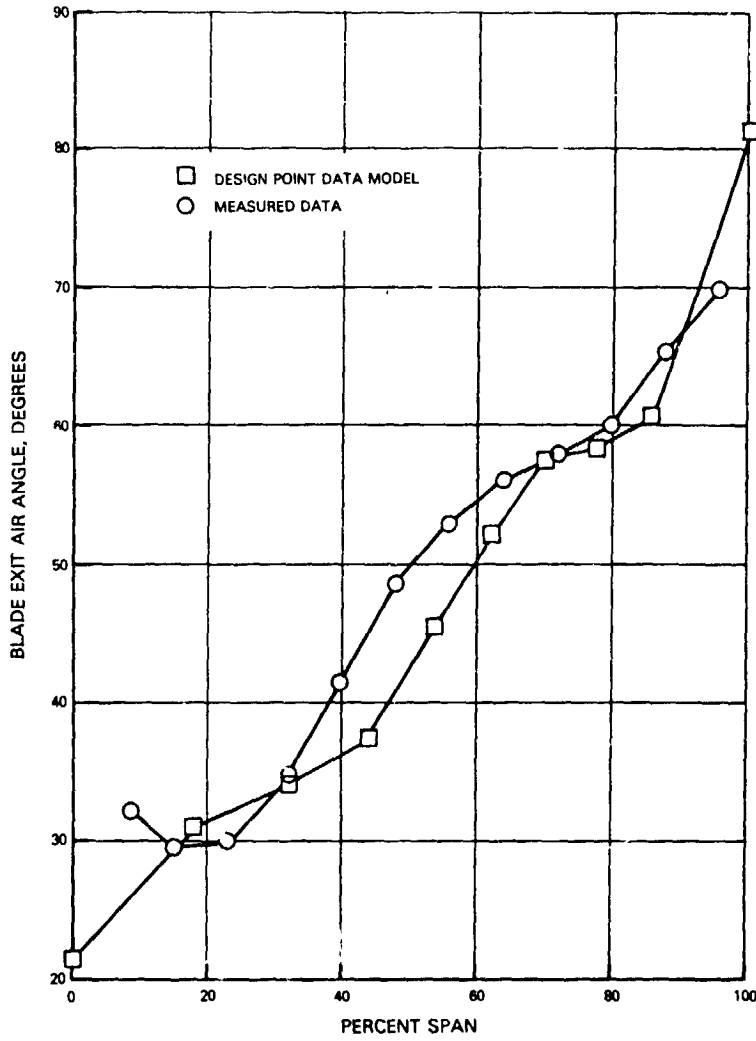


Figure 5.3.3-3 Spanwise Blade Exit Air Angle

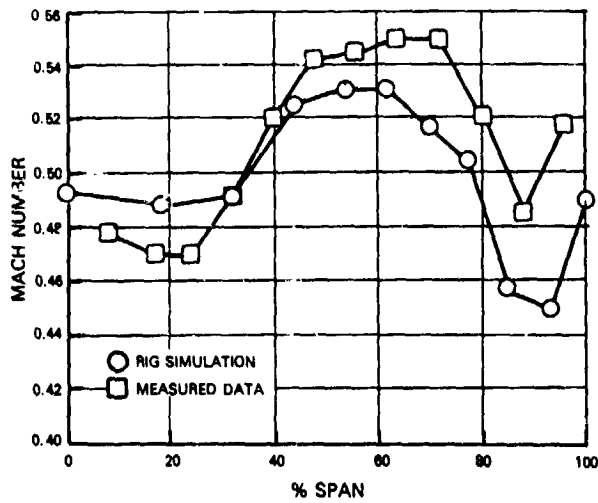


Figure 5.3.3-4 Spanwise Blade Exit Mach Number

A summary of vane and blade internal aerodynamics is presented in Table 5.3.3-II. This table compares predicted integrated core/low spool aerodynamics to the rig simulation. In general, simulation data for the vane are close to the design intent, particularly at the mean section. The difference in the root and tip values is expected because of the inherent limitations of the design analysis. Also, as expected, the aerodynamic differences produced by the design are more pronounced in the relative frame, as shown by the simulation data for the blade inlet root and tip sections. Of particular interest is this appreciable difference in blade incidence and its effect on stage efficiency. This is shown in Figures 5.3.3-5 and -6. Figure 5.3.3-5 shows the spanwise profiles of the blade inlet air angle for the design pressure ratio of 4.0 and varying corrected speed using the design point simulation for the base case (corrected speed of 244). Also shown is the blade design metal angle. It is noteworthy to point out that the design metal angle accounts for vane loss and combustor exit temperature profiles of an engine rather than rig environment. Consequently, the calculated blade inlet air angle profile in Figure 5.3.3-5 are flatter than the metal angle profile. As shown, negative incidence dominates in the 0 to approximately 70 percent span region in relation to the design metal angle. From this point, positive incidence, with the attendant high pressure loss, is prevalent. At the higher corrected speed, less of the blade leading edge span operates at positive incidence. The opposite effect occurs at lower corrected speeds.

TABLE 5.3.3-II

INTERNAL AERODYNAMICS*

<u>Vane</u>	<u>ROOT</u>		<u>MEAN</u>		<u>TIP</u>	
α in (deg.)	(90.0)	90.0	(90.0)	90.0	(90.0)	90.0
α out (deg.)	(11.6)	15.9	(10.6)	10.5	(9.1)	4.0
Mn in	(0.09)	0.09	(0.08)	0.08	(0.07)	0.06
Mn out	(1.01)	0.78	(0.93)	0.95	(0.87)	0.75
Θ gas (deg.)	(78.4)	74.1	(79.7)	79.5	(80.9)	86.0
<u>Blade</u>						
β in (deg.)	(32.7)	67.9	(41.5)	38.89	(59.2)	105.9
β out (deg.)	(16.3)	8.4	(17.2)	16.5	(18.1)	27.3
Mn in	(0.38)	0.23	(0.25)	0.22	(0.15)	0.05
Mn out	(1.23)	1.22	(1.25)	1.25	(1.30)	1.04
Θ Gas (deg.)	(131.0)	103.7	(122.7)	128.5	(102.7)	46.8
α out (deg.)	(38.3)	21.2	(43.5)	42.5	(48.6)	81.3
Mn out	(0.56)	0.49	(0.54)	0.53	(0.54)	0.48

*Values in parentheses are for the restaggered integrated core/low spool design. Values not in parentheses are simulation data at the design point.

ORIGINAL PAGE IS
OF POOR QUALITY

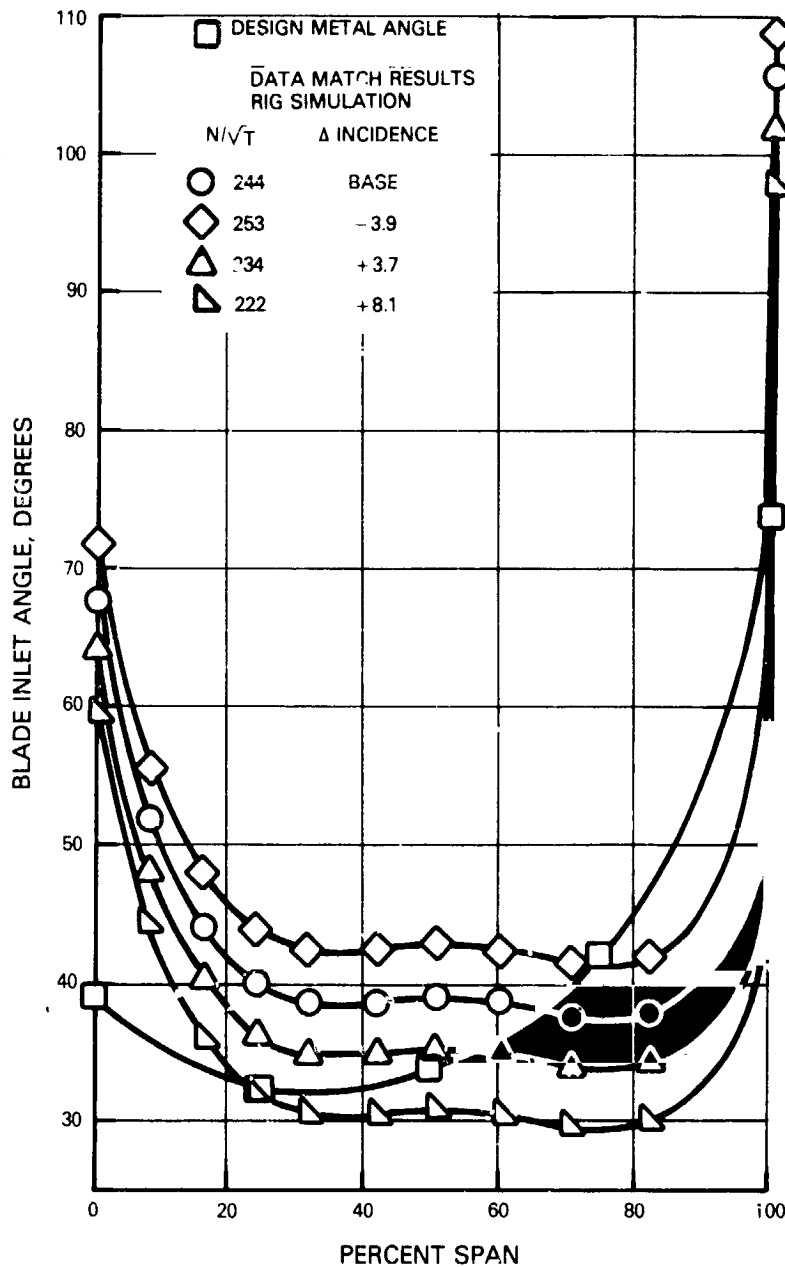


Figure 5.3.3-5 Spanwise Profile of Blade Inlet Air Angle

The advantage of minimizing the amount of positive incidence is apparent in Figure 5.3.3-6, which shows stage efficiency for the data in the preceding figure. At the root section, where incidence is negative for the entire range of speeds, the level of efficiency is constant. However, efficiency decreases with lower levels of corrected speed since more of the airfoil span is subjected to positive incidence. This explains the increase in stage efficiency at corrected speeds higher than the design level (Figure 5.3.1-1).

A spanwise comparison of design and streamline simulation data for blade turning is shown in Figure 5.3.3-7. In comparison to the design, the simulation data show a reduction in turning at the root, indicating that less work is being performed in this area. The midspan region is in agreement with the design, while the tip shows more work being accomplished than predicted by the design. This contrast in design and simulation data is largely attributed to the difference in blade inlet angle.

ORIGINAL PAGE IS
OF POOR QUALITY

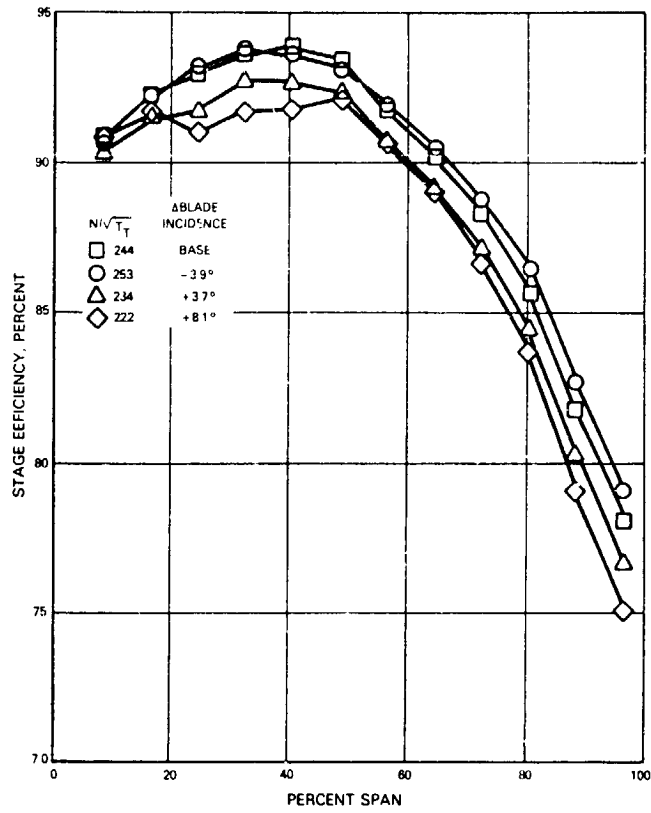


Figure 5.3.3-6 Blade Spanwise Efficiency

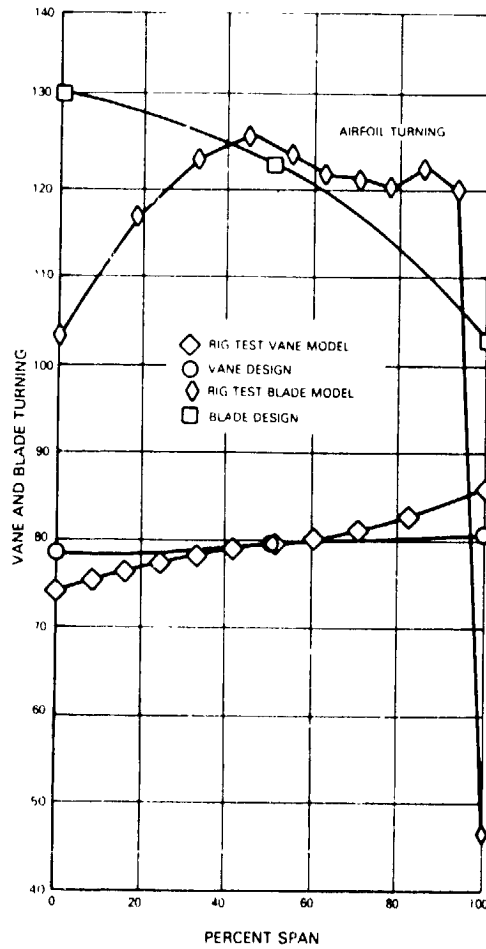


Figure 5.3.3-7 Blade and Vane Turning Characteristics

5.3.4 Secondary Flow System Performance Characterization Studies

The evaluation of secondary flow system performance involved a series of separate investigations to examine the effect of different component flow rate changes on overall turbine performance. The investigation included the main TOBI (tangential on-board injection) flow sensitivity test, mini TOBI flow sensitivity test and compressor end seal leakage test. Test results are presented in the following sections.

In addition, a related rig test was completed to determine the blade inlet supply pressure. Pertinent results from this test are summarized in Section 5.3.4.1, while additional information such as the test rig description, instrumentation and test sequence is contained in Appendix A.

5.3.4.1 Turbine Blade Supply Pressure Test

The turbine blade cooling supply system is based on a pressure-balanced tangential on-board injection system. This design eliminates the requirement for inner and outer TOBI seals.

As part of the high-pressure turbine performance program, a flow test of the tangential on-board injection system was conducted to verify the level of blade cooling air supply pressure. For this test, an existing rotating disk rig was modified to the Energy Efficient Engine configuration. Figure 5.3.4-1 shows how a scaled Energy Efficient Engine tangential on-board injection cascade and vortex plate were added to the existing rig to simulate the Energy Efficient Engine system. Pressure and temperature instrumentation was installed as indicated in Figure 5.3.4-2. Rotating pressure taps were located on the disk to determine pressure rise.

A summary of the test results is shown in Figure 5.3.4-3. Extrapolated to integrated core/low spool engine sea level takeoff performance, the data indicate a blade coolant supply pressure of 53 percent of the compressor discharge total pressure versus a predicted pressure of 54 percent of the compressor discharge total pressure. Since the test program was successful in that the minimum design assumptions were verified, no further analysis or testing was conducted. The minimum allowable supply pressure is 51 percent of compressor discharge total pressure.

5.3.4.2 Tangential On-Board Injection (TOBI) Nozzle Flow Characterization Studies

A series of tests was performed to assess the aerodynamic behavior of the blade and mini TOBI nozzles in maintaining a positive blade supply pressure and acceptable rim cavity temperatures. Testing was conducted by varying the nozzle flow rates a percentage above and below the design rate. The conditions are listed in Table 4 1-I under Phase II.

The results of the tests are summarized in Table 5.3.4-1. Overall, these results show that temperatures and pressures in the front rim cavity are insensitive to TOBI flow rate changes.

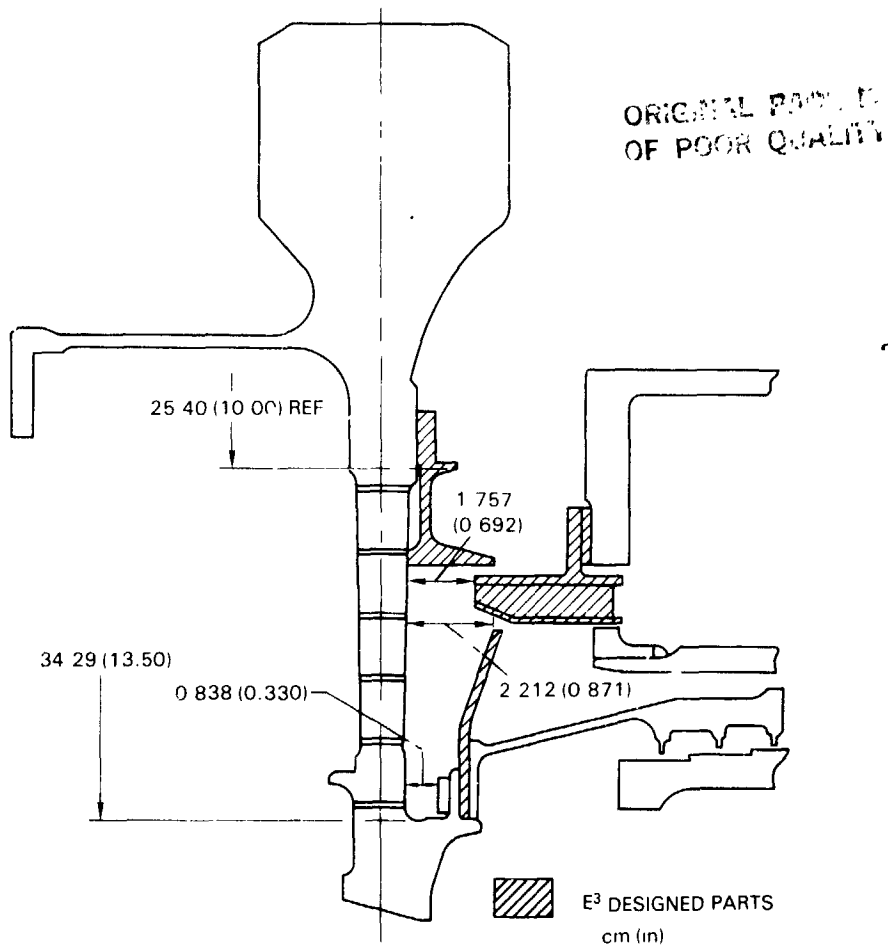


Figure 5.3.4-1 Tangential On-Board Injection System Rig Geometry

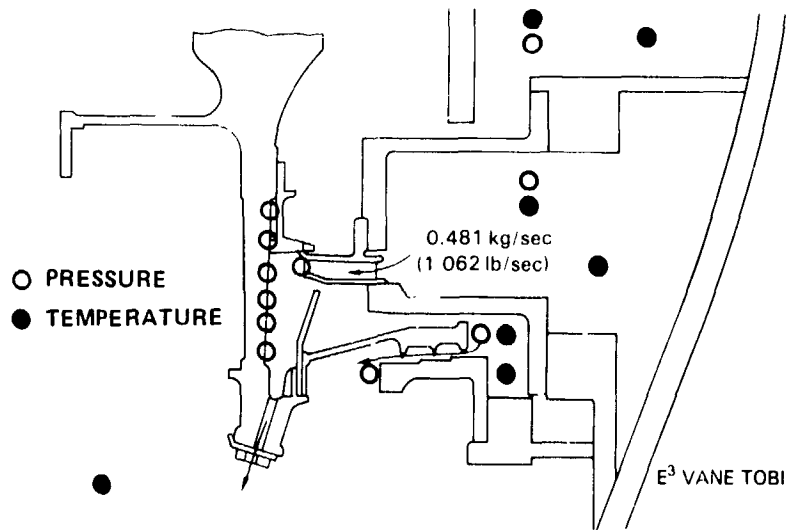


Figure 5.3.4-2 Tangential On-Board Injection Rig Instrumentation Locations

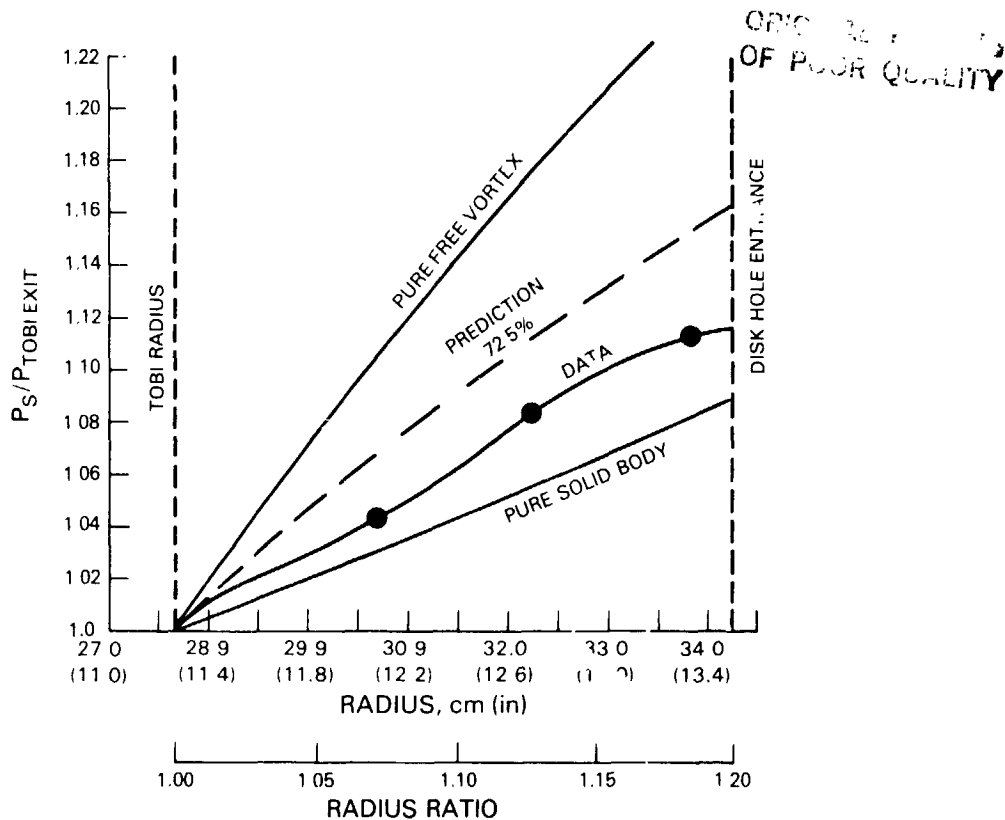


Figure 5.3.4-3 Tangential On-Board Injection Rig Radial Pressures

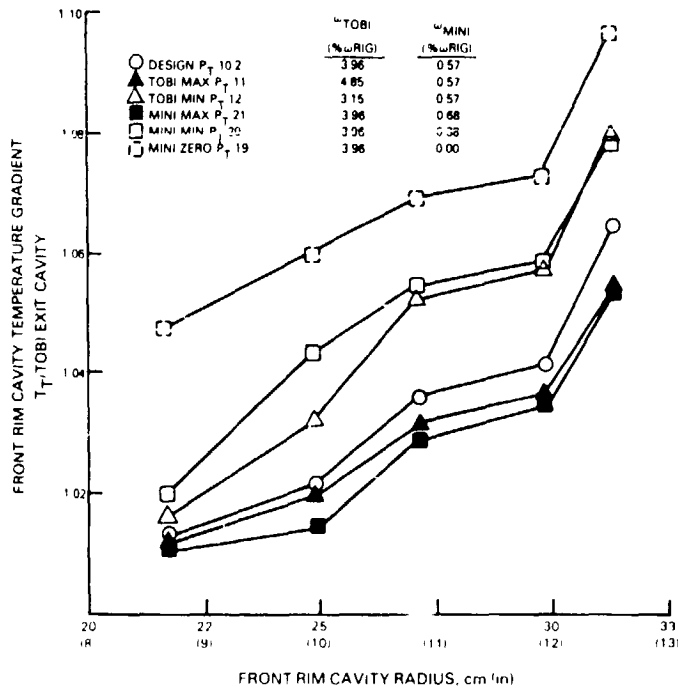
Figure 5.3.4-4 presents a summary of rim cavity temperature trends at the different test conditions in Table 5.3.4-I. The trends indicate that overflowing the nozzles lowered the cavity temperatures, as expected. However, the temperature gradient did not increase significantly with either a 20 percent reduction in blade TOBI flow or a 33 percent reduction in mini TOBI flow. Moreover, complete elimination of flow from the mini TOBI did not cause a dramatic increase in temperatures. This result suggests that the cavity flowfield contained a much higher level of induced swirl than anticipated and this sufficiently reduces the windage shear effects. Thus, for the type of design in the Energy Efficient Engine high-pressure turbine, the loss of preswirled air from the mini TOBI does not produce a detrimental temperature increase in the front rim cavity.

The effect of main TOBI flow variations on front rim pressure levels is shown in Figure 5.3.4-5. As indicated, neither increasing nor decreasing the flow rate imparts any substantial effect in the cavity flowfield. Consequently, a positive blade supply pressure level is assured. Changes to the exit velocity did not produce a noticeable change in the swirl level of the TOBI air to substantially change the front rim swirl characteristics.

The small decrease in static pressure measured with a lower flow rate is corroborated by the corresponding small increase in the rim temperature. This is clearly shown in Figure 5.3.4-6, where the rim temperature rise is only 16.6°C (30°F) at the minimum flow condition compared to the design condition.

TABLE 5.3.4-1
HIGH-PRESSURE TURBINE FRONT RIM CAVITY DATA

Radius cm (in)	Rim Cavity Pressure MPa (psia)	% PT IN	Pr/Pr I	R/R1	Mach I	TOBI Exit Temps °C (°F)	Solid body factor	Ptcalc MPa (psia)	TrI/TEC
Design Point - 10.....									
22.0 (8.7)	0.223 (32.36)	49.1047	1	1		35 (95)			1.01277
25 (10)	0.227 (32.86)	49.8634	1.01545	1.14943	.261431	37 (100)	.45232	0.238 (34.4591)	1.02190
27.6 (10.9)	0.229 (33.17)	50.3338	1.02503	1.25287	.249423	42 (108)	.479982	0.239 (34.6371)	1.03650
30 (12)	0.230 (33.42)	50.7132	1.03276	1.37931	.226390	43 (111)	.437282	0.239 (34.6344)	1.04197
32.0 (12.6)	0.230 (33.29)	50.5159	1.02874	1.44828	.192429	51 (124)	.376422	0.236 (34.1609)	1.06569
PT IN	0.454 (65.9)	100				TT IN 315 (599)			
PT-30.4 (12.0)	0.389 (56.48)	85.7056				TEC 31 (88)			
Zero Mini Point - 19.....									
22.0 (8.7)	0.225 (32.61)	49.1262	1	1		45 (113)			1.04753
25 (10)	0.227 (32.87)	49.5179	1.00797	1.14943	.188045	48 (120)	.366645	0.232 (33.6908)	1.06033
27.6 (10.9)	0.228 (33.14)	49.9247	1.01625	1.25287	.201294	51 (125)	.393963	0.235 (34.0895)	1.06947
30 (12)	0.230 (33.37)	50.2712	1.02331	1.37931	.191275	52 (127)	.375140	0.236 (34.2325)	1.07313
32.0 (12.6)	0.228 (33.06)	49.8042	1.01380	1.44828	.133691	60 (140)	.265586	0.231 (33.4755)	1.09689
PT IN	0.458 (66.38)	100				TT IN 316 (602)			
PT-30.4 (12.0)	0.225 (32.57)	49.0660				TEC 30 (87)			
Min Mini Point - 20.....									
22.0 (8.7)	0.227 (32.86)	49.5925	1	1		36 (97)			1.02015
25 (10)	0.229 (33.22)	50.1358	1.01096	1.14943	.220312	43 (110)	.425283	0.237 (34.3f25)	1.04396
27.6 (10.9)	0.230 (33.4)	50.4075	1.01643	1.25287	.202403	46 (116)	.393058	0.237 (34.3677)	1.05495
30 (12)	0.232 (33.64)	50.7697	1.02374	1.37931	.193022	47 (118)	.375629	0.238 (34.5255)	1.05861
32.0 (12.6)	0.230 (33.34)	50.3169	1.01461	1.44828	.137530	53 (129)	.270667	0.233 (33.7835)	1.07875
PT IN	0.457 (66.26)	100				TT IN 316 (601)			
PT-30.4 (12.0)	0.304 (44.11)	66.5711				TEC 30 (86)			
Max Mini Point - 21.....									
22.0 (8.7)	0.224 (32.42)	48.9506	1	1		32 (90)			1.01103
25 (10)	0.227 (32.98)	49.7962	1.01727	1.14943	.276327	33 (92)	.523483	0.240 (34.7767)	1.01471
27.6 (10.9)	0.230 (33.33)	50.3246	1.02807	1.25287	.263986	37 (100)	.504045	0.241 (34.9844)	1.02941
30 (12)	0.232 (33.67)	50.8380	1.03656	1.37931	.245369	39 (103)	.470192	0.242 (35.1105)	1.03493
32.0 (12.6)	0.231 (33.52)	50.6115	1.03393	1.44828	.208896	45 (114)	.404855	0.238 (34.5551)	1.05515
PT IN	0.457 (66.23)	100				TT IN 314 (598)			
PT-30.4 (12.0)	0.451 (65.36)	98.6864				TEC 28 (84)			
Min TOBI Point - 15.....									
22.0 (8.7)	0.223 (32.29)	48.5345	1	1		38 (101)			1.01630
25 (10)	0.226 (32.74)	49.2109	1.01394	1.14943	.248350	43 (110)	.478784	0.237 (34.1755)	1.03261
27.6 (10.9)	0.227 (32.99)	49.5867	1.02168	1.25287	.232256	49 (121)	.452403	0.236 (34.2526)	1.05254
30 (12)	0.230 (33.34)	50.1127	1.03252	1.37931	.225573	51 (124)	.440652	0.238 (34.5427)	1.05797
32.0 (12.6)	0.229 (33.02)	49.6317	1.02261	1.44828	.170855	58 (138)	.328465	0.232 (33.6997)	1.08333
PT IN	0.459 (66.53)	100				TT IN 310 (590)			
PT-30.4 (12.0)	0.391 (56.74)	85.2848				TEC 33C (92)			
Max TOBI Point - 18.....									
22.0 (8.7)	0.226 (32.83)	49.3981	1	1		32 (90)			1.01289
25 (10)	0.230 (33.38)	50.2257	1.01675	1.14943	.272159	34 (94)	.516635	0.242 (35.1430)	1.02026
27.6 (10.9)	0.232 (33.69)	50.6921	1.02620	1.25287	.255107	37 (100)	.487314	0.243 (35.2499)	1.03131
30 (12)	0.234 (33.98)	51.1285	1.03503	1.37931	.234019	39 (103)	.448683	0.243 (35.3006)	1.03683
32.0 (12.6)	0.233 (33.86)	50.9479	1.03137	1.44828	.230963	45 (113)	.389267	0.240 (34.8269)	1.05525
PT IN	0.458 (66.46)	100				TT IN 315 (600)			
PT-30.4 (12.0)	0.391 (56.7)	85.3145				TEC 28 (83)			



ORIGINAL COPY

Figure 5.3.4-4 Front Rim Cavity Sensitivity to TOBI Flow Rate Variations

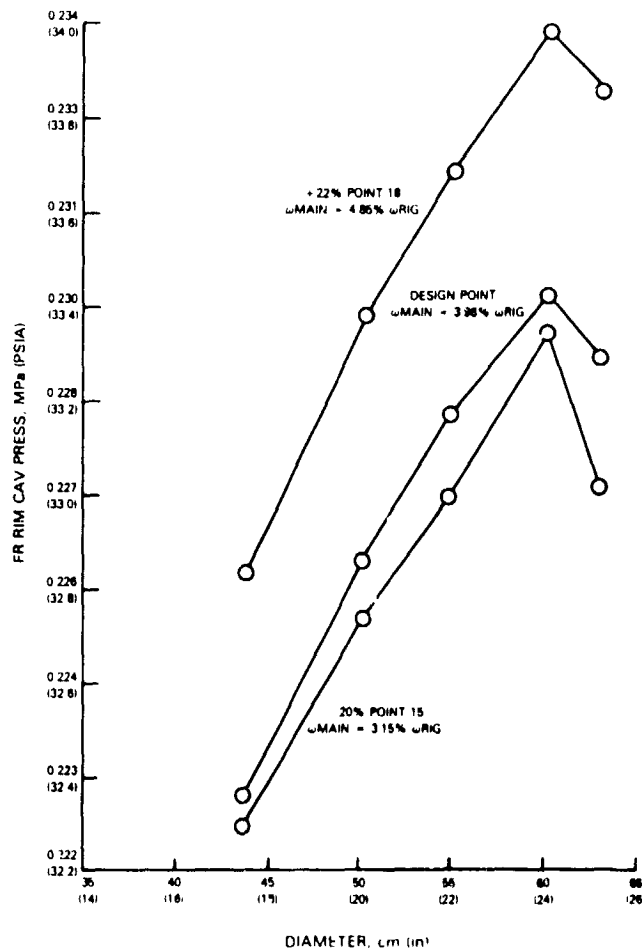


Figure 5.3.4-5 Rim Cavity Pressures with Blade TOBI Flow Rate Variations

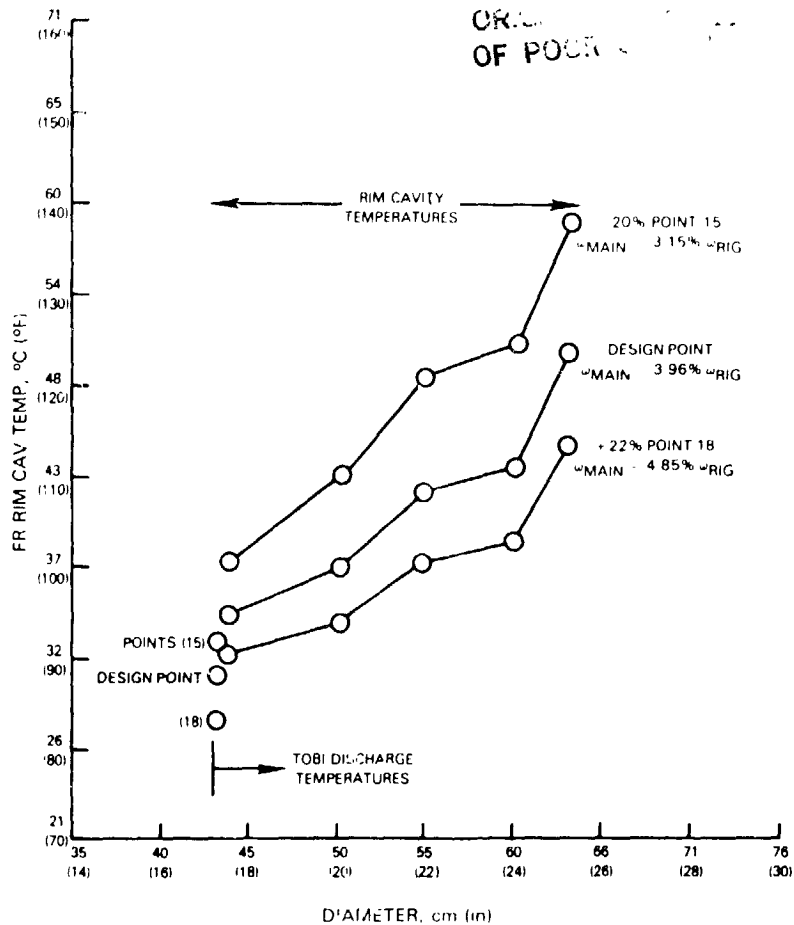


Figure 5.3.4-6 Rim Cavity Temperatures with Blade TOBI Flow Rate Variations

Similar results are presented in Figure 5.3.4-7 for variations in the mini TOBI flow rate. Again, the pressure level differences between the design and off-design conditions are small. The corresponding temperature levels are also small, as indicated in Figure 5.3.4-8.

The information in Figure 5.3.4-9 shows the calculated swirl factor in the front cavity. As indicated, there is a gradual loss in swirl strength as the flow approaches the rim. These results are consistent with previous data trends as well as the pressure gradient results in Figure 5.3.4-10.

5.3.4.3 Compressor End Seal Study

This test evaluated the influence of compressor discharge seal flow rates on the pressure distribution in the front disk cavity and the blade TOBI supply plenum as well as the resultant effects on blade coolant flow. Testing showed that the seal, which is a 9-knife edge geometry, performed as designed. Changes in flow rates had little, if any, effect on the performance of the secondary flow system. The blade supply pressure is insensitive to changes in the seal clearance. In addition, as shown in Figure 5.3.4-11, the design prediction is in good agreement with the code flow and rig measurements.

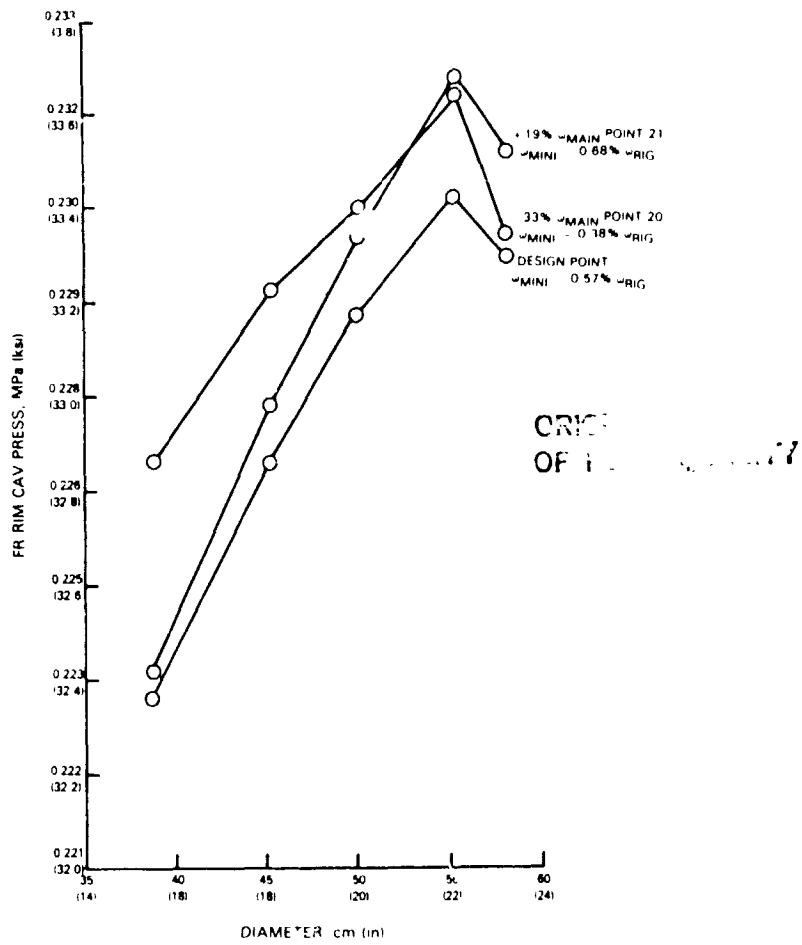


Figure 5.3.4-7 Rim Cavity Pressures with Mini TOBI Flow Rate Variations

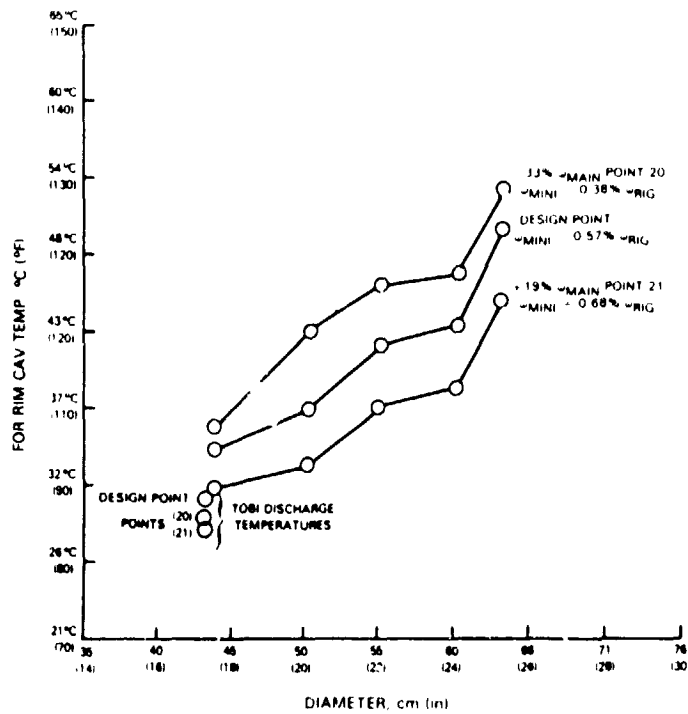


Figure 5.3.4-8 Rim Cavity Temperatures with Mini TOBI Flow Rate Variations

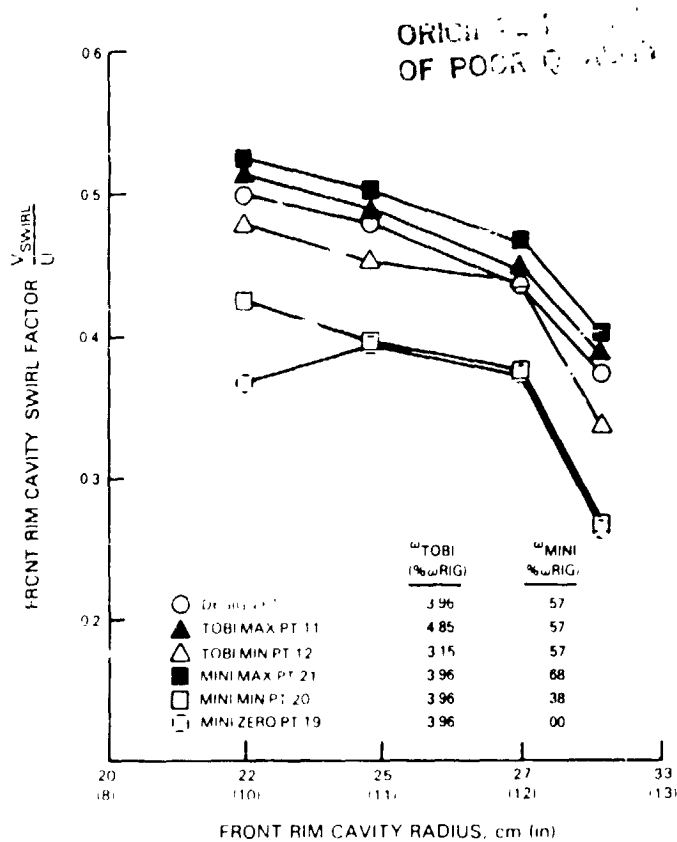


Figure 5.3.4-9 Front Rim Cavity Sensitivity to Swirl Level Difference

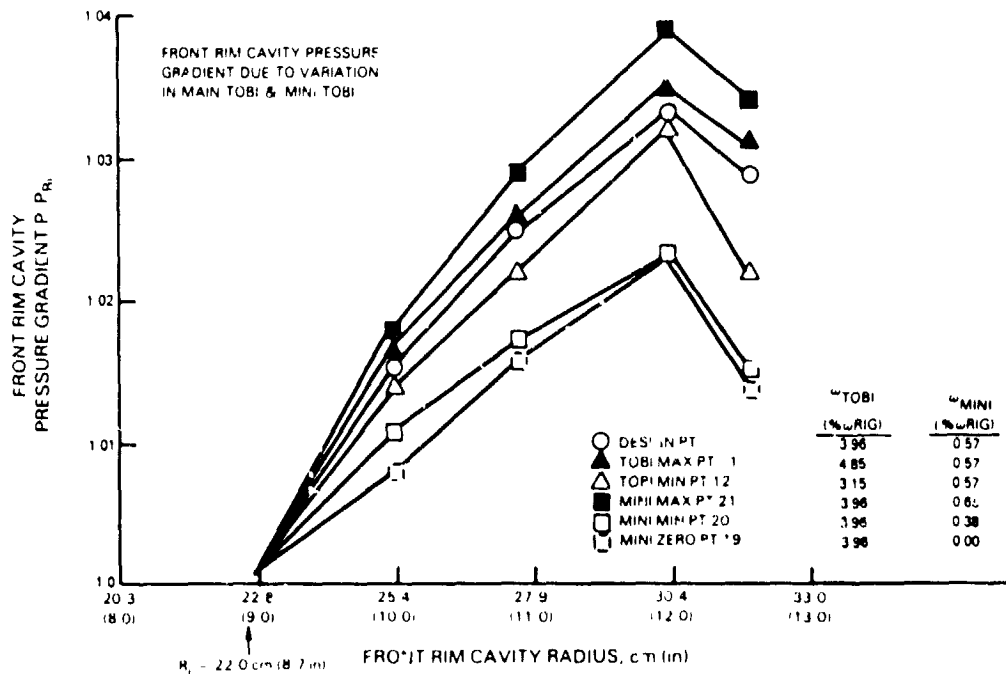


Figure 5.3.4-10 Front Rim Cavity Sensitivity to Pressure Variation

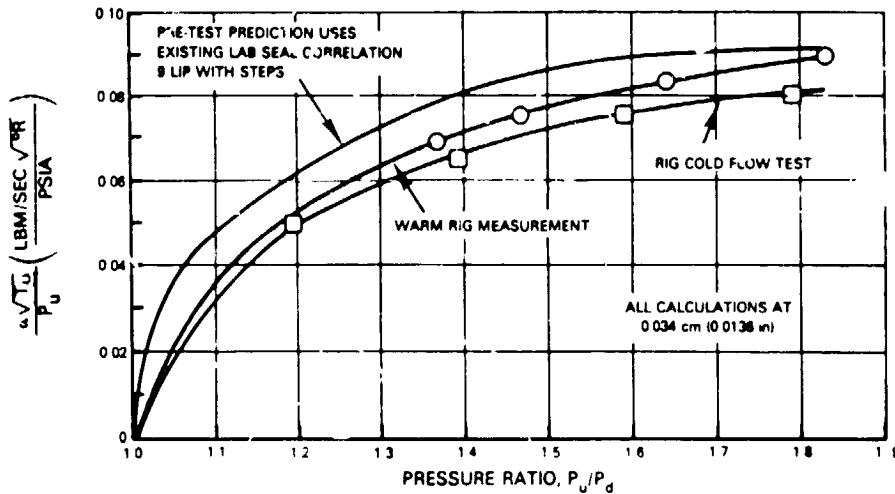


Figure 5.3.4-11 High-Pressure Compressor Discharge End Seal Leakage Study Results

5.3.4.4. Vane Leakage Study

Leakage rates in the vane attachment area were calculated and compared to levels predicted during the evolution of the turbine design. Attachment leakage rates were calculated by deducting pretest vane foil and blade outer seal flows and vane platform estimates from the measured total flow of the vane assembly. The results presented in Table 5.3.4-II indicate that the effects of thermals and vane loadings reduced attachment leakage to values close to the flight propulsion system preliminary definition.

TABLE 5.3.4-1

VANE ATTACHMENT LEAKAGES

	FLIGHT PROPULSION SYSTEM	EXISTING FEATHER SEAL EXPERIENCE	UPDATE BASED ON LEAKAGE TEST PROGRAM	UPDATE BASED ON HPT RIG COLD FLOW TESTS	HPT WARM RIG RESULTS
<u>Vane Inner Diameter</u>					
Front	0.05	0.05	0.22	0.04	0.15
Mid	0.11	0.22	0.35	0.78	0.23
Rear	0.40	0.46	0.44	1.58	0.38
Inner Diameter Total	0.56	0.73	1.01	2.40	0.76
<u>Vane Outer Diameter</u>					
Front	0.13	0.25	0.18	0.20	0.12
Mid	0.13	0.25	0.34	0.47	0.16
Rear	0.21	0.26	0.30	0.40	0.25
Outer Diameter Total	0.47	0.77	0.82	1.07	0.53
Vane Attach Total (± Rig Flow)	1.03	1.50	1.83	3.47	1.29

5.4 POST-TEST INSPECTION RESULTS

All rotating hardware, the outer case assembly and outer airseal assembly of the high-pressure turbine rig were disassembled and inspected. In general, all parts were in excellent condition.

Post-test visual inspection of rig instrumentation showed that the pressure and temperature sensors, along with associated hardware accessories, maintained their pre-test condition. In addition, post-test system validity checks for temperature and pressure data acquired during rig testing indicated measurement accuracies consistent with pretest error/accuracy predictions and provided an excellent correlation between estimated and actual data.

No distress was observed on the blades, vanes and outer air seals. The excellent condition of these components is shown in Figure 5.4-1 through 5.4-3. No evidence of cooling air hole plugging was noted with these components.

Also, there was no indication of seal rubbing with the high-compressor discharge seal, rear thrust balance seal and the No. 4-5 bearing compartment buffer air seal. Dark line marks on the discharge seal land at the 3 o'clock position indicated that the knife edges may have been very close to the land at this location. However, there was no appreciable rub.

While the majority of component parts associated with the aerodynamics of the rig was in excellent condition, the No. 4 bearing showed some minor distress. Scoring marks were noted on the inner surfaces of the No. 4 bearing oil scoop, the No. 4 bearing front carbon seal plate, and the outer diameter surface of the No. 4 bearing hub. These were the result of the oil scoop and the carbon seal plate spinning on the No. 4 bearing hub. Most rig-associated components were also in excellent condition. Teardown inspection showed that the reason for binding of the traverse instrumentation ring was insufficient axial clearance between the rotating ring and stationary parts. Galling and metal pickup were visible inboard of the front 'W' seal on these parts, as shown in Figure 5.4-4.

5.5 SUMMARY OF RESULTS

The Energy Efficient Engine high-pressure turbine component was successfully tested over a range of conditions that simulated operation of the integrated core/low spool at both intermediate and high power levels. There were no major difficulties that prevented the acquisition of performance data. The good mechanical operation of the test rig was verified by the excellent post-test condition of the test components.

The main result is that the measured turbine rig efficiency of 88.5 percent surpassed both the rig design goal of 86.5 percent and the estimated component efficiency for the integrated core/low spool of 87.1 percent. Furthermore, this efficiency measurement was repeatable, indicating that no performance deterioration occurred during the test. When comparing this measured efficiency to that of the uncooled rig, there is only a 2.6 percent penalty, in efficiency from cooling and leakage flows.

ORIGINAL SOURCE OF
OF POOR QUALITY

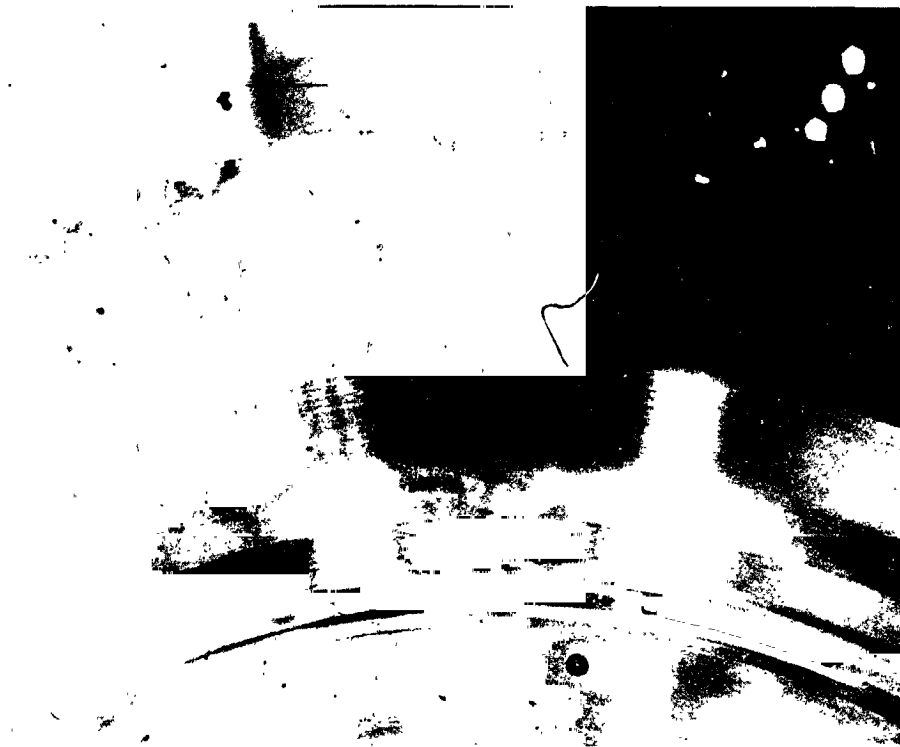


Figure 5.4-1 High-Pressure Turbine Rotating Disk Assembly



Figure 5.4-2 Post-Test Condition of Turbine Vanes

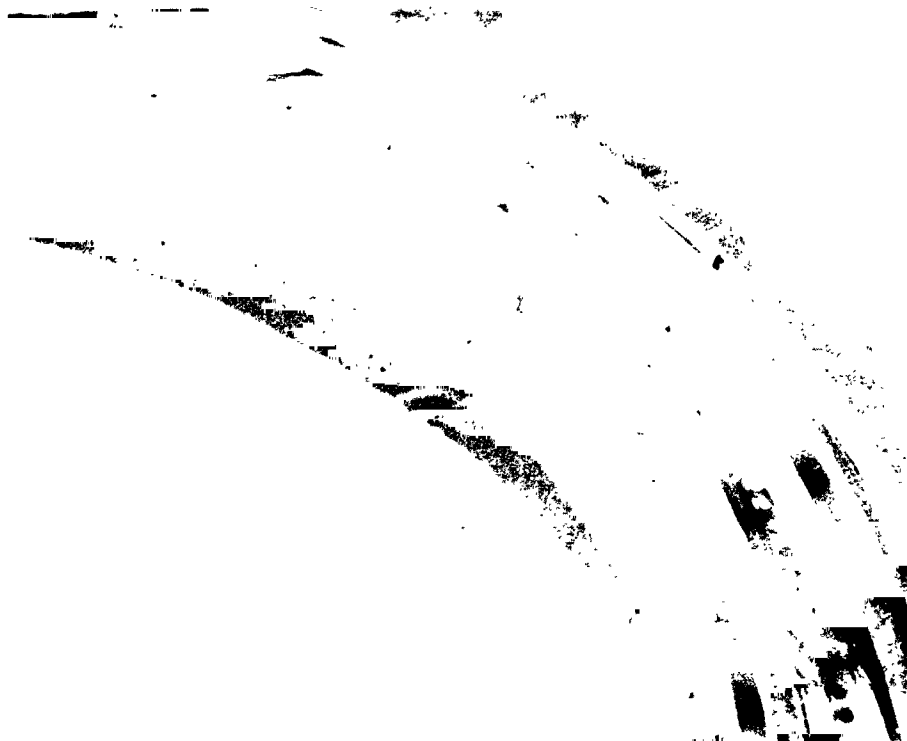


Figure 5.4-3 High-Pressure Turbine Outer Air Seal Segments

Vane performance, as documented by cascade testing, was generally in good agreement with results from the preceding Uncooled Rig Test program and the design prediction. Measured pressure loss was at predicted levels, and showed the expected increase in loss at higher exit Mach numbers. Typically, the endwalls exhibited the highest loss, while the midspan showed the lowest loss. Operation at high Reynolds numbers produced no change in loss characteristics.

Of particular importance, cascade testing demonstrated the effectiveness of the vane cooling scheme. Results indicate that the cooling film from the vane leading edge remains attached over the entire suction surface to provide a higher than predicted cooling effectiveness. This suggests that the design of a second-generation vane for this turbine configuration could require less coolant.

The high level of stage efficiency along with the good vane performance indicates that the blade performed at higher than expected levels. Performance trends showed the typical increase in loss with higher exit Mach number throughout the transonic region. This is a result of the low loss blade design and trailing edge cooling ejection. The analysis of blade performance also showed that testing engine hardware in a rig configuration imparts slight compromises in performance.

The turbine secondary flow system performed according to the design intent. Characterization studies showed that system performance, in particular the pressure-balanced tangential on-board injection system, is insensitive to flow and pressure variations.

ORIGINAL FACE IS
OF POOR QUALITY



Figure 5.4-4 High-Pressure Turbine Full Stage Rig Exit Probe Instrumentation Ring Showing Galling and Metal Pickup

SECTION 6.0 CONCLUDING REMARKS

A single-stage turbine configuration is attractive from the aspects of cost, weight and maintainability. However, in comparison to a two-stage turbine, these benefits can be compromised by a lower level of performance. The results from this test have demonstrated that it is possible to minimize the performance decrement with a highly-loaded, transonic, single-stage design.

This test has provided an opportunity to evaluate the numerous technology features in the Energy Efficient Engine single stage high-pressure turbine component. Besides high rim speed operation, which is a prerequisite for higher pressure ratio engines in the future, testing has also shown that substantial improvements in performance can be achieved with advances in airfoil aerodynamics and sealing technology. In several instances, results have indicated where additional performance gains could be attained, should a design update be contemplated.

The results of this test have wide application. Many of the advanced concepts, such as airfoil design, are directly applicable to commercial and military engines planned in the near future. These concepts also establish the technology base for the design of far-term fuel efficient turbofan engines.

APPENDIX A
BLADE TANGENTIAL ON-BOARD INJECTION SYSTEM -- RELATED TESTING

INTRODUCTION

In a supporting test, the flow and pressure characteristics of the blade tangential on-board injection (TOBI) system were assessed to verify the design assumptions and overall efficiency of the pressure-balanced system in the Energy Efficient Engine high-pressure turbine component. Testing was conducted with an available turbine development test rig at the Middletown, Connecticut Test Facility.

TEST CONFIGURATION

To maintain the integrity of the rotating instrumentation and slip ring, no changes were made to the existing rig disk. The disk hole entrances of the rig disk were at a radius of 34.29 cm (13.50 in), and the remaining vortex chamber dimensions were scaled from this point holding radius ratios constant. Thus, the TOBI radius in the rig was 28.605 cm (11.262 in), as indicated in Figure A-1. A limitation imposed by the disk, which does not fit the modeling, occurs at the vortex plate bolt circle. The net effect was a 40 percent reduction in available flow area.

TEST PROGRAM

To effectively model the TOBI conditions in the integrated core/low spool at sea level takeoff, three parameters were held constant. These included a TOBI exit Mach number of 1.05, an air-to-disk velocity ratio of 1.68 and a radial-to-tangential air velocity ratio of 0.027. In order to satisfy these conditions, the rig speed was maintained at 6580 rpm with the TOBI nozzle pressure ratio set at 2.0. In addition, the TOBI supply air temperature was established to minimize heat transfer effects on disk temperatures.

An investigation of off-design conditions was limited to various TOBI pressure ratios with a constant disk speed. Pressure ratios ranging from 1.2 to 2.5 were tested. During these tests, TOBI inlet temperature was varied to maintain minimum disk temperature gradients. Table A-1 shows the test conditions established for the rig program.

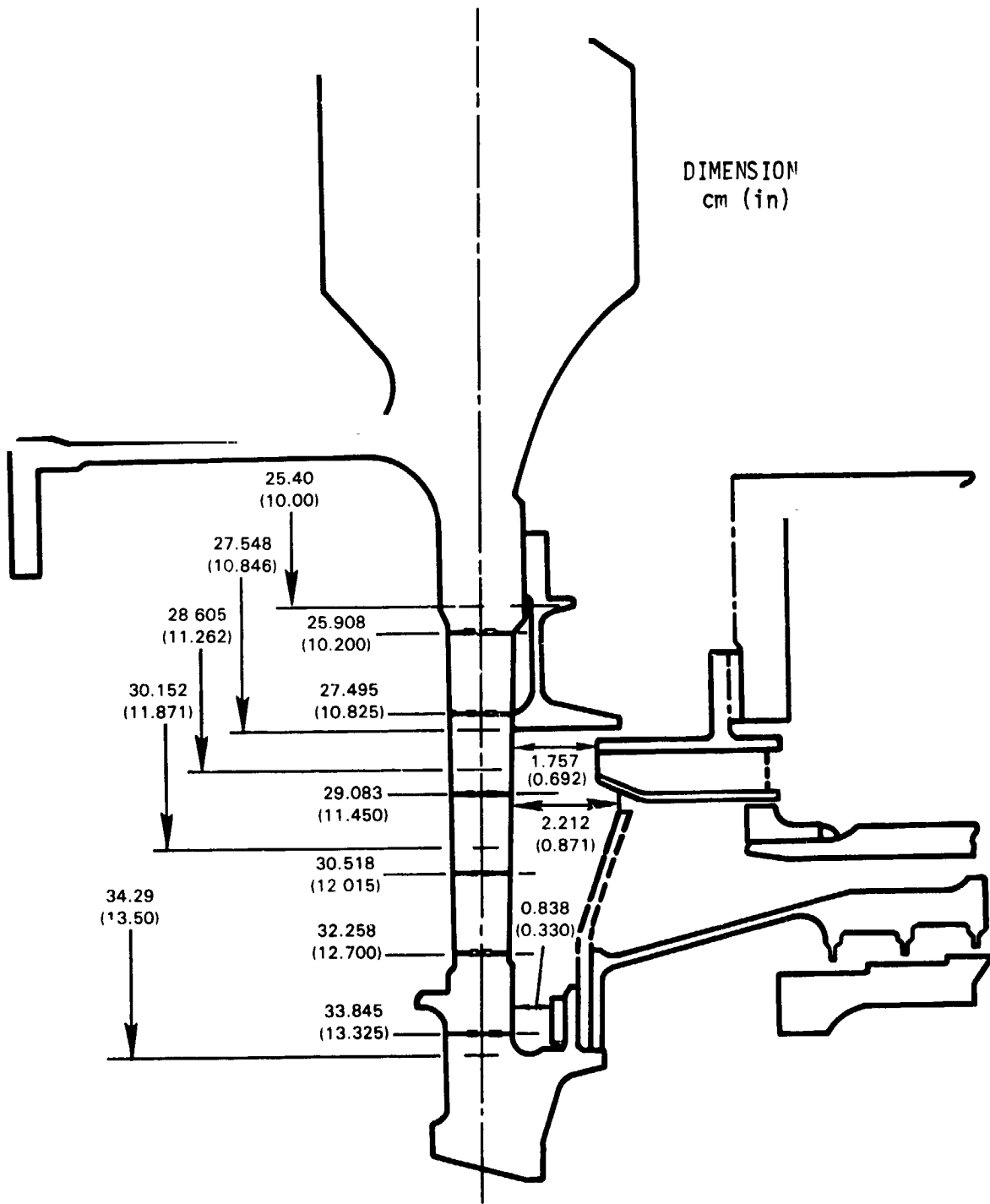


Figure A-1 Energy Efficient Engine Tangential On-Board Injection Rig Geometry

TABLE A-I
TEST RIG PROGRAM

<u>Pressure Ratio Across TOBI</u>	<u>RPM</u>	<u>TOBI Inlet Temperature °C (°F)</u>
1.2	0	37 (100)
1.4	0	37 (100)
1.6	0	37 (100)
2.0	0	37 (100)
2.5	0	37 (100)
2.0	0	37 (100)
1.2	6580	101 (214)
1.4	6580	113 (236)
1.6	6580	121 (250)
2.0	6580	132 (270)
2.5	6580	132 (270)
2.0	6580	132 (270)

TABLE B-I
FULL STAGE TURBINE WARM RIG TEST RESULTS

<u>PHASE 1</u>		
<u>TEST*</u> <u>POINT</u>	<u>PRESS</u> <u>RATIO</u>	<u>SPEED</u> <u>PARA.</u>
1	4.01	244.8
2	4.03	234.1
3	3.91	222.3
4	3.98	253.1
5	3.49	244.4
6	3.48	235.5
7	3.44	223.0
9	4.43	245.3
<u>PHASE 3</u>		
18	4.03	244.6
21	4.02	244.2
28	4.01	244.8
<u>PHASE 4</u>		
22	4.30	234.4
23	3.47	253.8
24	4.04	244.8
29	4.75	243.8

*For each test point, exit total pressure (in HgA), static pressure (in HgA), air angle (supplementary angles), and total temperature (°F), and efficiency are presented.

ORIGINAL PAGE IS
OF POOR QUALITY

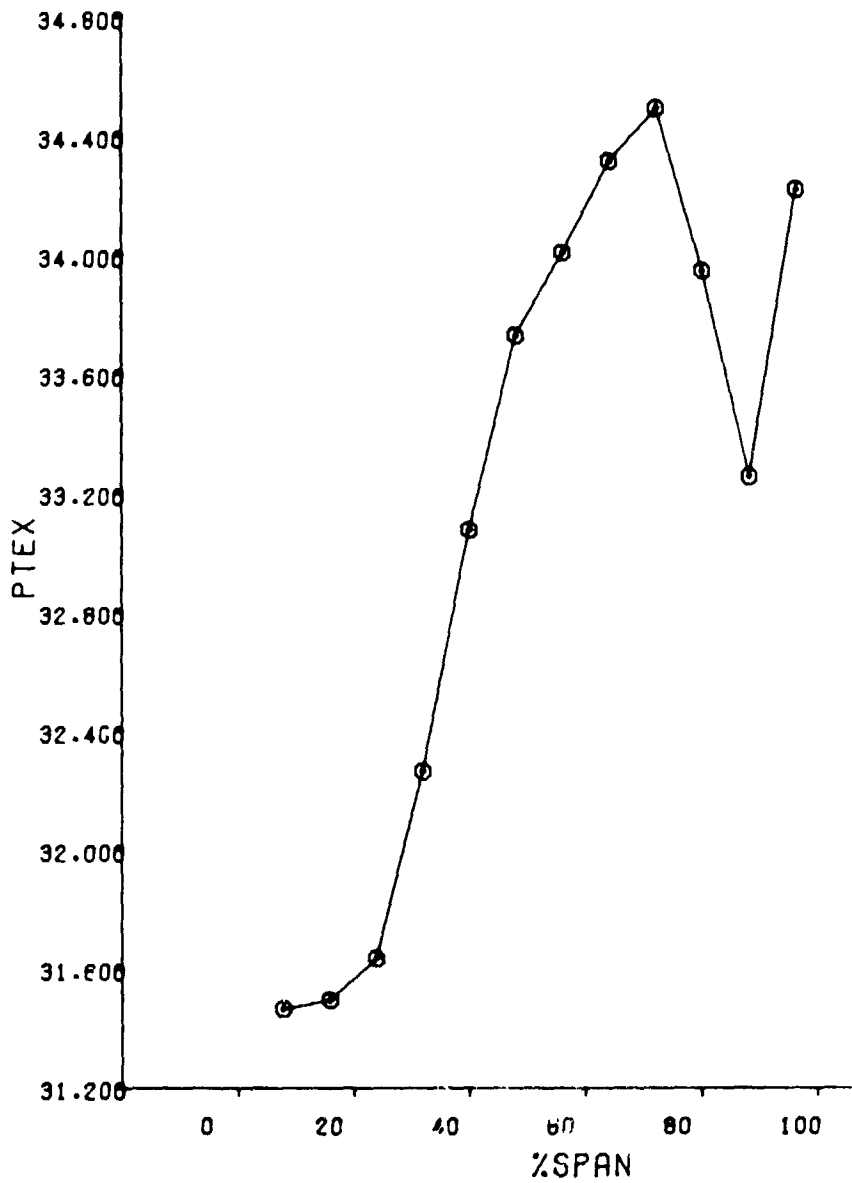


Figure B-1 Average Total Pressure Versus Span (Point 1)

ORIGINAL PAGE IS
OF POOR QUALITY

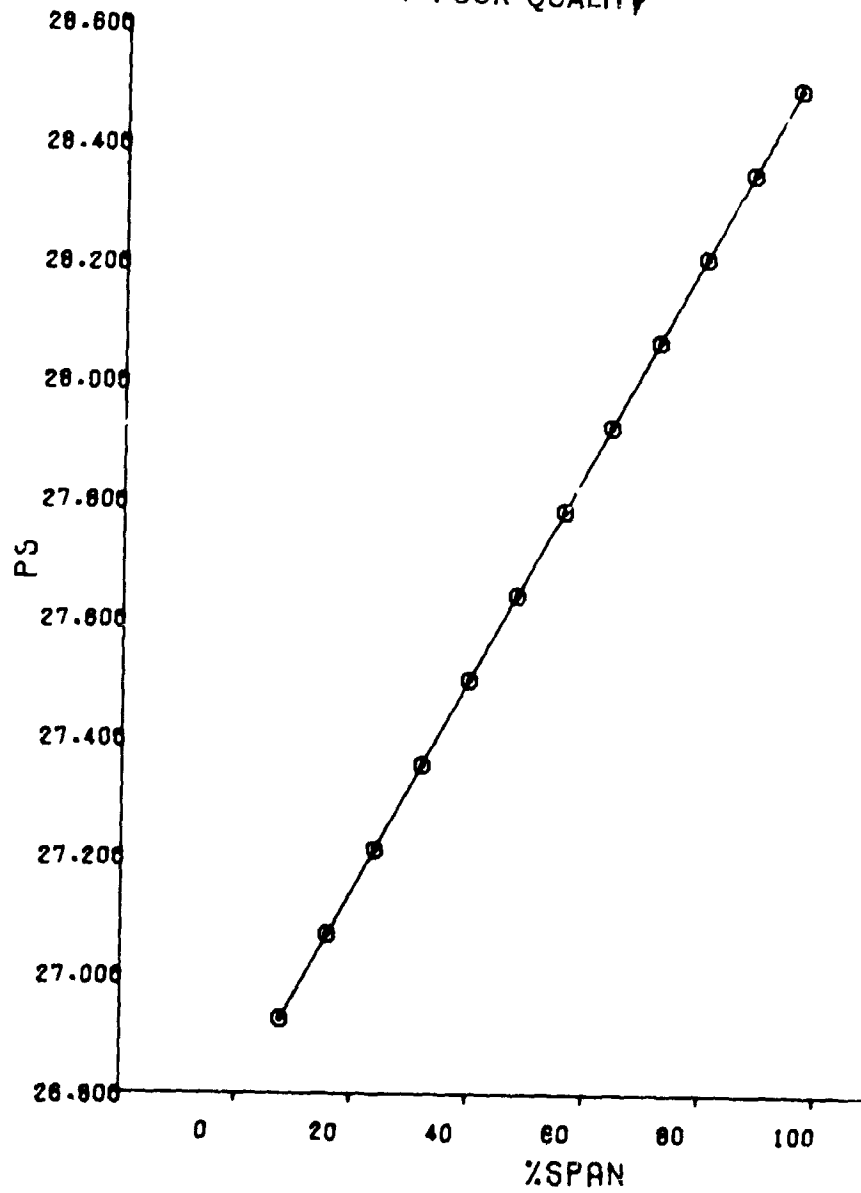


Figure B-2 Average Static Pressure Versus Span (Point 1)

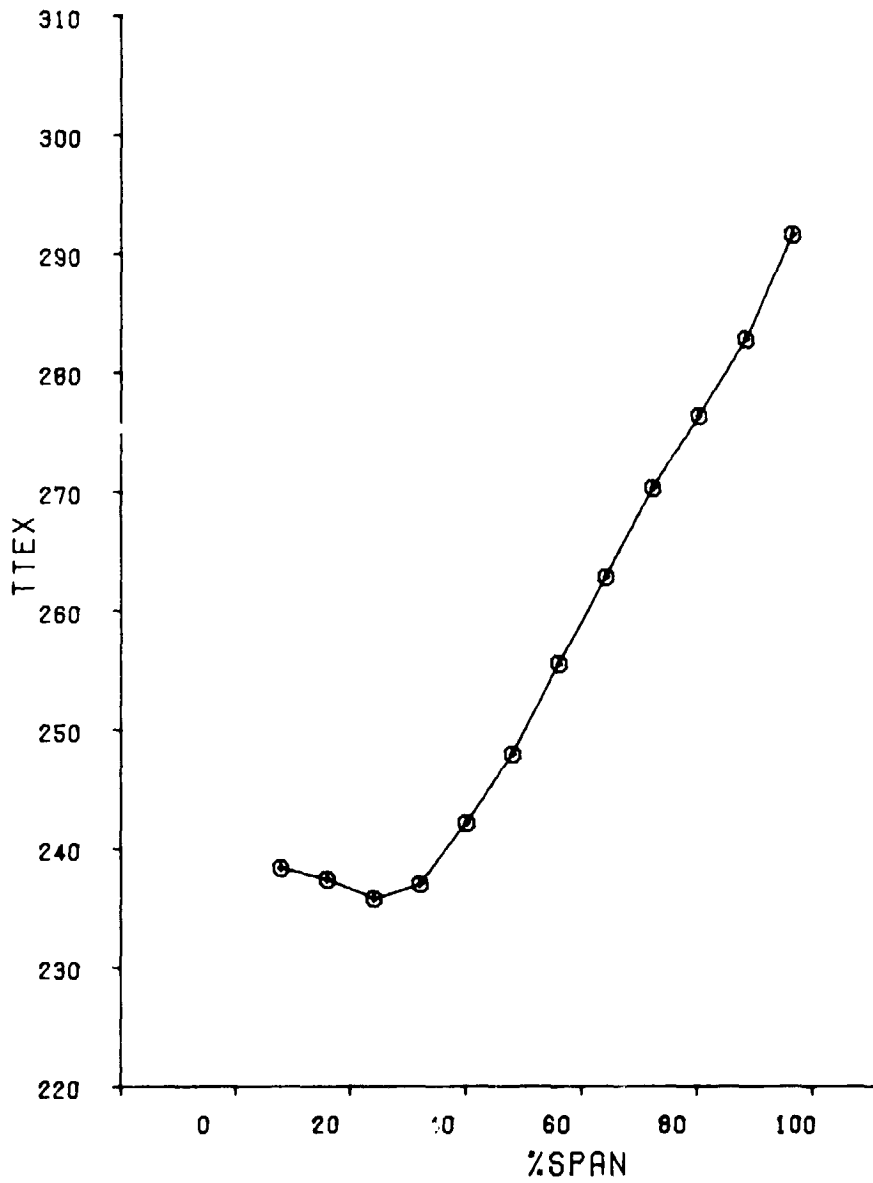


Figure B-3 Average Total Temperature Versus Span (Point 1)

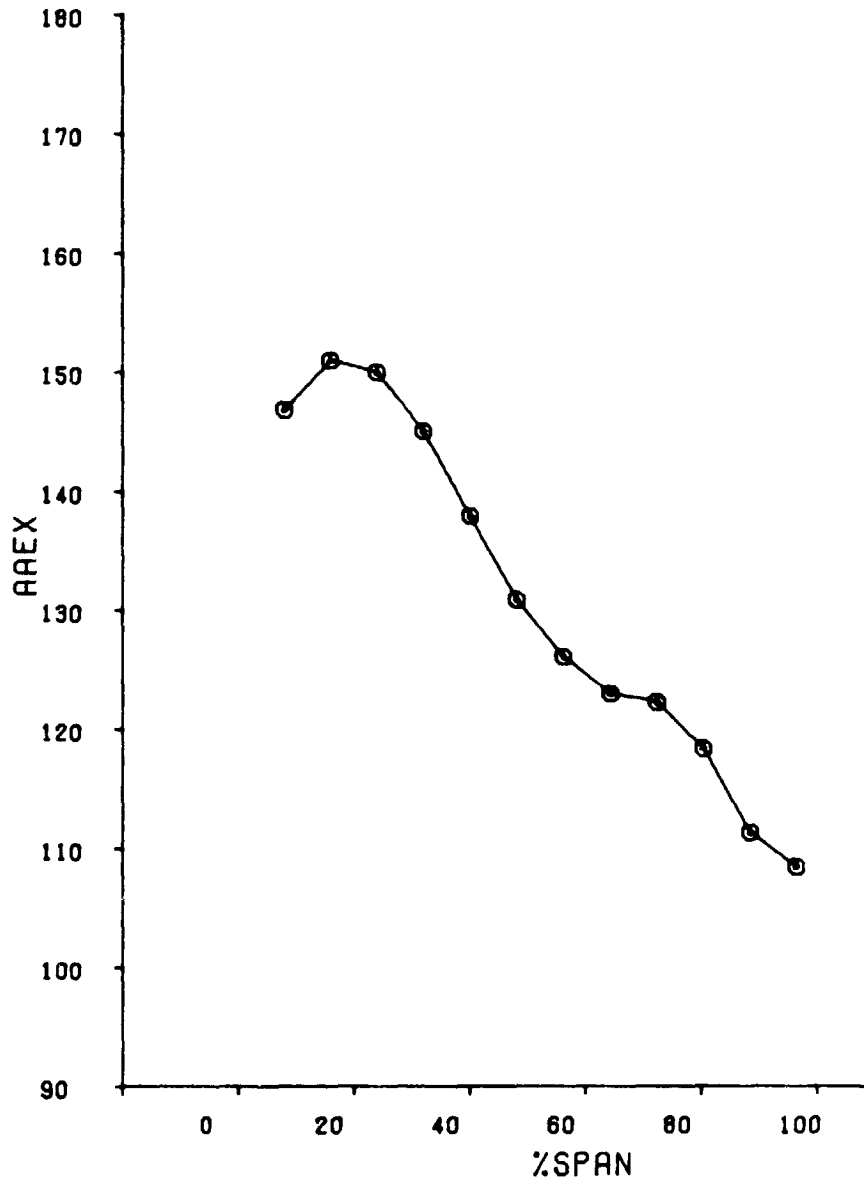


Figure B-4 Average Air Angle Versus Span (Point 1)

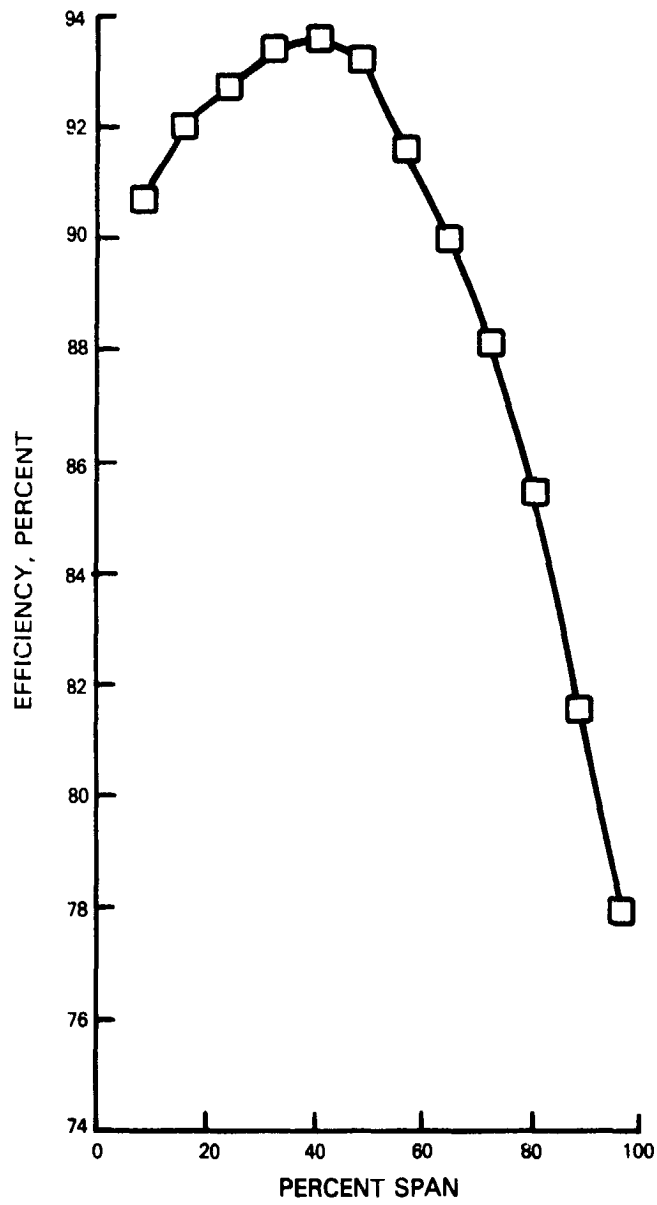


Figure B-5 Efficiency Versus Span (Point 1)

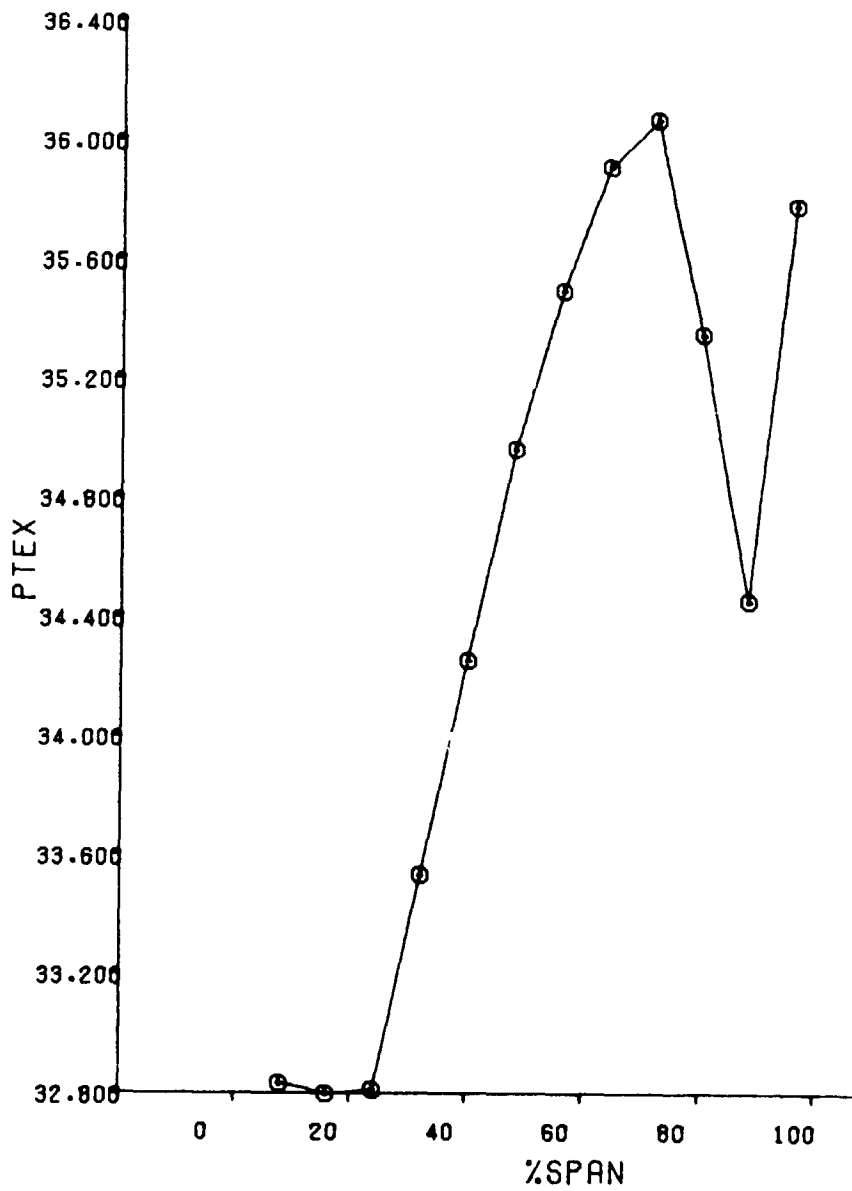


Figure B-6 Average Total Pressure Versus Span (Point 2)

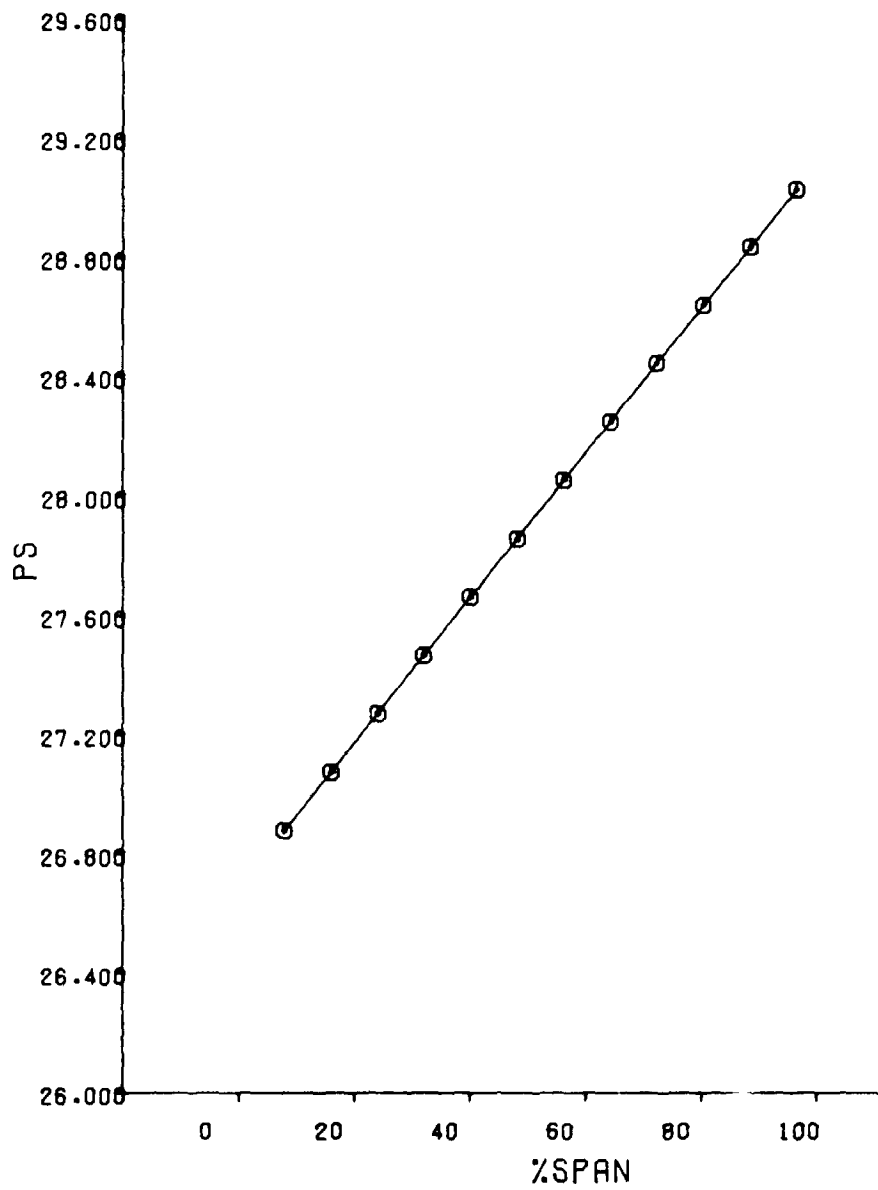


Figure B-7 Average Static Pressure Versus Span (Point 2)

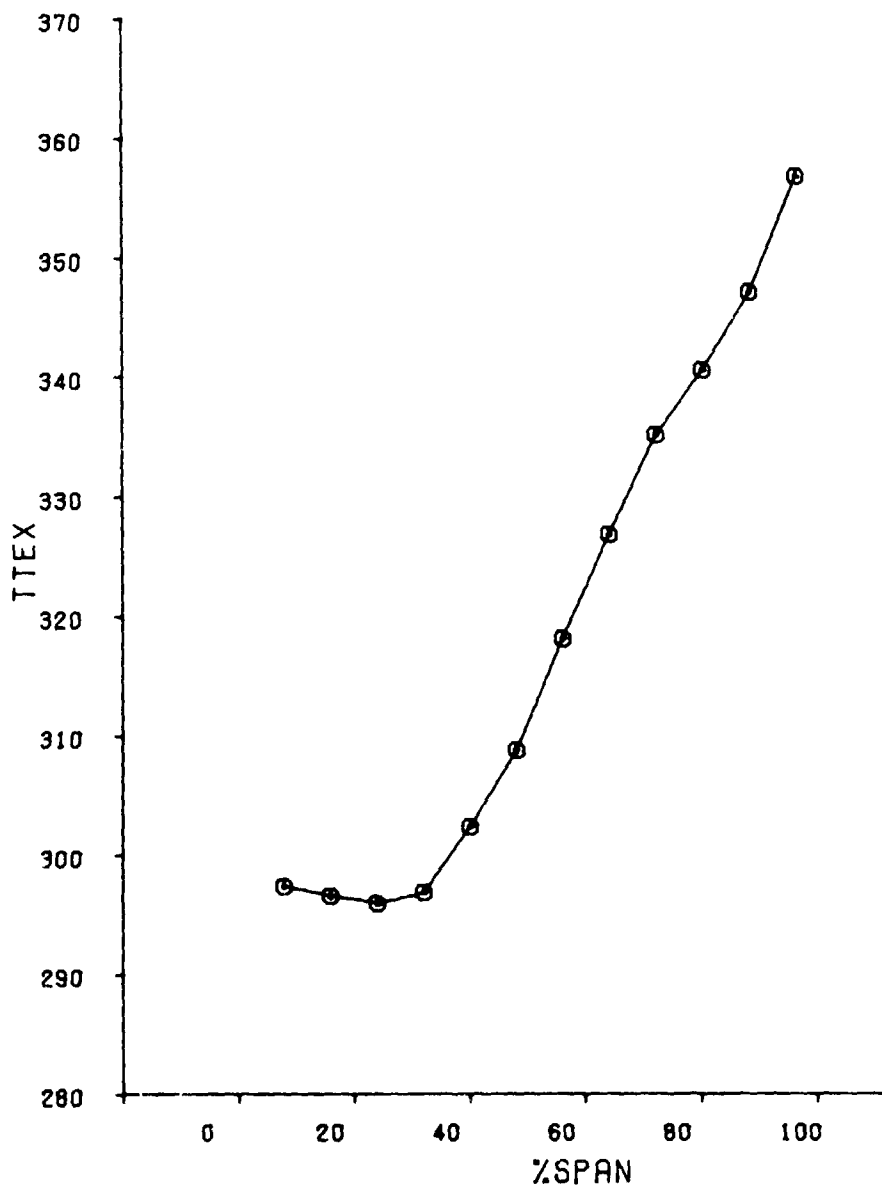


Figure B-8 Average Total Temperature Versus Span (Point 2)

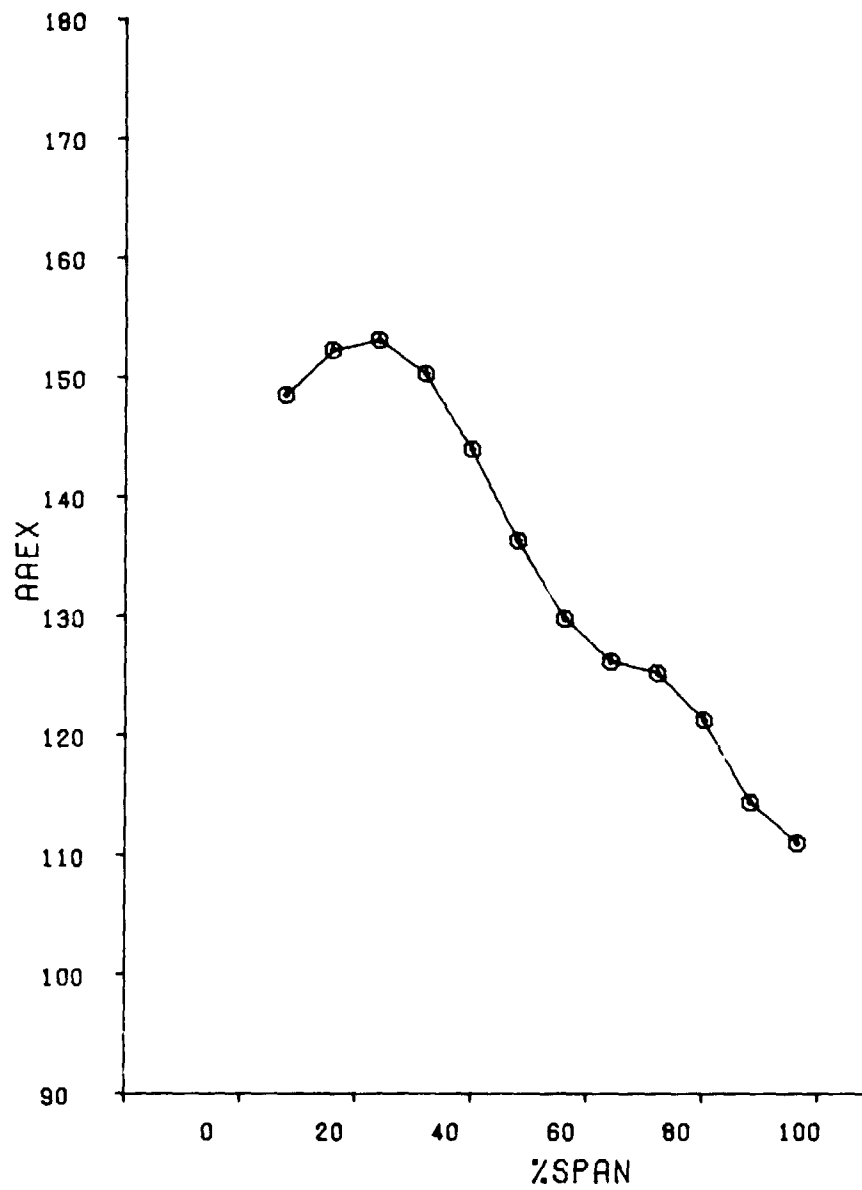


Figure B-9 Average Air Angle Versus Span (Point 2)

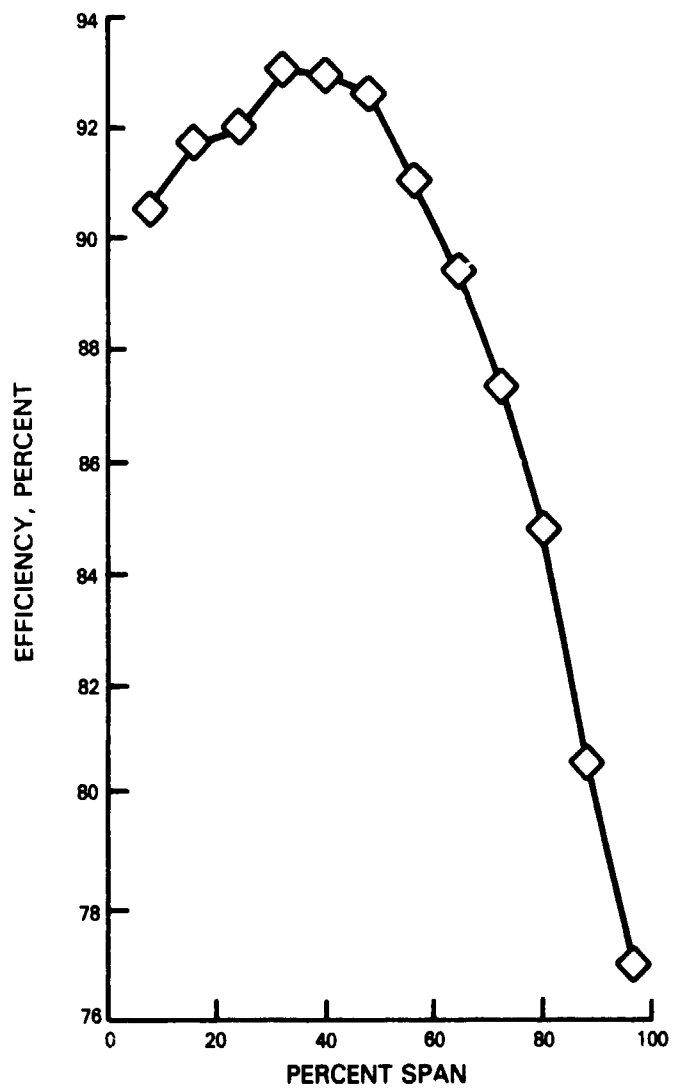


Figure B-10 Efficiency Versus Span (Point 2)

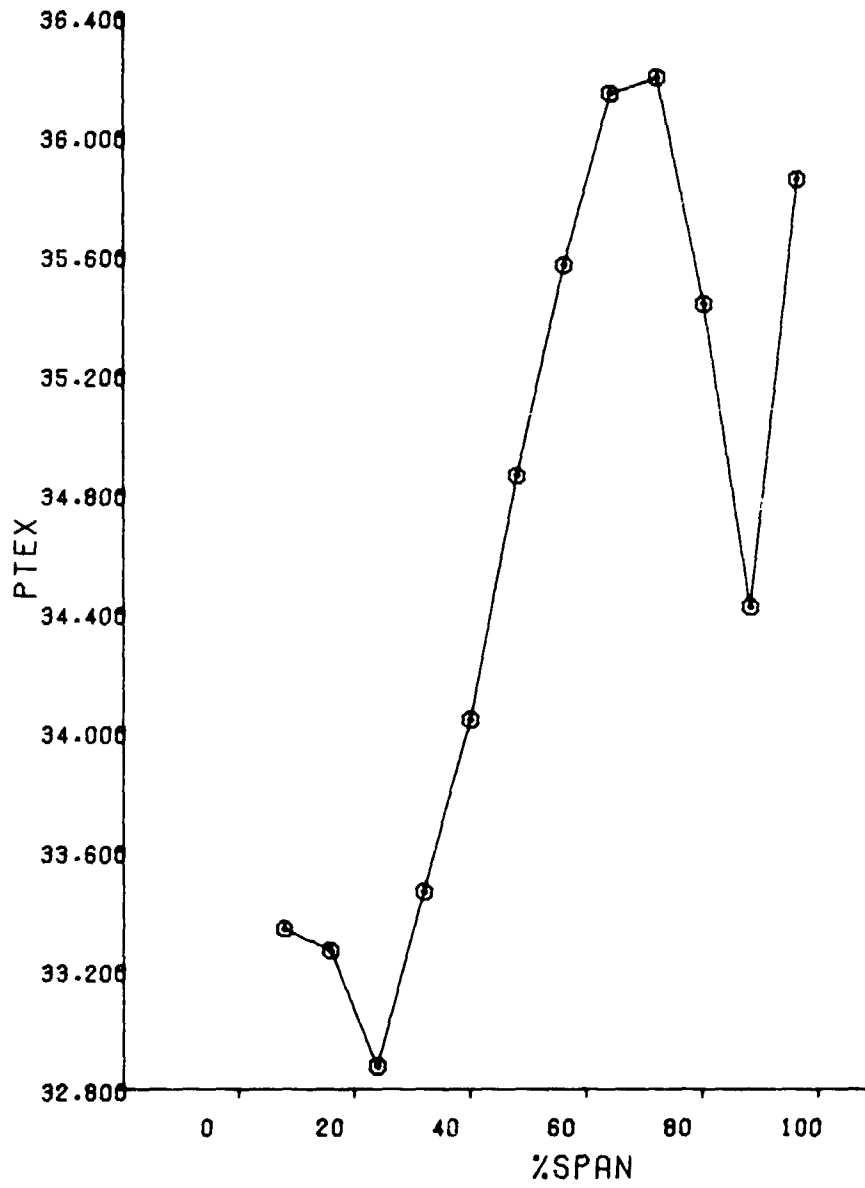


Figure B-11 Average Total Pressure Versus Span (Point 3)

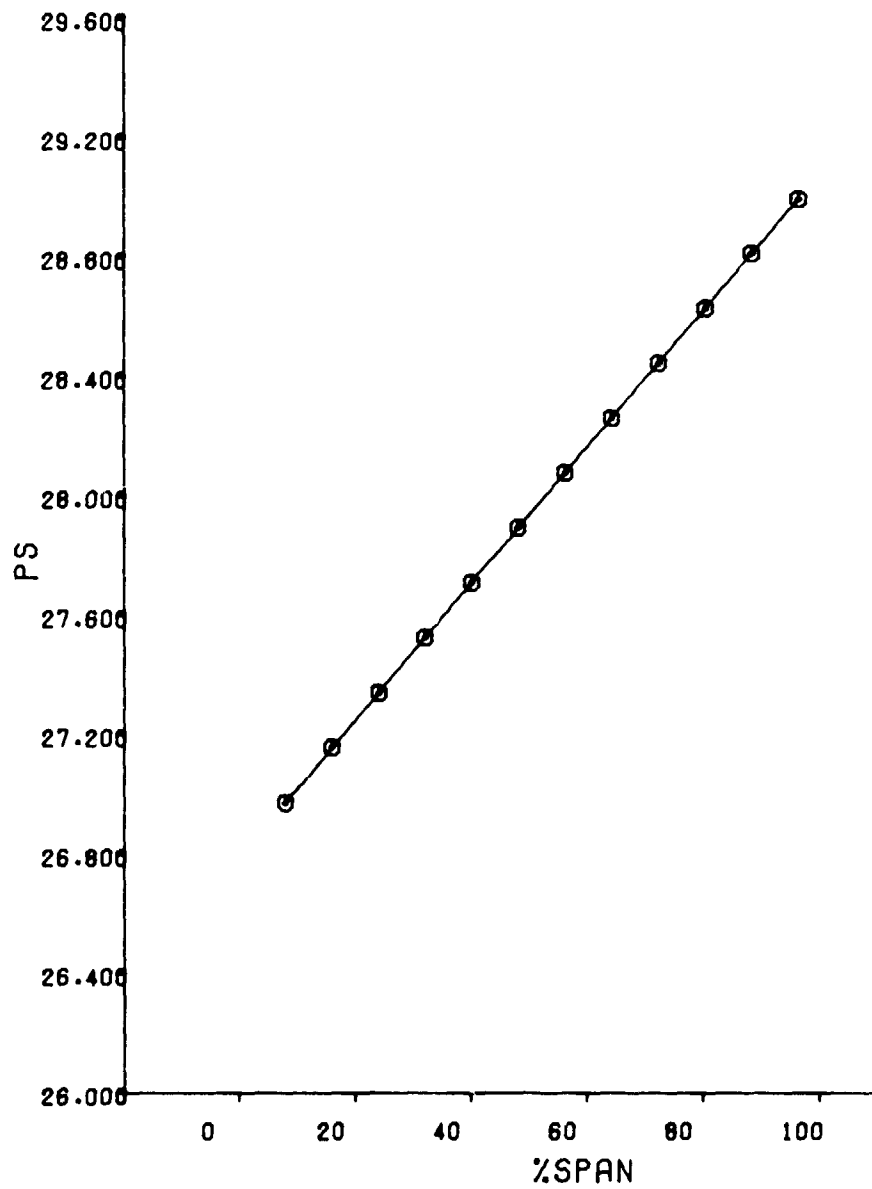


Figure B-12 Average Static Pressure Versus Span (Point 3)

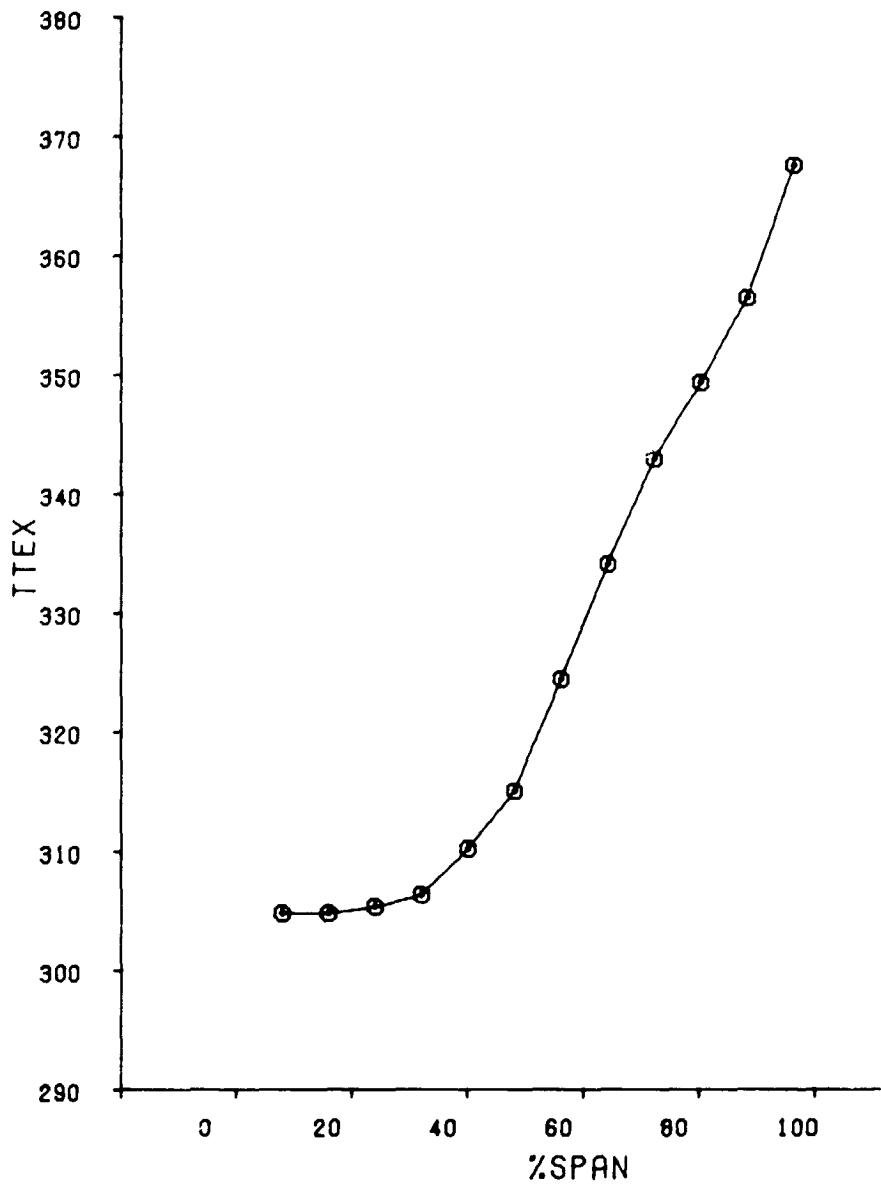


Figure B-13 Average Total Temperature Versus Span (Point 3)

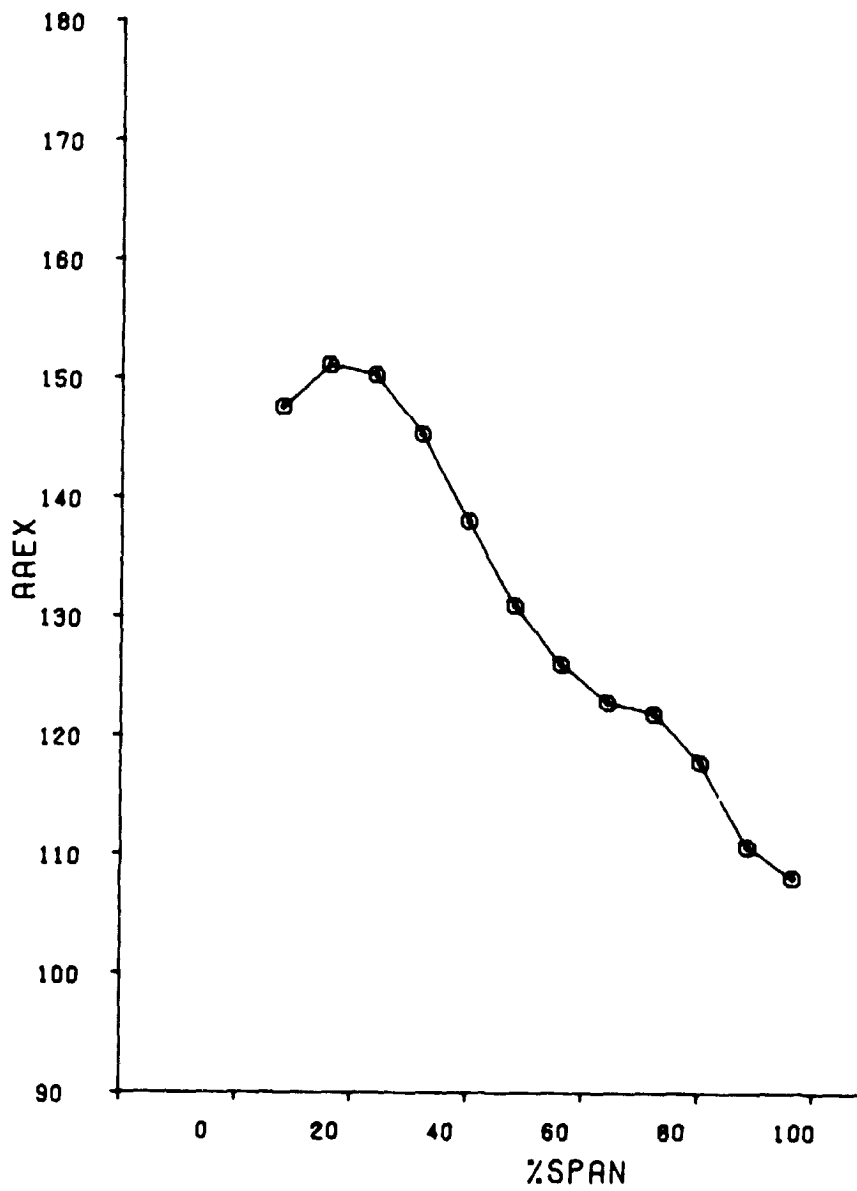


Figure B-14 Average Air Angle Versus Span (Point 3)

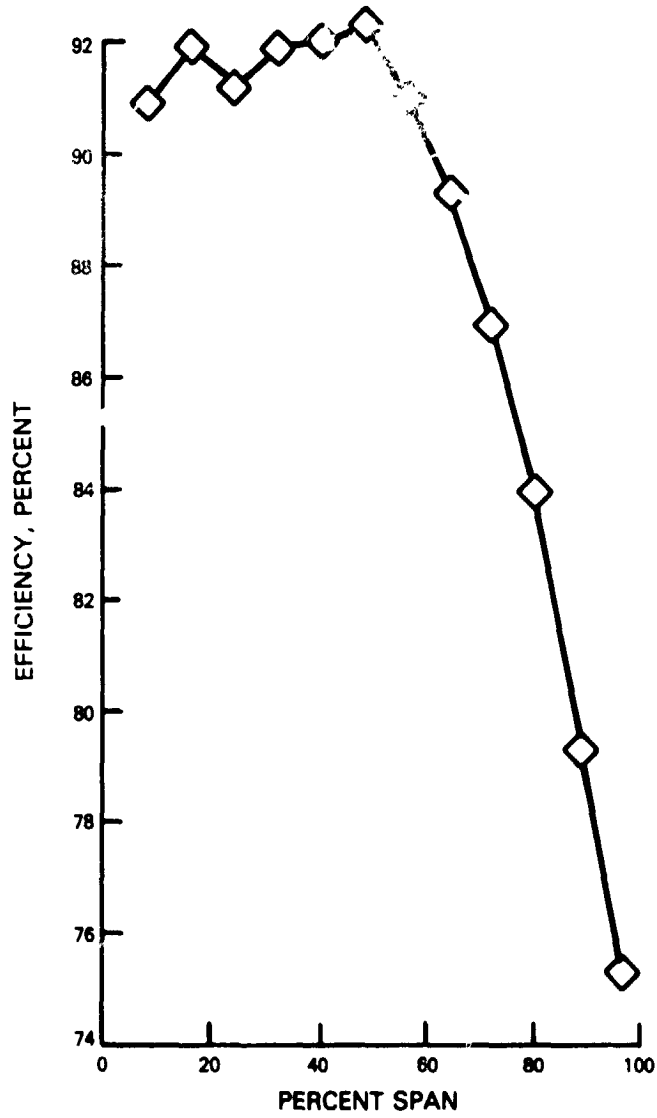


Figure B-15 Efficiency Versus Span (Point 3)

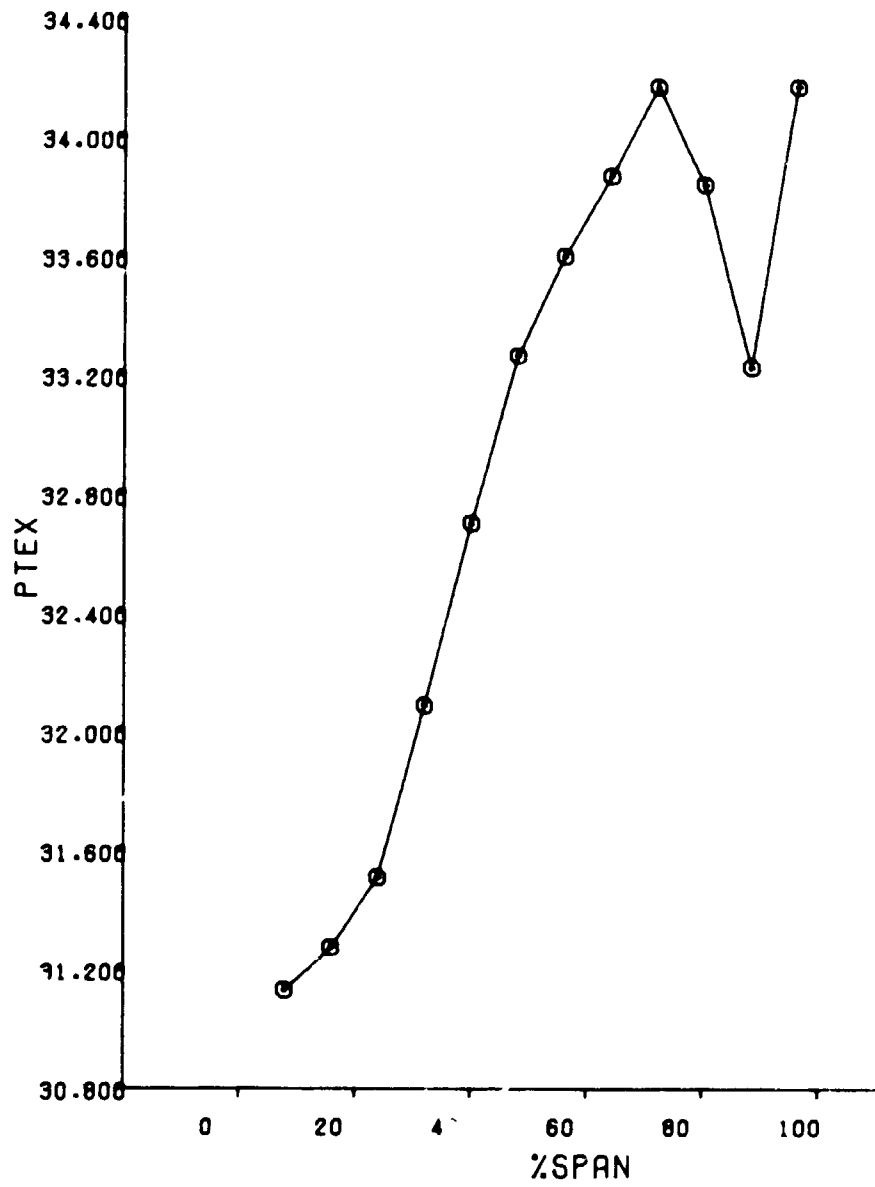


Figure B-16 Average Total Pressure Versus Span (Point 4)

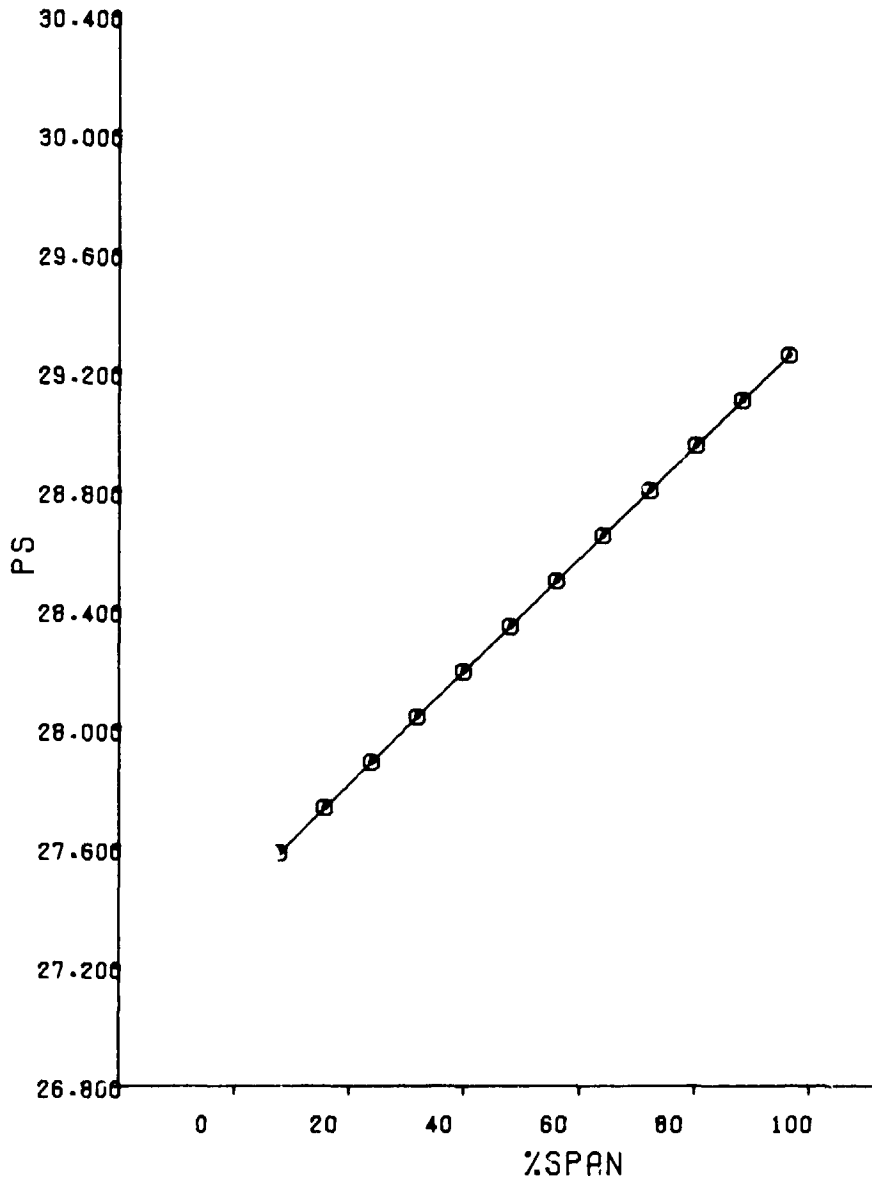


Figure B-17 Average Static Pressure Versus Span (Point 4)

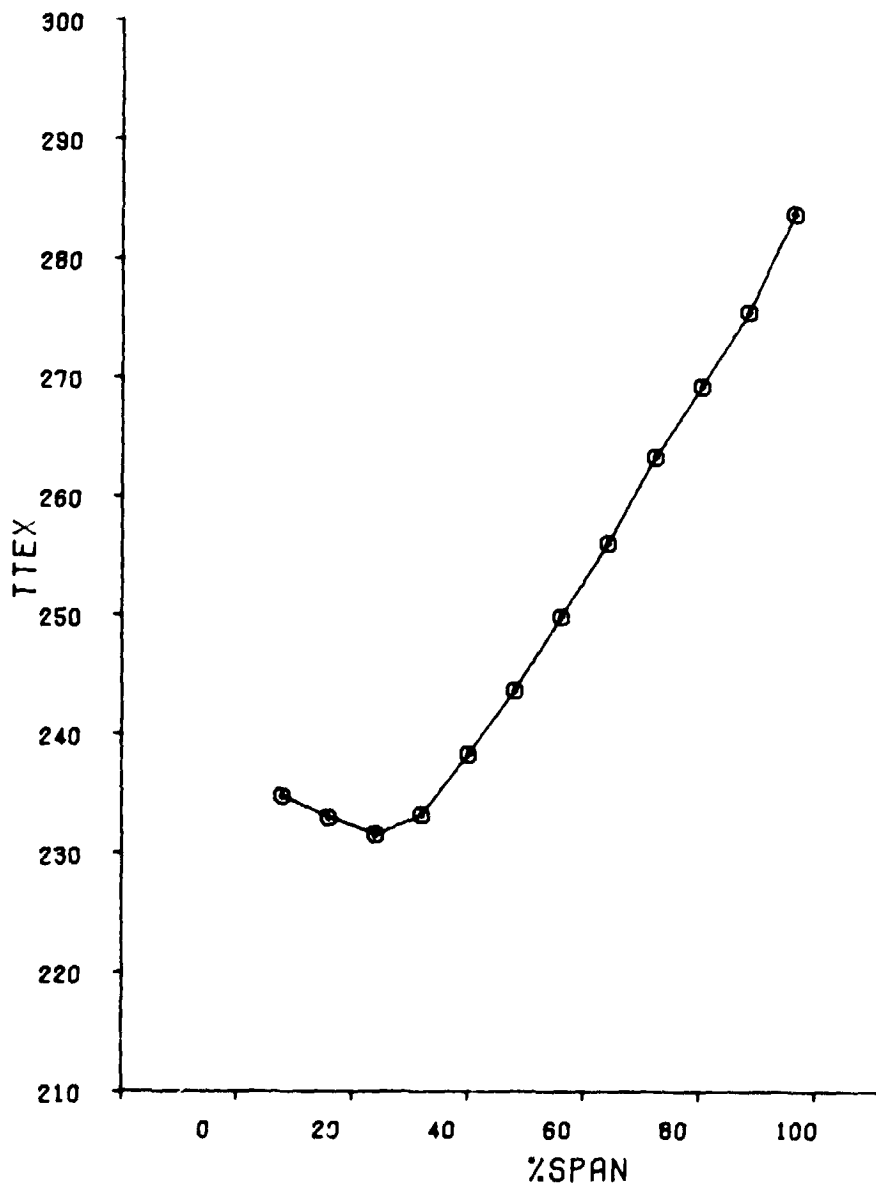


Figure B-18 Average Total Temperature Versus Span (Point 4)

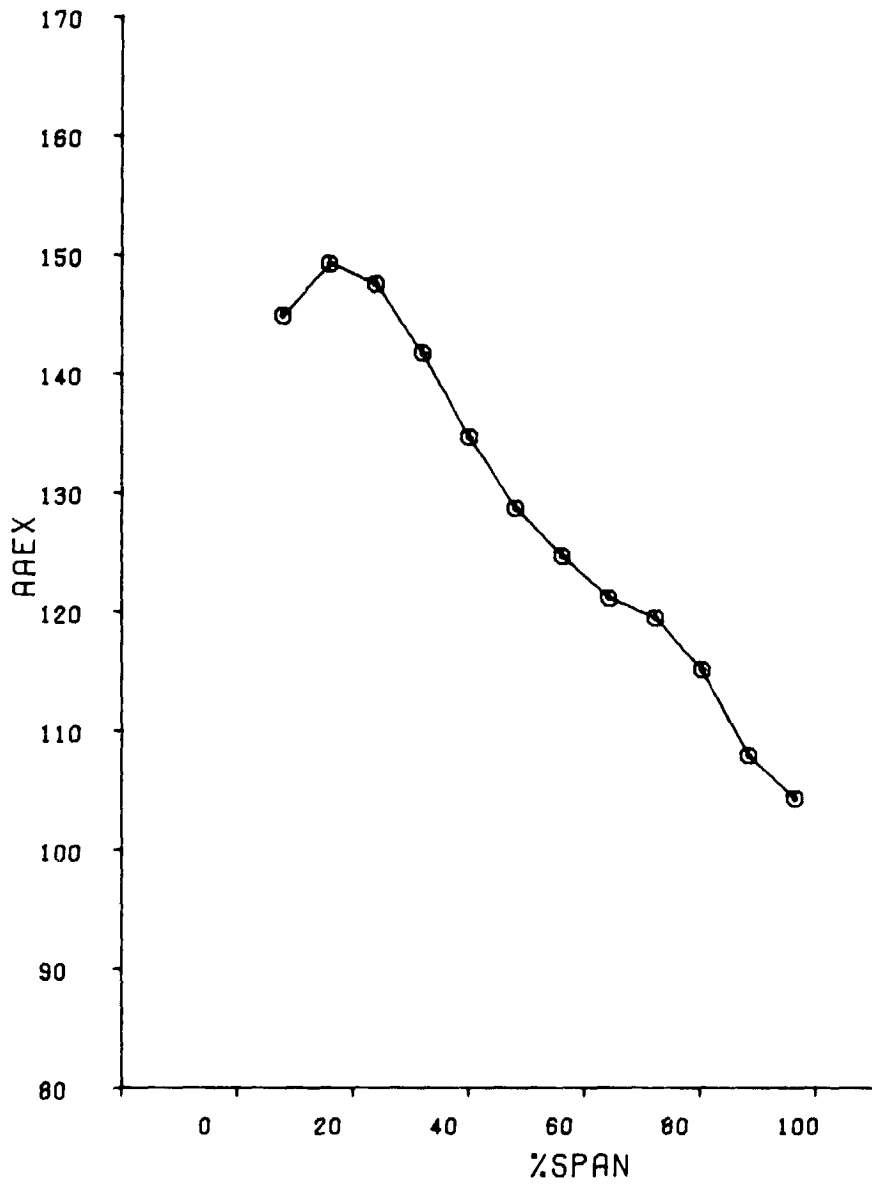


Figure B-19 Average Air Angle Versus Span (Point 4)

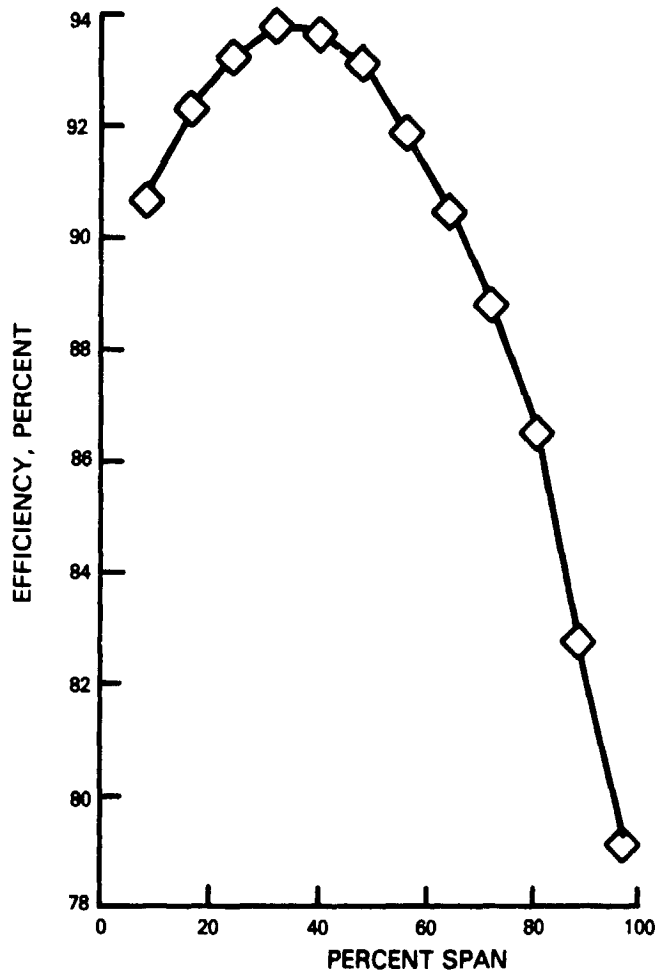


Figure B-20 Efficiency Versus Span (Point 4)

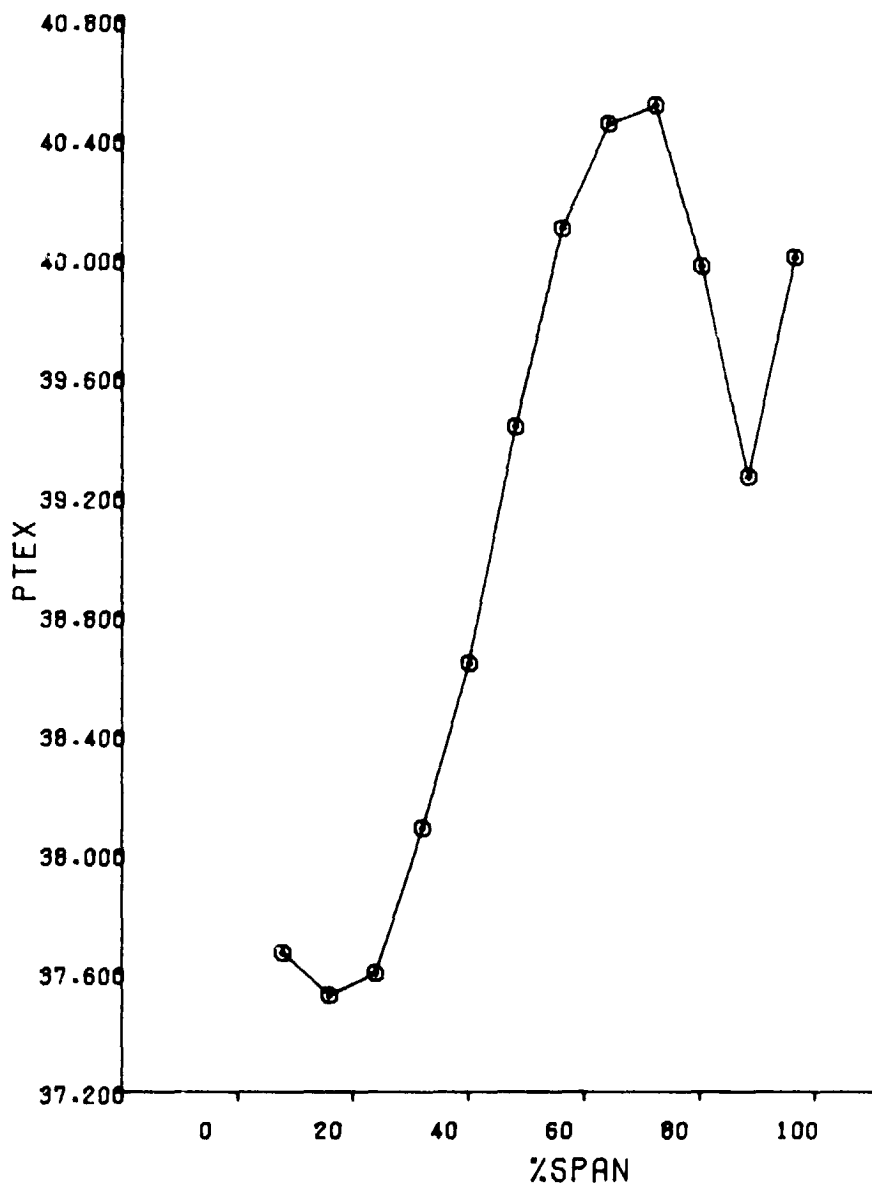


Figure B-21 Average Total Pressure Versus Span (Point 5)

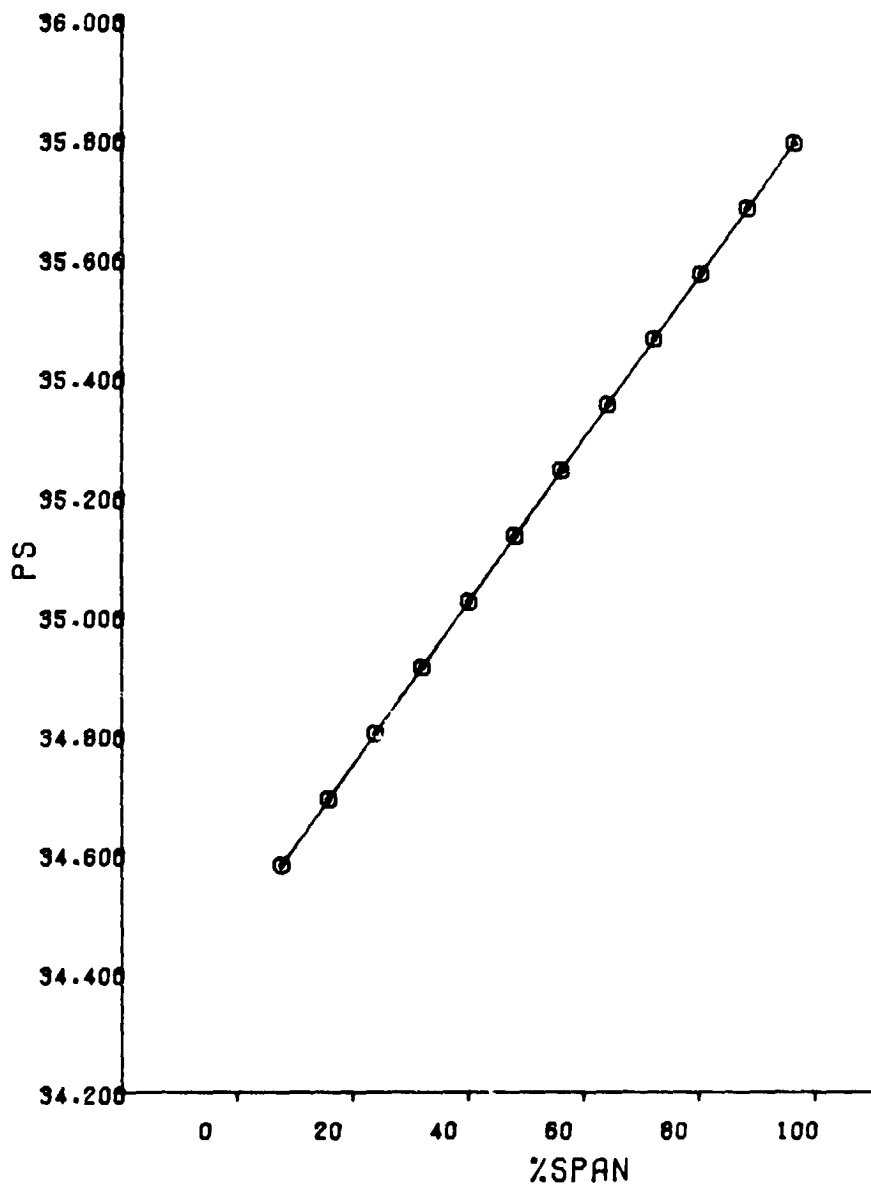


Figure B-22 Average Static Pressure Versus Span (Point 5)

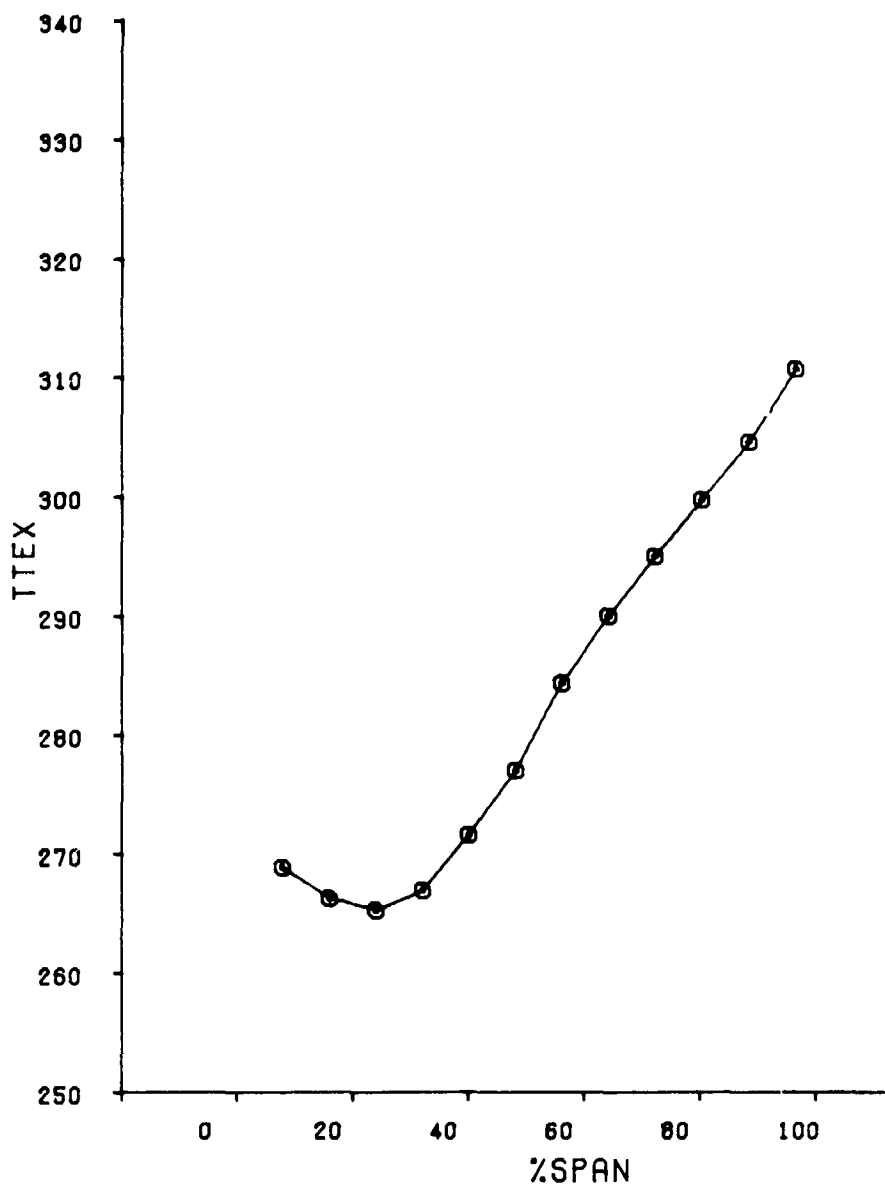


Figure B-23 Average Total Temperature Versus Span (r nt 5)

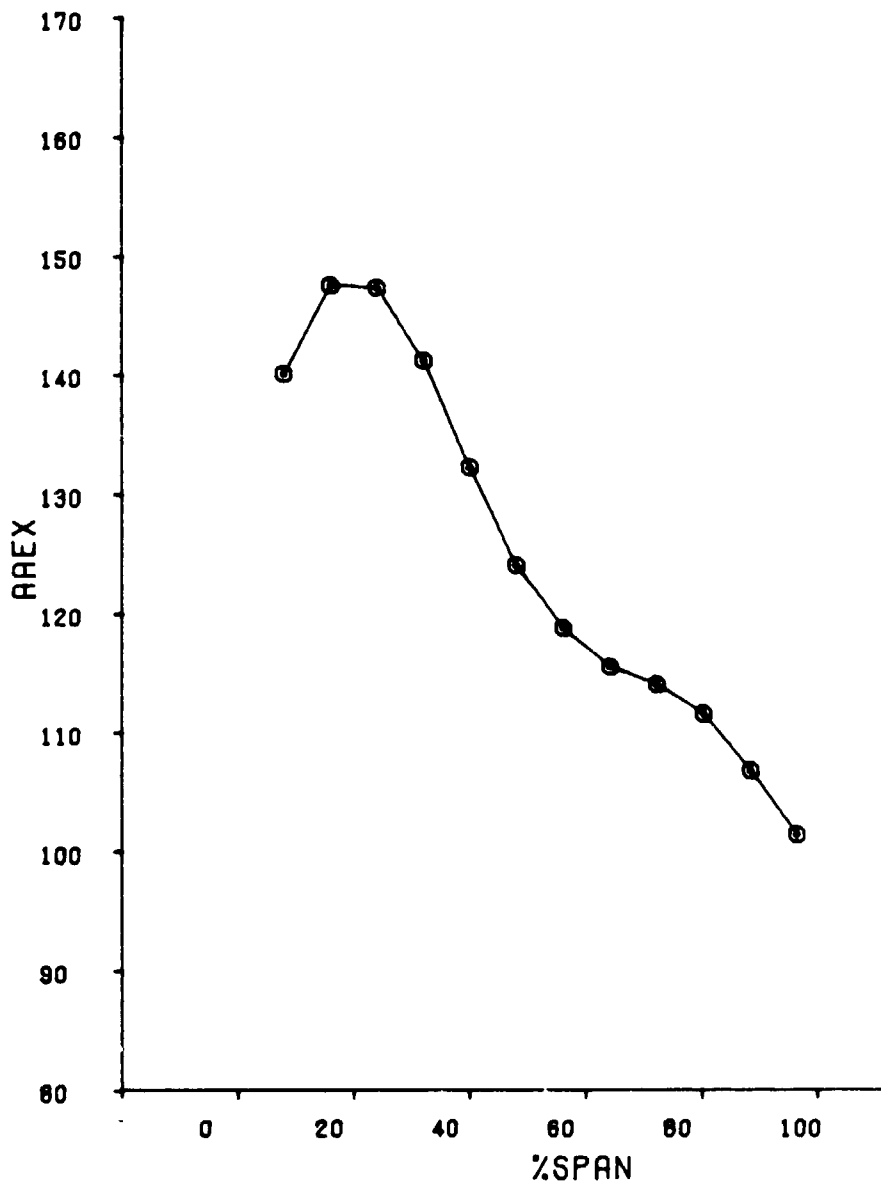


Figure B-24 Average Air Angle Versus Span (Point 5)

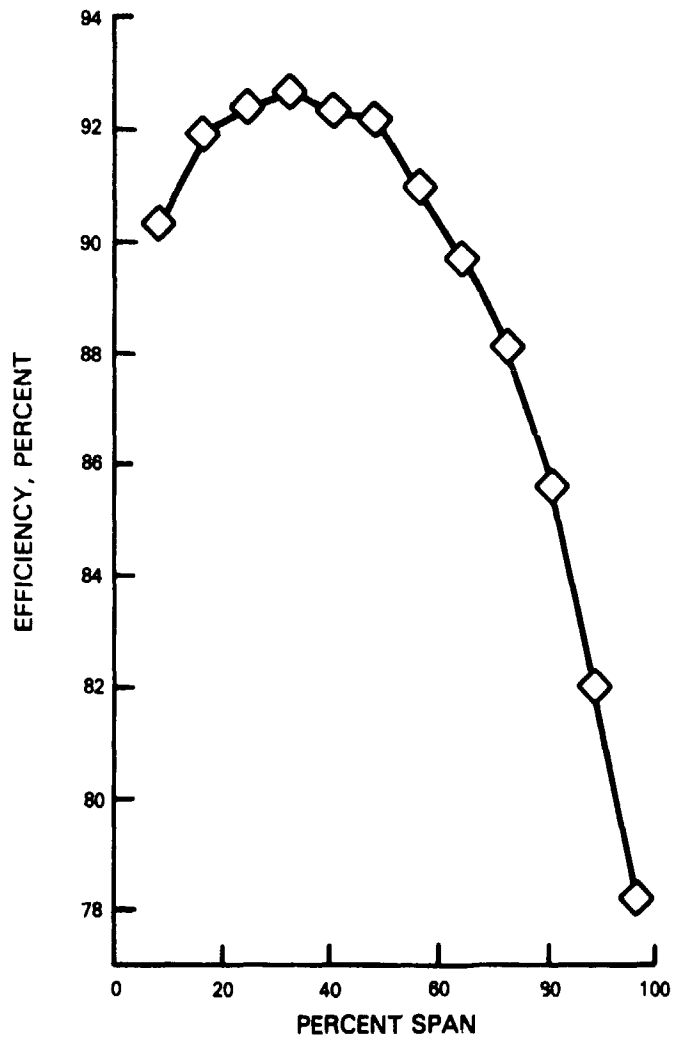


Figure B-25 Efficiency Versus Span (Point 5)

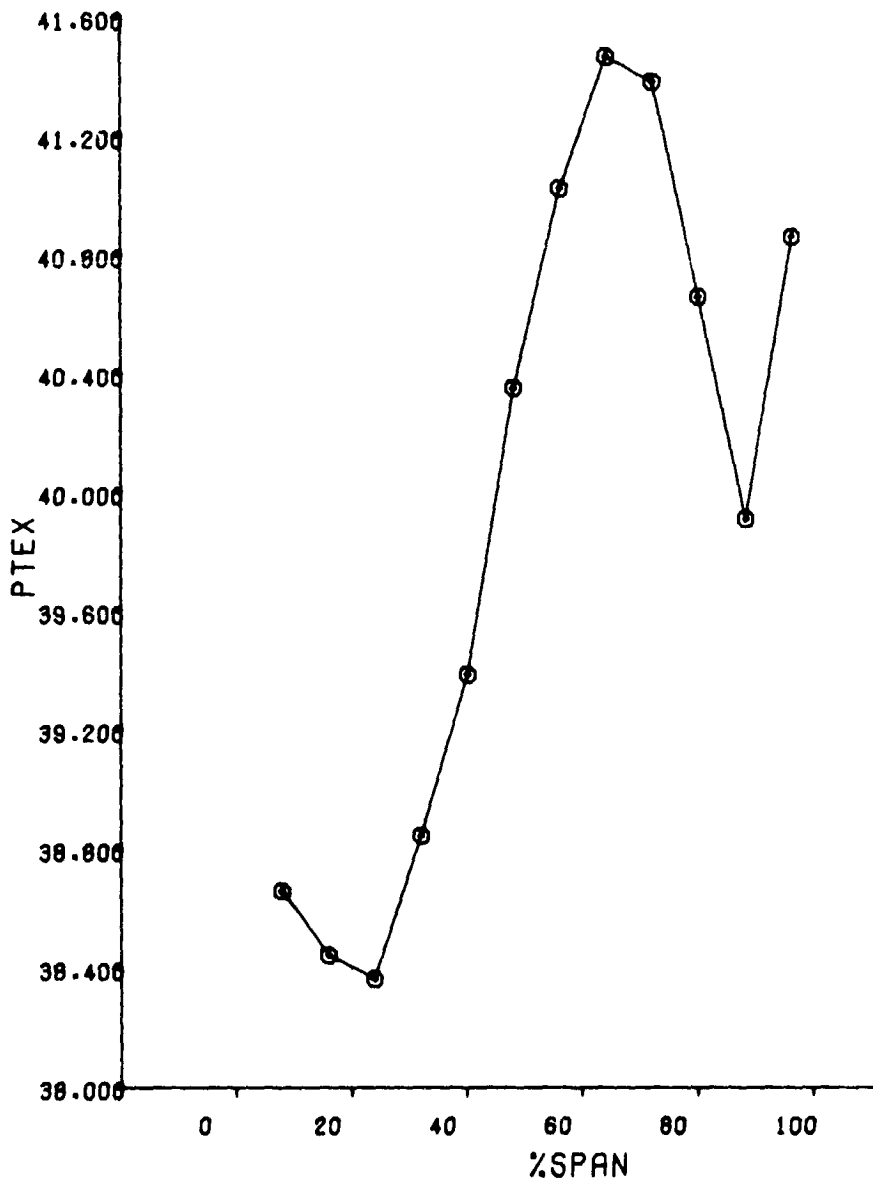


Figure B-26 Average Total Pressure Versus Span (Point 6)

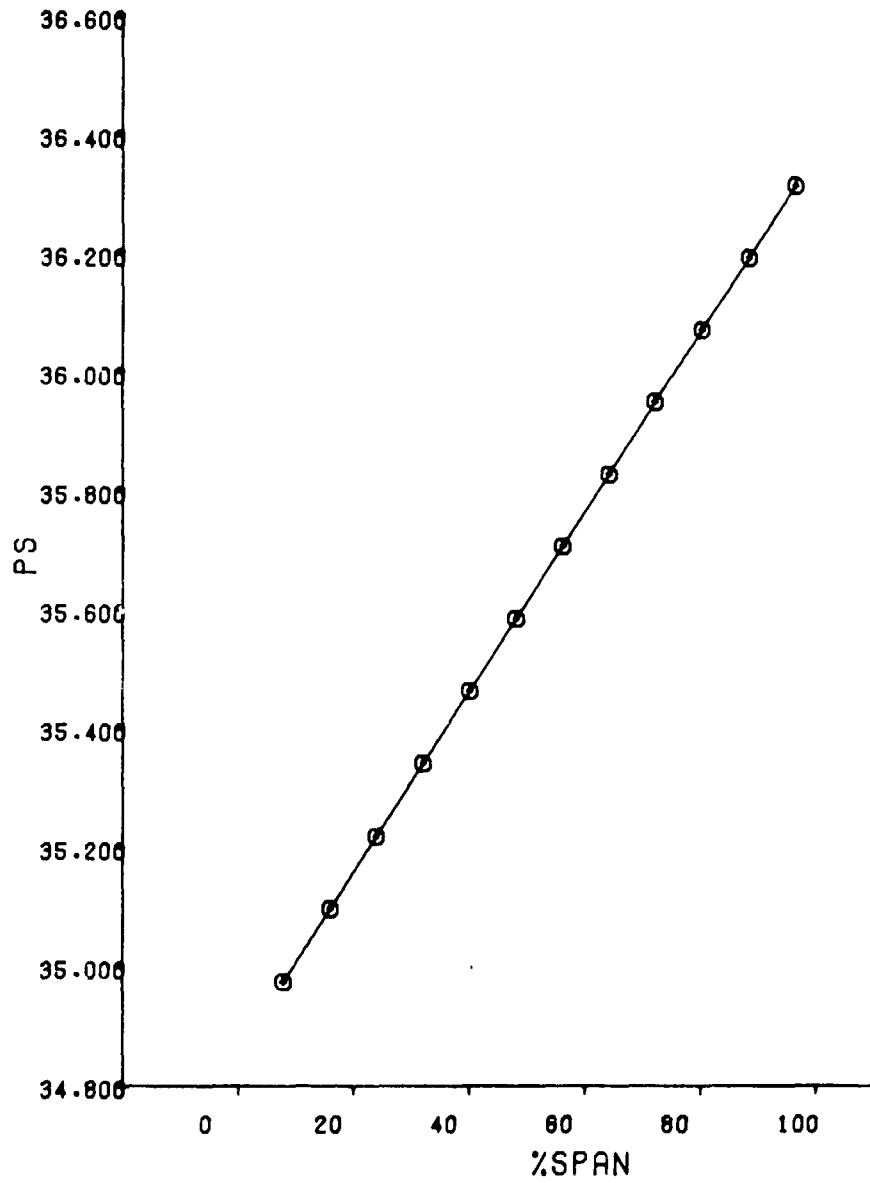


Figure B-27 Average Static Pressure Versus Span (Point 6)

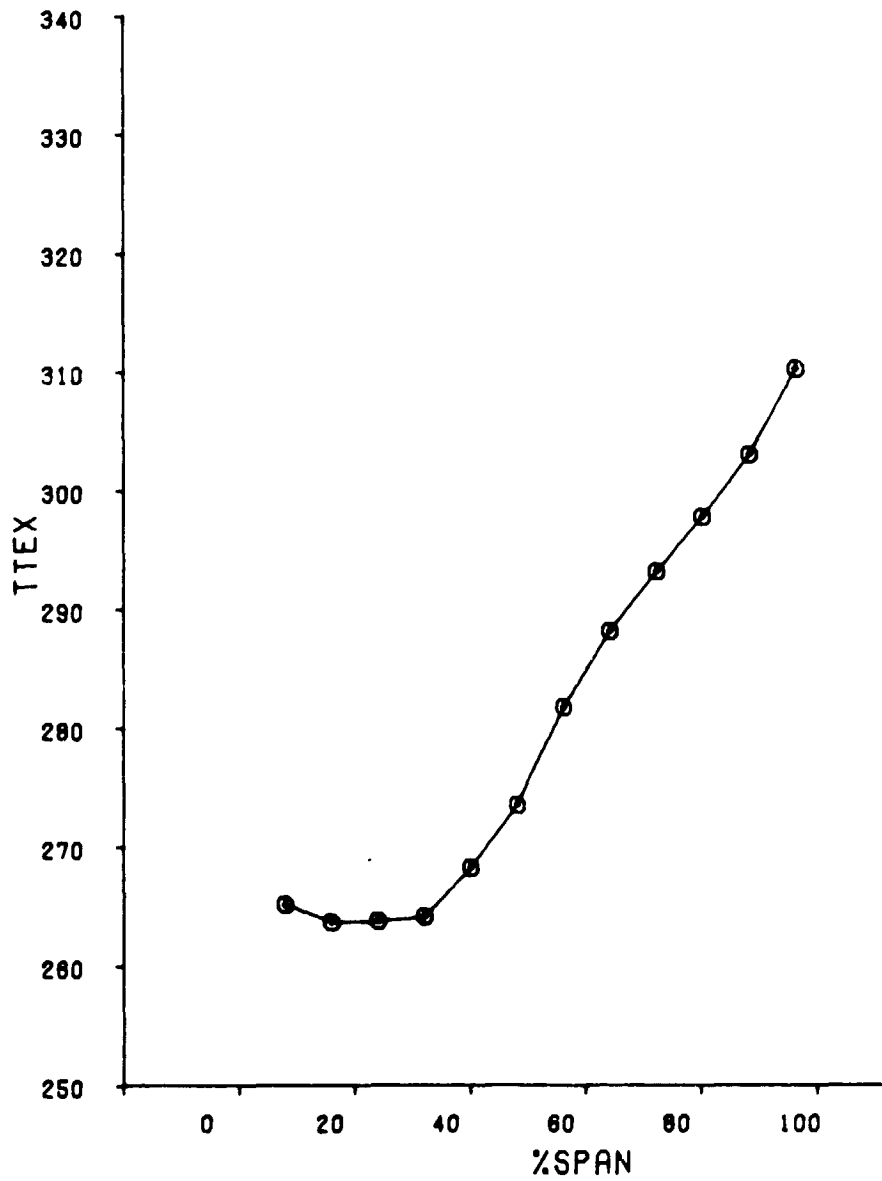


Figure B-28 Average Total Temperature Versus Span (Point 6)

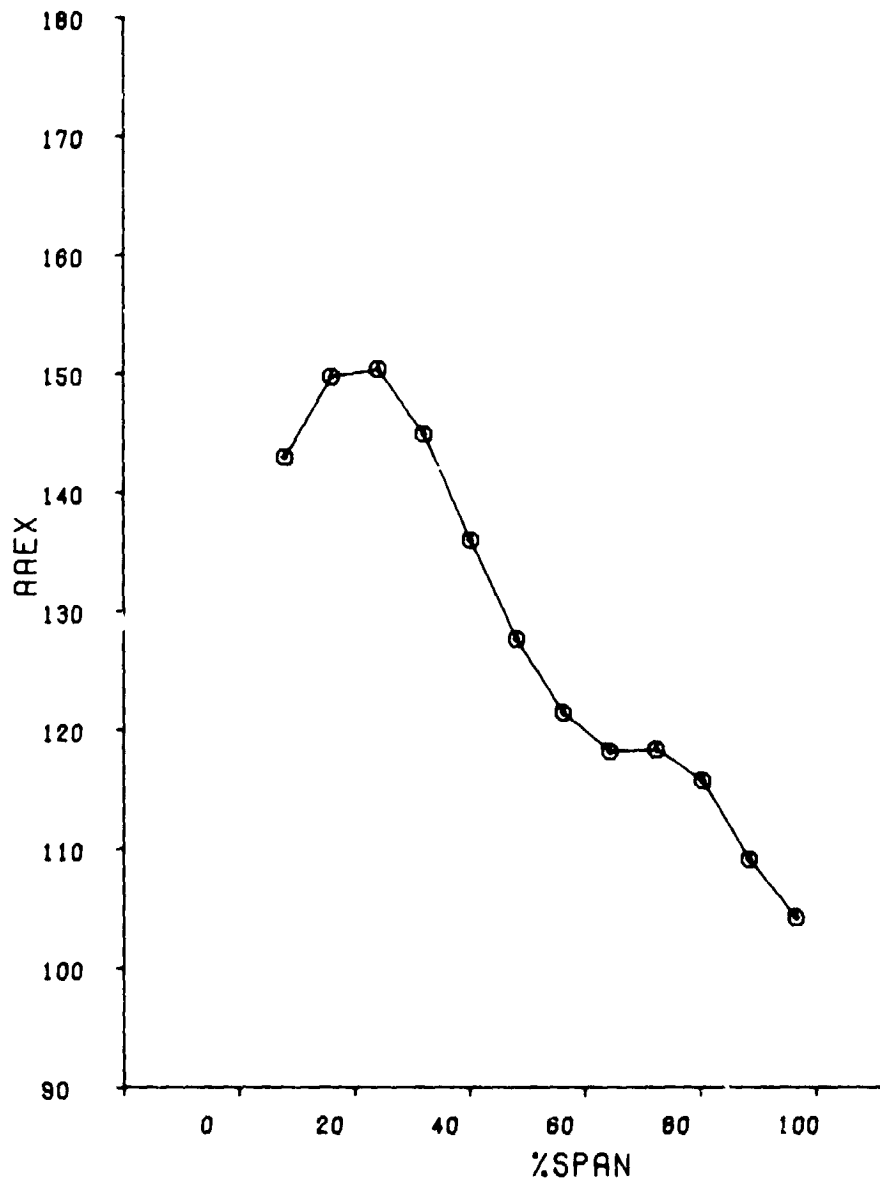


Figure B-29 Average Air Angle Versus Span (Point 6)

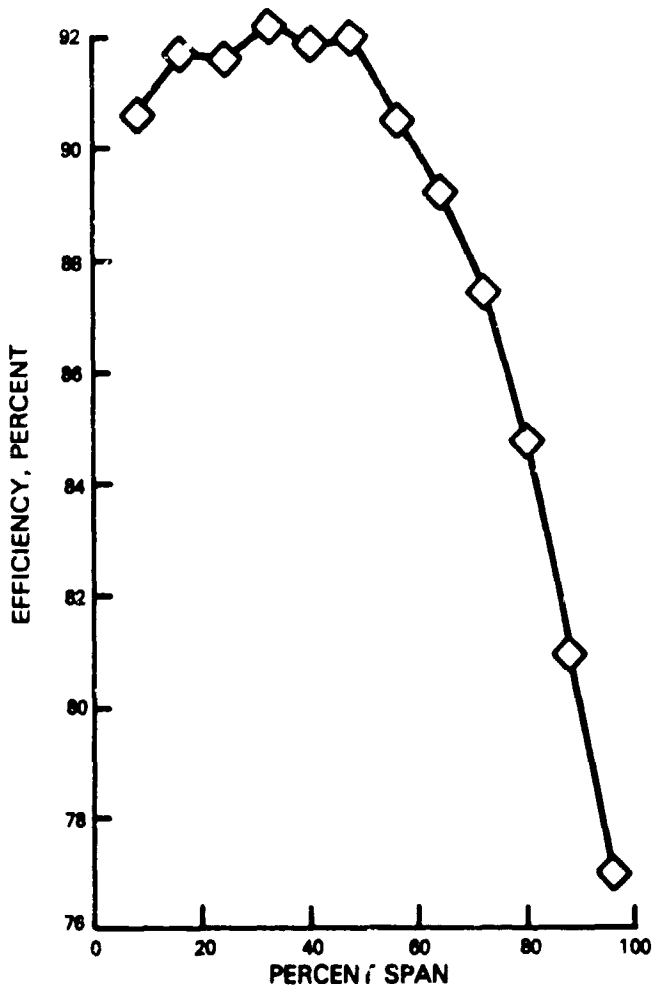


Figure B-30 Efficiency Versus Span (Point 6)

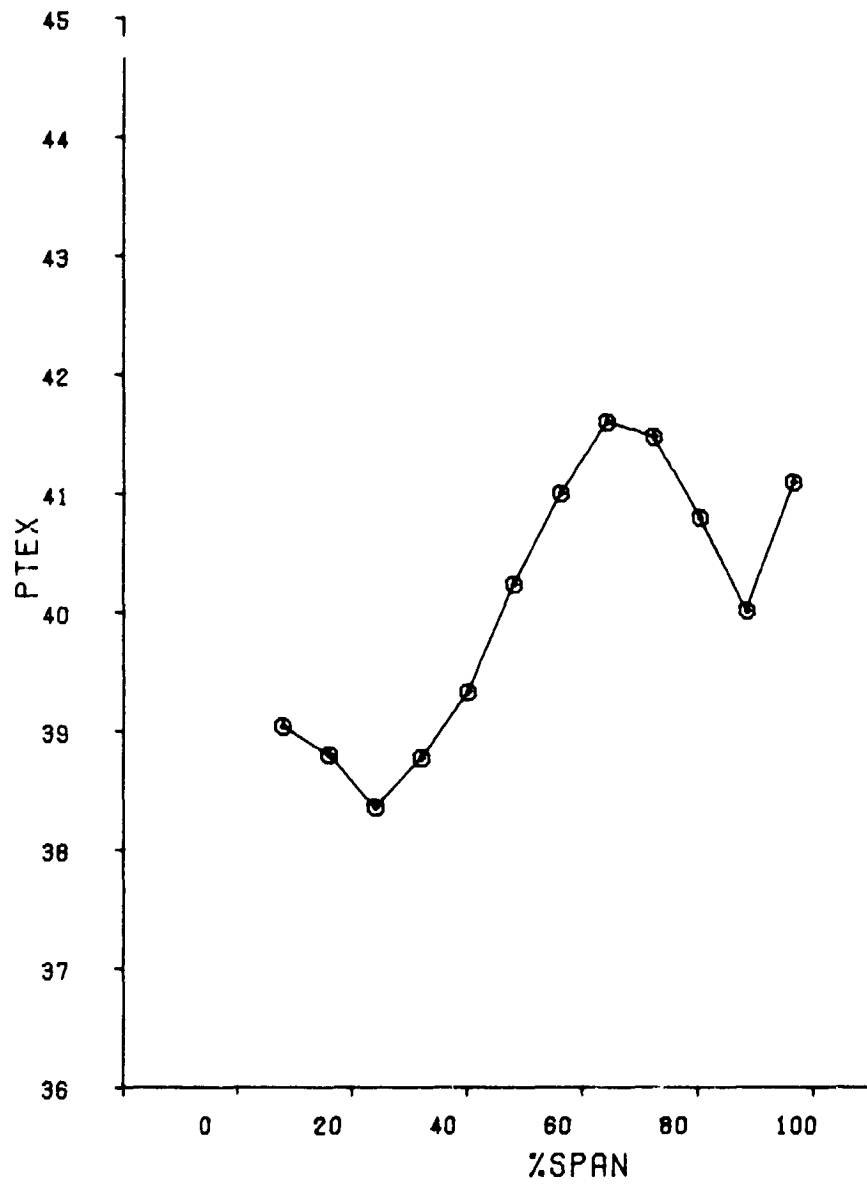


Figure B-31 Average Total Pressure Versus Span (Point 7)

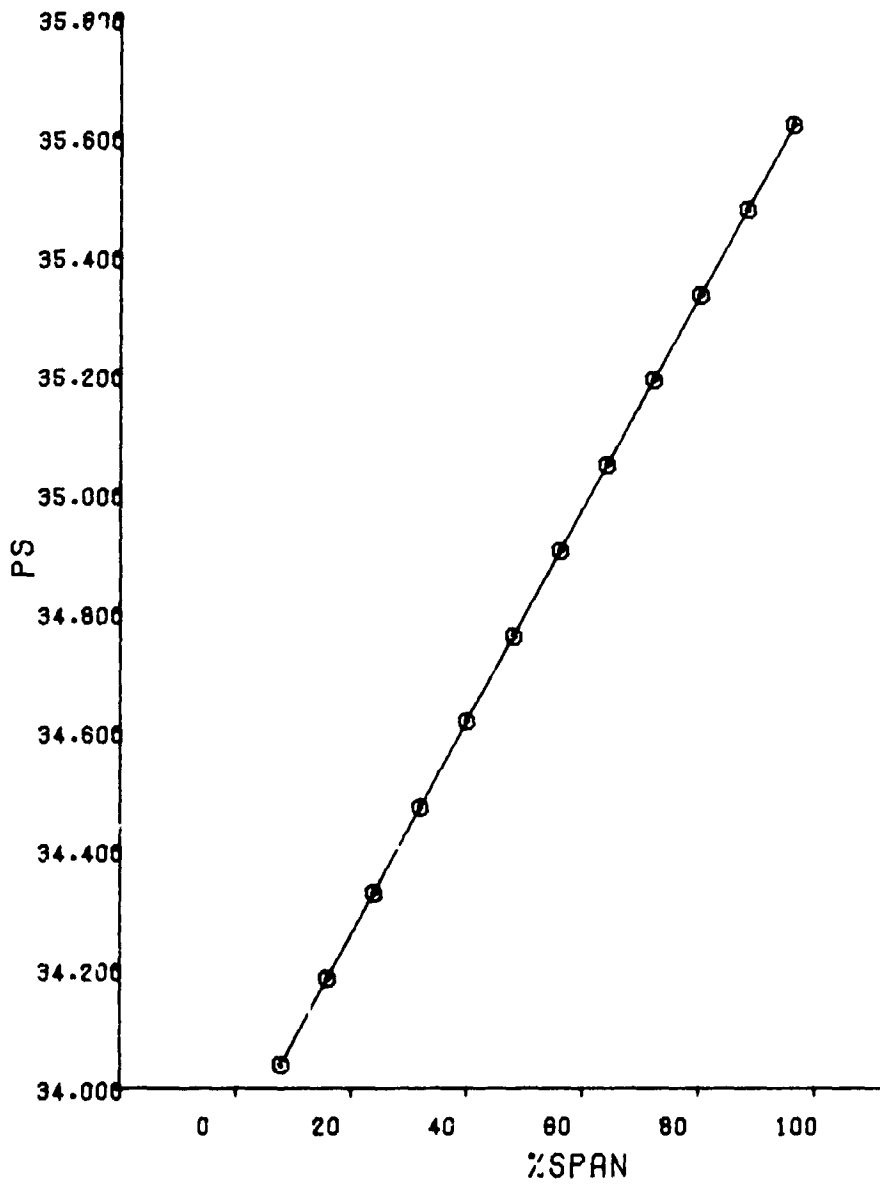


Figure B-32 Average Static Pressure Versus Span (Point 7)

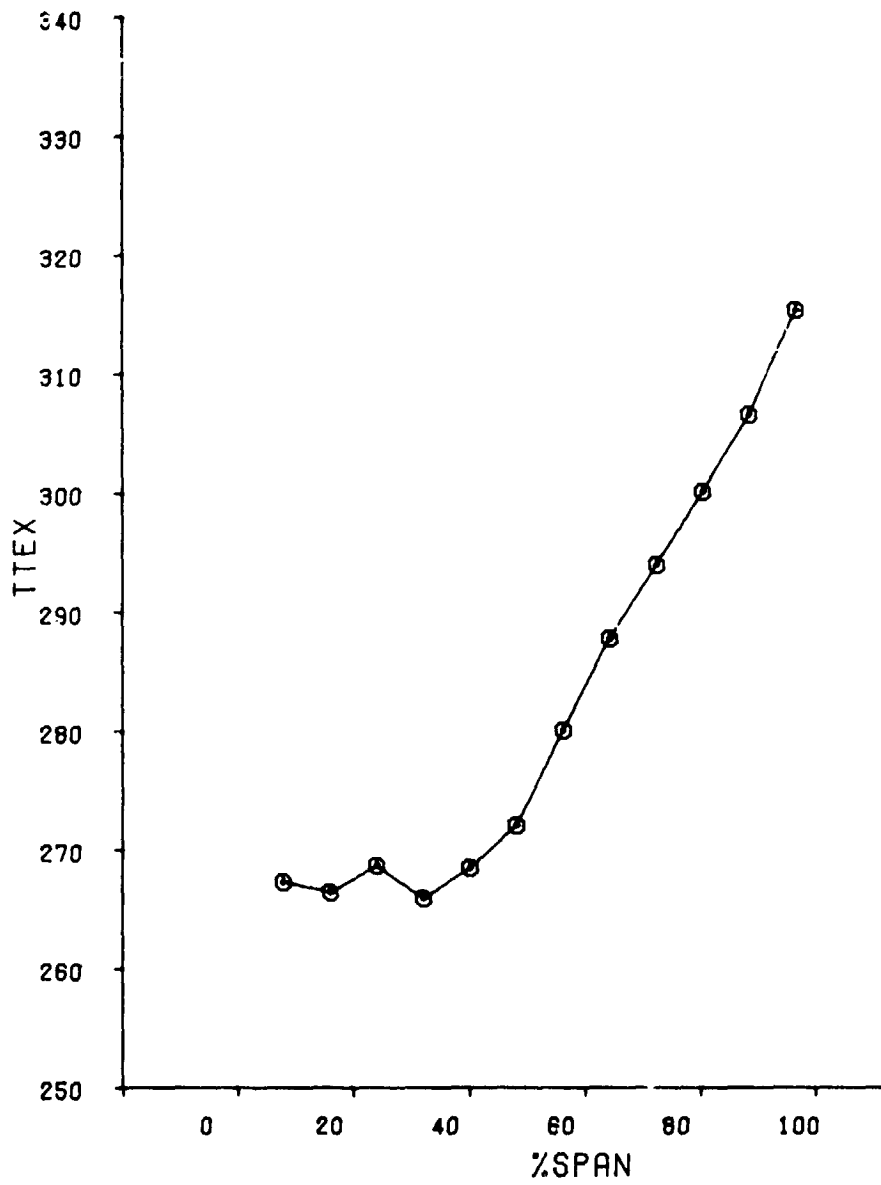


Figure B-33 Average Total Temperature Versus Span (Point 7)

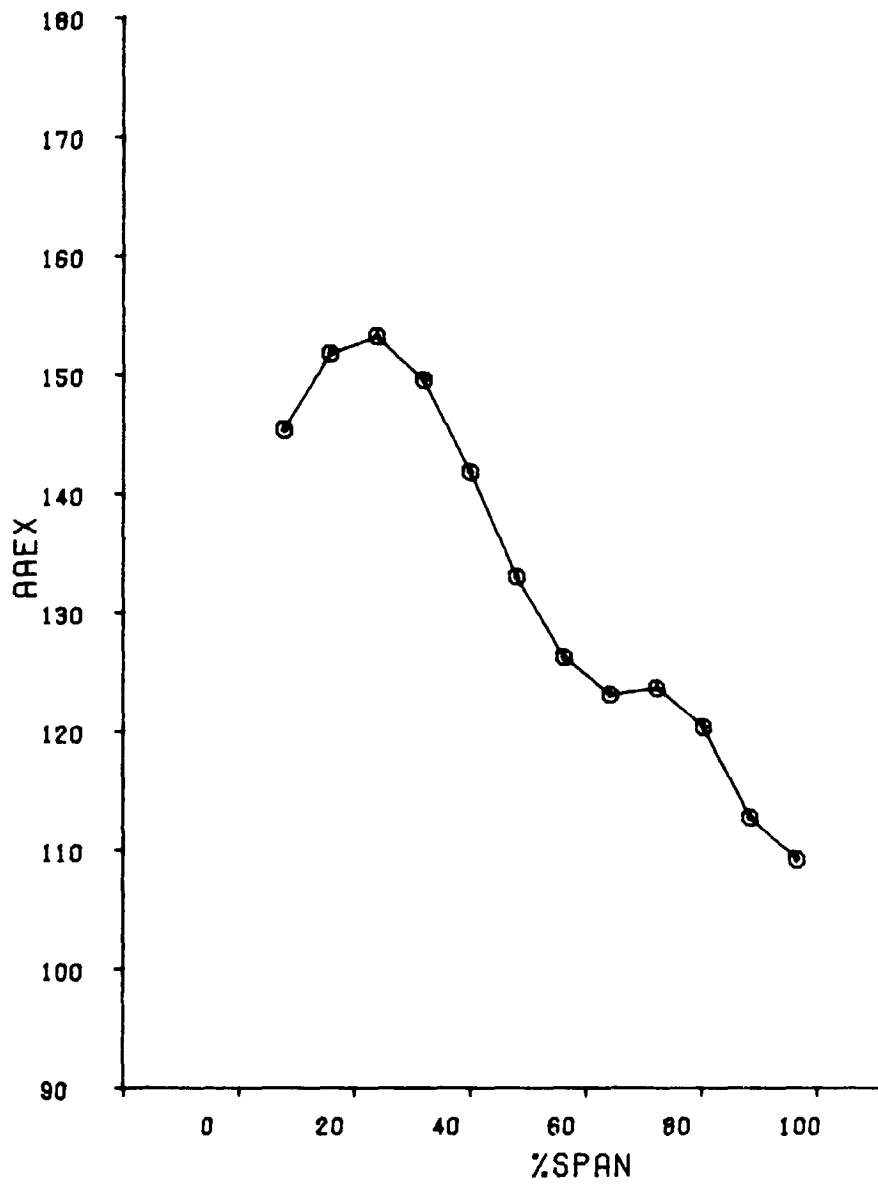


Figure B-34 Average Air Angle Versus Span (Point 7)

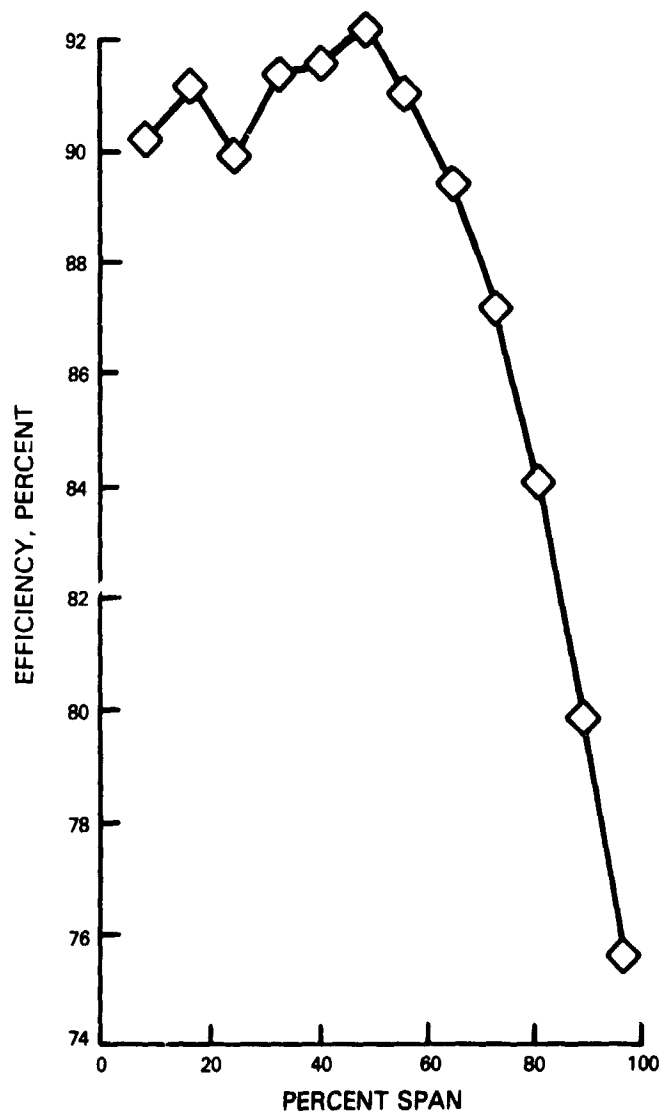


Figure B-35 Efficiency Versus Span (Point 7)

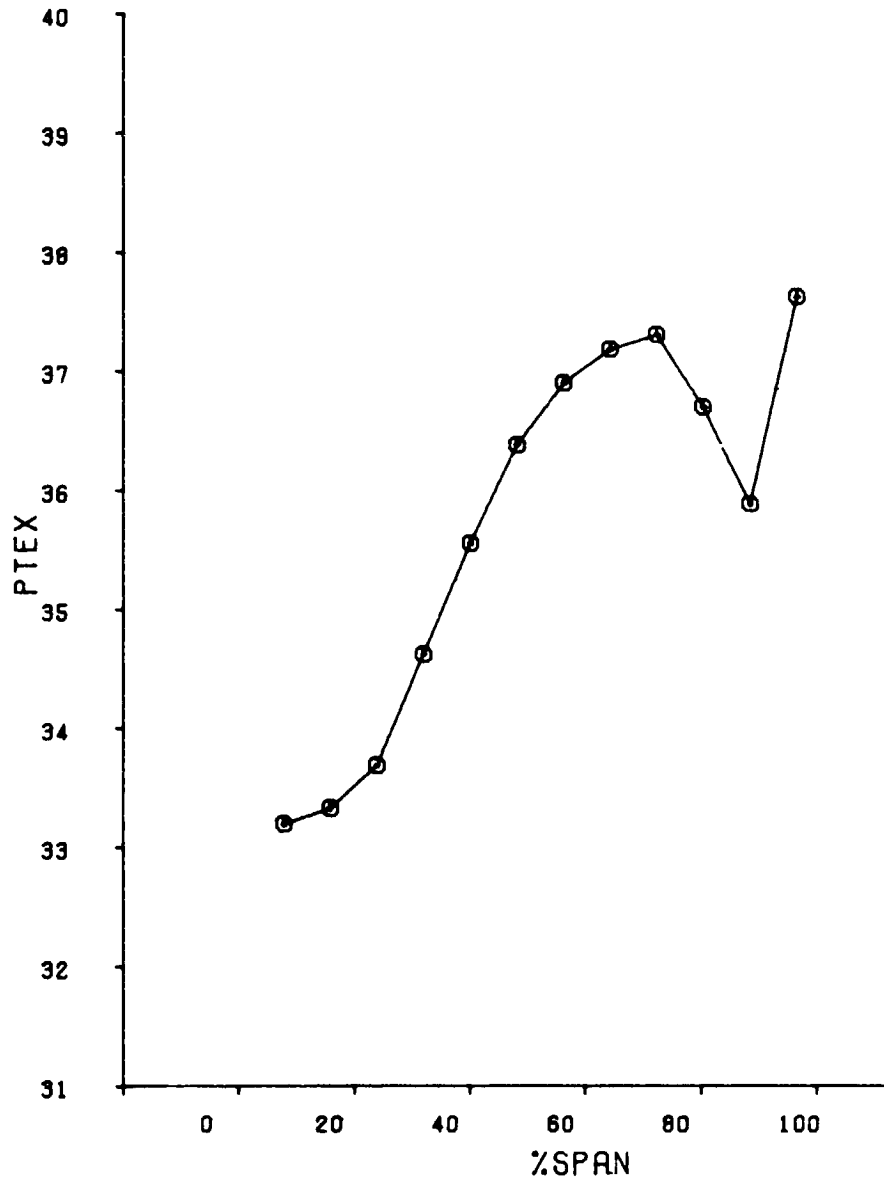


Figure B-36 Average Total Pressure Versus Span (Point 9)

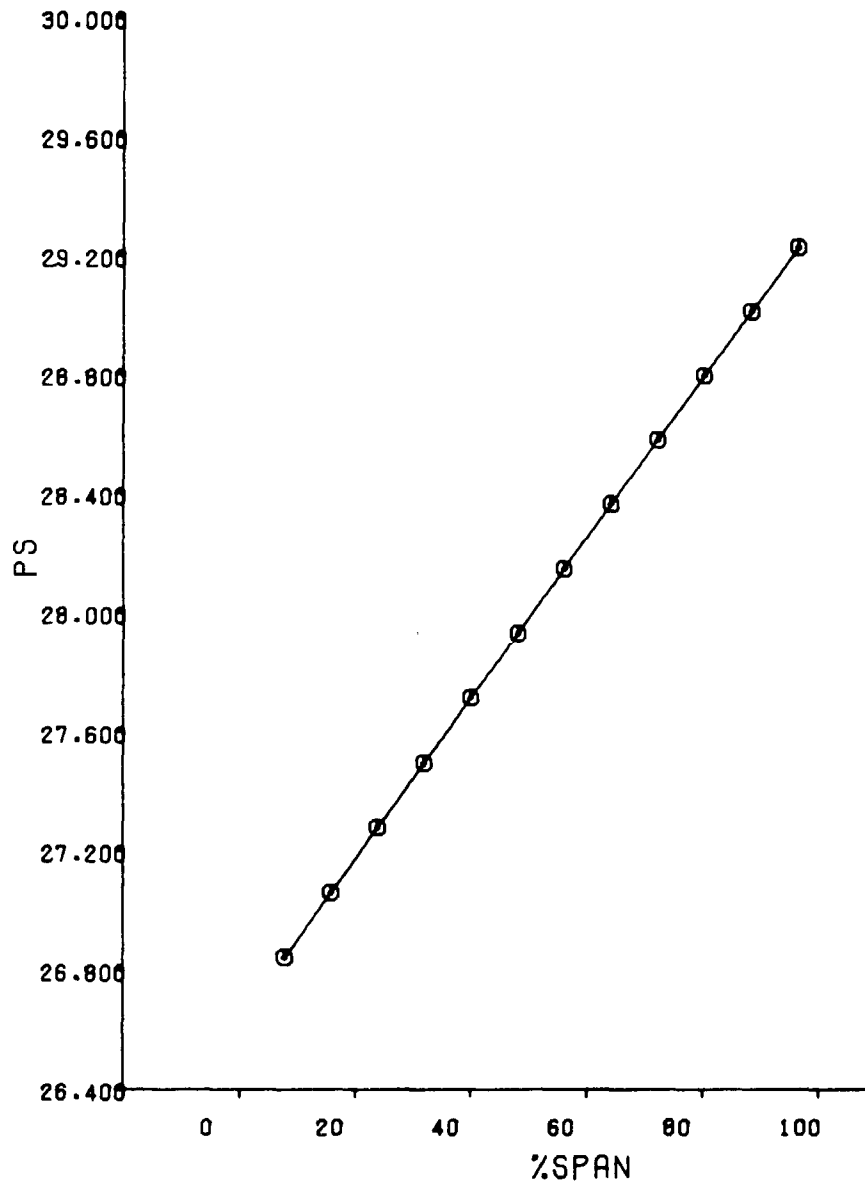


Figure B-37 Average Static Pressure Versus Span (Point 9)

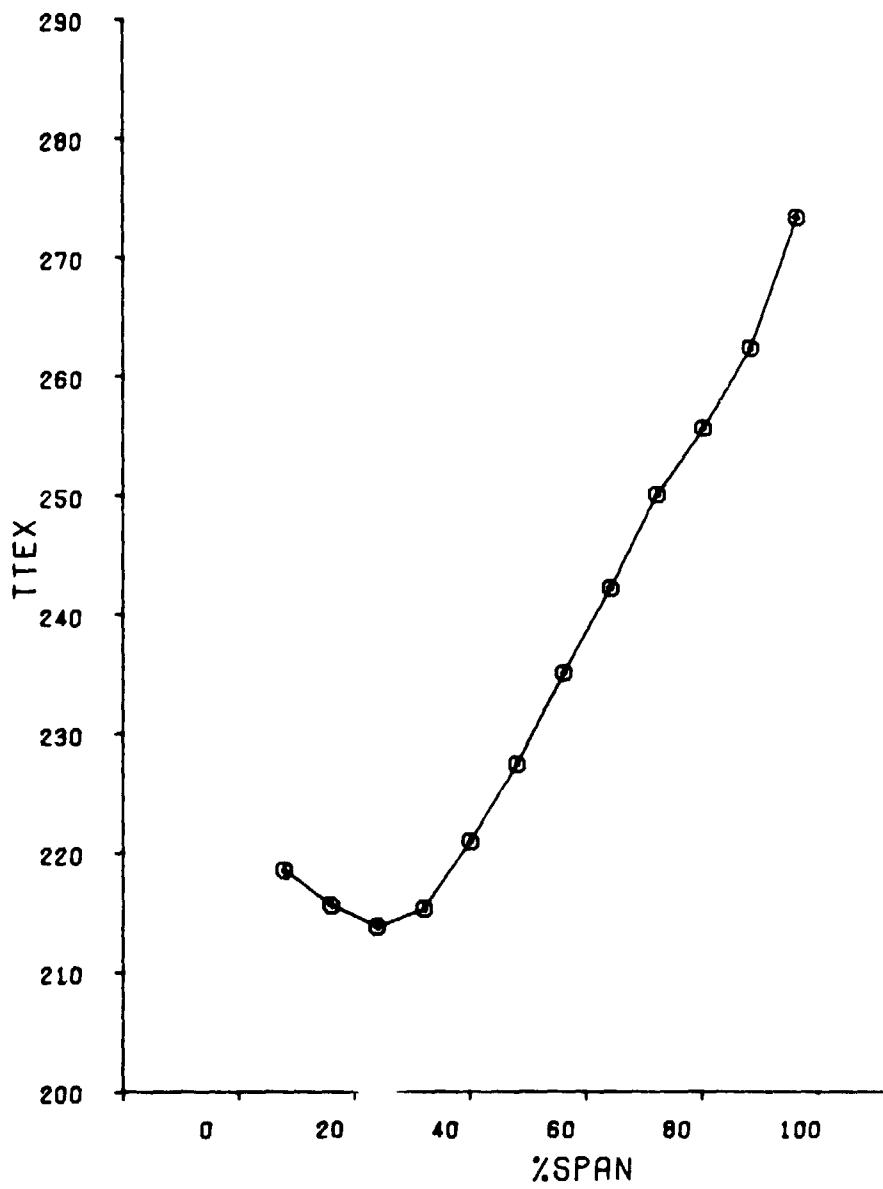


Figure B-38 Average Total Temperature Versus Span (Point 9)

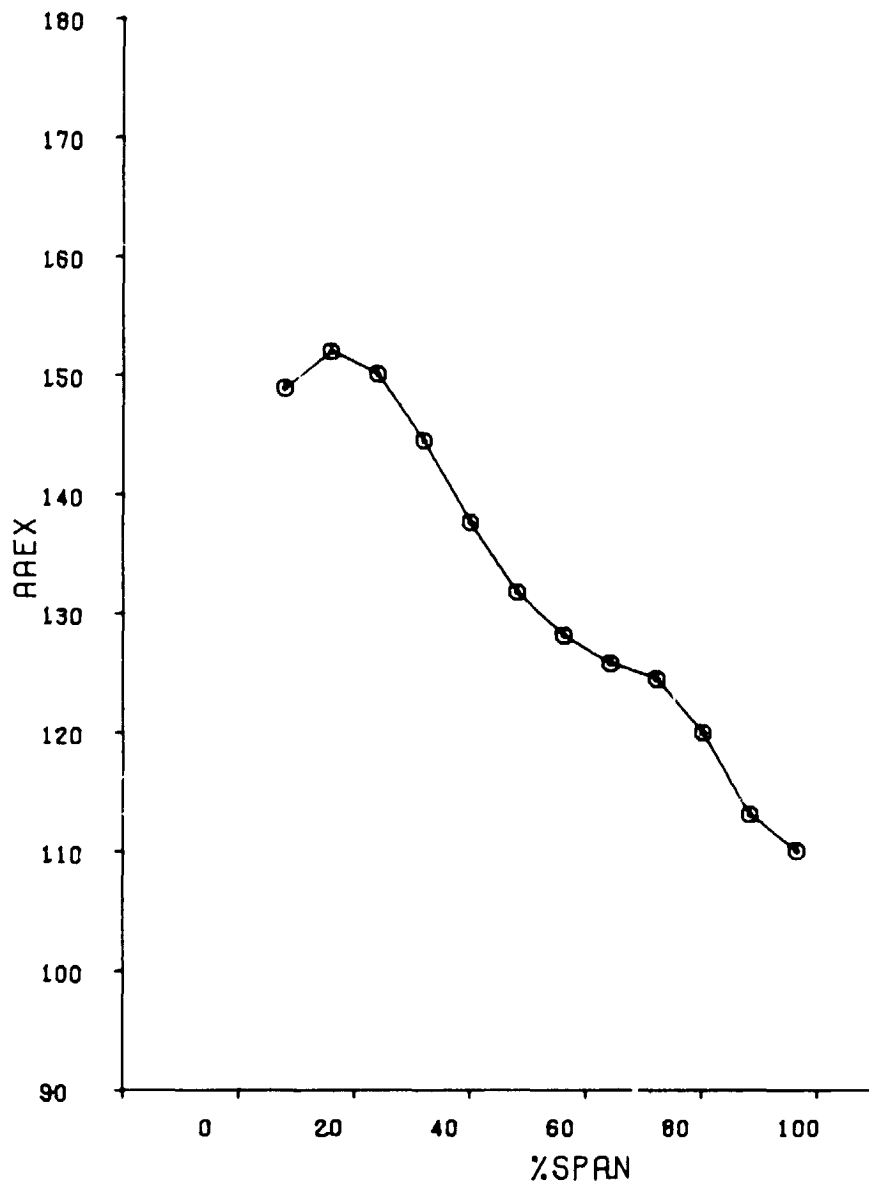


Figure B-39 Average Air Angle Versus Span (Point 9)

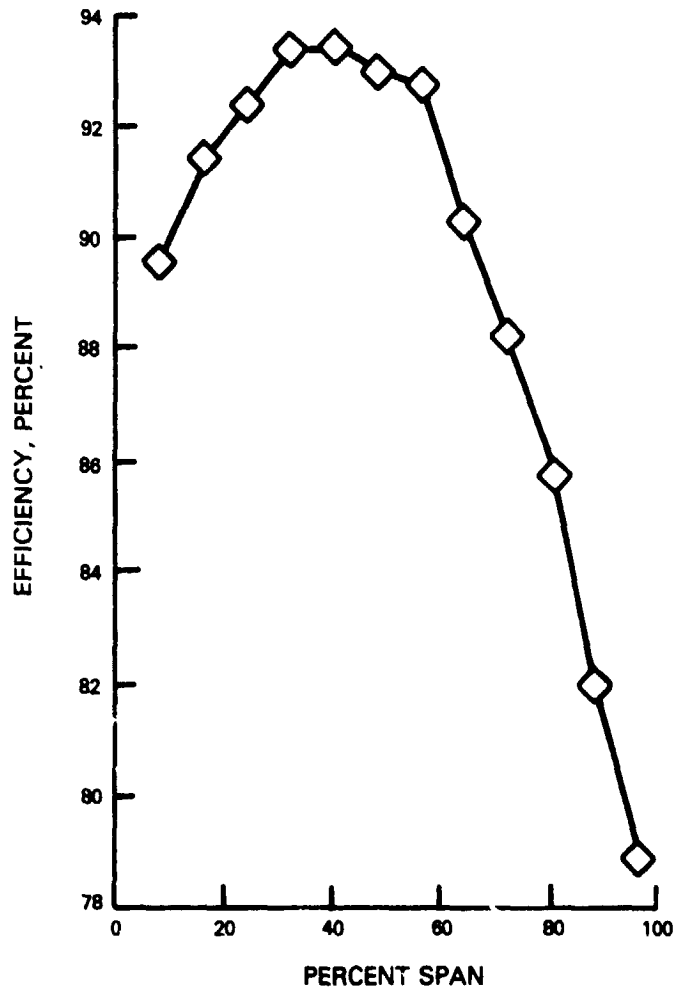


Figure B-40 Efficiency Versus Span (Point 9)

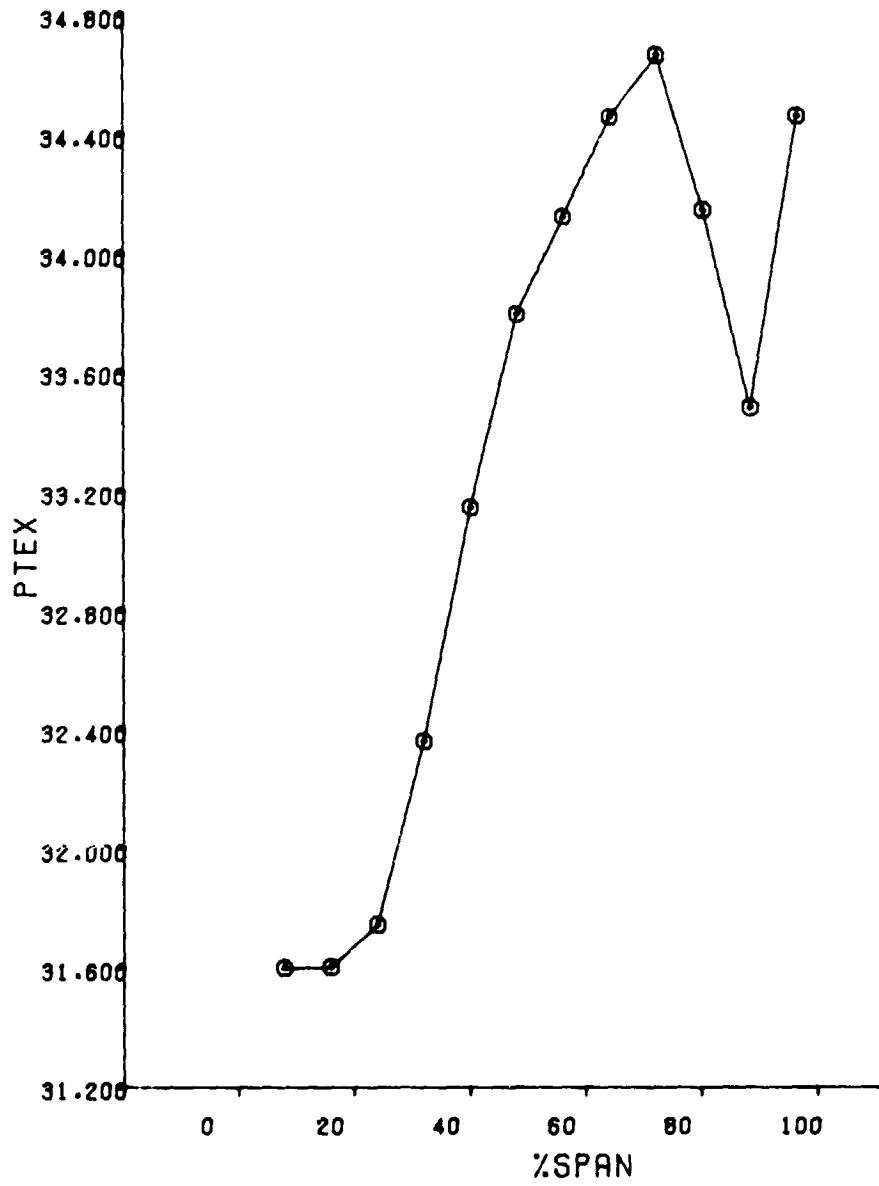


Figure B-41 Average Total Pressure Versus Span (Point 18)

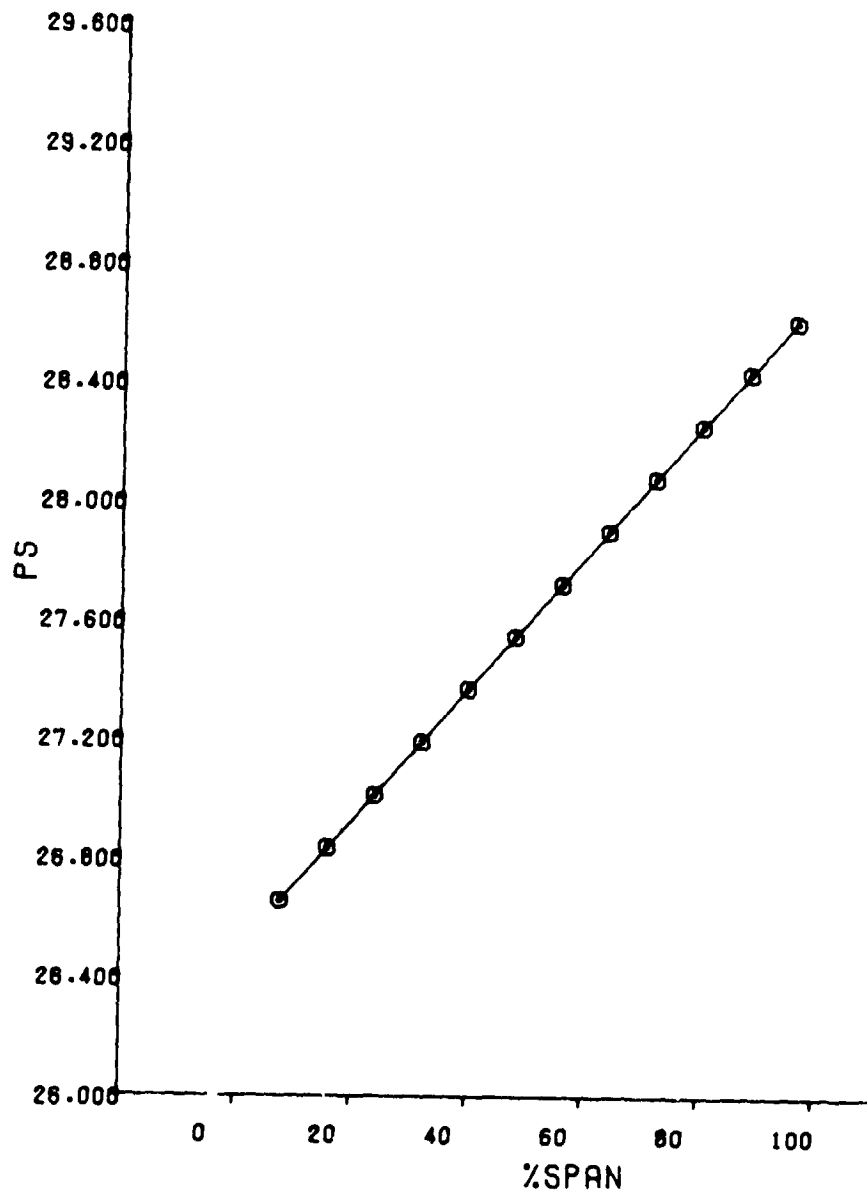


Figure B-42 Average Static Pressure Versus Span (Point 18)

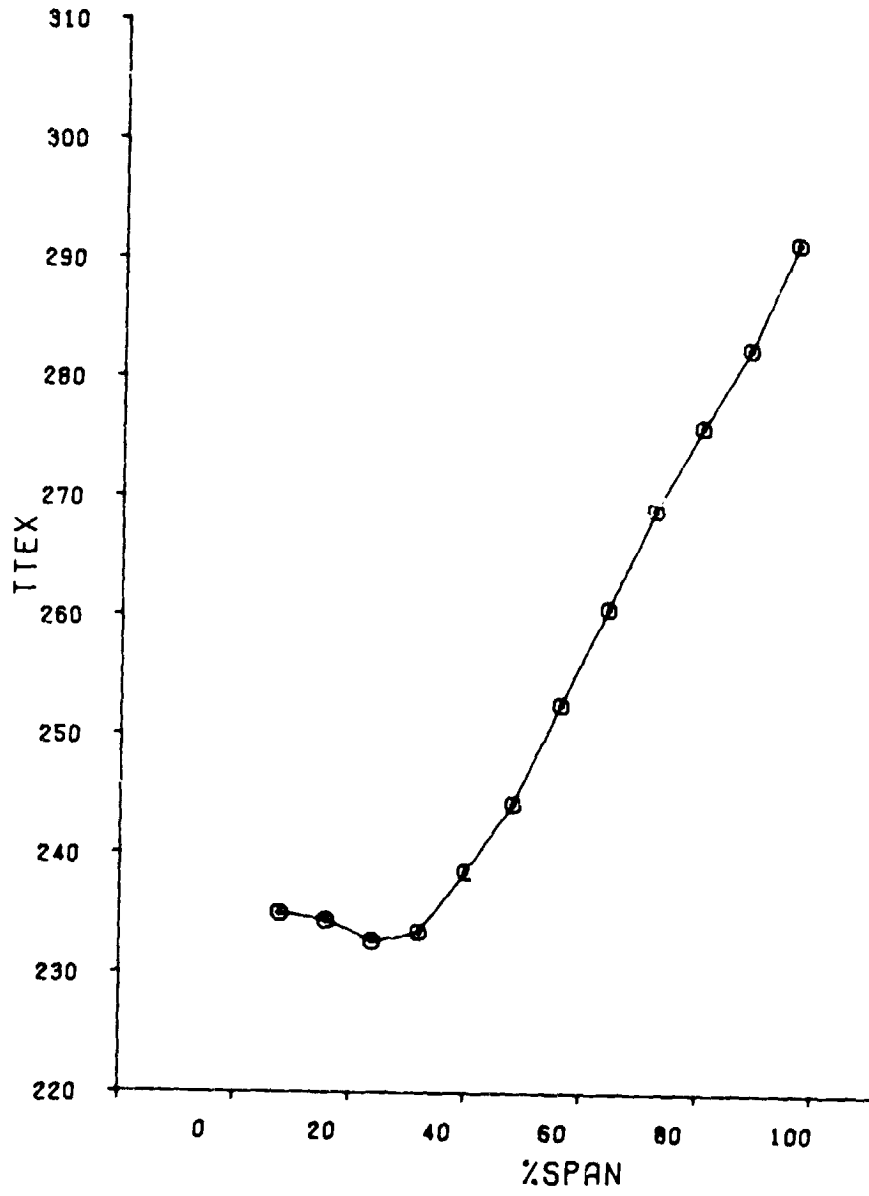


Figure B-43 Average Total Temperature Versus Span (Point 18)



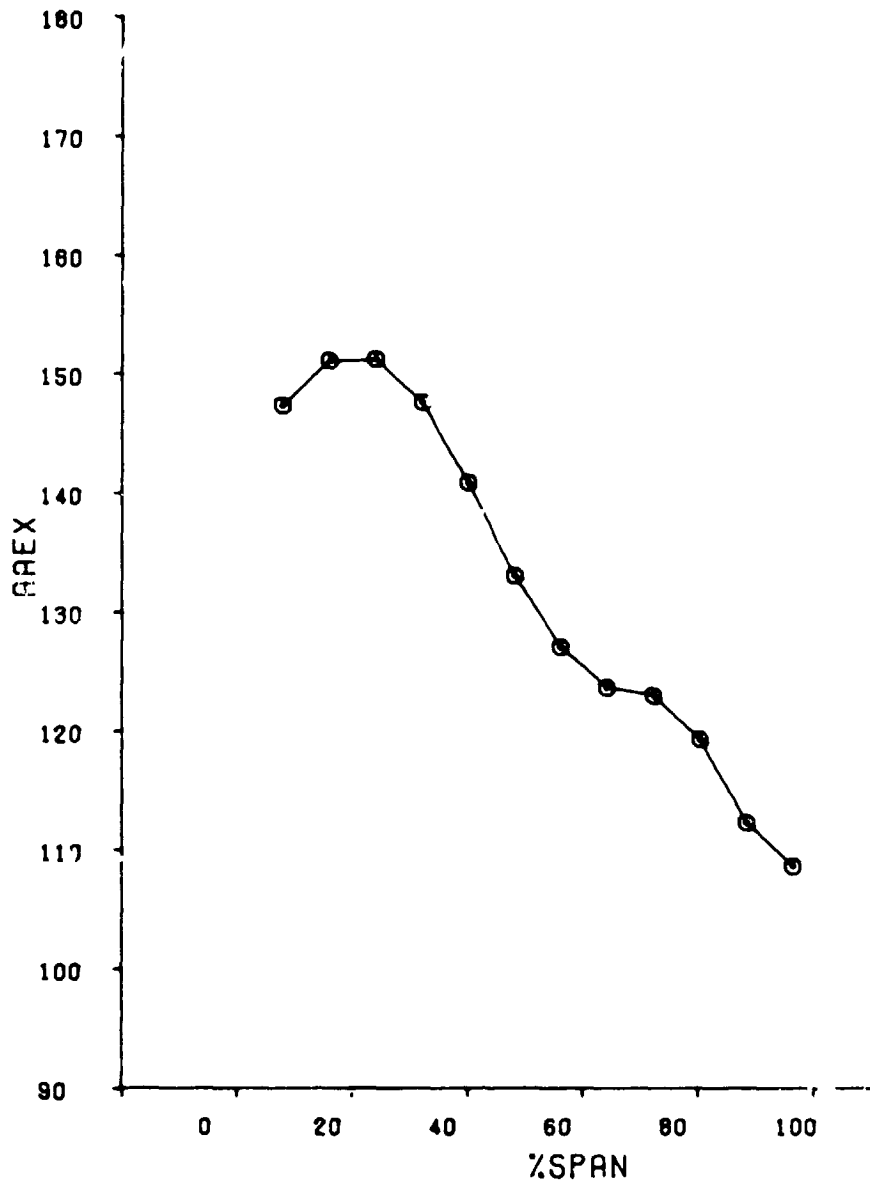


Figure B-44 Average Air Angle Versus Span (Point 18)

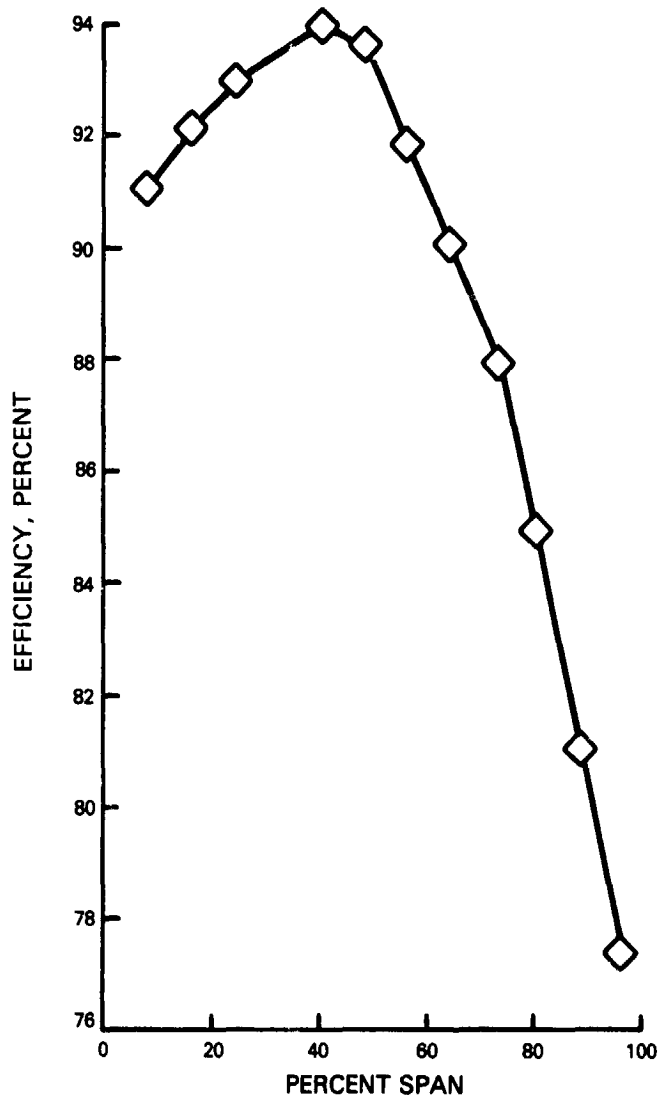


Figure B-45 Efficiency Versus Span (Point 18)

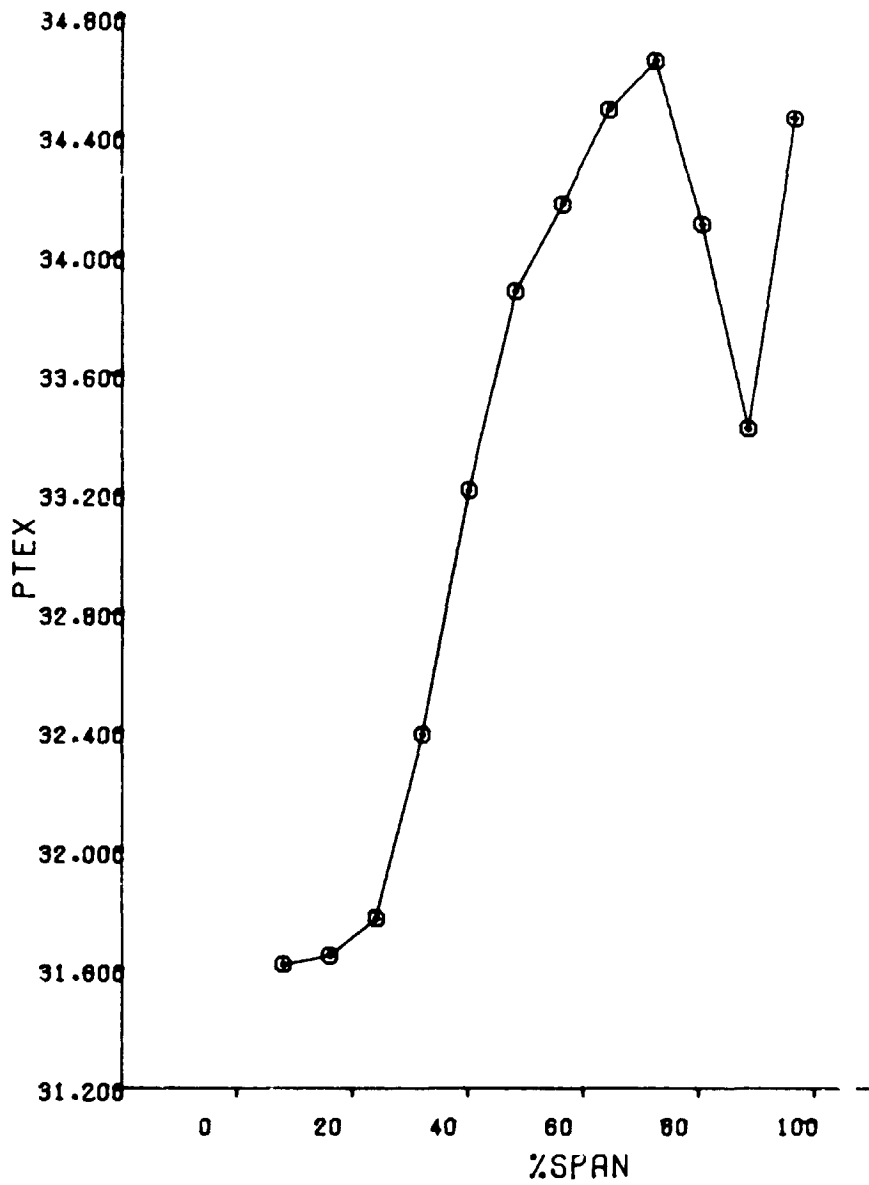


Figure B-46 Average Total Pressure Versus Span (Point 21)

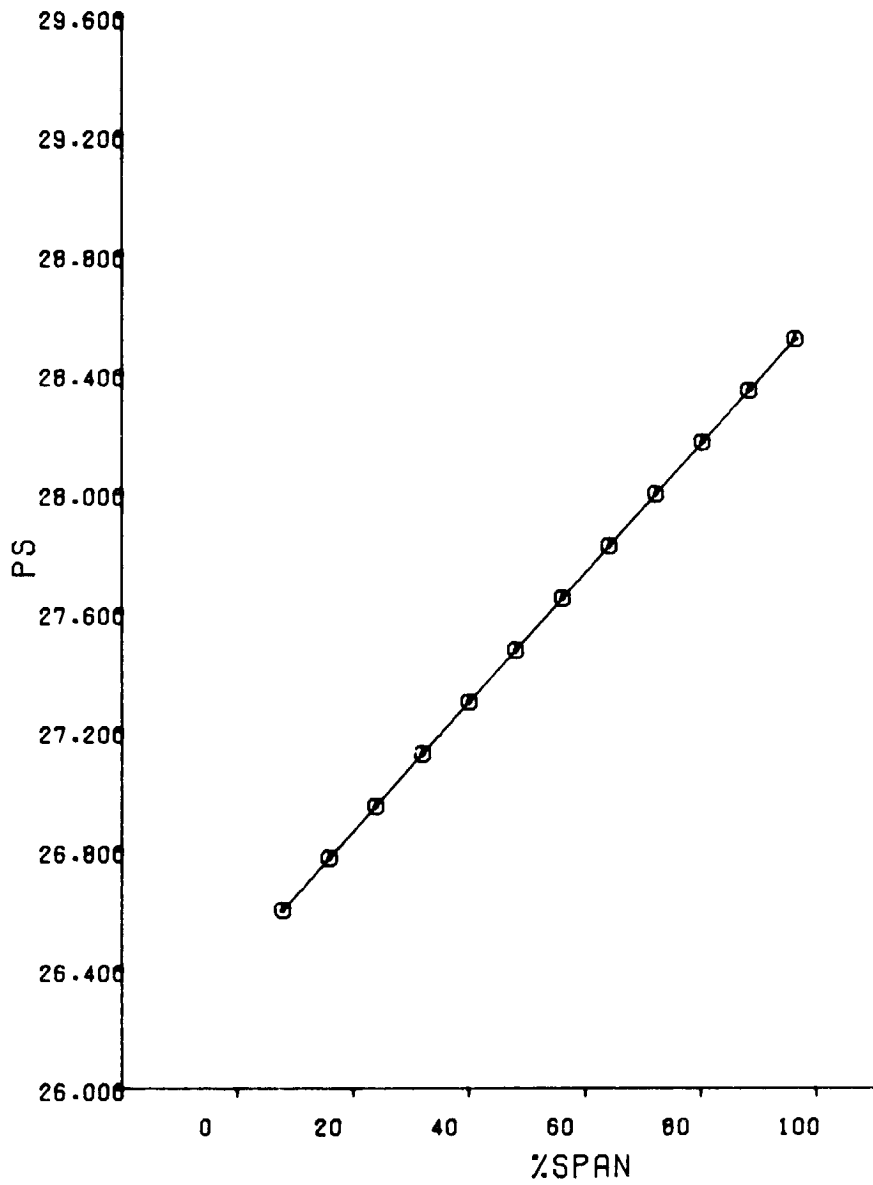


Figure B-47 Average Static Pressure Versus Span (Point 21)

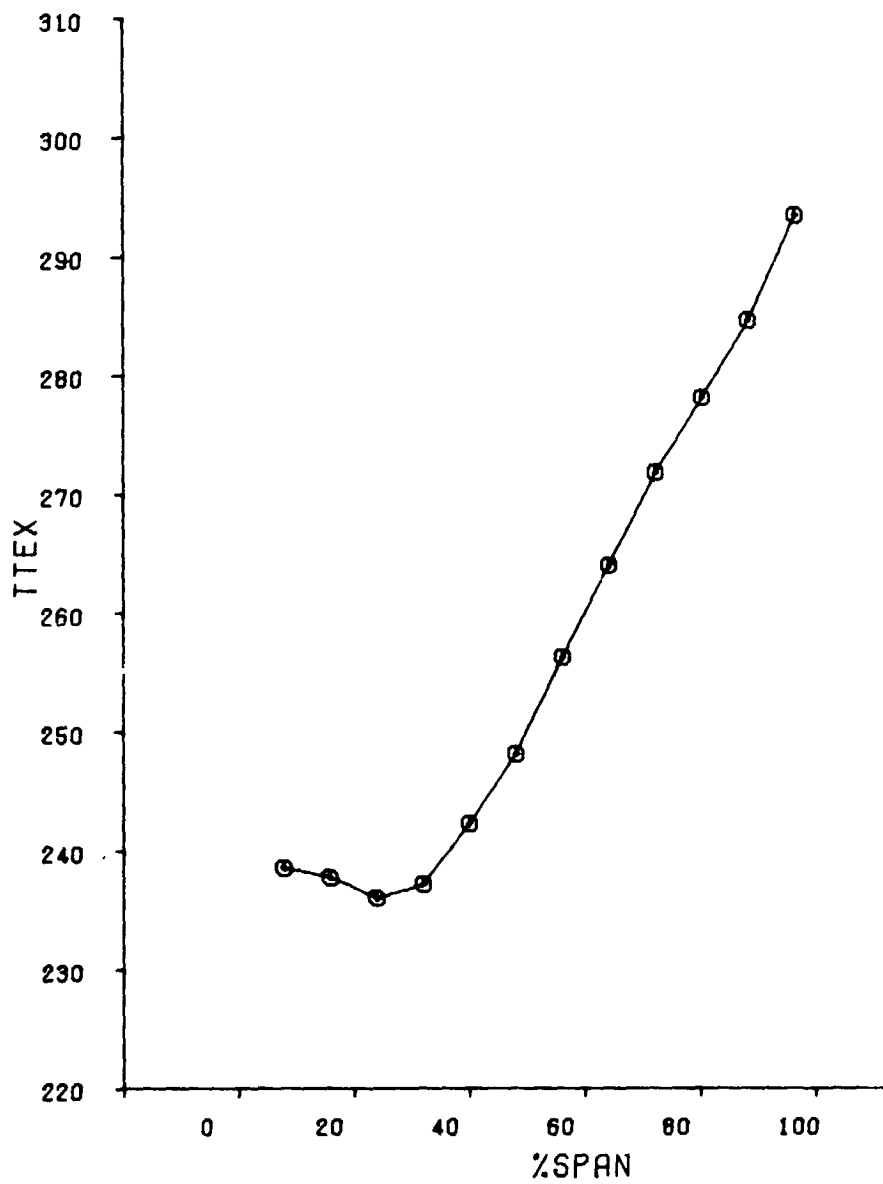


Figure B-48 Average Total Temperature Versus Span (Point 21)

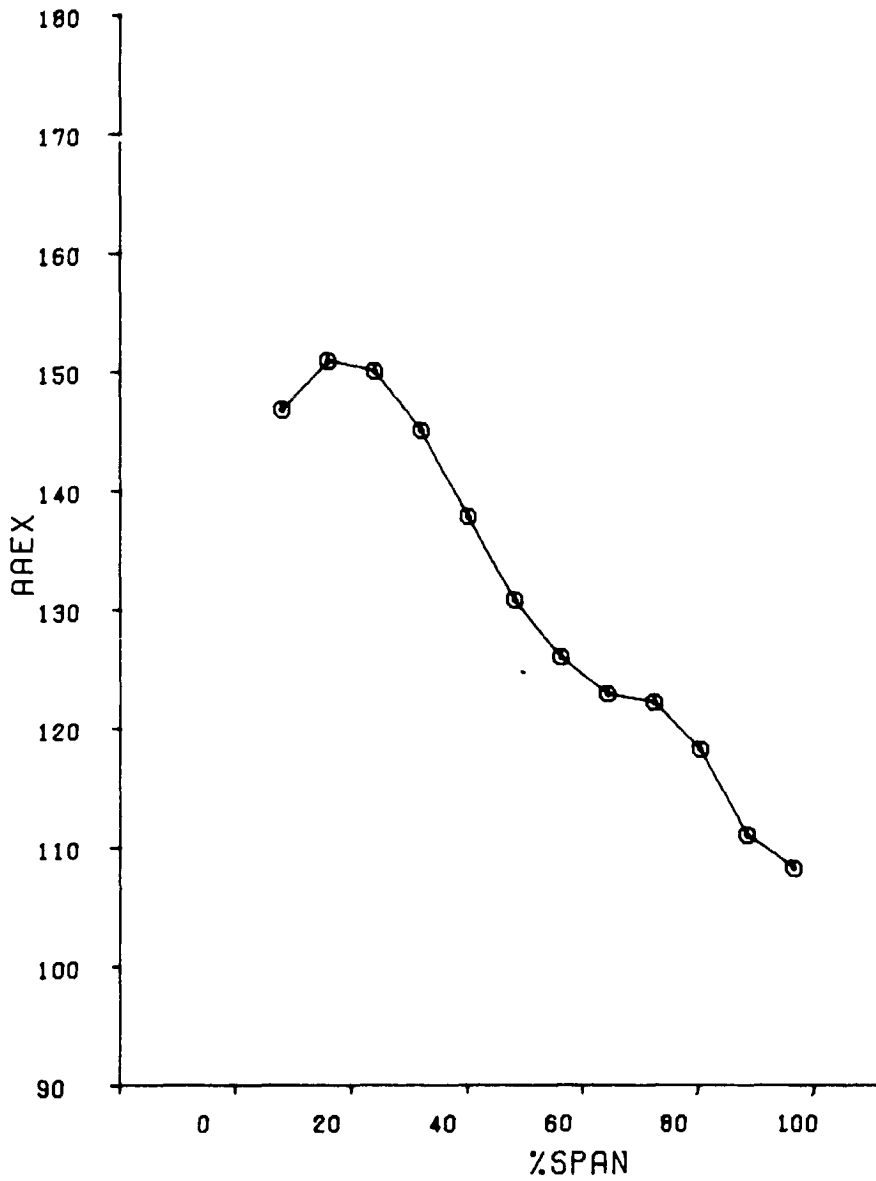


Figure B-49 Average Air Angle Versus Span (Point 21)

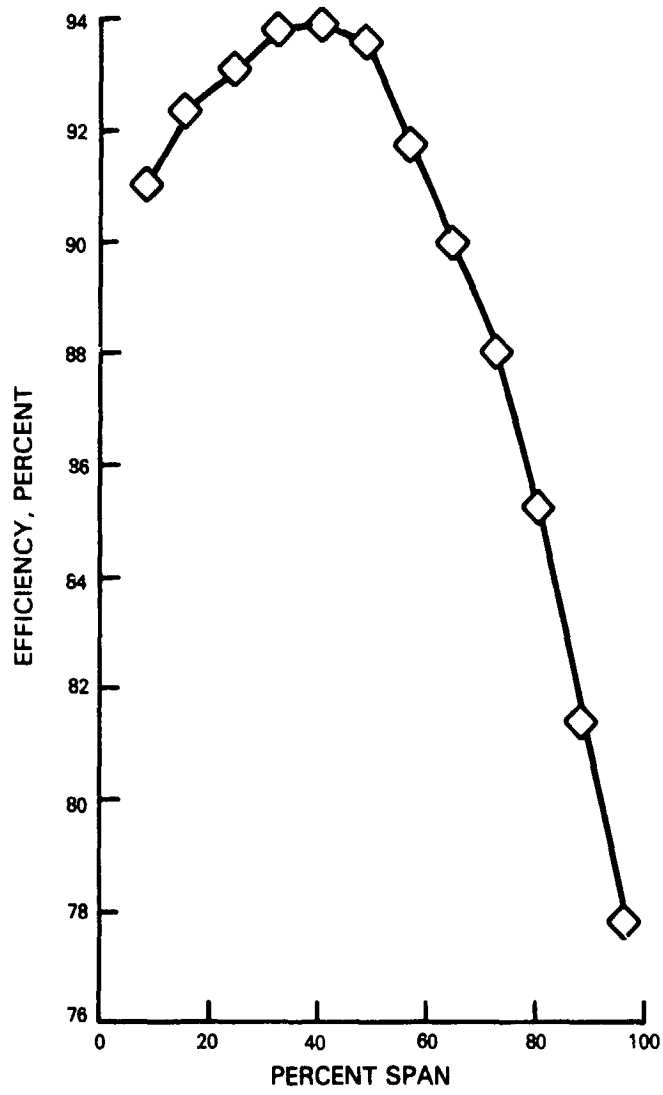


Figure B-50 Efficiency Versus Span (Point 21)

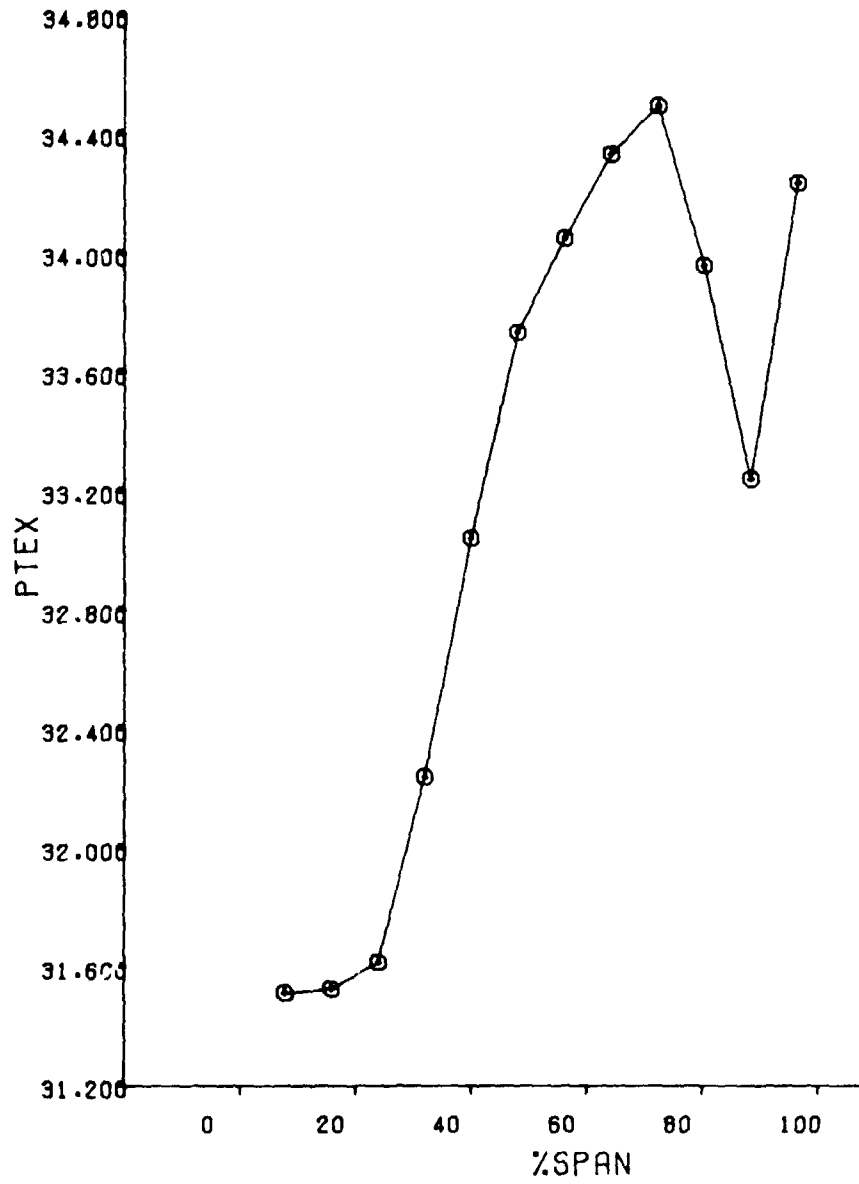


Figure B-51 Average Total Pressure Versus Span (Point 28)

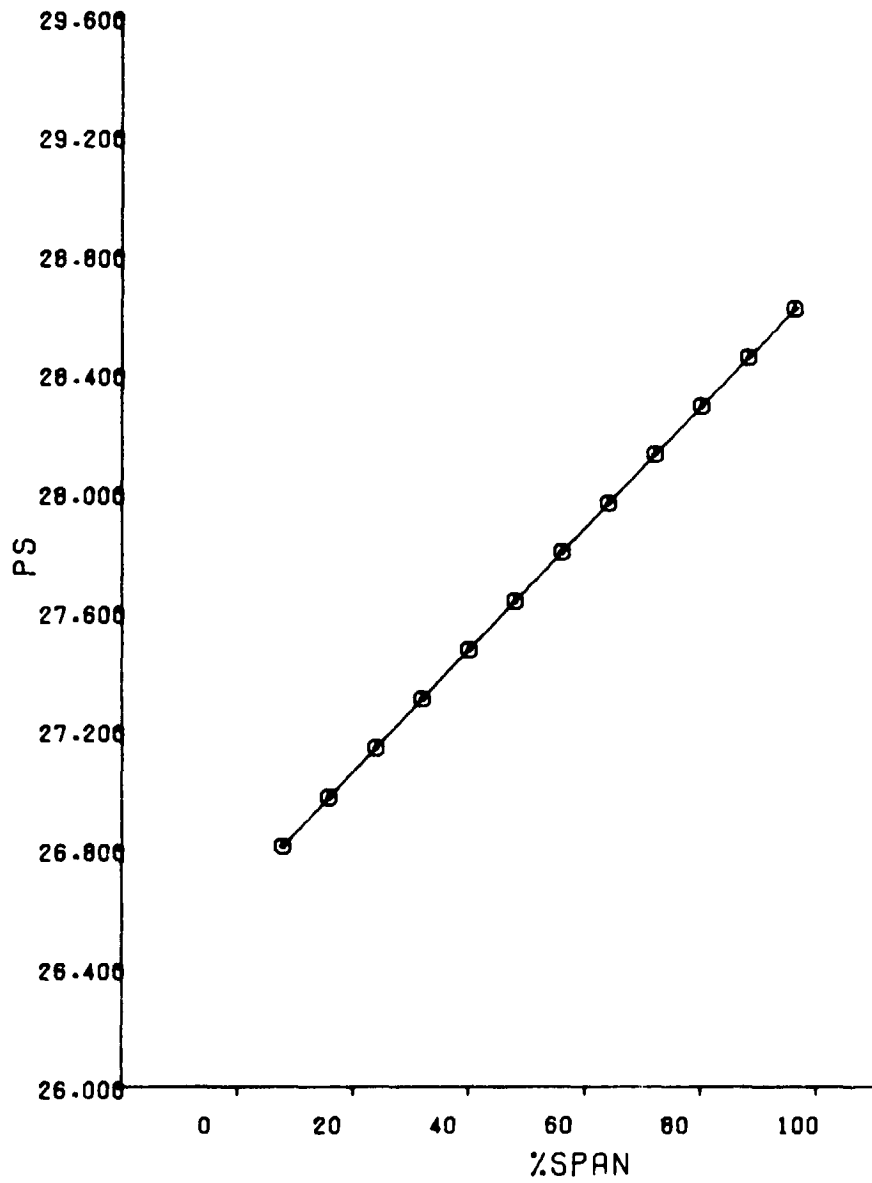


Figure B-52 Average Static Pressure Versus Span (Point 28)

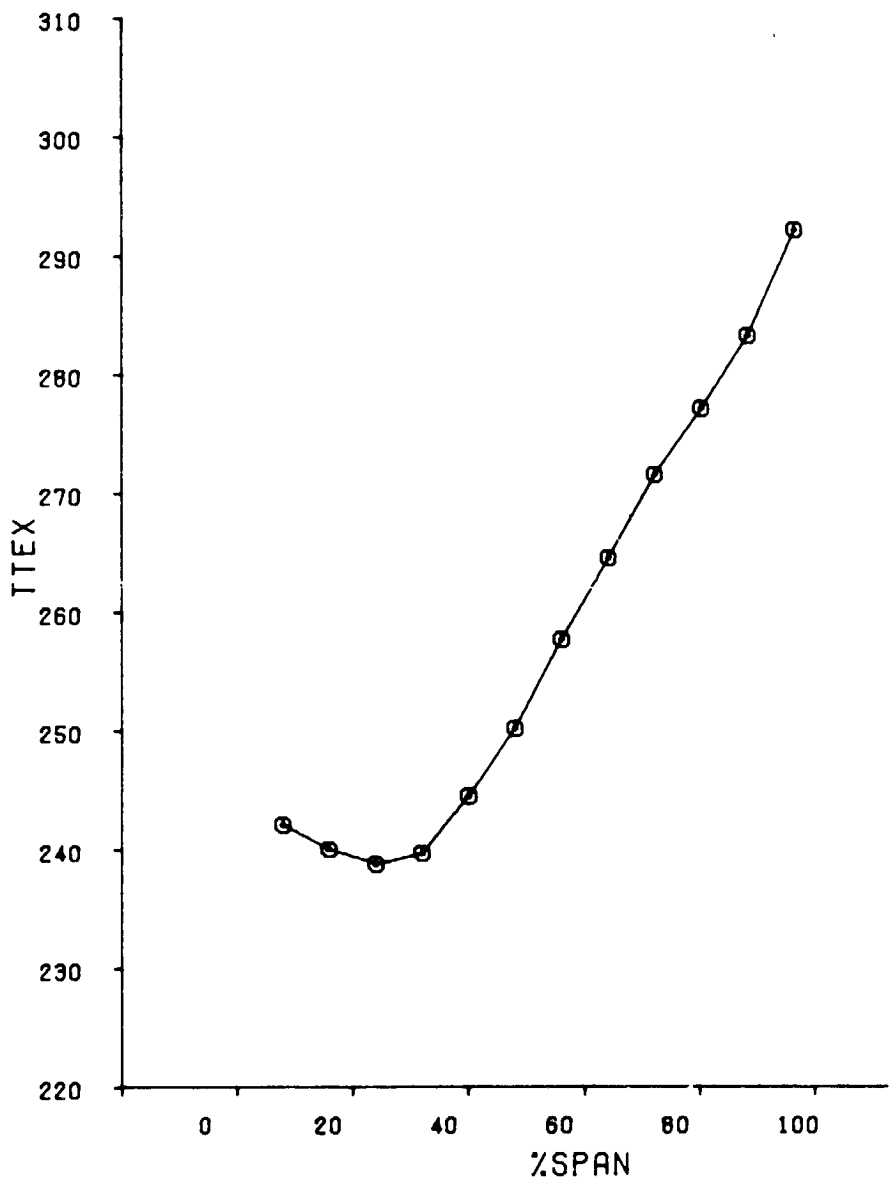


Figure B-53 Average Total Temperature Versus Span (Point 28)

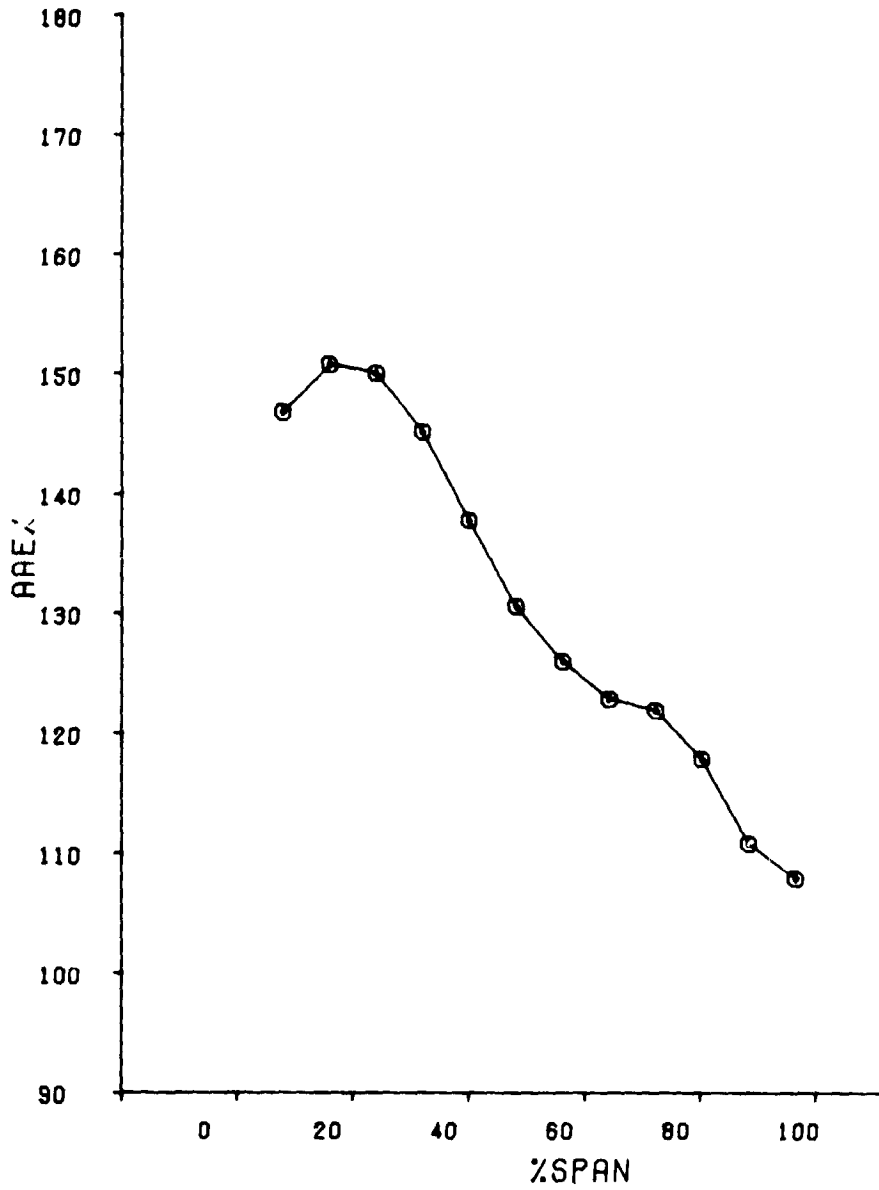


Figure B-54 Average Air Angle Versus Span (Point 28)

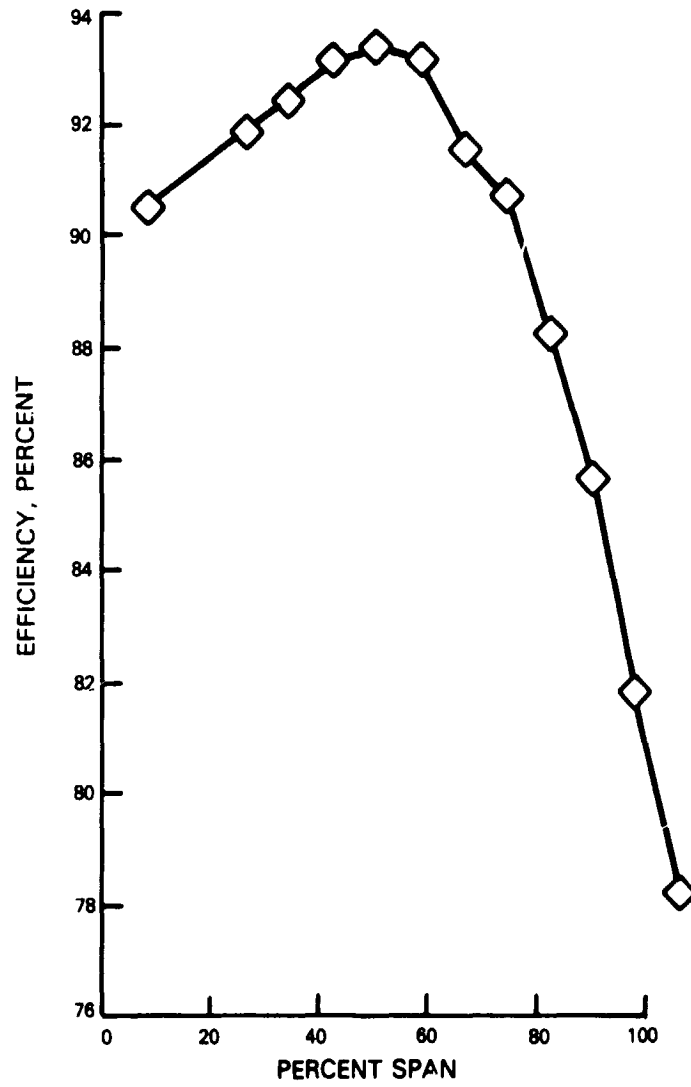


Figure B-55 Efficiency Versus Span (Point 28)

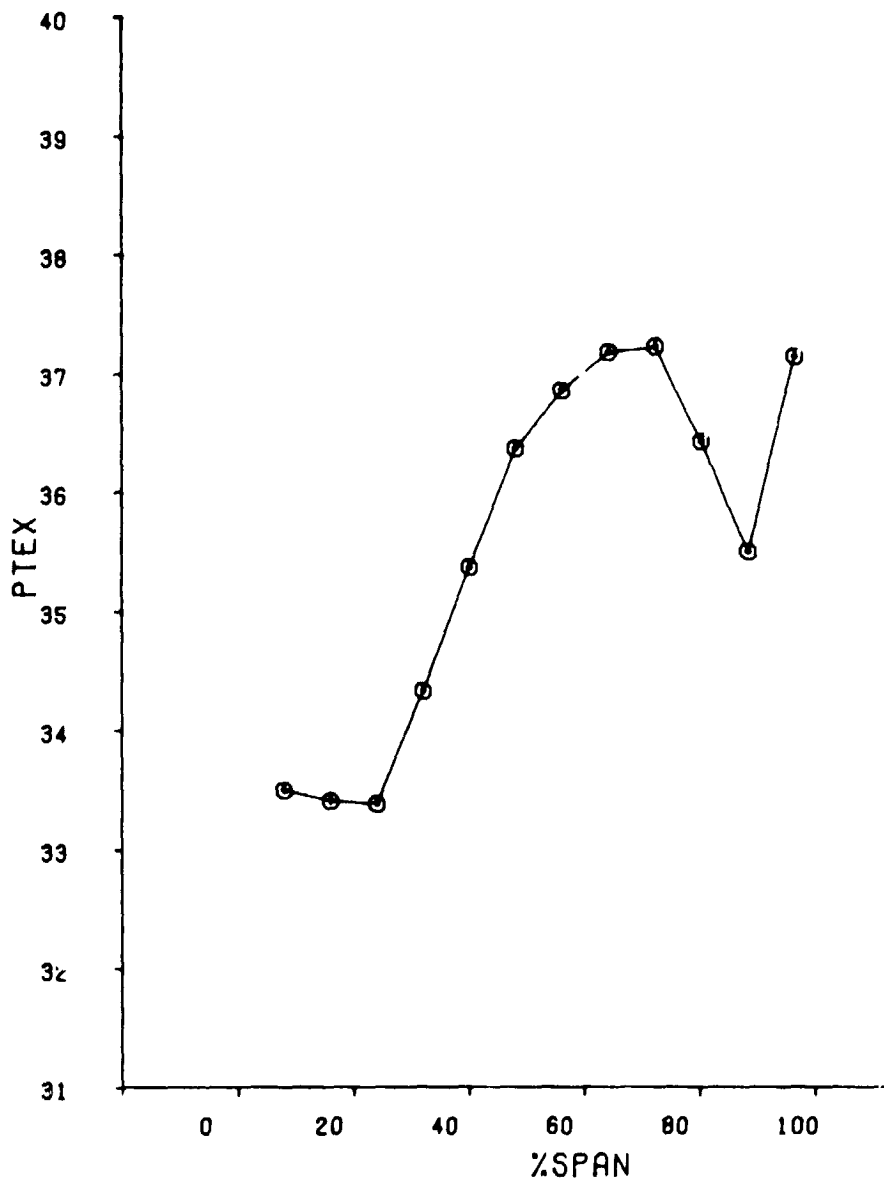


Figure B-56 Average Total Pressure Versus Span (Point 22)

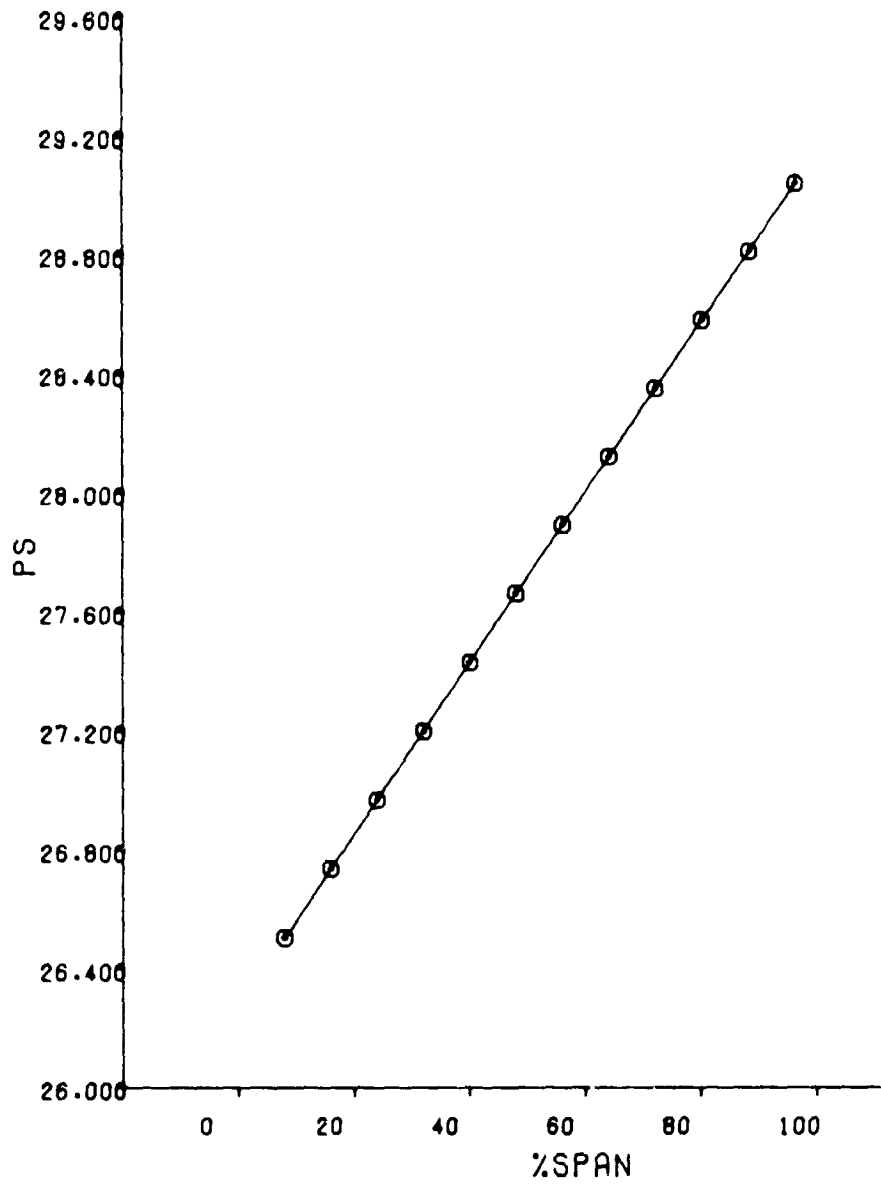


Figure B-57 Average Static Pressure Versus Span (Point 22)

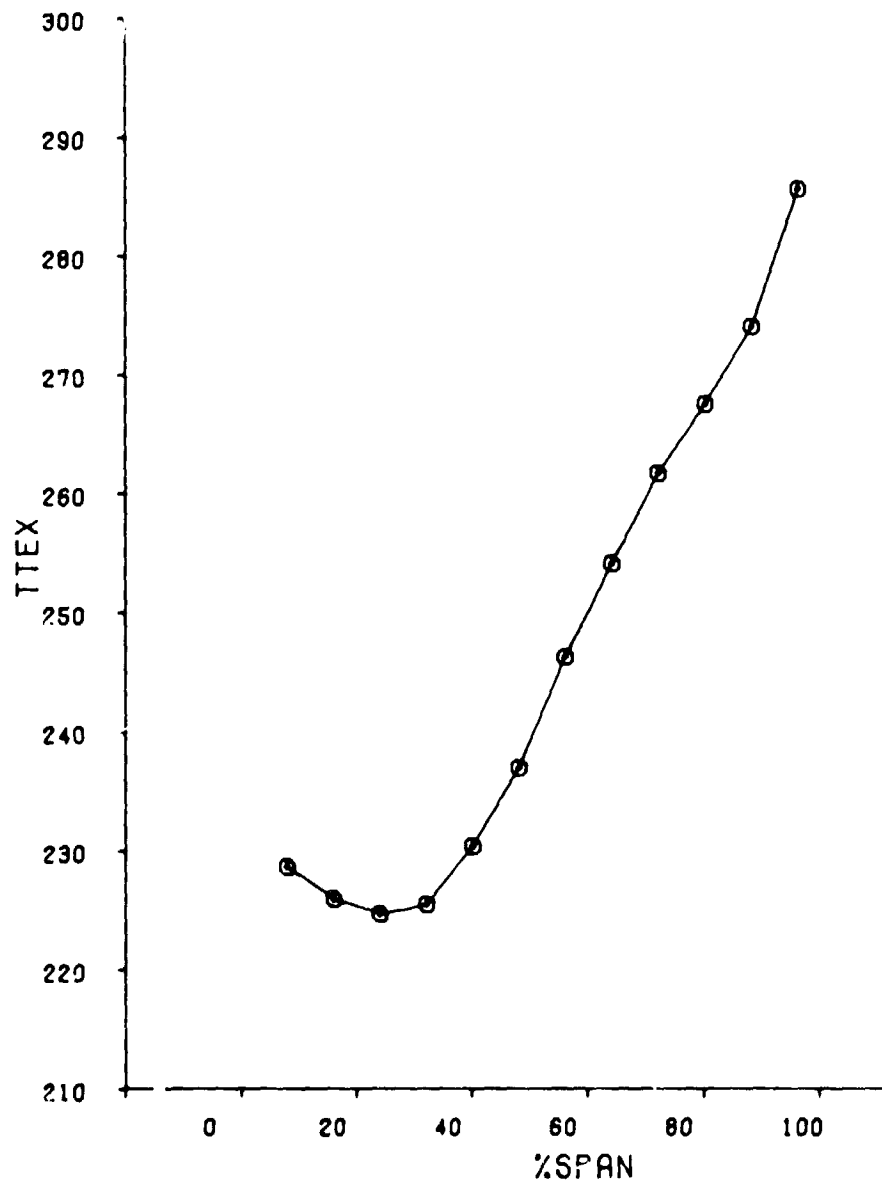


Figure B-58 Average Total Temperature Versus Span (Point 22)

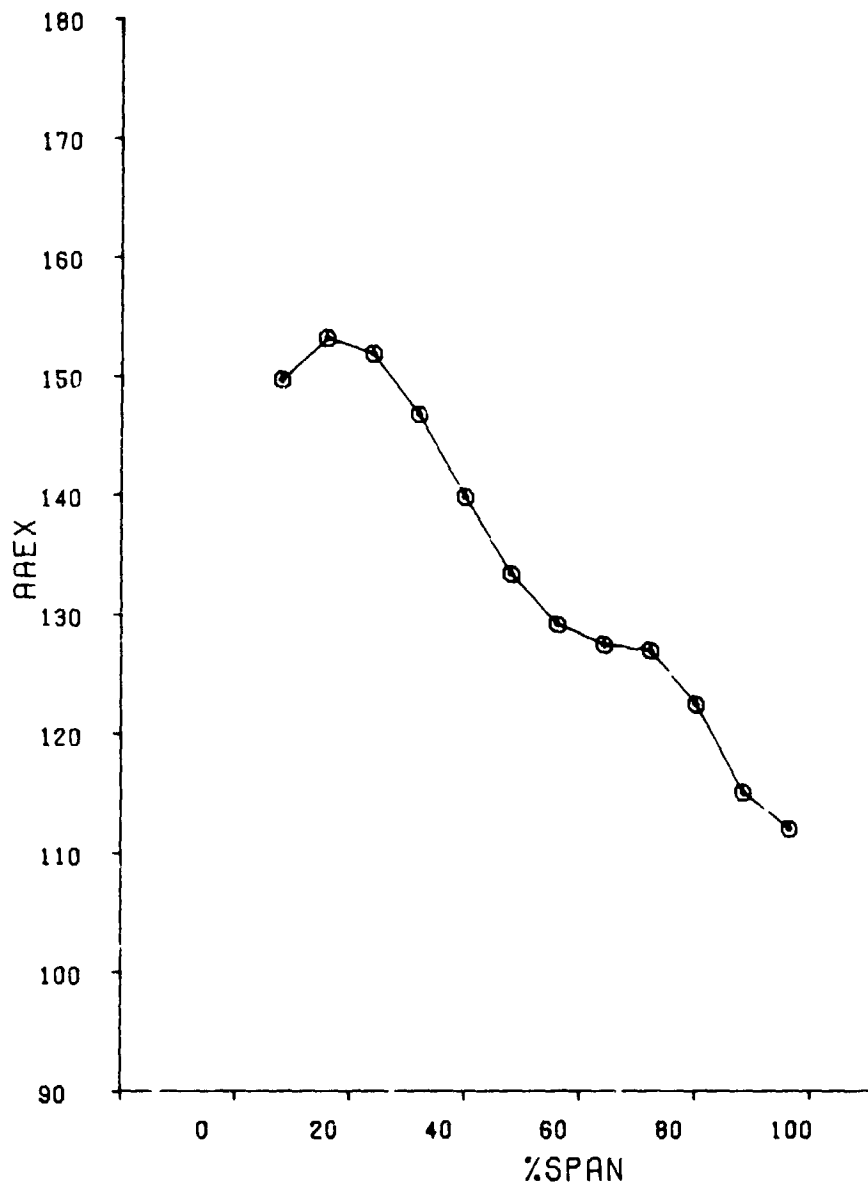


Figure B-59 Average Air Angle Versus Span (Point 22)

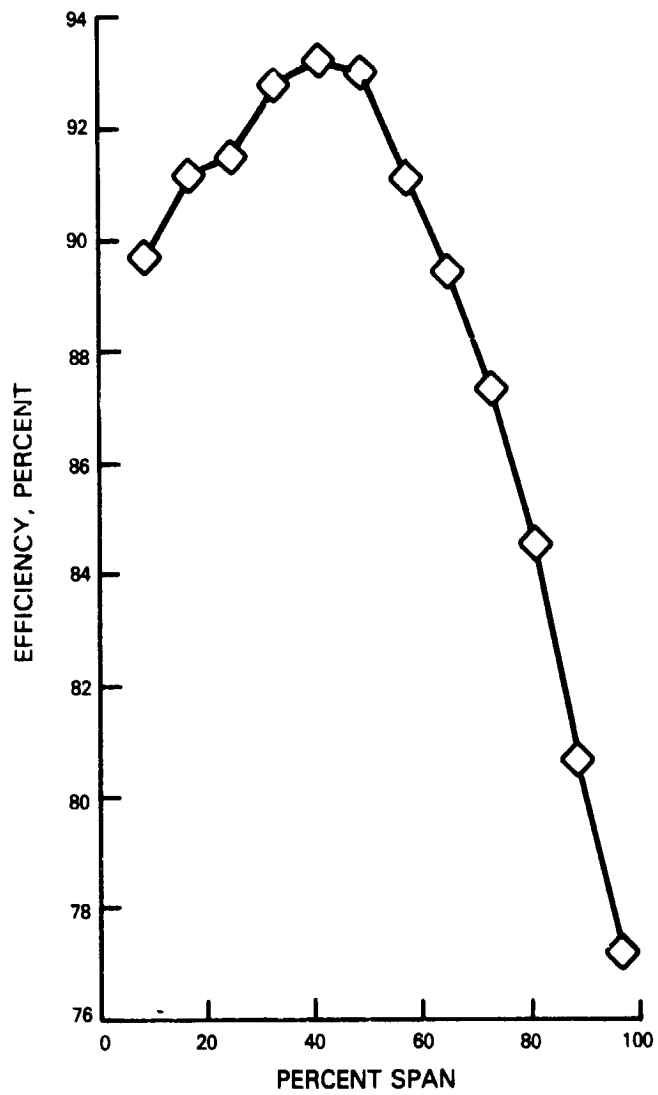


Figure B-60 Efficiency Versus Span (Point 22)

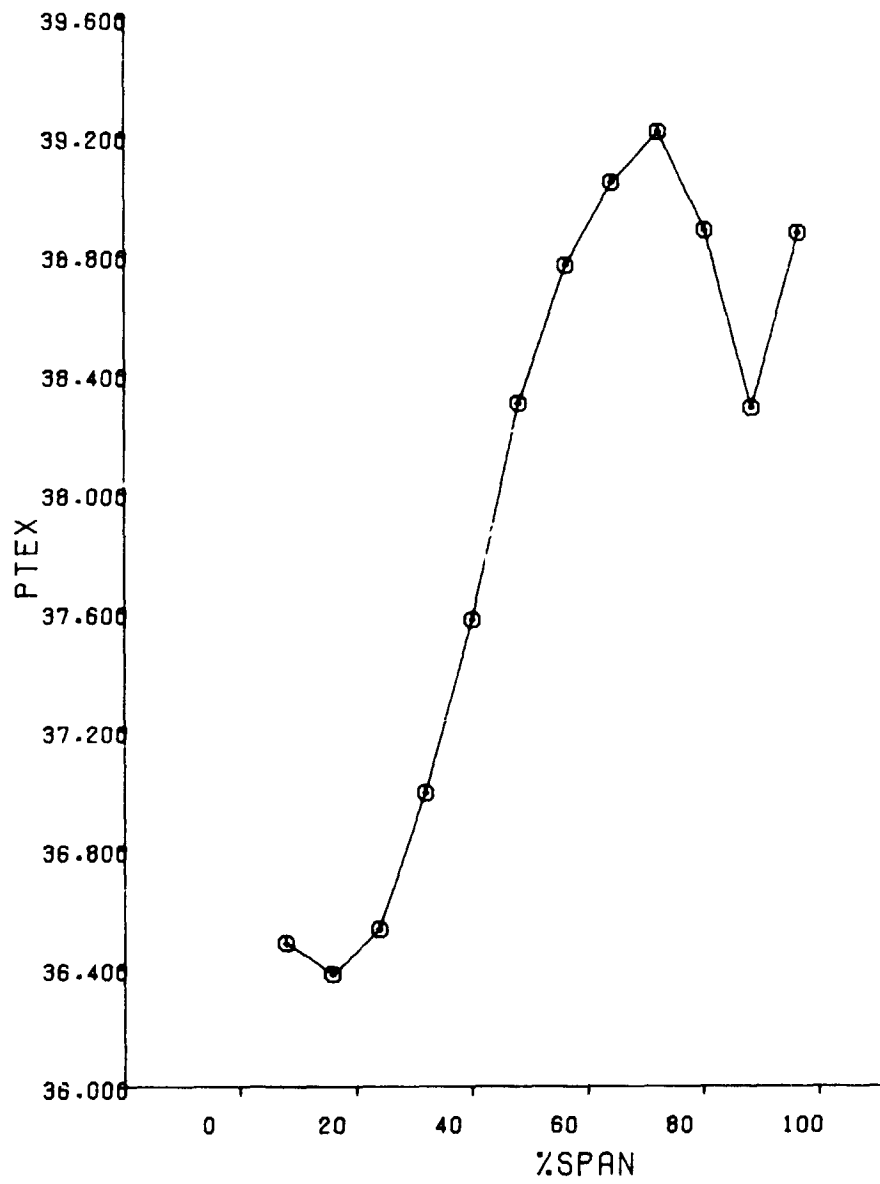


Figure B-61 Average Total Pressure Versus Span (Point 23)

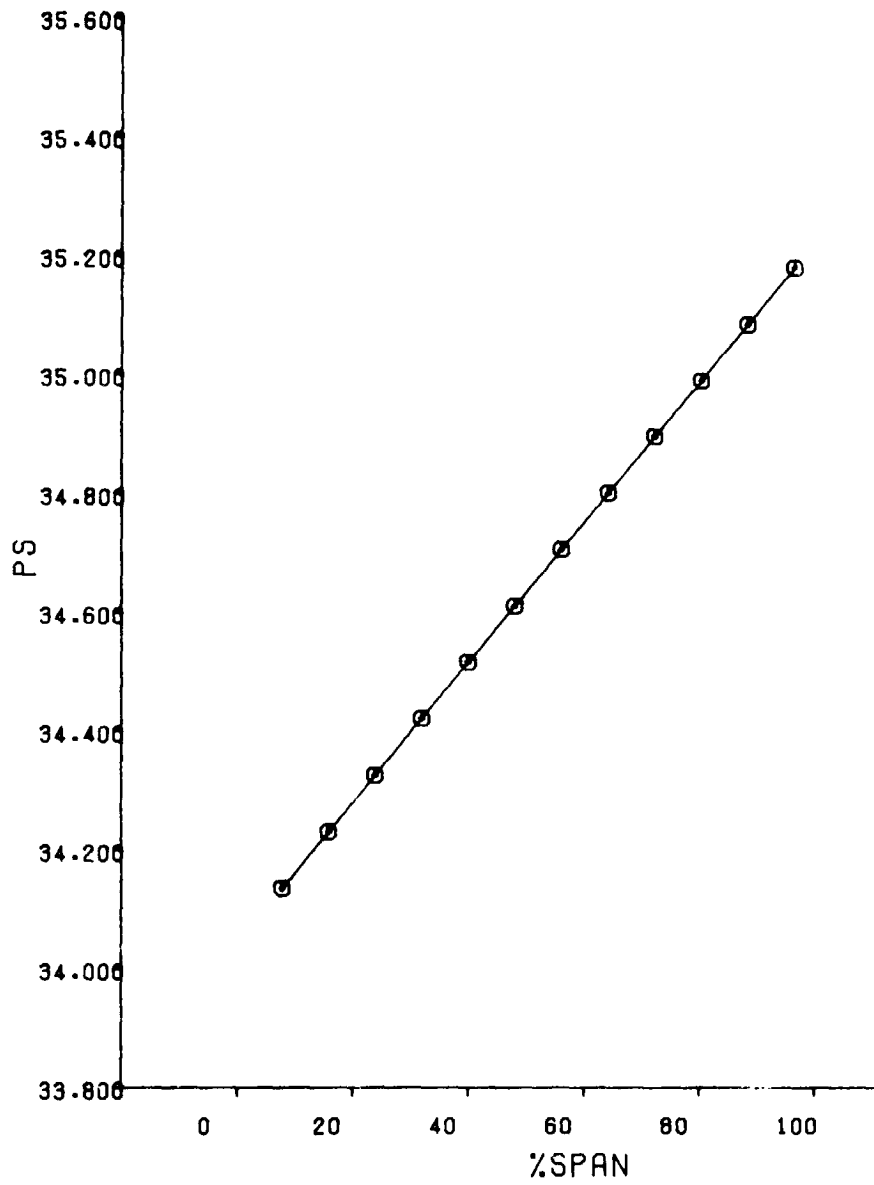


Figure B-62 Average Static Pressure Versus Span (Point 23)



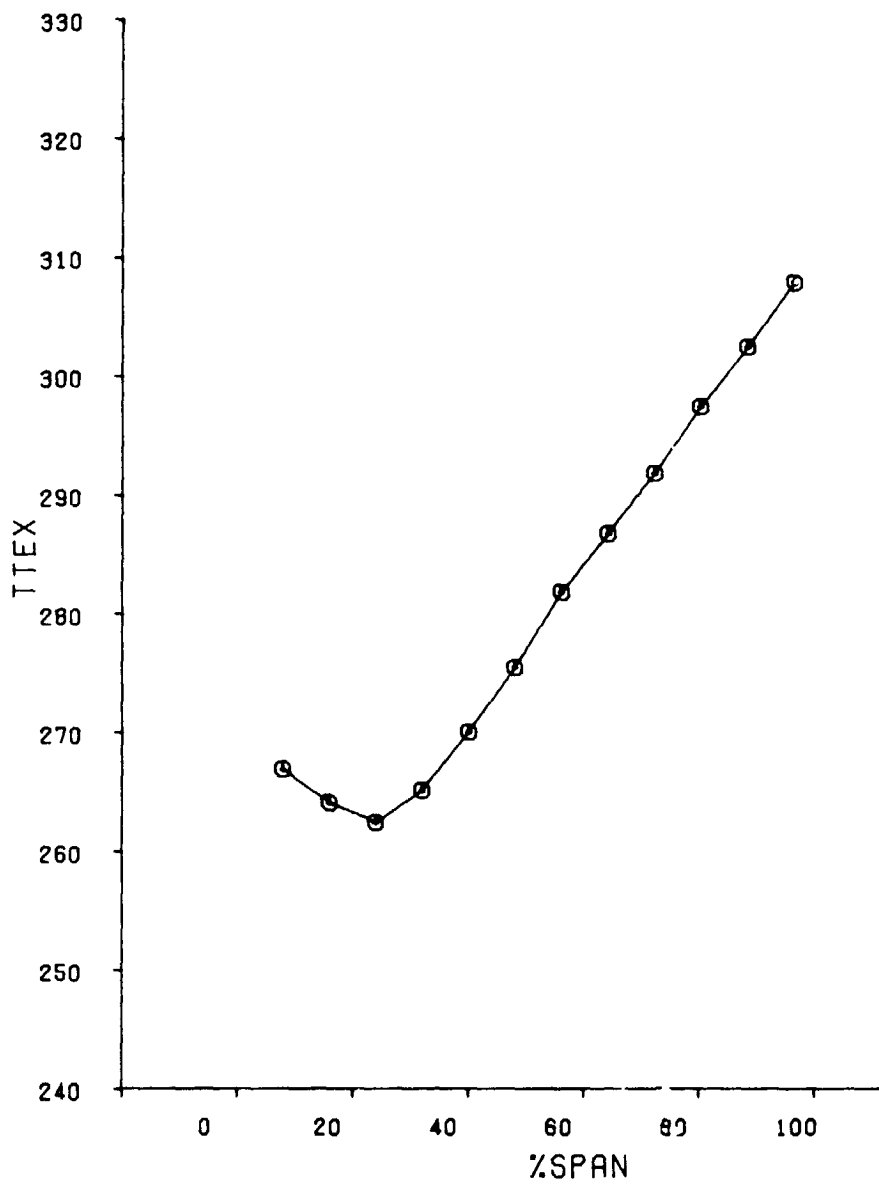


Figure B-63 Average Total Temperature Versus Span (Point 23)

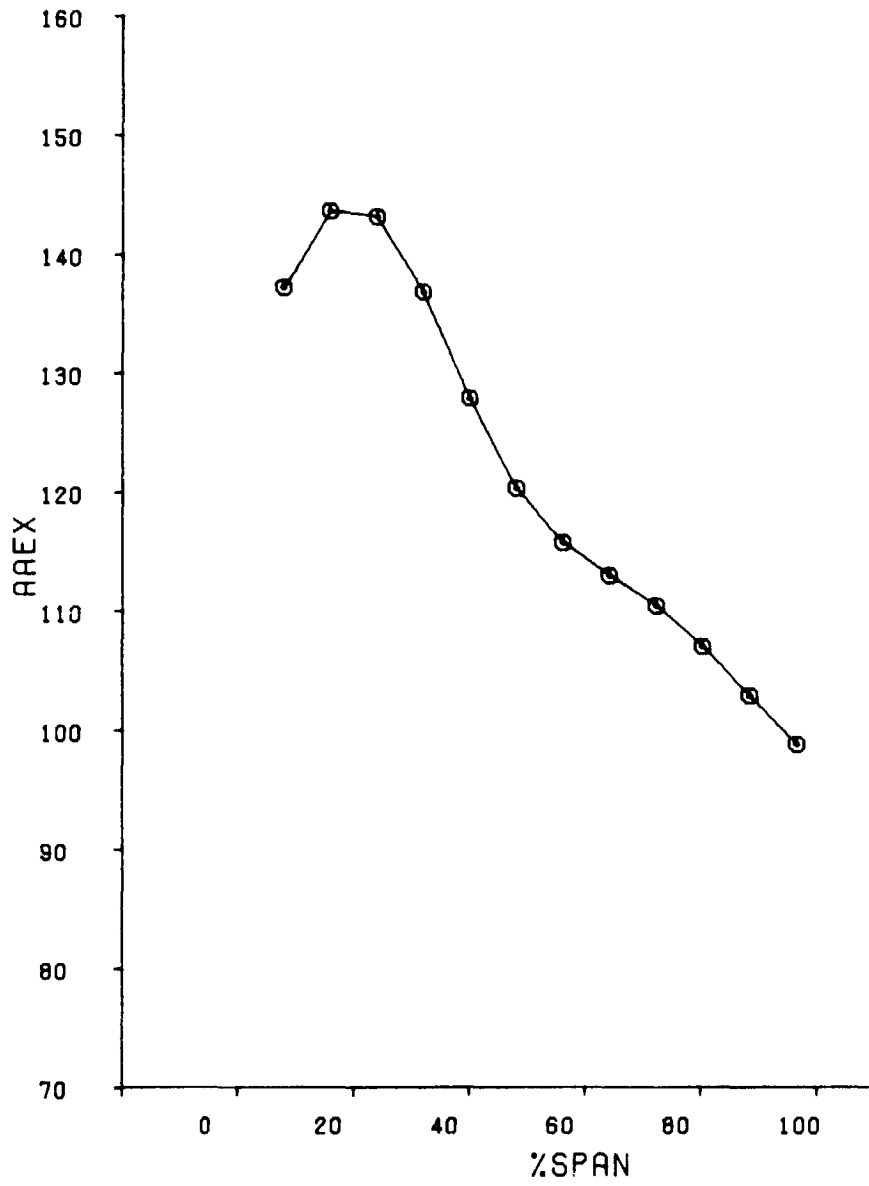


Figure B-64 Average Air Angle Versus Span (Point 23)

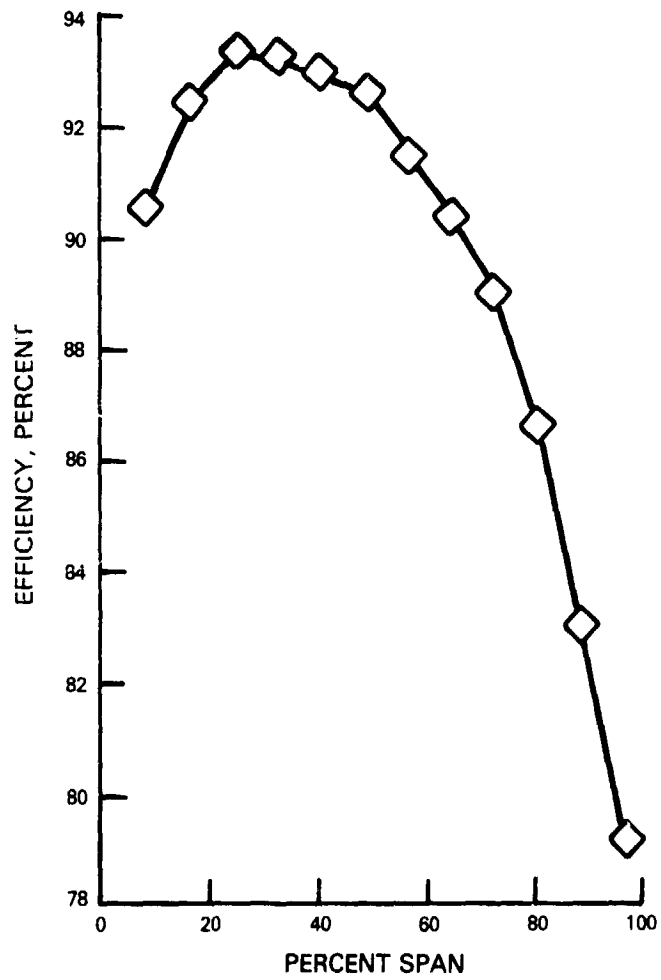


Figure B-65 Efficiency versus Span (Point 23)

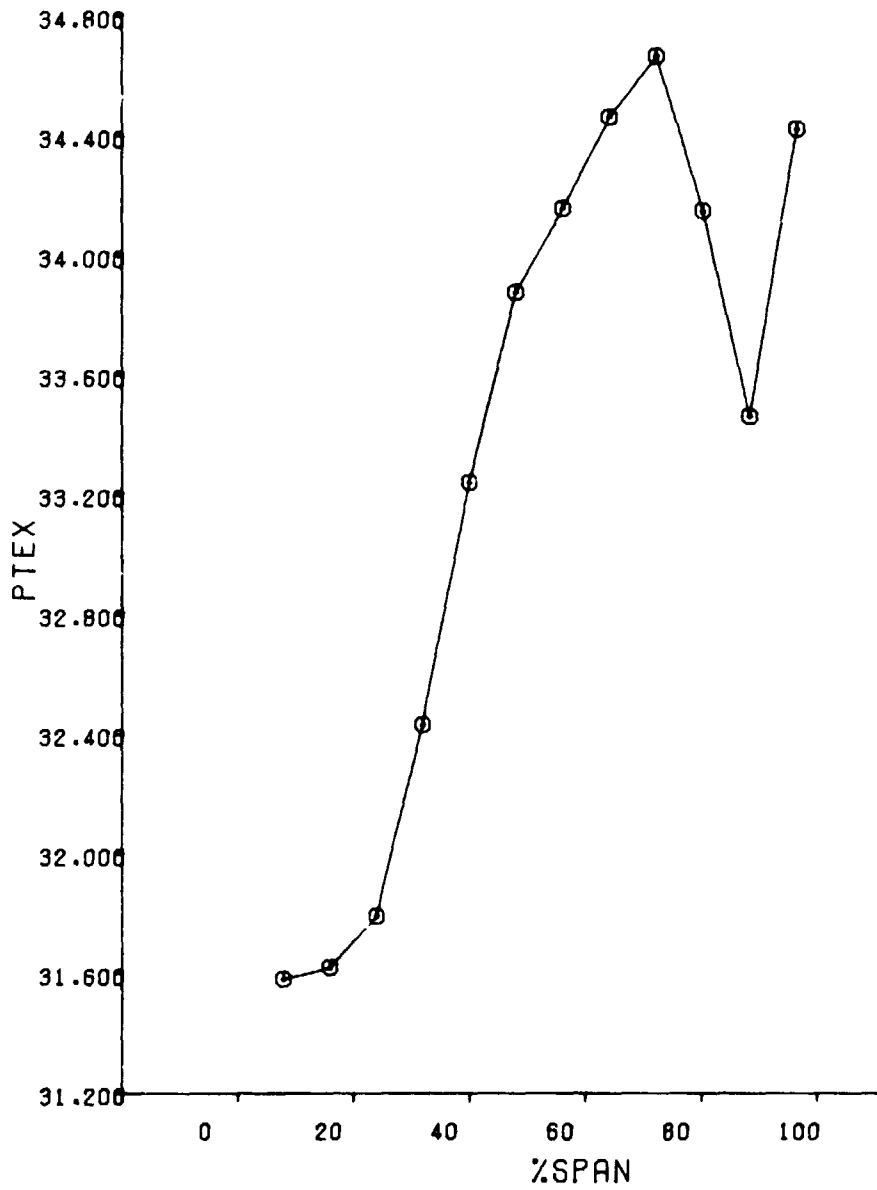


Figure B-66 Average Total Pressure Versus Span (Point 24)

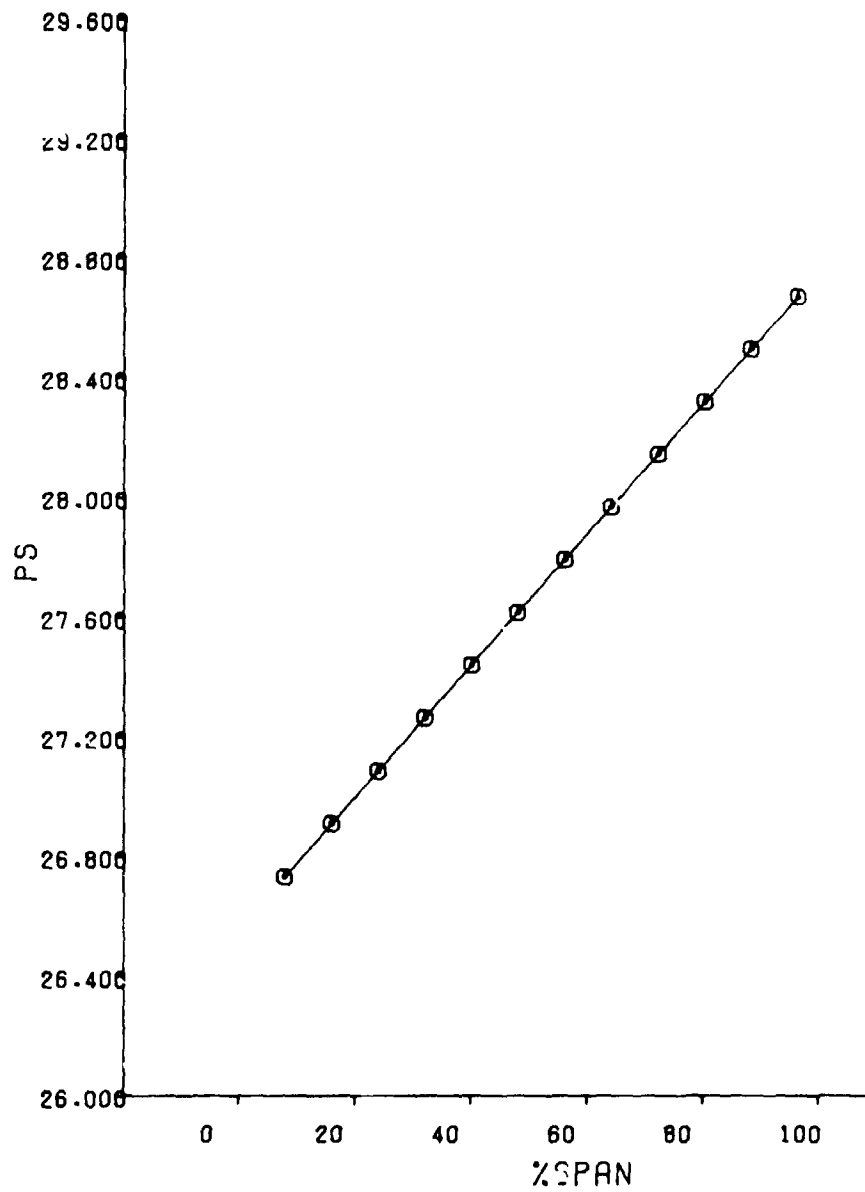


Figure B-67 Average Static Pressure Versus Span (Point 24)

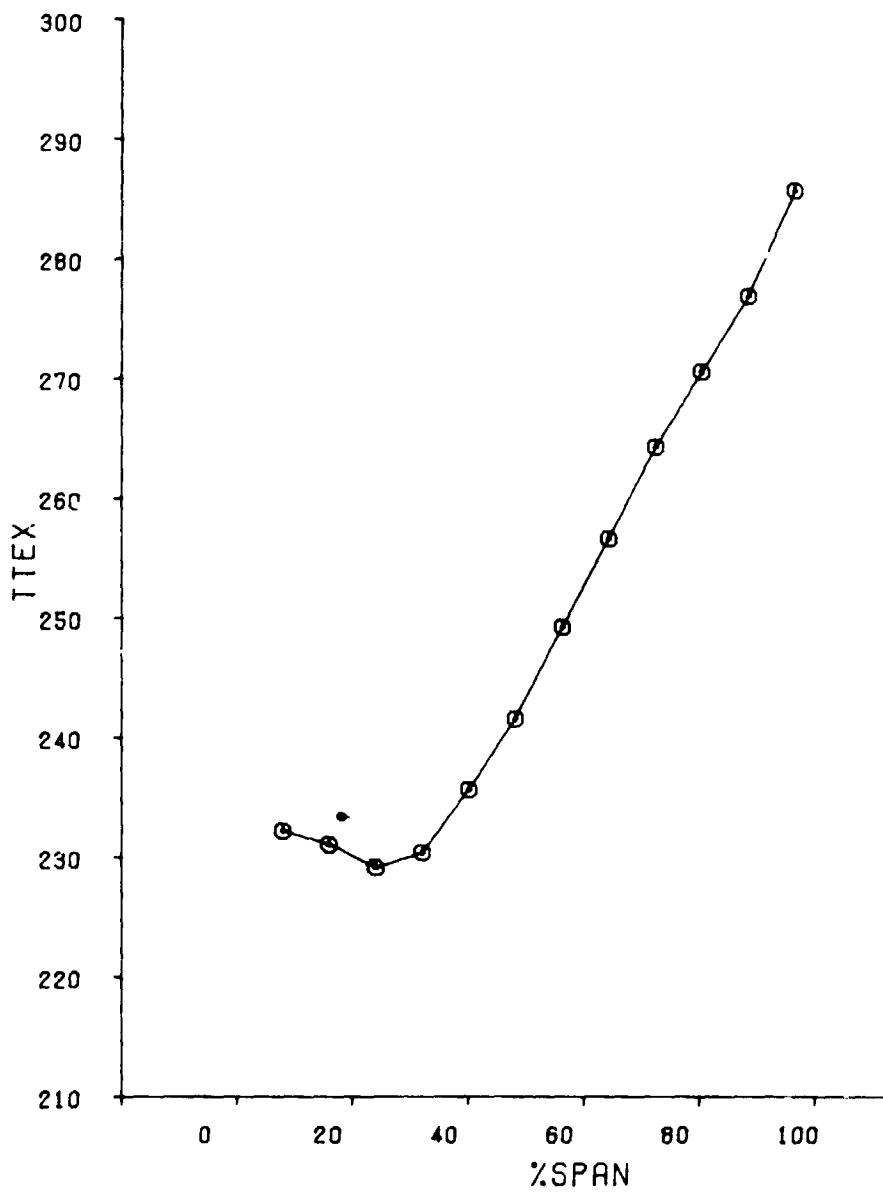


Figure B-68 Average Total Temperature Versus Span (Point 24)

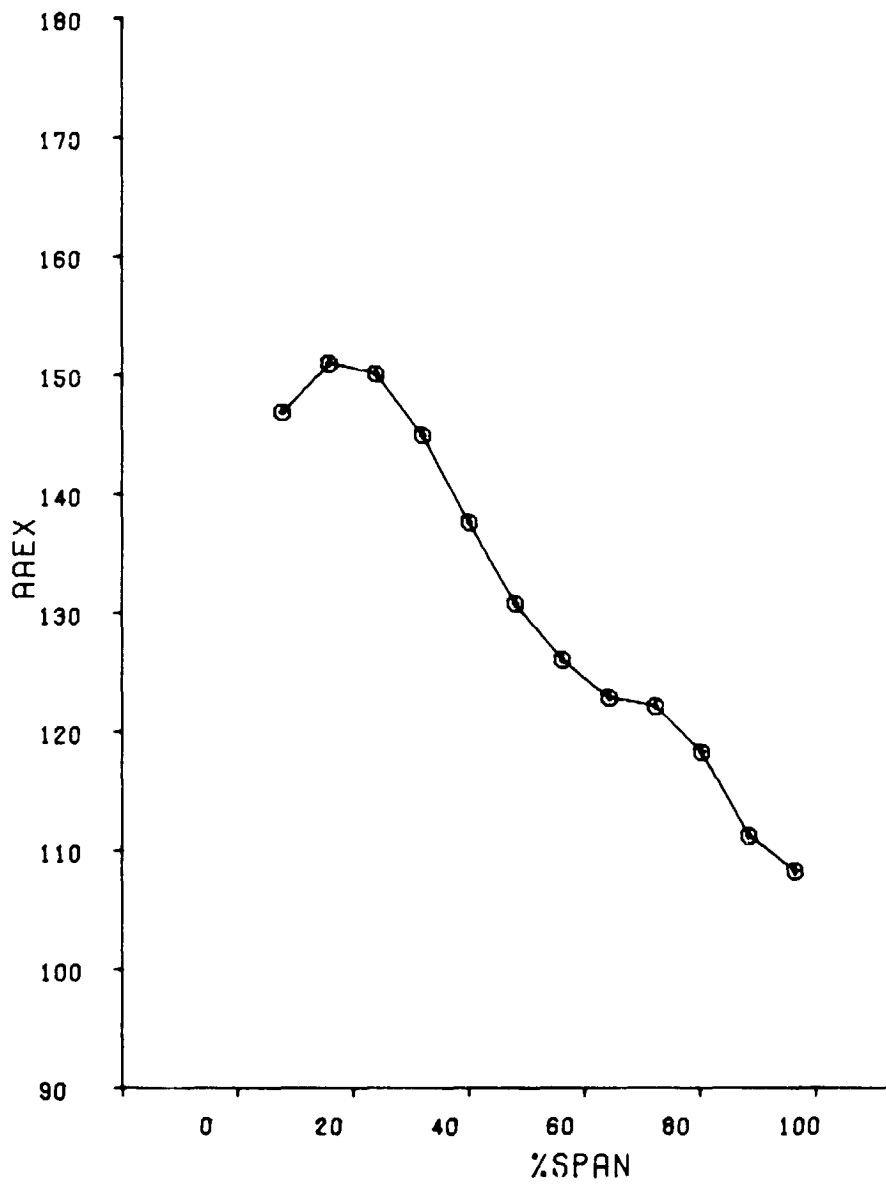


Figure B-69 Average Air Angle Versus Span (Point 24)

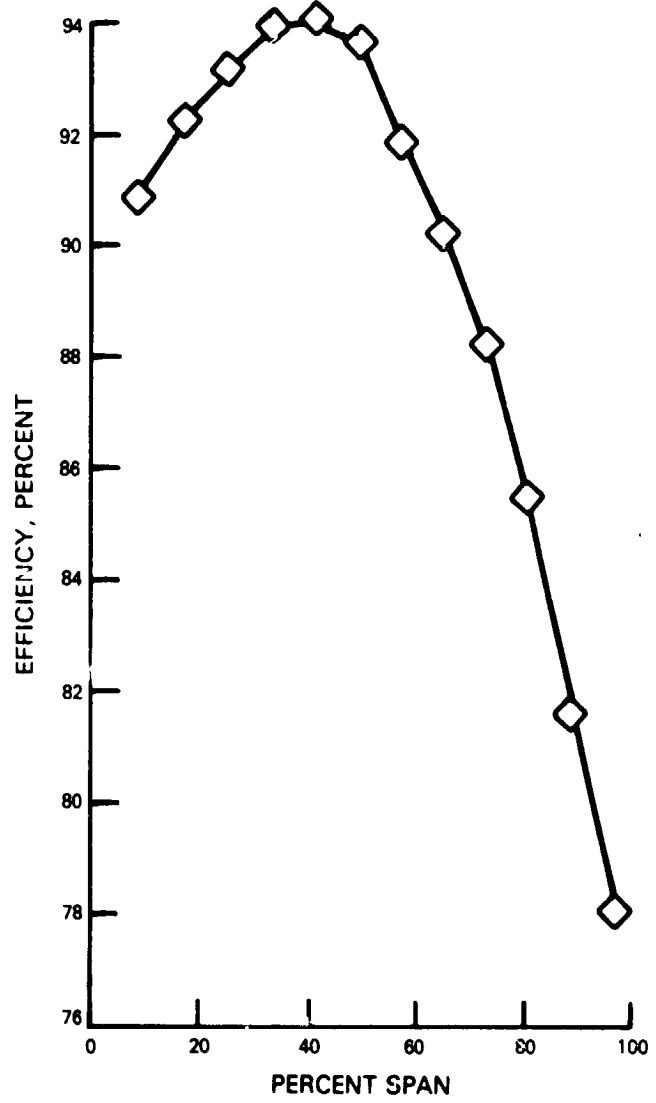


Figure B-70 Efficiency Versus Span (Point 24)

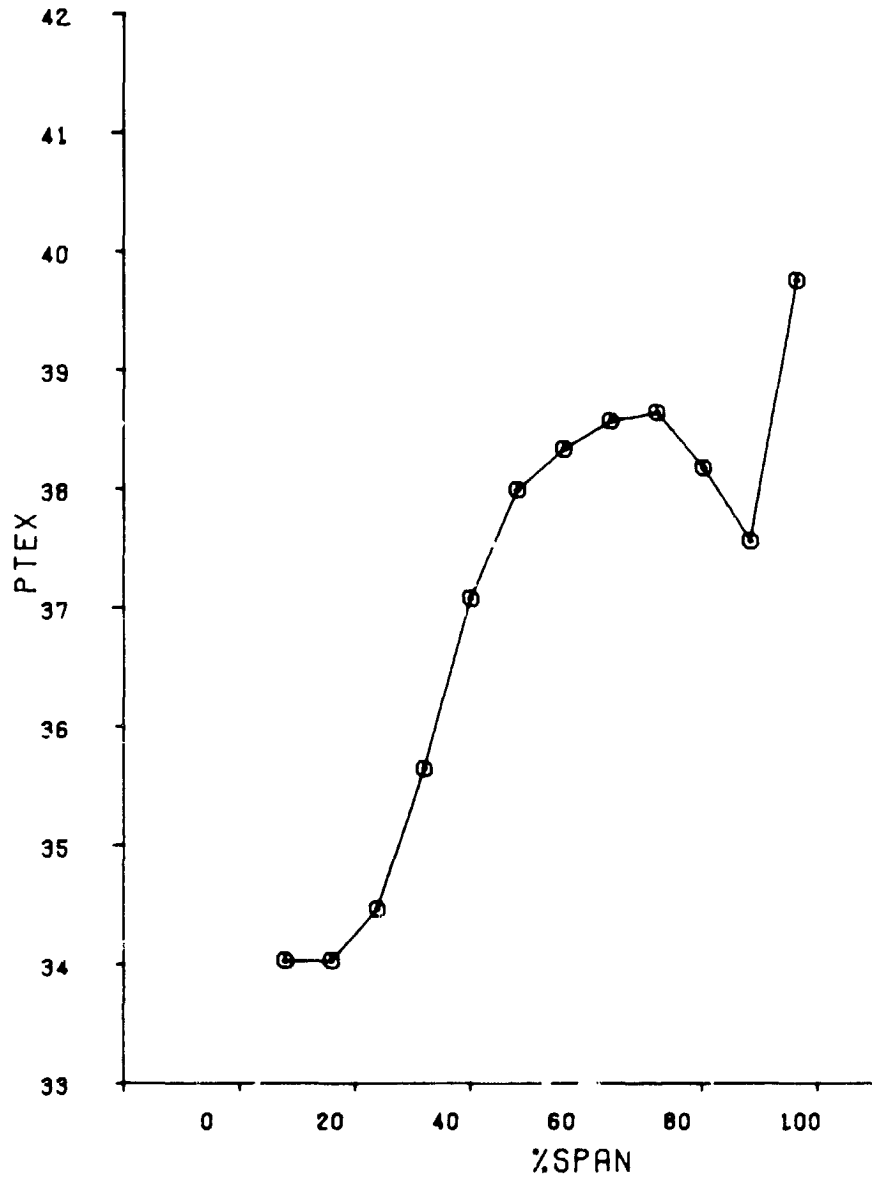


Figure B-71 Average Total Pressure Versus Span (Point 2^a)

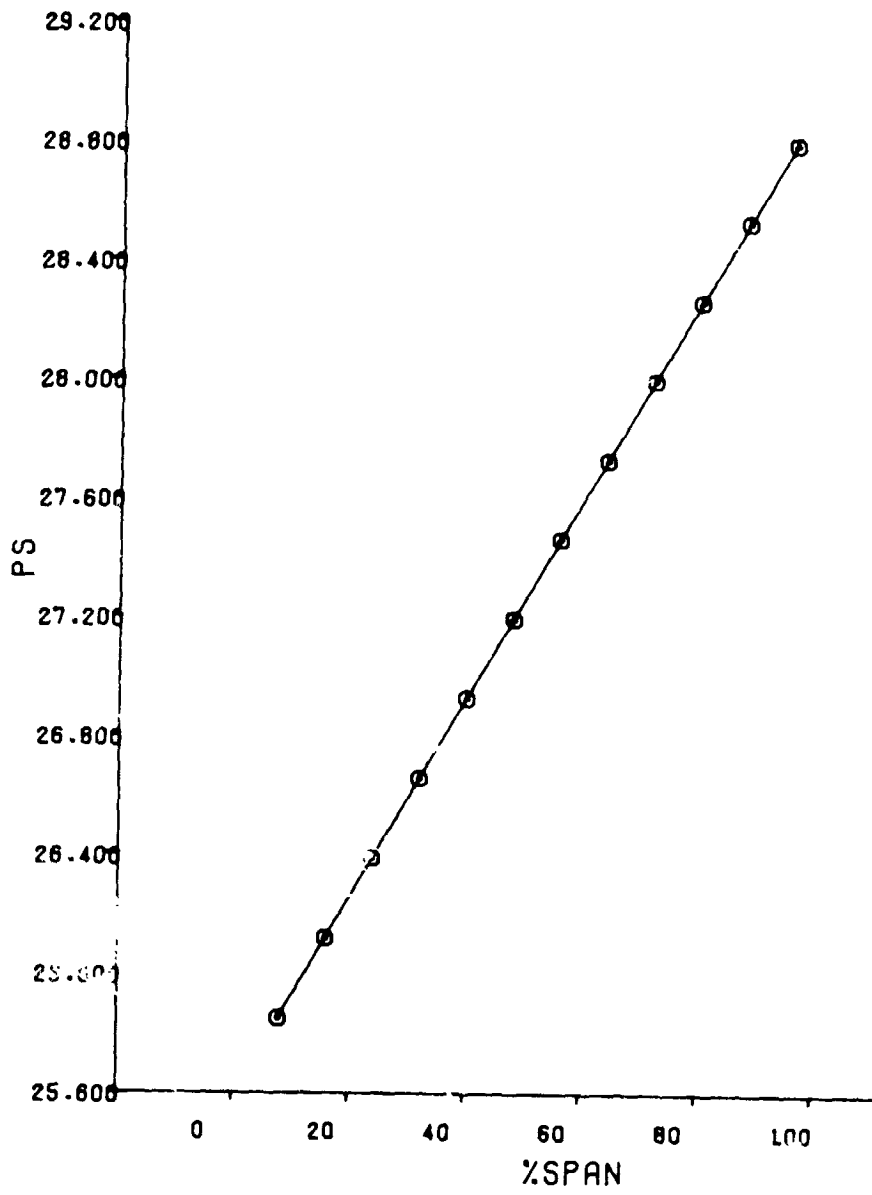


Figure B-72 Average Static Pressure Versus Span (Point 29)

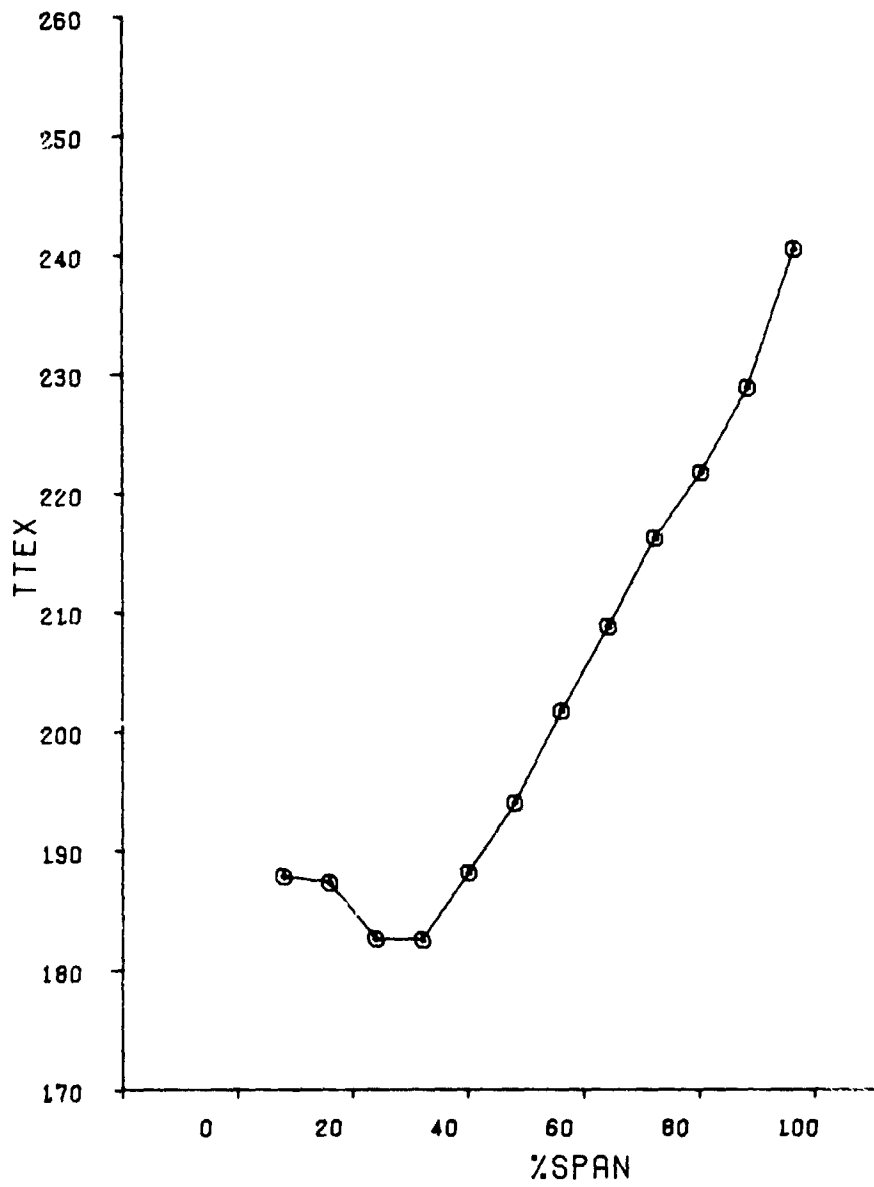


Figure B-73 Average Total Temperature Versus Span (Point 29)

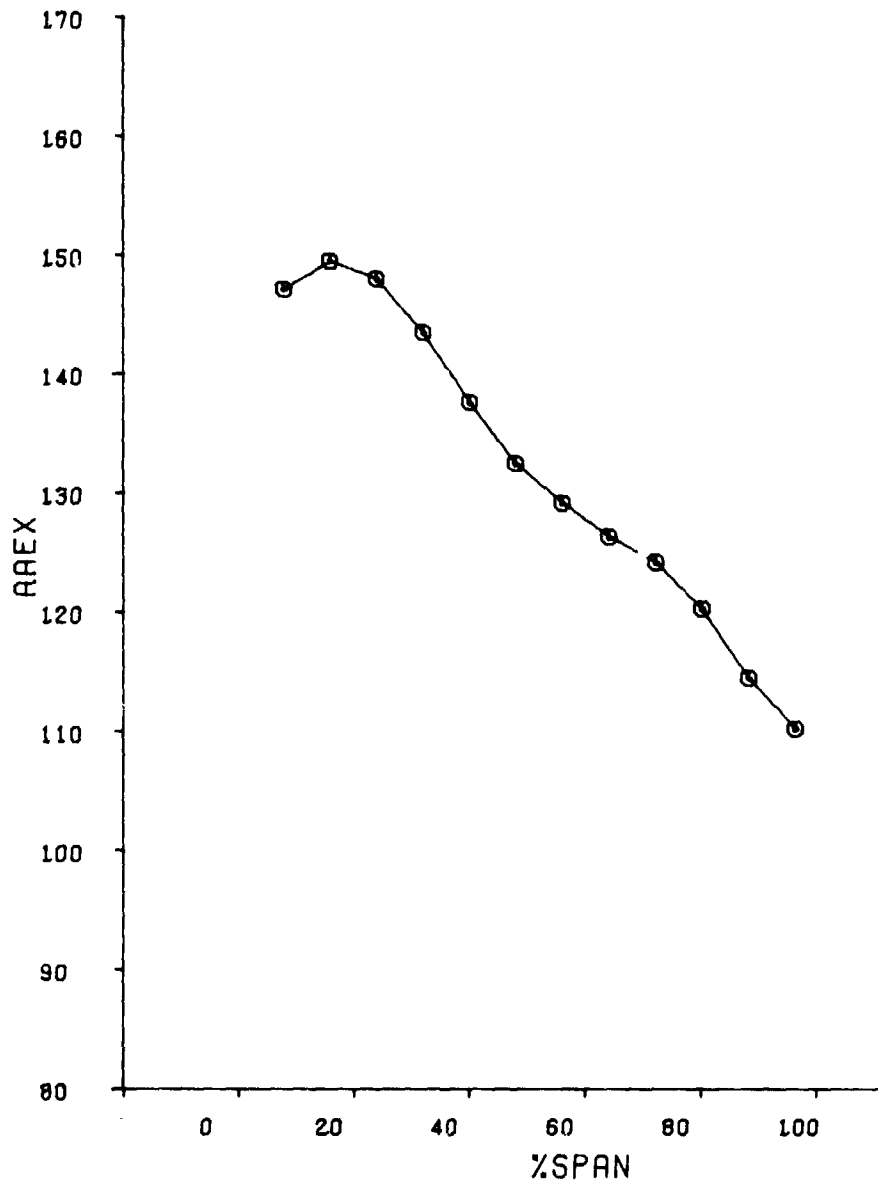


Figure B-74 Average Air Angle Versus Span (Point 29)

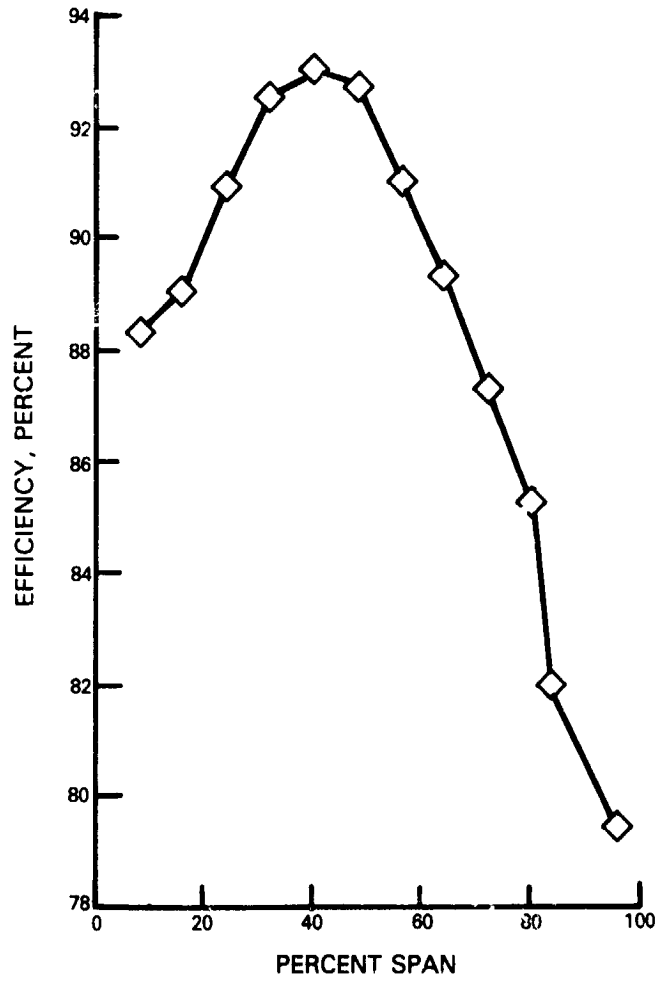


Figure B-75 Efficiency Versus Span (Point 29)

TABLE B-II
HIGH PRESSURE TURBINE CASCADE TEST RESULTS

PHASE 1

<u>TEST*</u> <u>POINT</u>	<u>MACH</u> <u>NUMBER</u>
1	0.70
2	0.85
3	0.91
4	1.0
5	1.08
6	1.19
7	0.56

PHASE 2

8	0.92
9	0.92

*For each test point, the exit total pressure (in HgA), static pressure (in HgA), air angle, vane loss ($\Delta P_T/P_T$), and pressure distribution are presented.

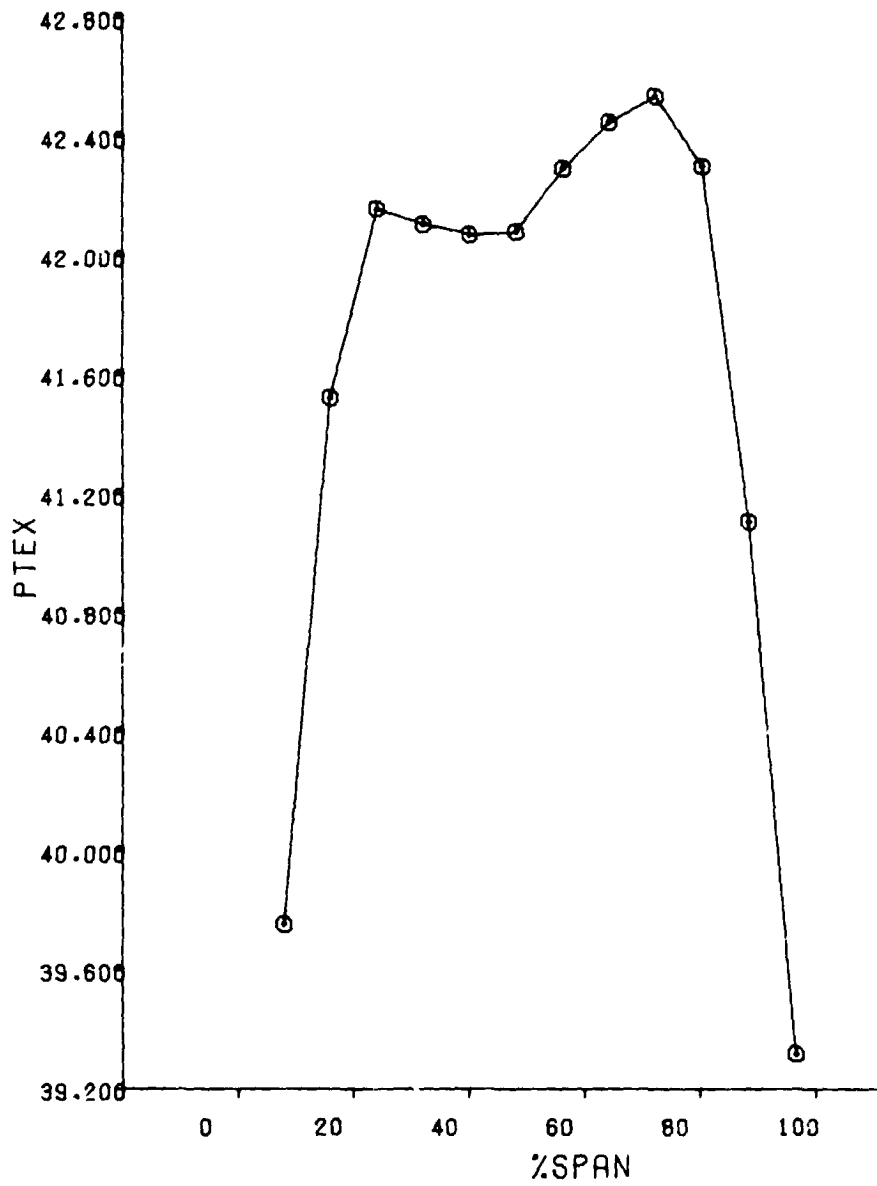


Figure B-76 Average Total Pressure Versus Span (Point 1)

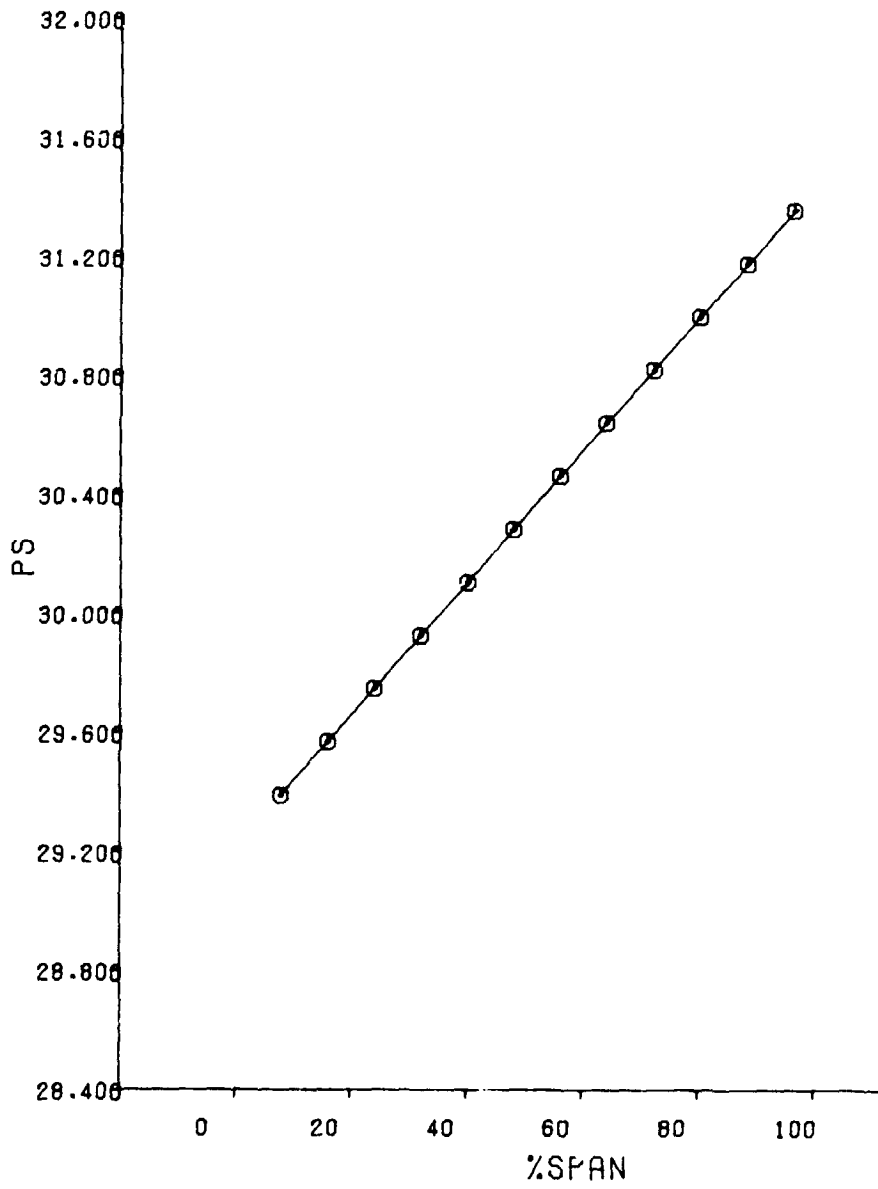


Figure B-77 Average Static Pressure Versus Span (Point 1)

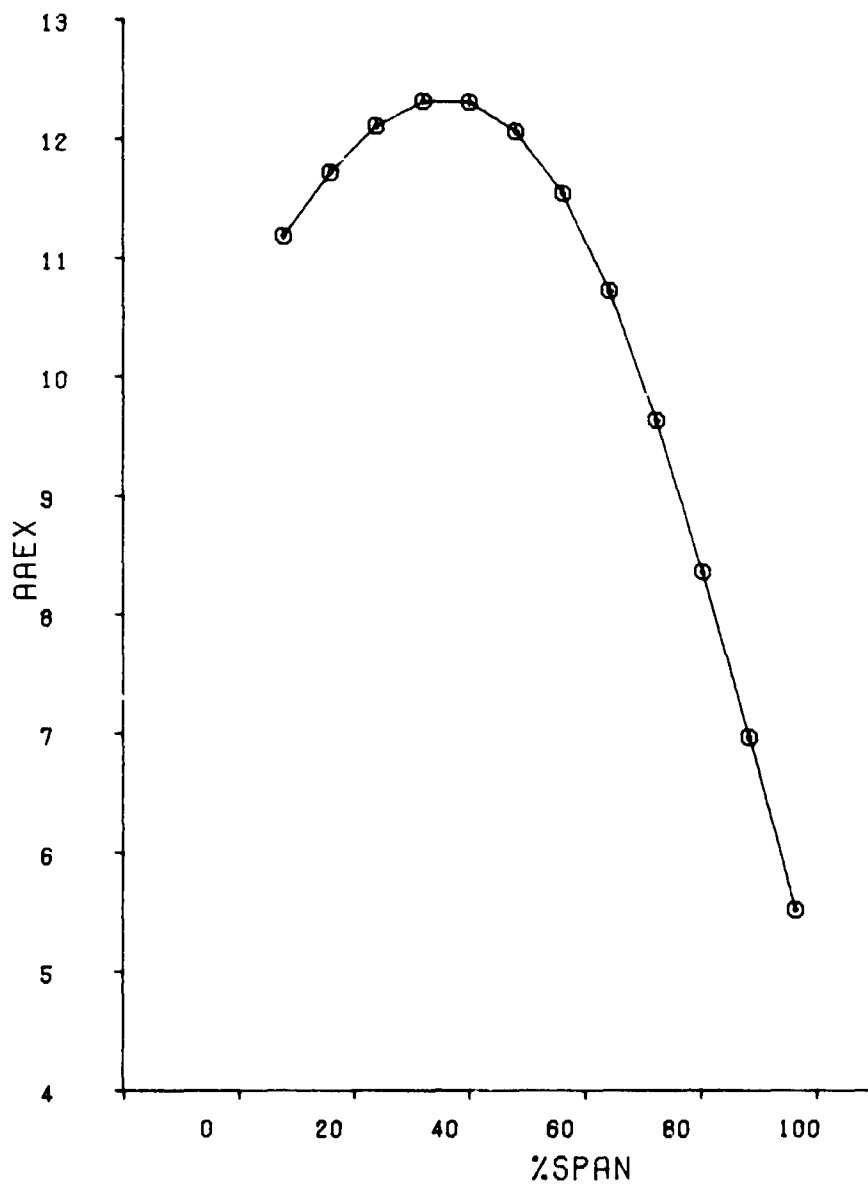


Figure B-78 Average Air Angle Versus Span (Point 1)

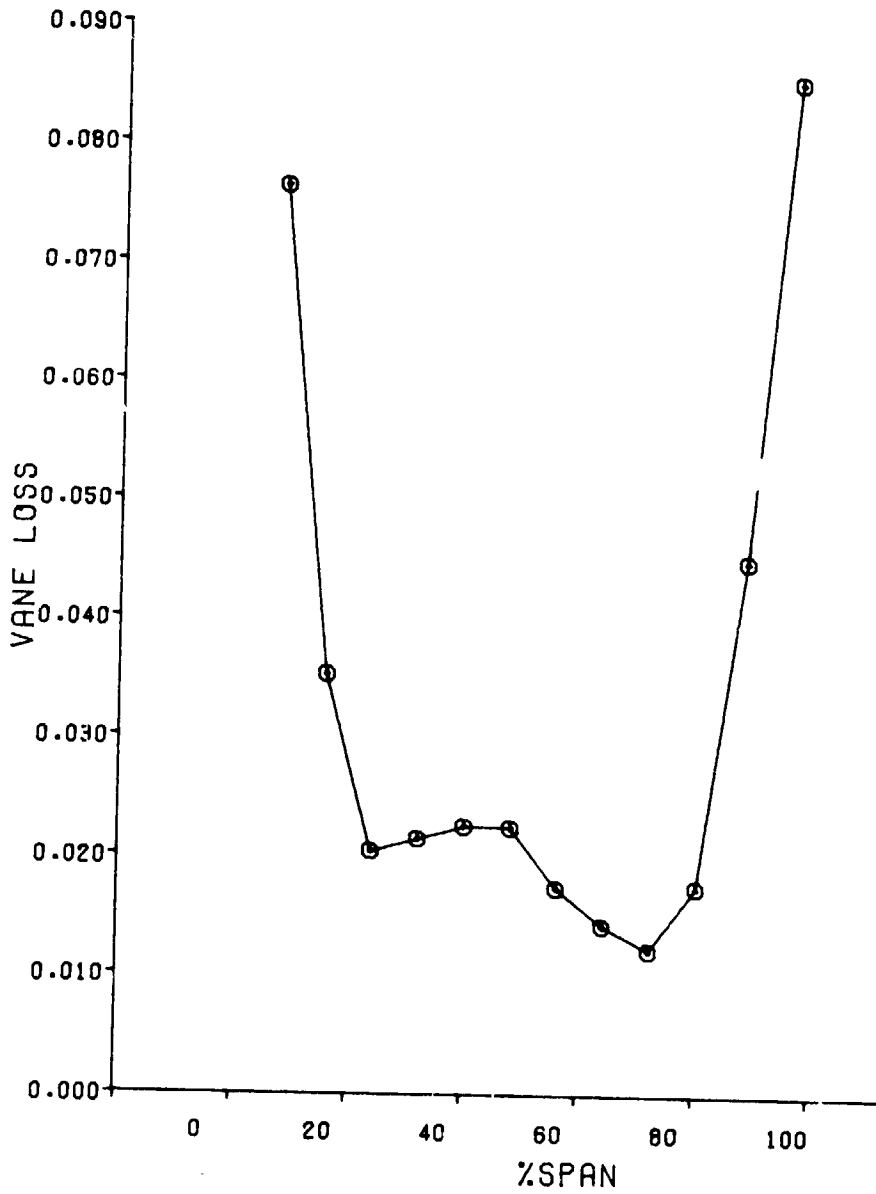


Figure B-79 Vane Loss Versus Span (Point 1)

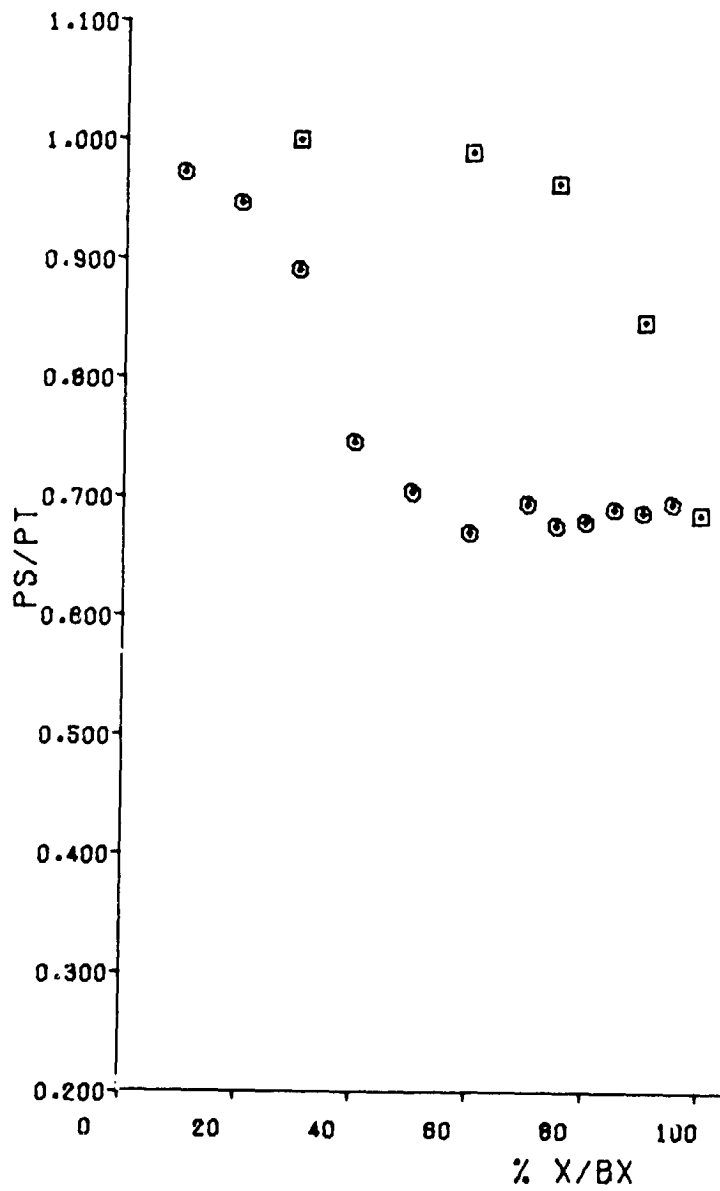


Figure B-80 Vane Pressure Distribution at 11 Percent Span (Point 1)

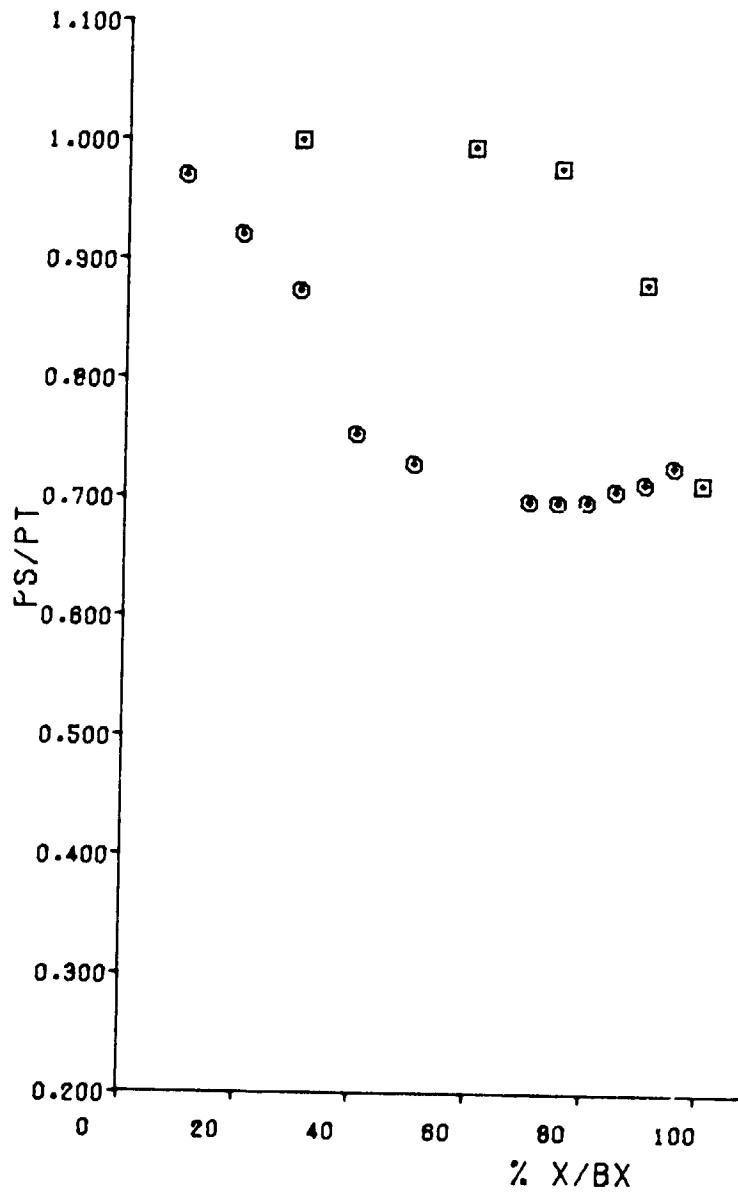


Figure B-81 Vane Pressure Distribution at 50 Percent Span (Point 1)

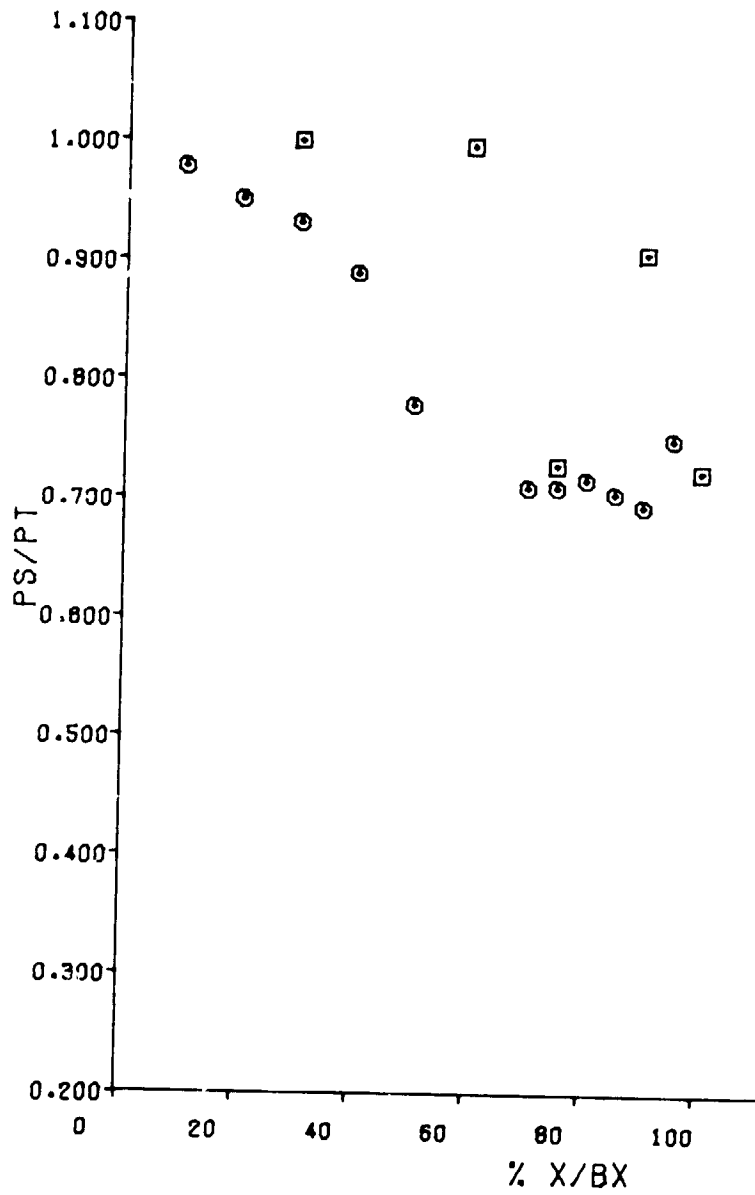


Figure B-82 Vane Pressure Distribution at 89 Percent Span (Point 1)

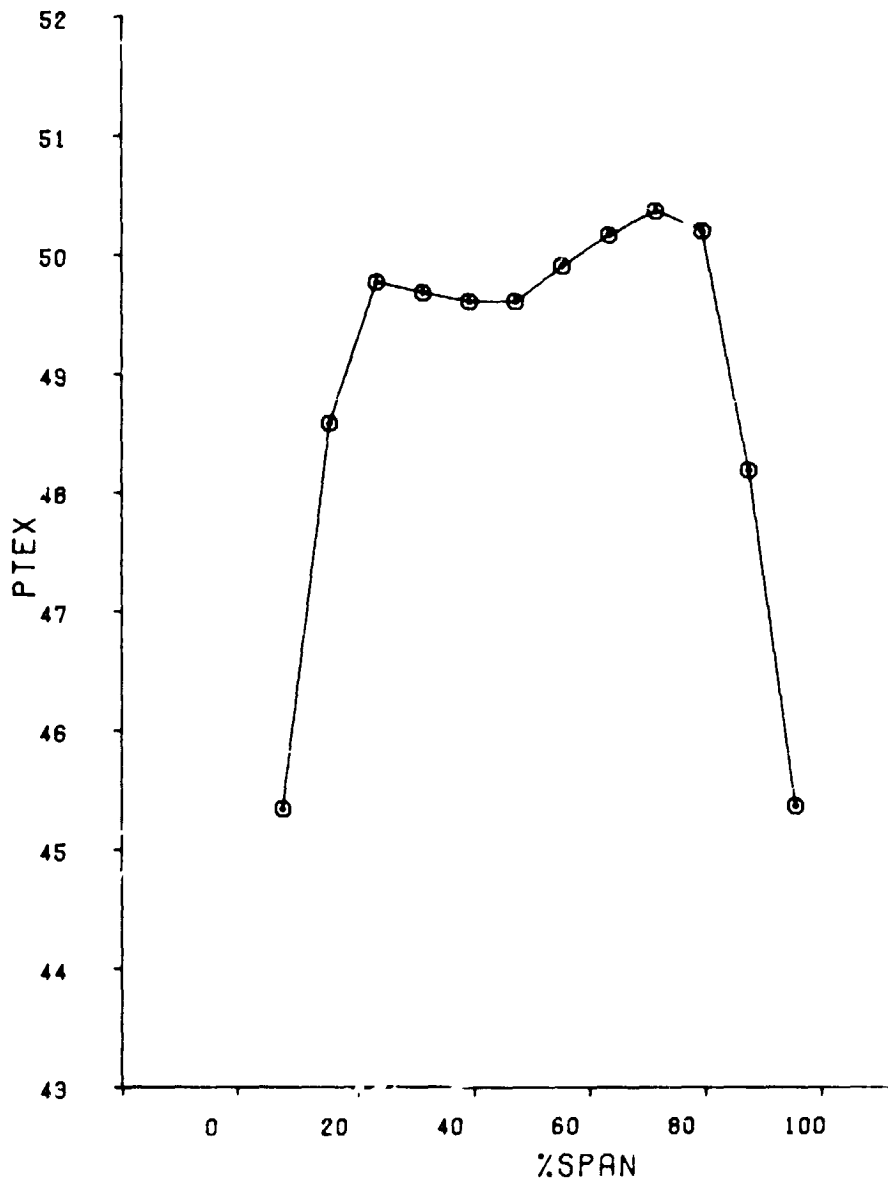


Figure B-83 Vane Average Total Pressure Versus Span (Point 2)

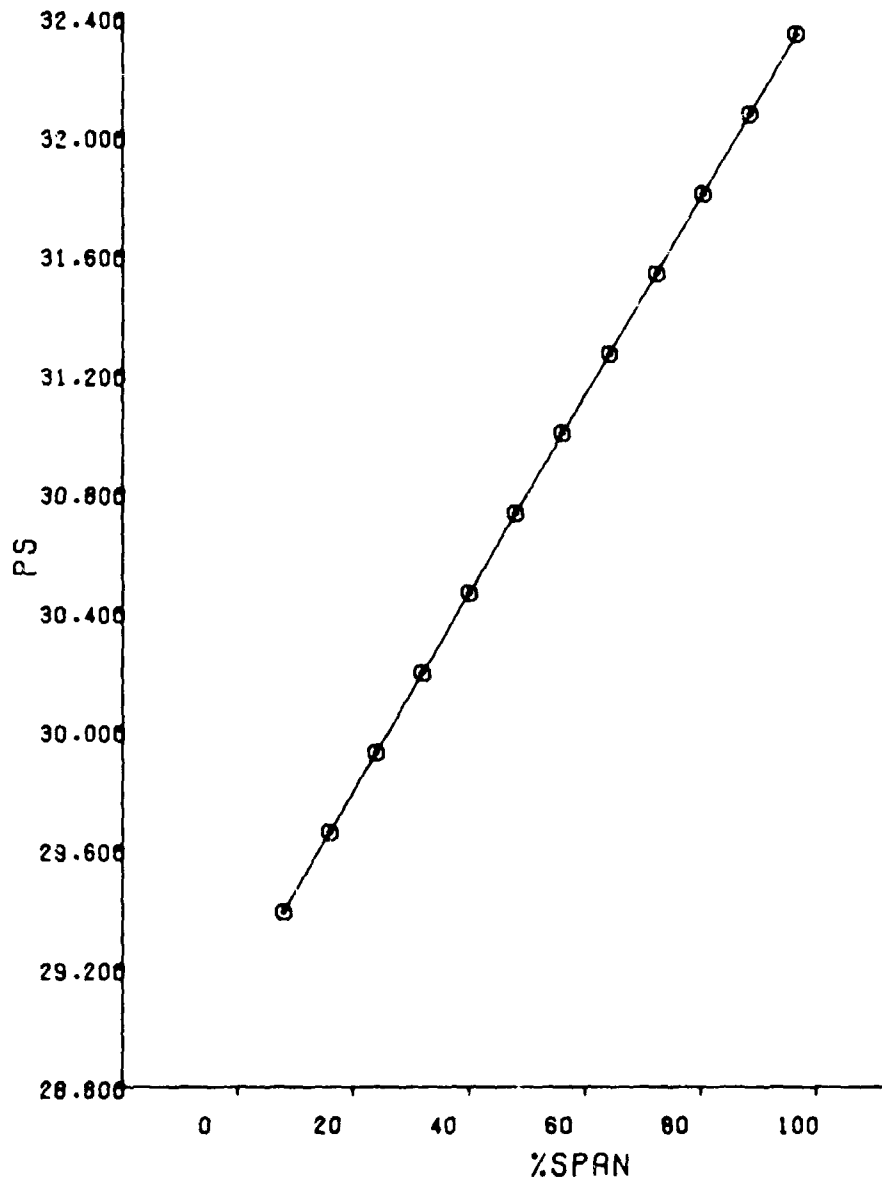


Figure B-84 Vane Average Static Pressure Versus Span (Point 2)

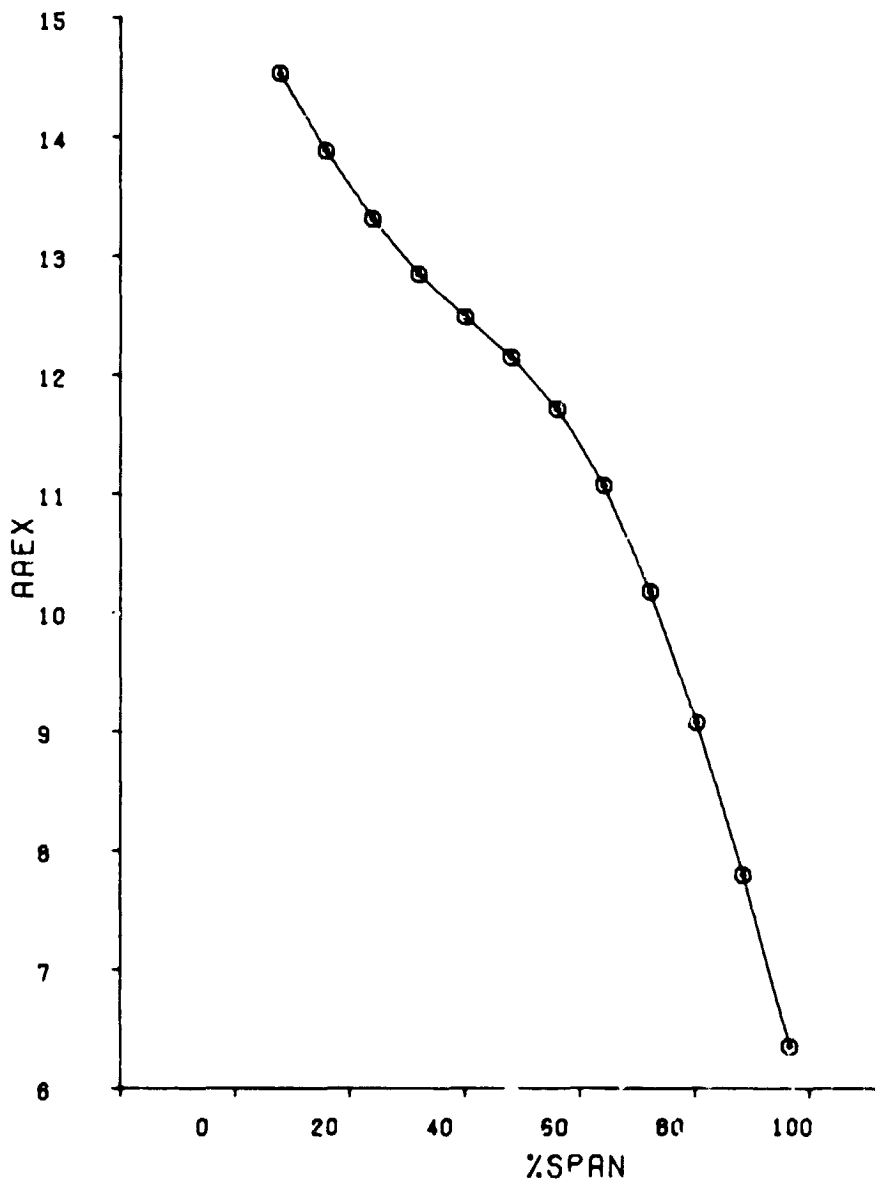


Figure B-85 Vane Average Air Angle Versus Span (Point 2)

425

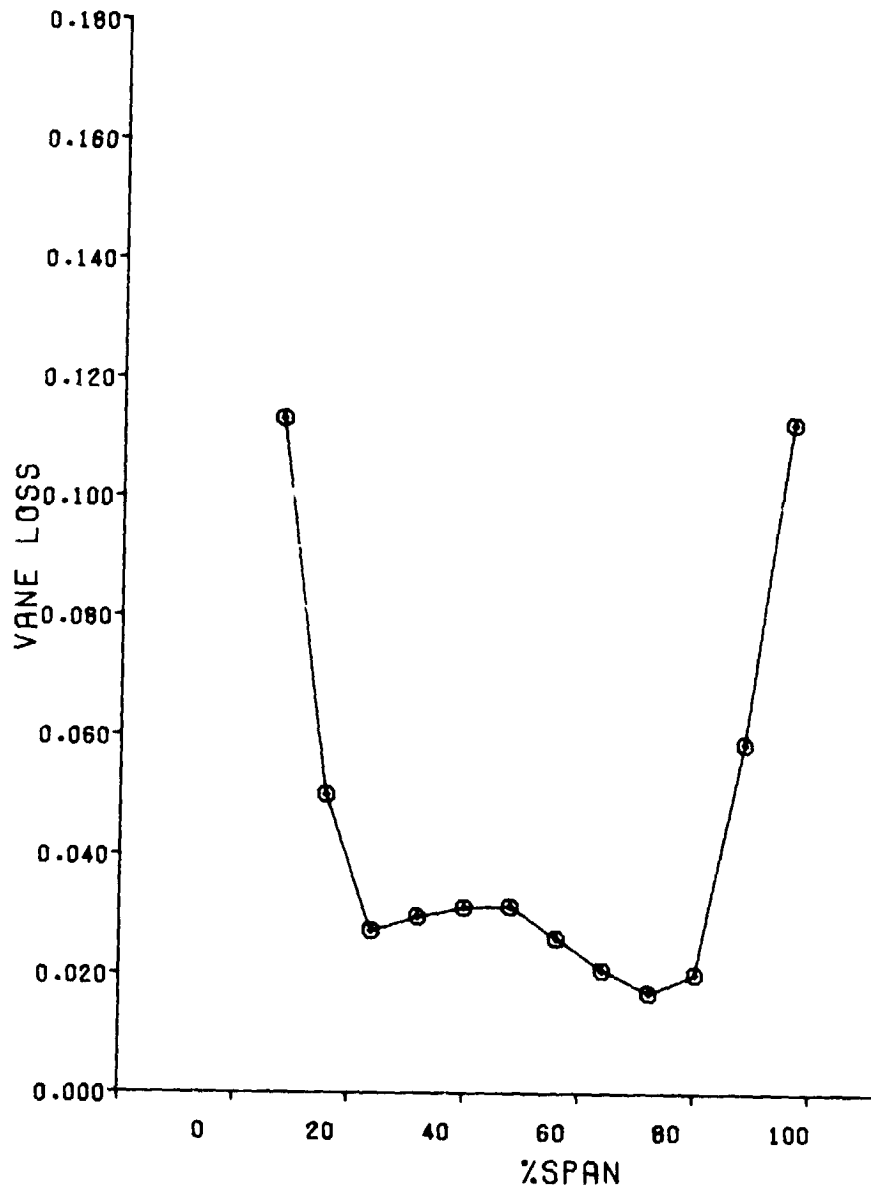


Figure B-86 Vane Loss Versus Span (Point 2)

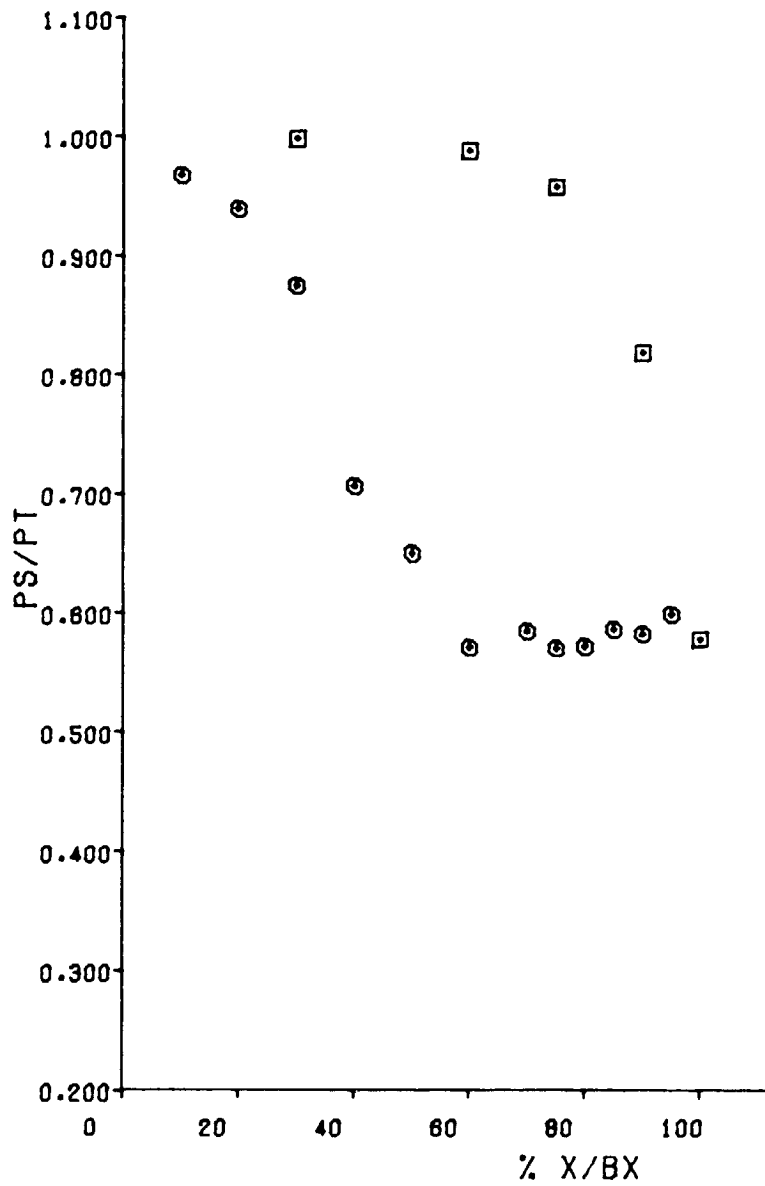


Figure B-87 Vane Pressure Distribution at 11 Percent Span (Point 2)

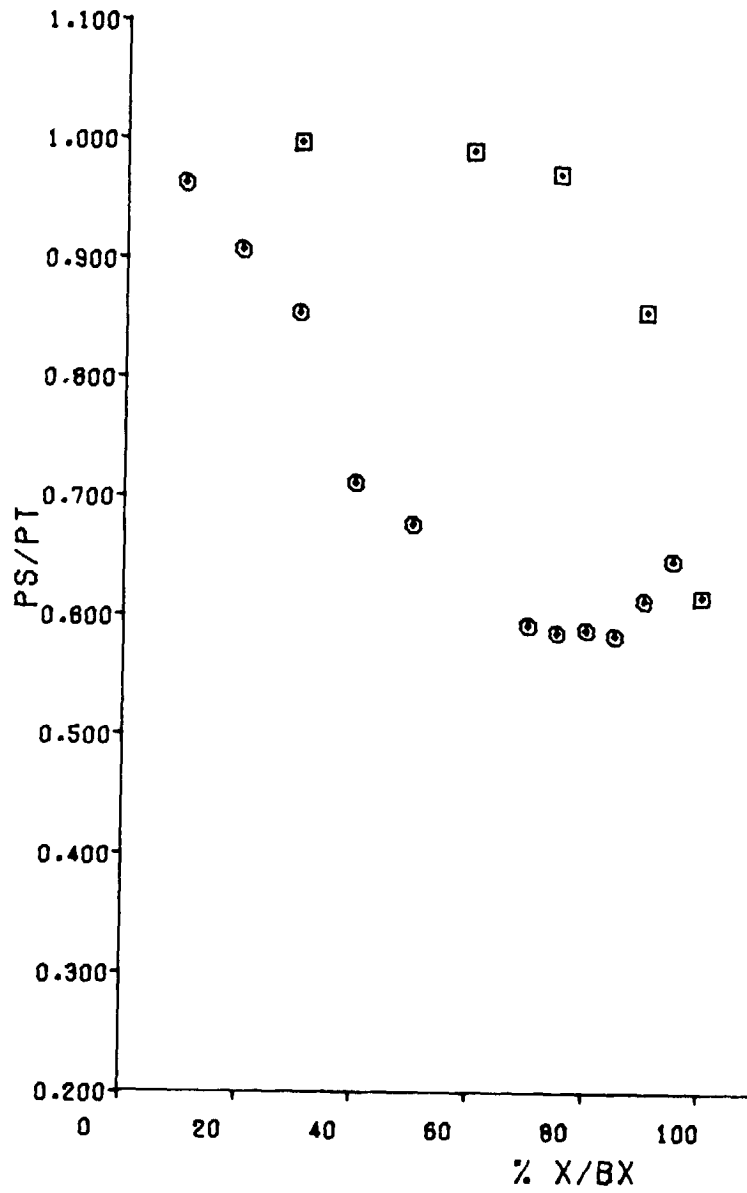


Figure B-88 Vane Pressure Distribution at 50 Percent Span (Point 2)

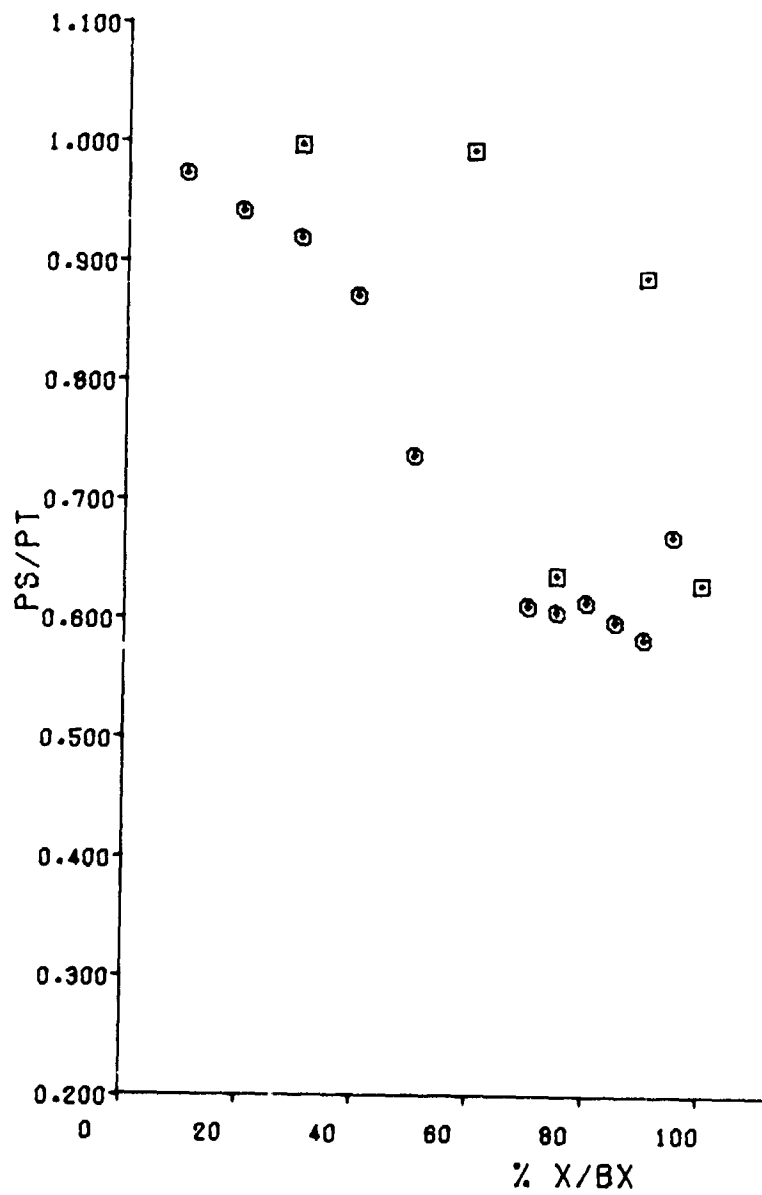


Figure B-89 Vane Pressure Distribution at 89 Percent Span (Point 2)

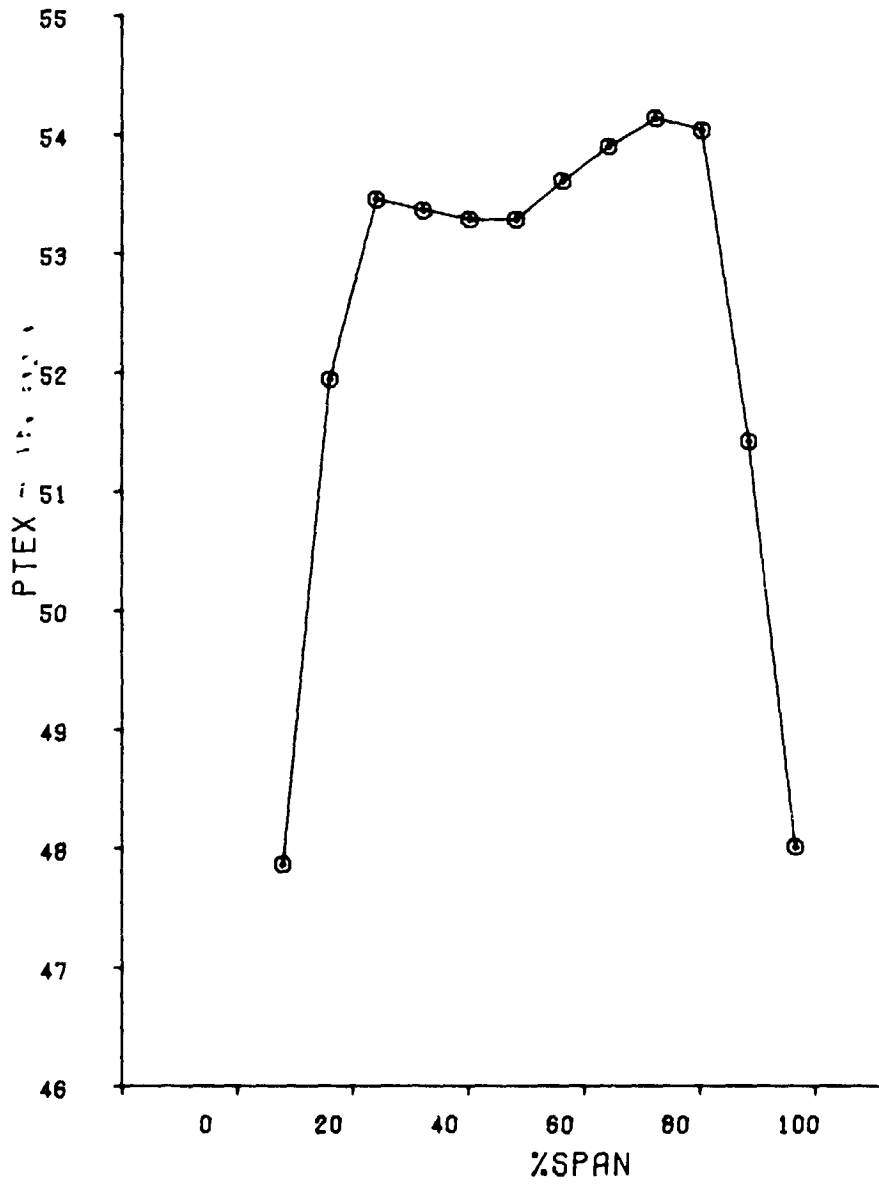


Figure B-90 Vane Average Total Pressure Versus Span (Point 3)

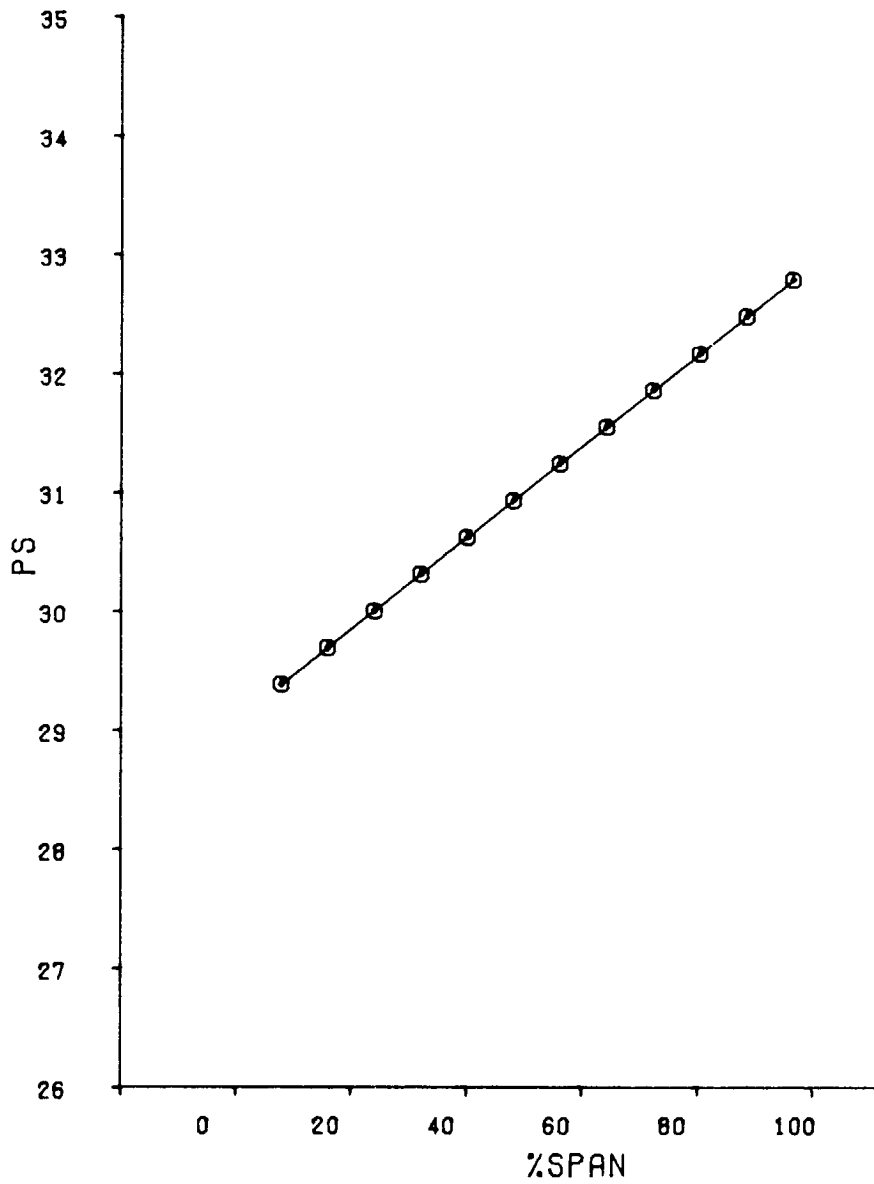


Figure B-91 Vane Average Static Pressure Versus Span (Point 3)

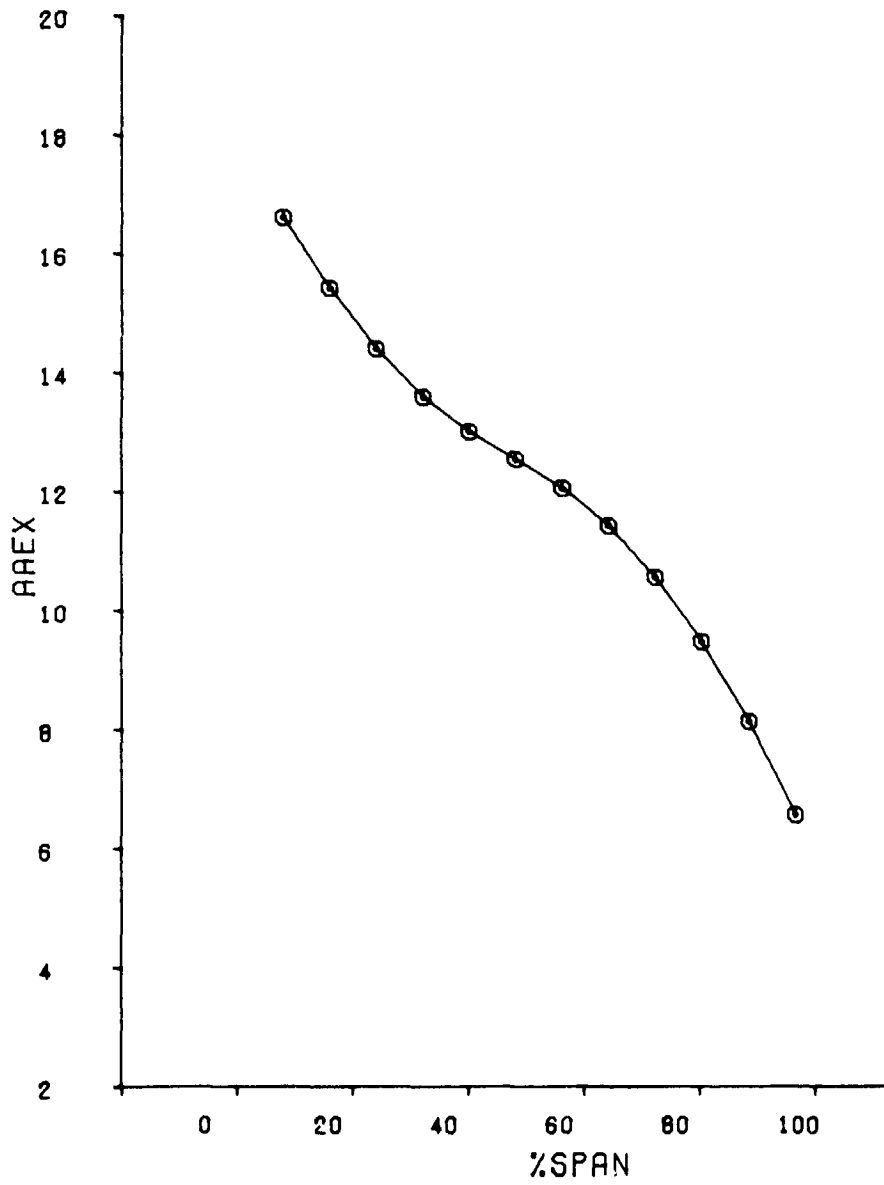


Figure B-92 Vane Average Air Angle Versus Span (Point 3)

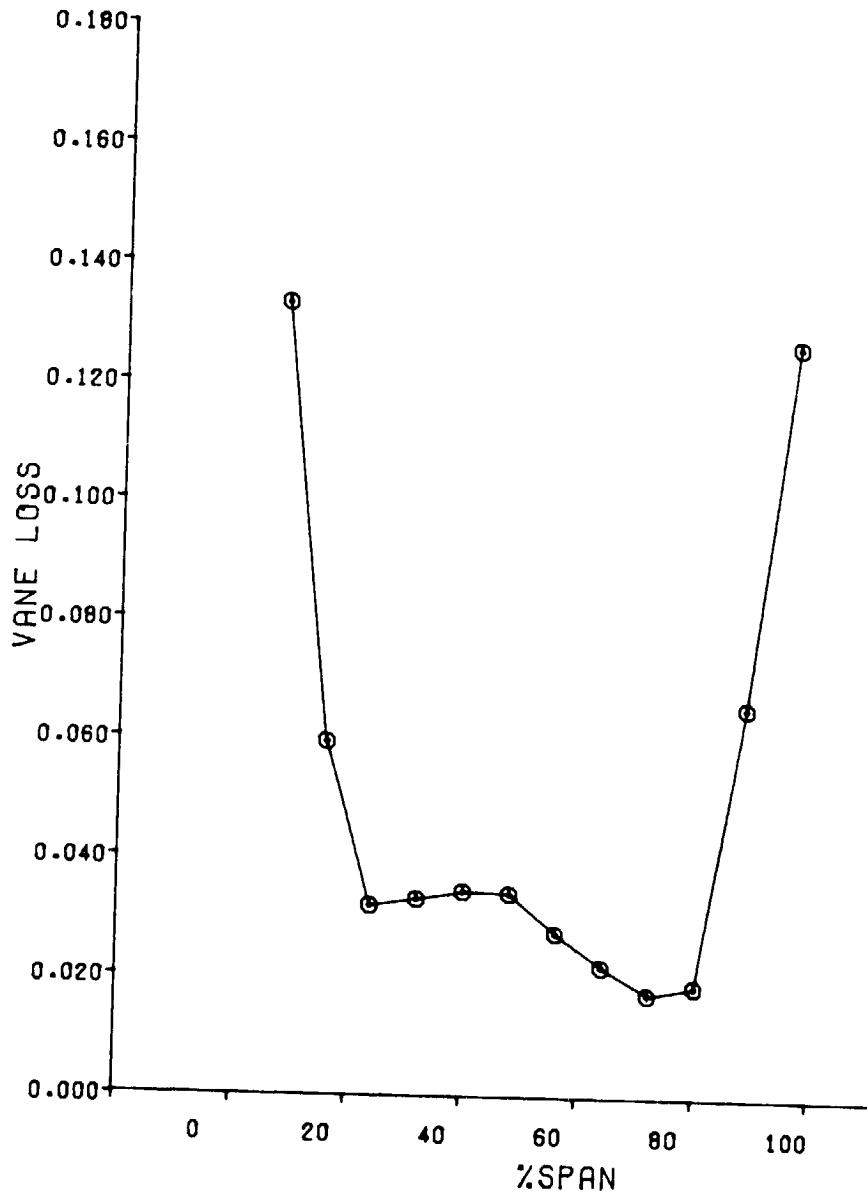


Figure B-93 Vane Loss Versus Span (Point 3)

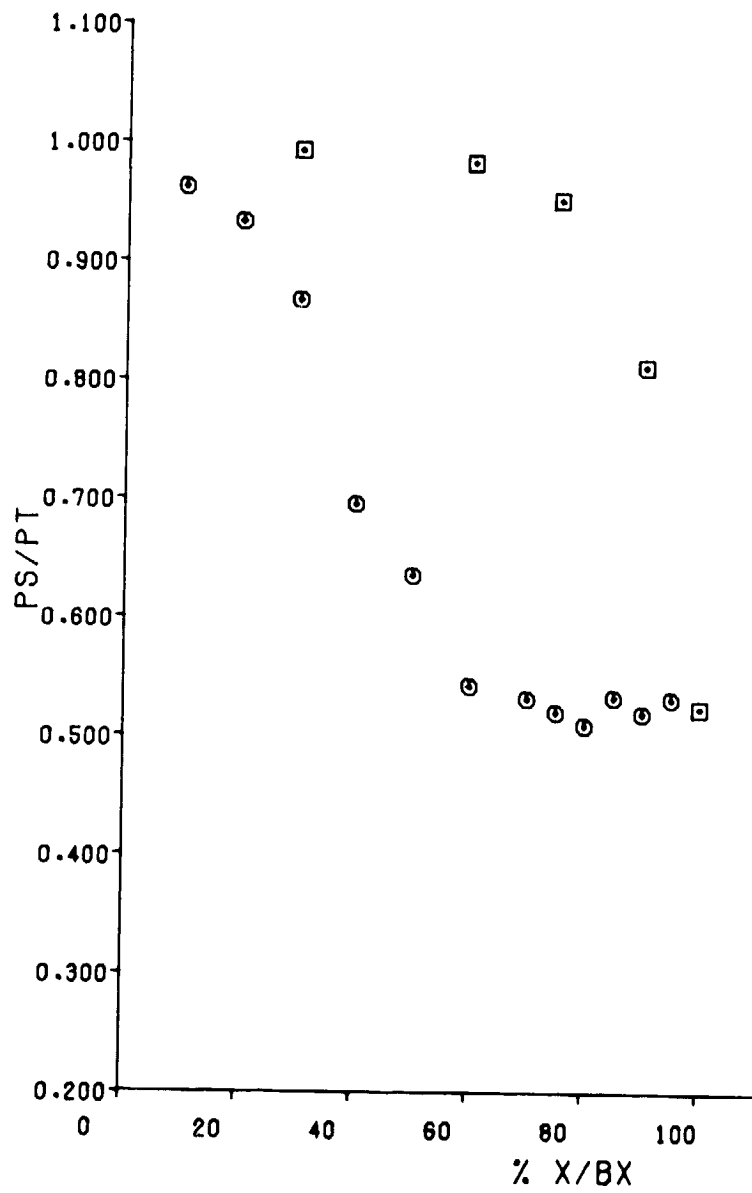


Figure B-94 Vane Pressure Distribution at 11 Percent Span (Point 3)

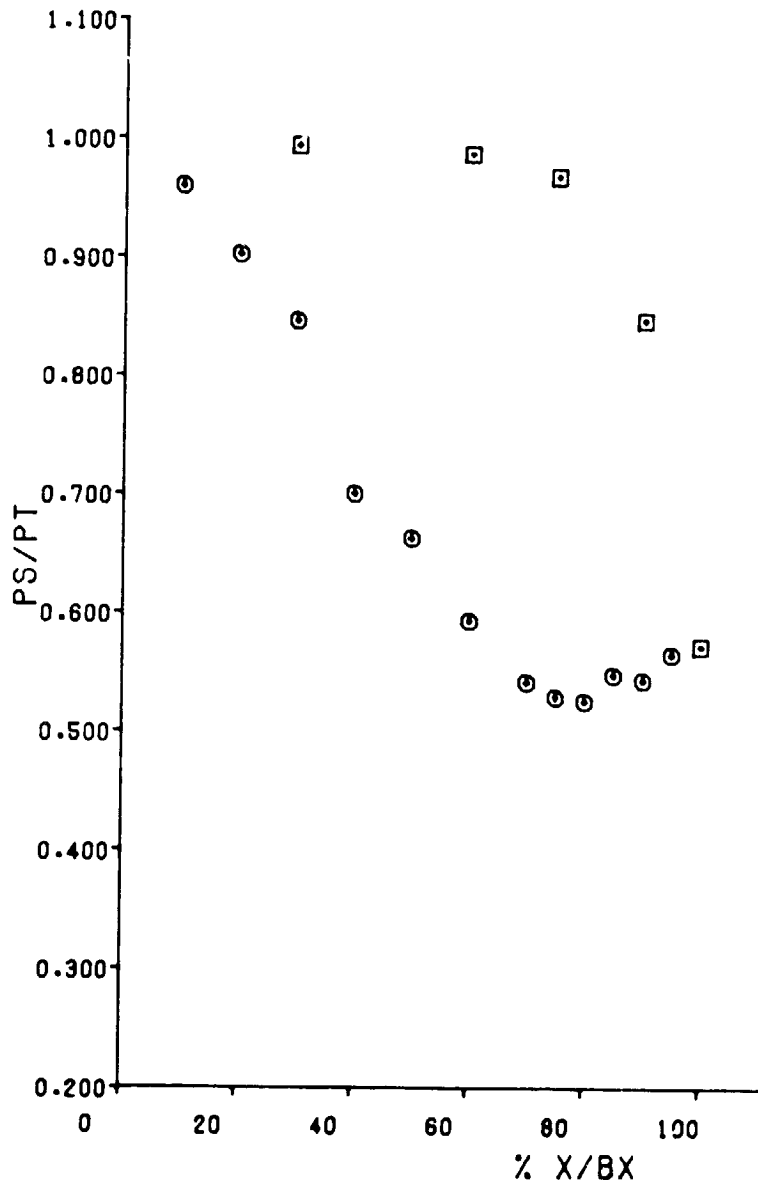


Figure B-95 Vane Pressure Distribution at 50 Percent Span (Point 3)

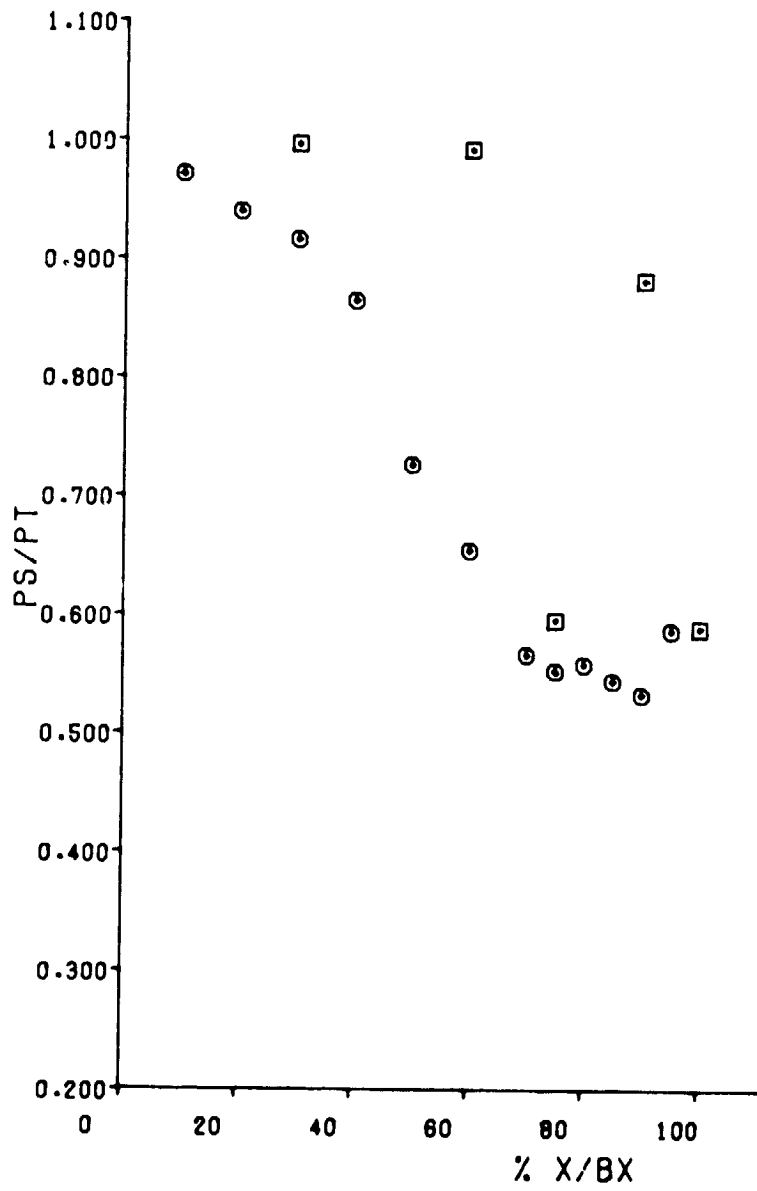


Figure B-96 Vane Pressure Distribution at 89 Percent Span (Point 3)

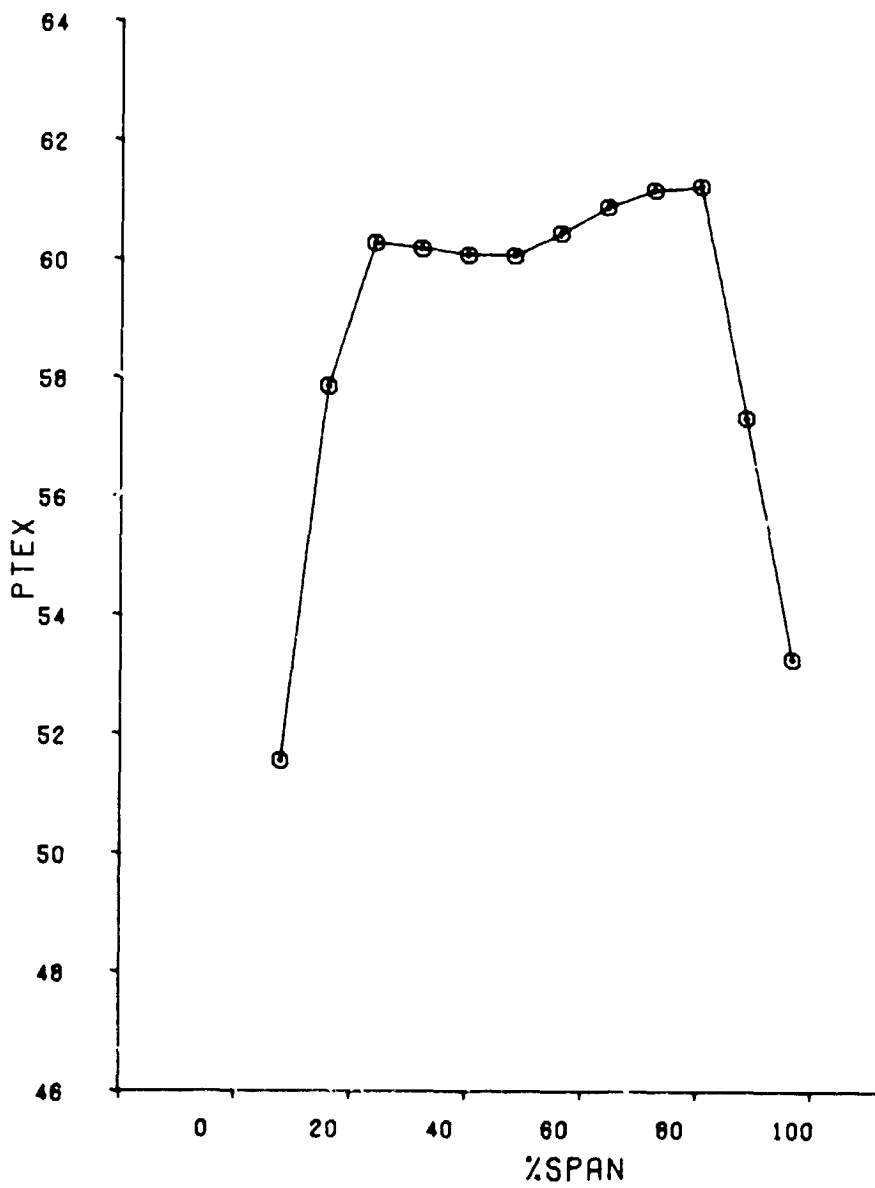


Figure B-97 Vane Average Total Pressure Versus Span (Point 4)

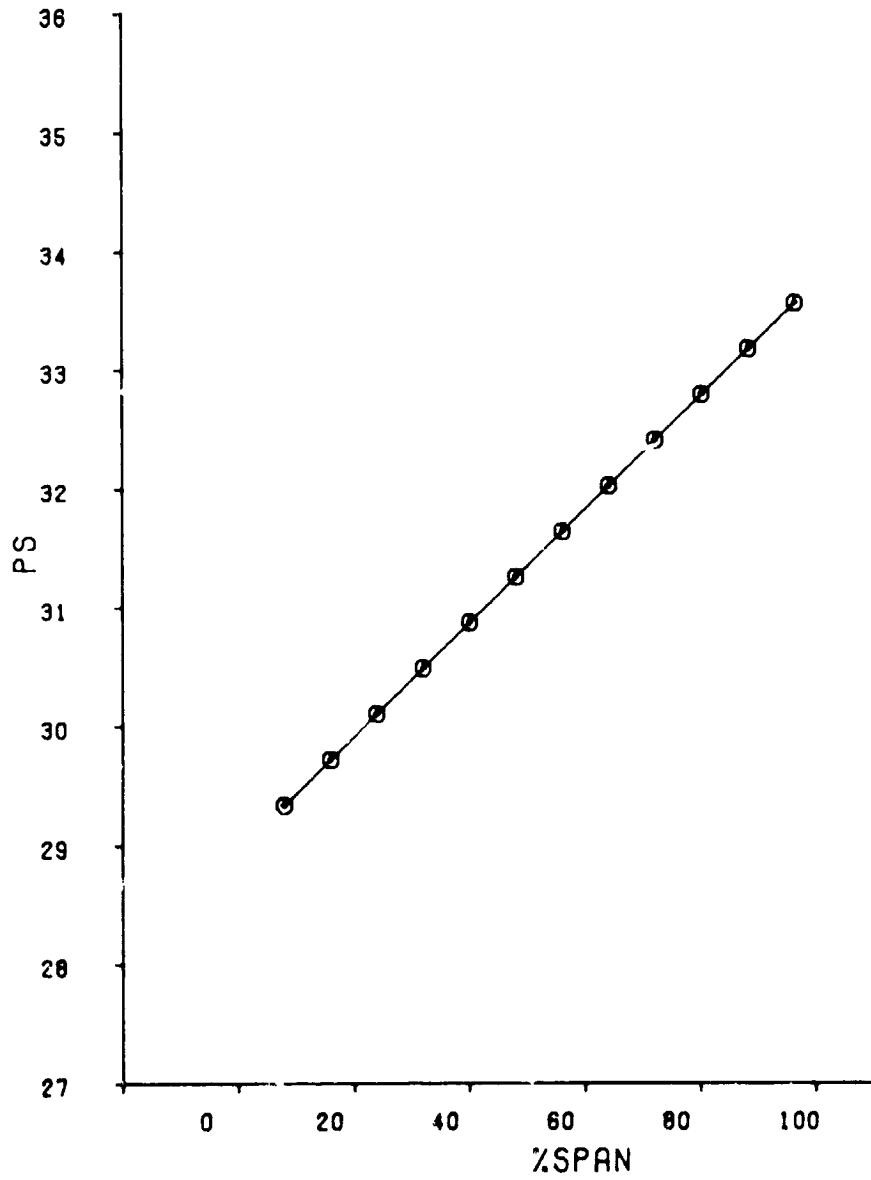


Figure B-98 Vane Average Static Pressure Versus Span (Point 4)

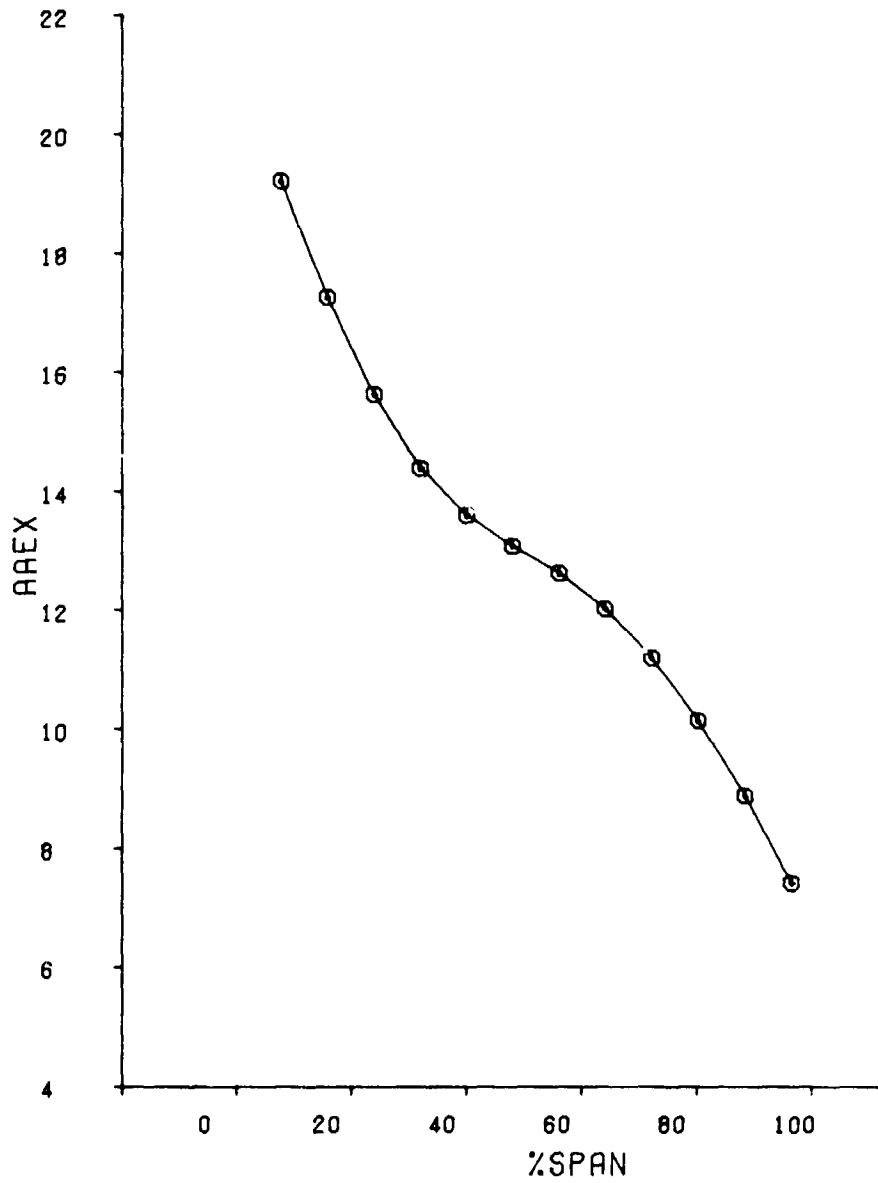


Figure B-99 Vane Average Air Angle Versus Span (Point 4)

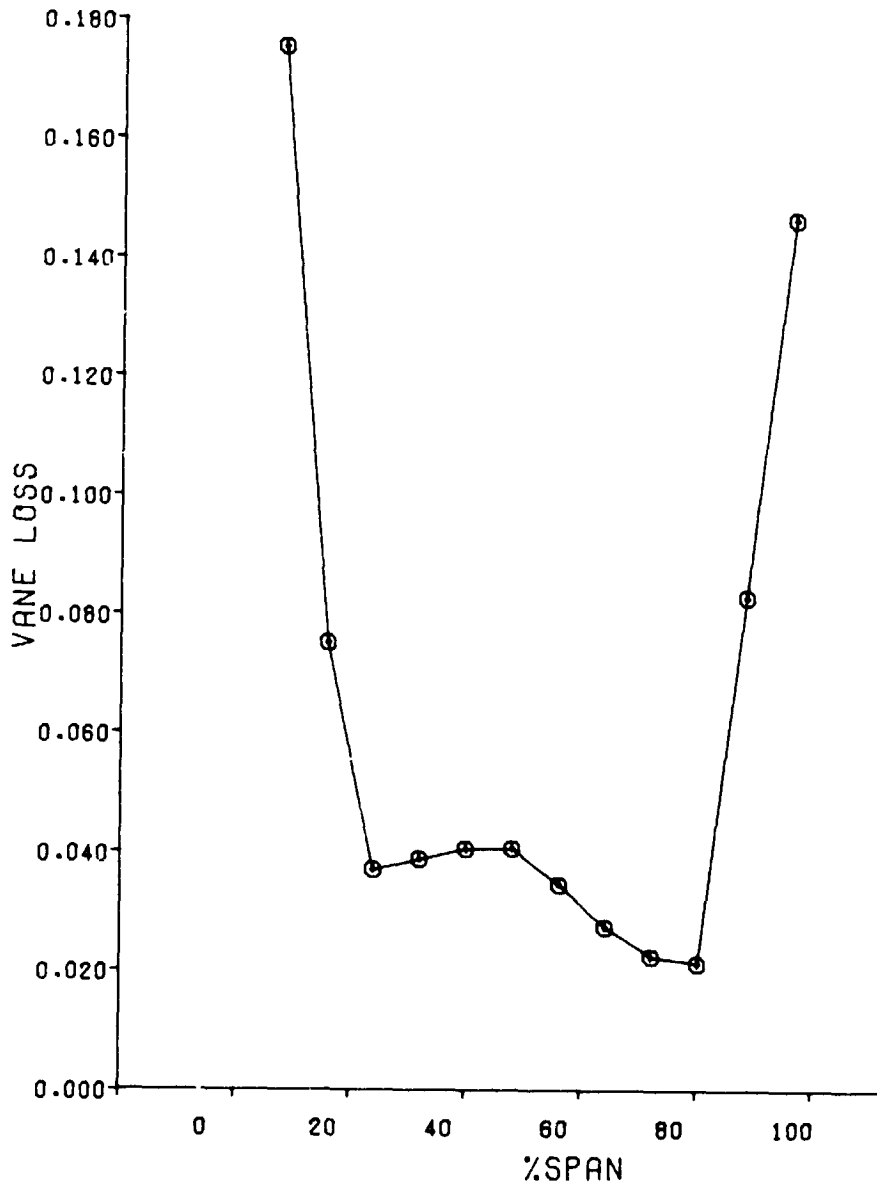


Figure B-100 Vane Loss Versus Span (Point 4)

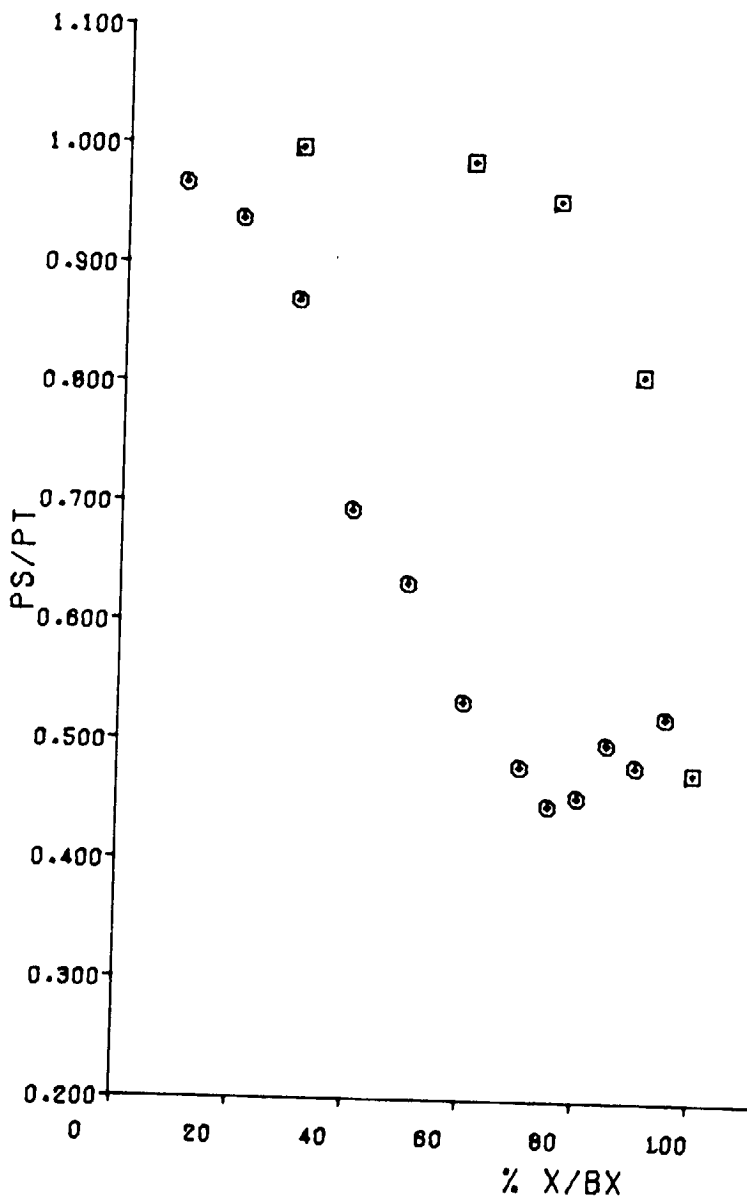


Figure B-101 Vane Pressure Distribution at 11 Percent Span (Point 4)

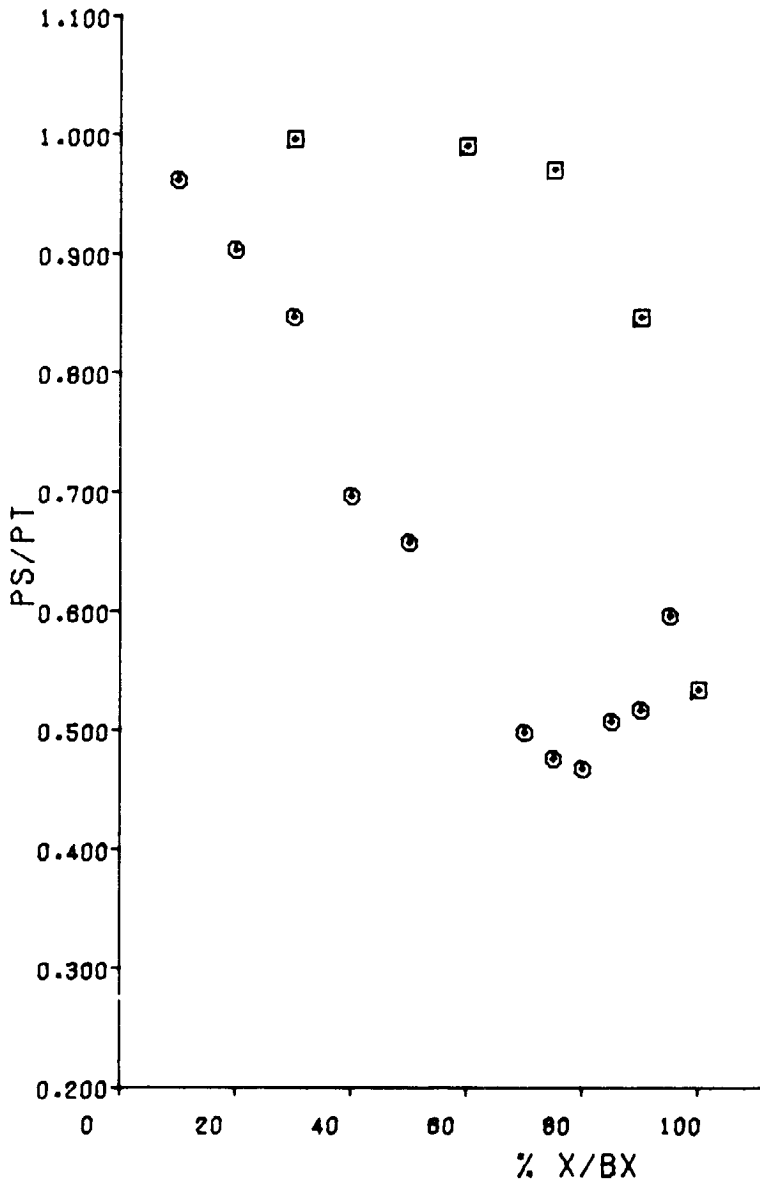


Figure B-102 Vane Pressure Distribution at 50 Percent Span (Point 4)

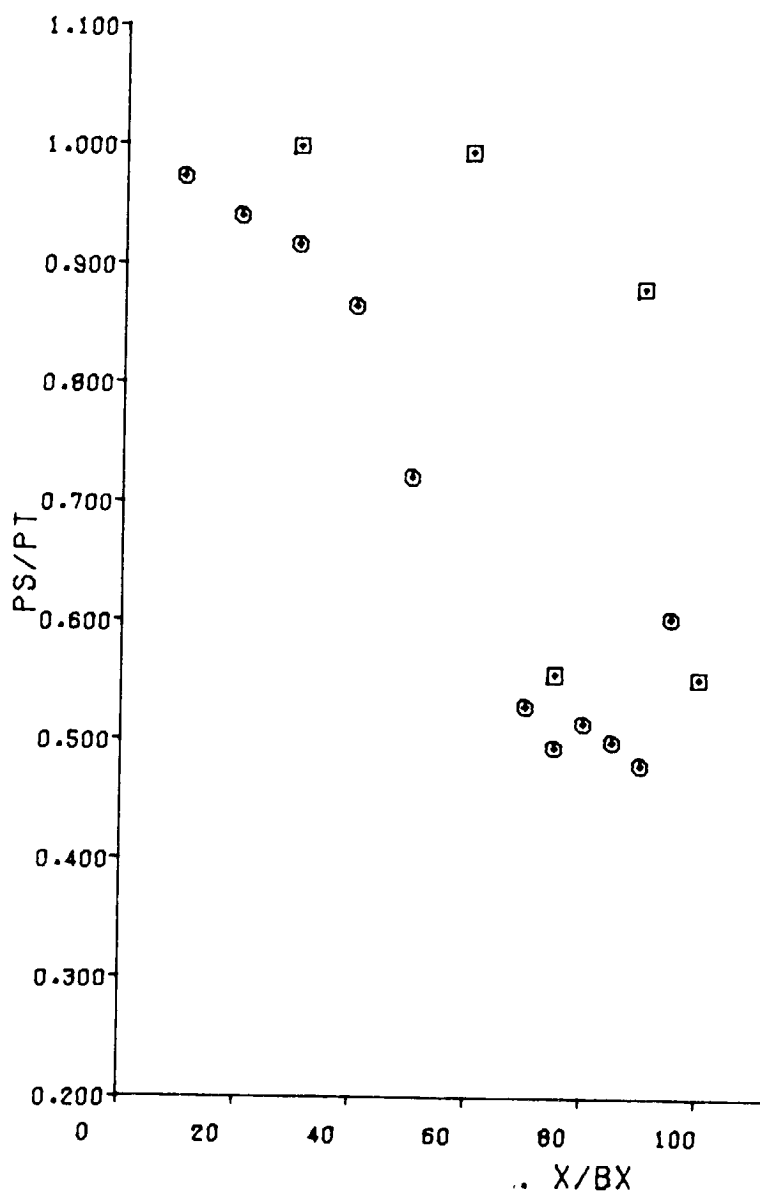


Figure B-103 Vane Pressure Distribution at 89 Percent Span (Point 4)

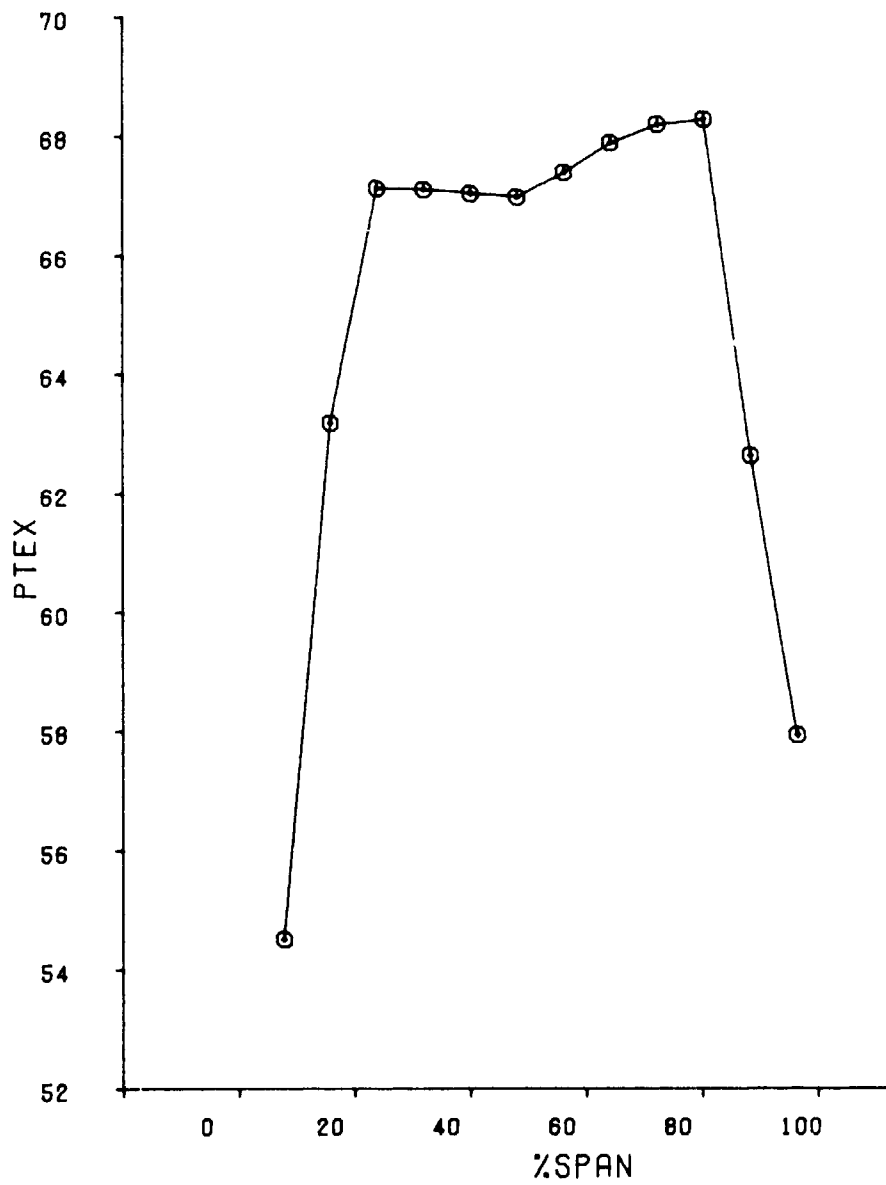


Figure B-104 Vane Average Total Pressure Versus Span (Point 5)

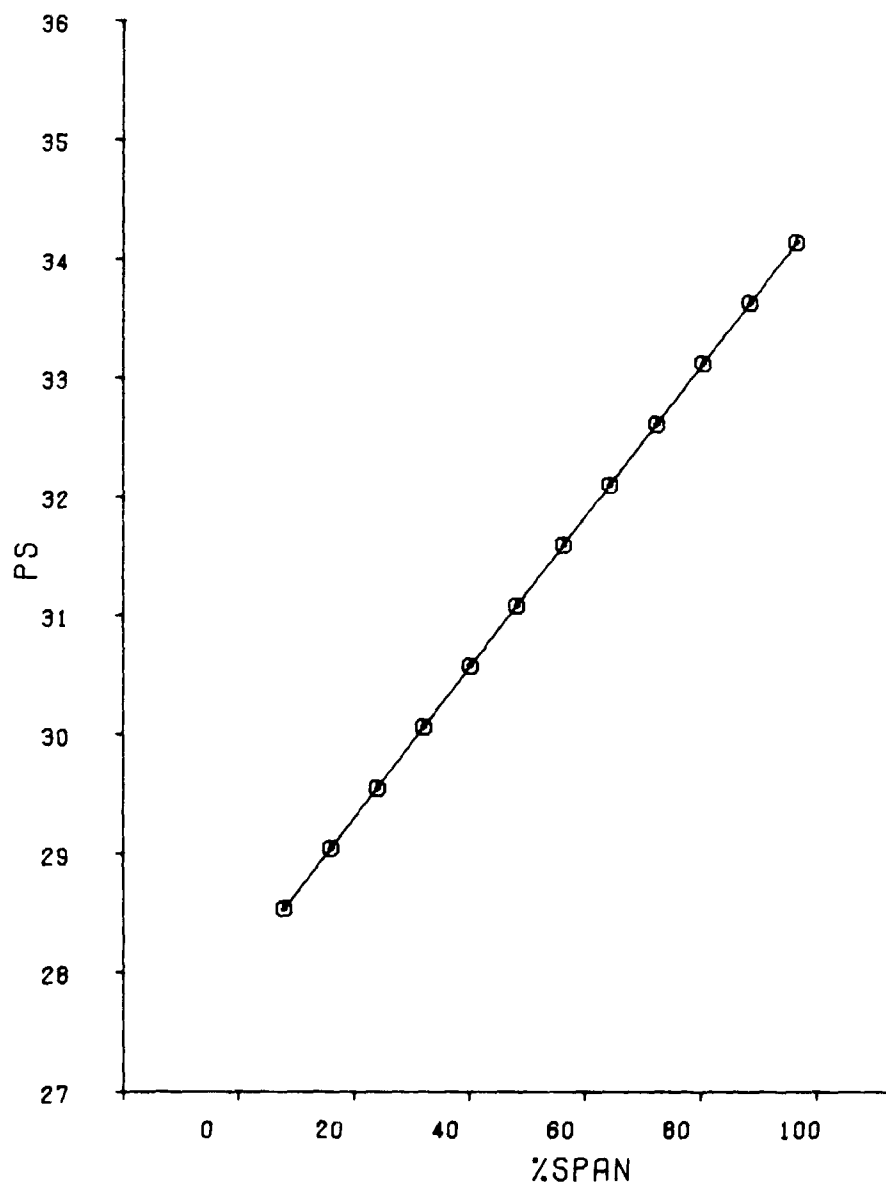


Figure B-105 Vane Average Static Pressure Versus Span (Point 5)

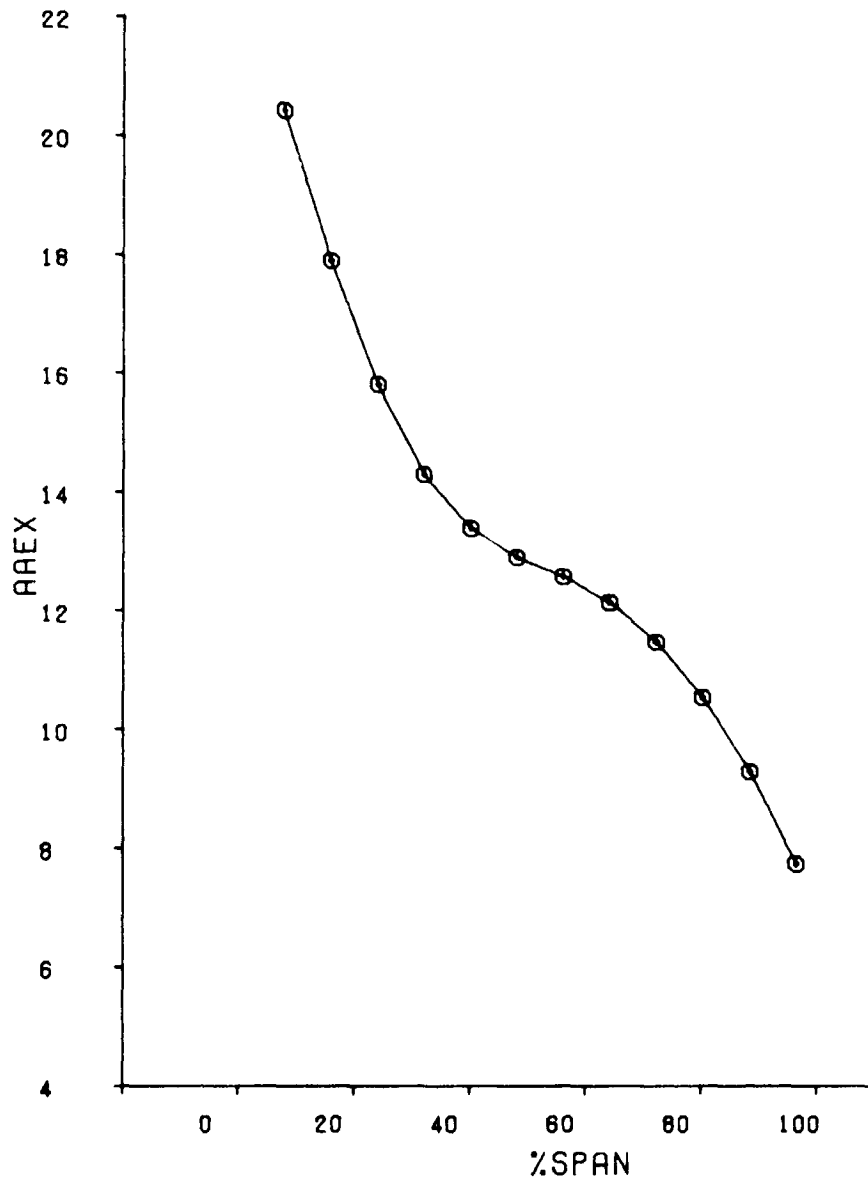


Figure B-106 Vane Average Air Angle Versus Span (Point 5)

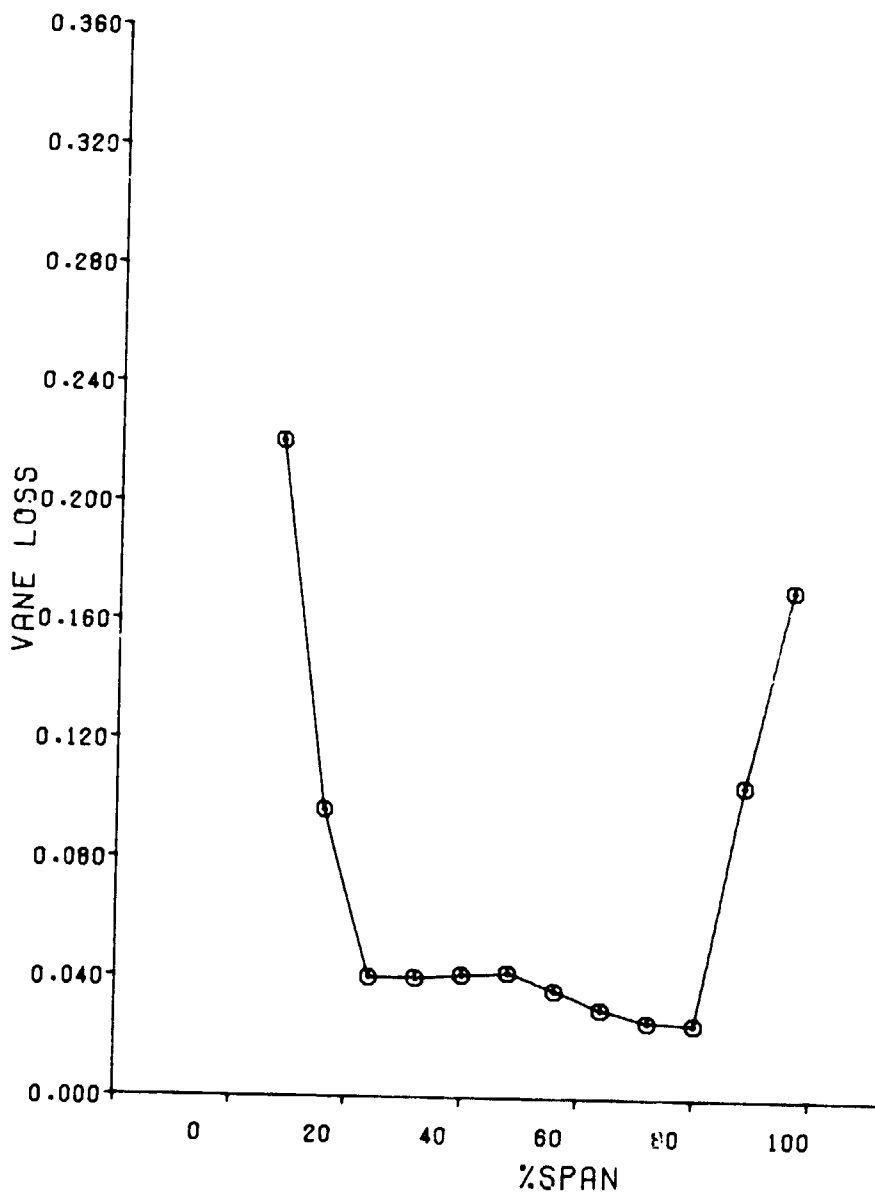


Figure B-107 Vane Loss Versus Span (Point 5)

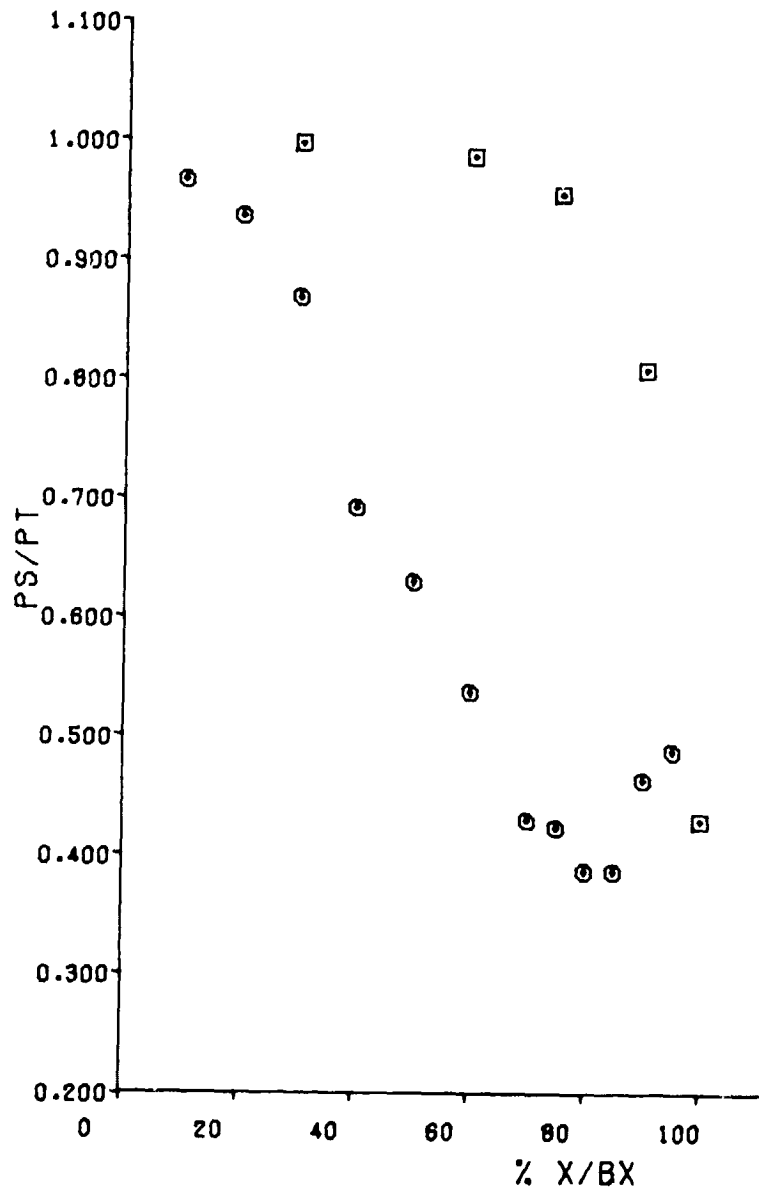


Figure B-108 Vane Pressure Distribution at 11 Percent Span (Point 5)

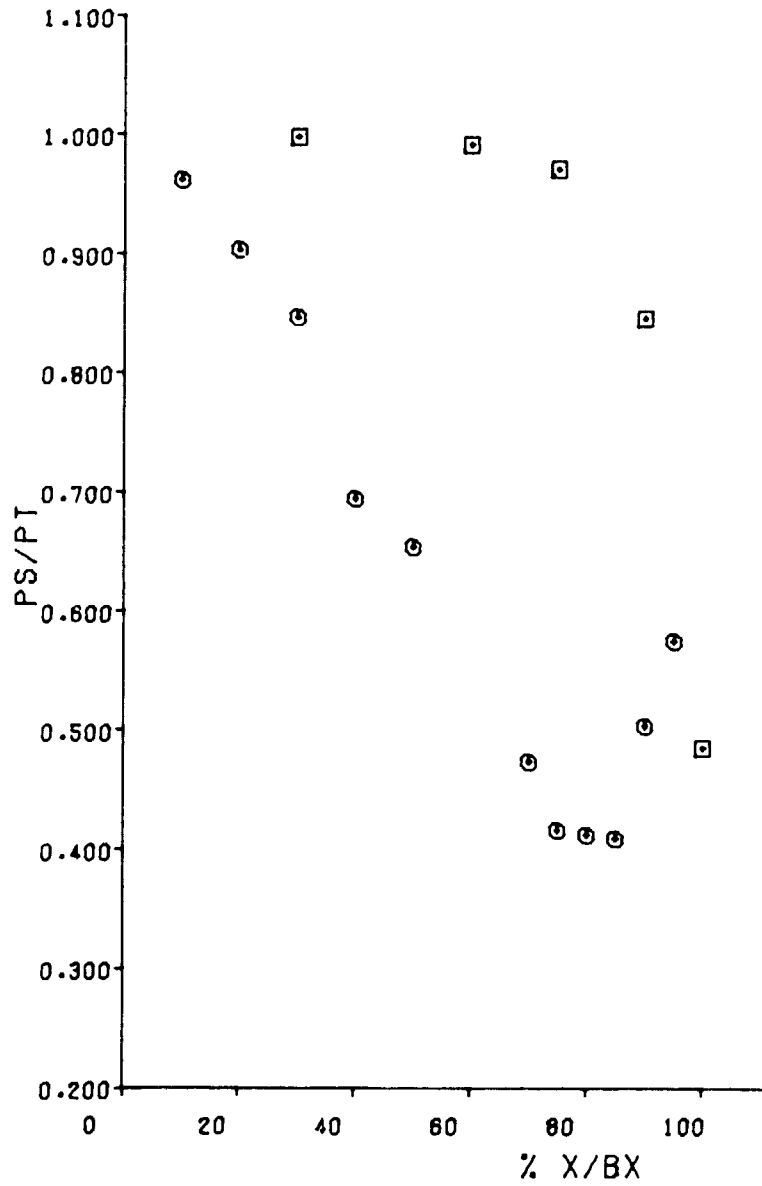


Figure B-109 Vane Pressure Distribution at 50 Percent Span (Point 5)

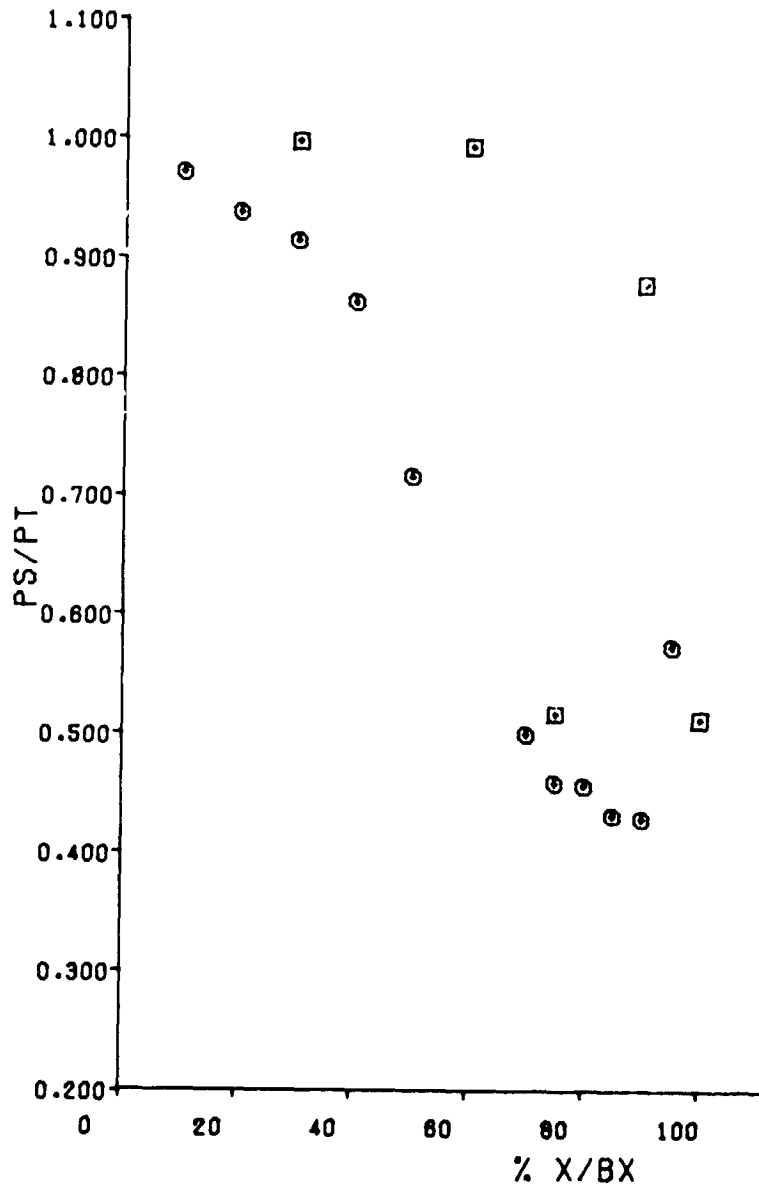


Figure B-110 Vane Pressure Distribution at 89 Percent Span (Point 5)

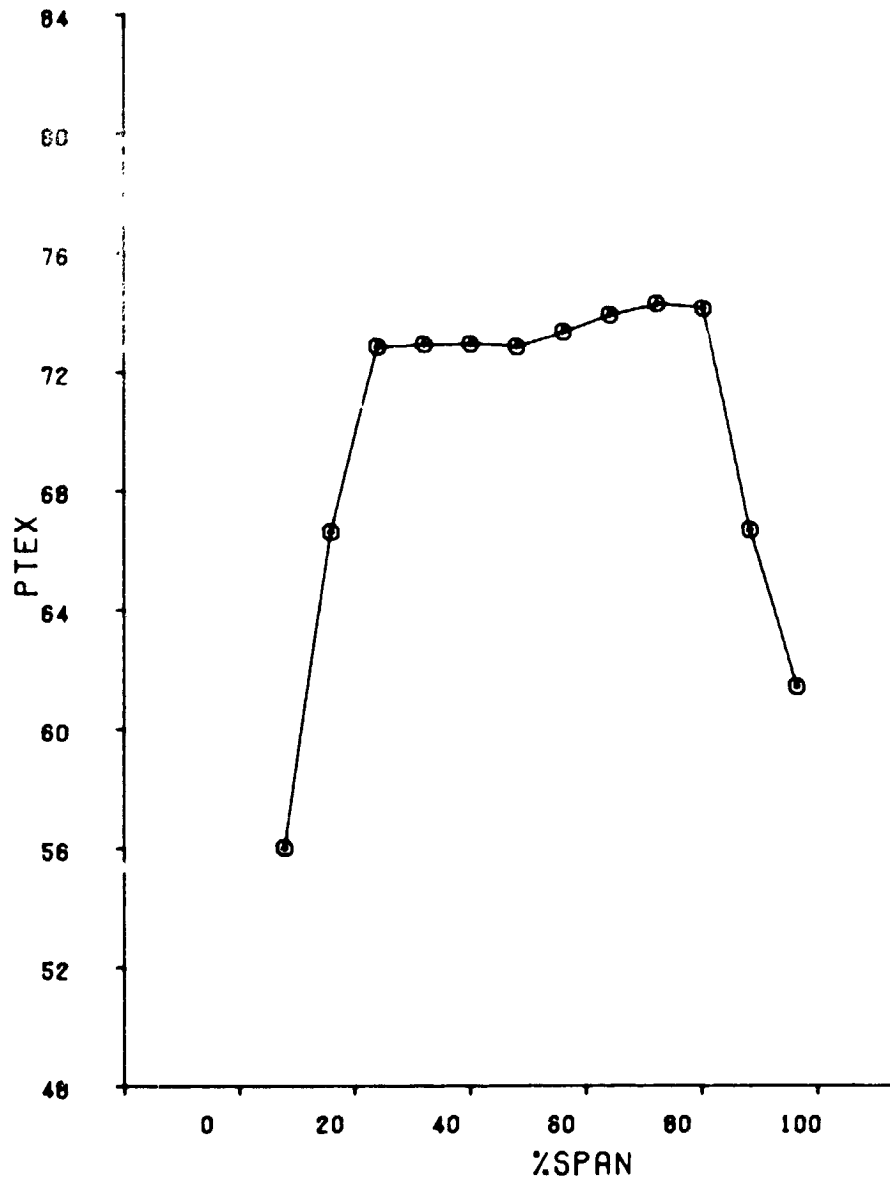


Figure B-11 Vane Average Total Pressure Versus Span (Point 6)

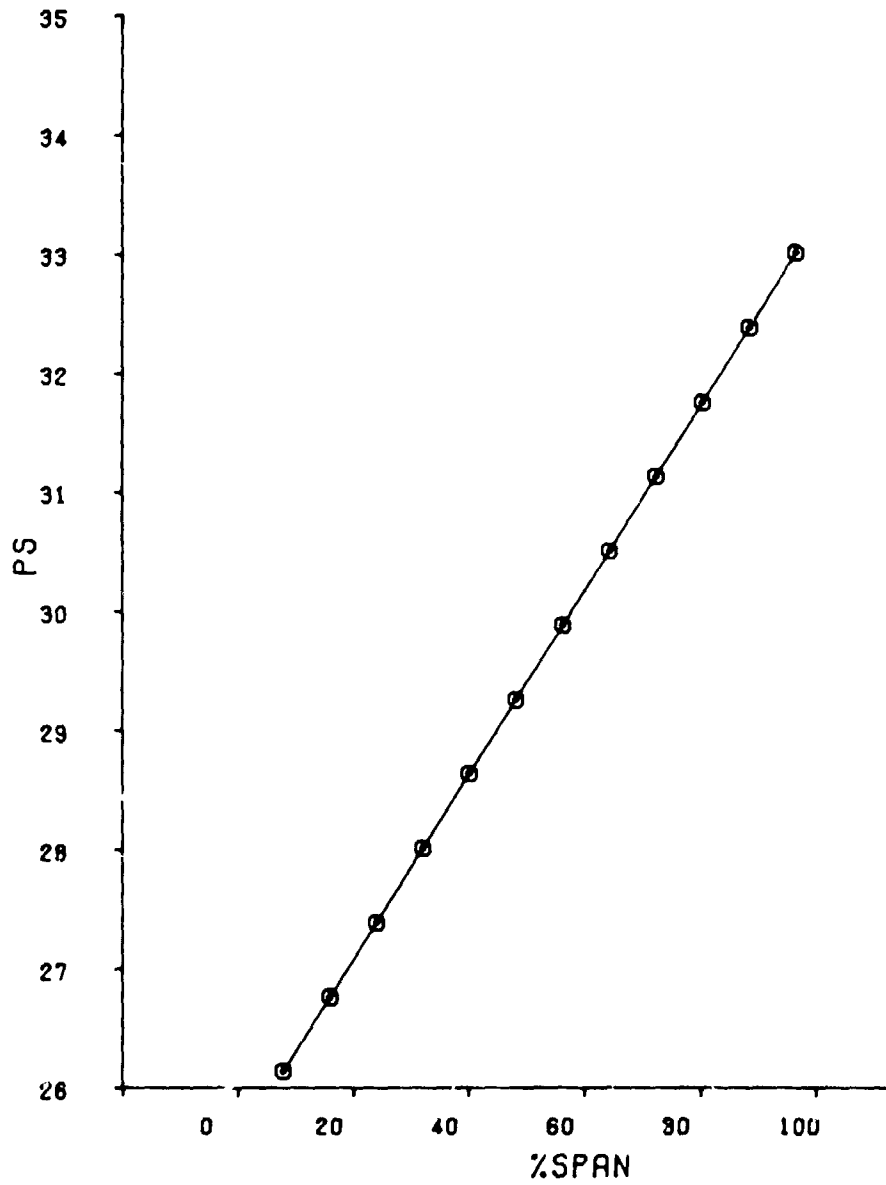


Figure B-112 Vane Average Static Pressure Versus Span (Point 6)

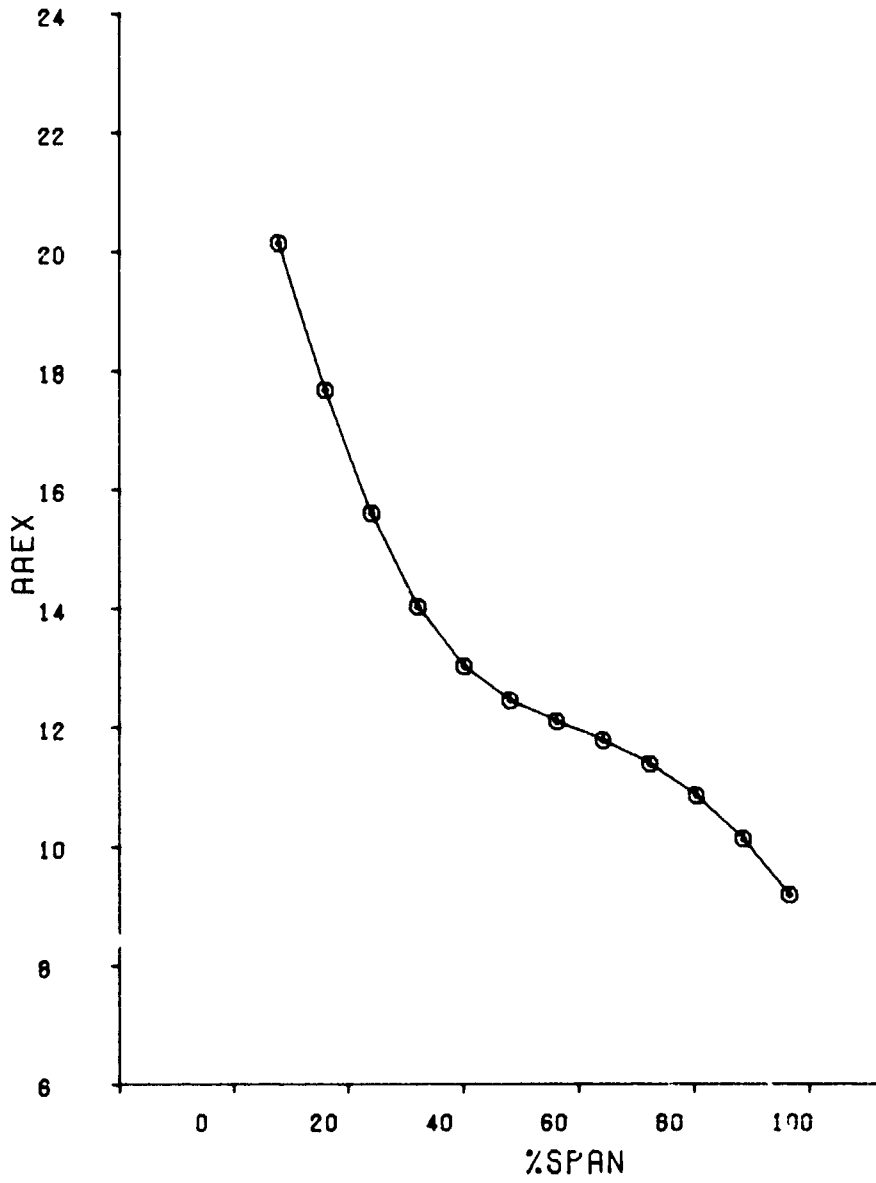


Figure B-113 Vane Average Air Angle Versus Span (Point 6)

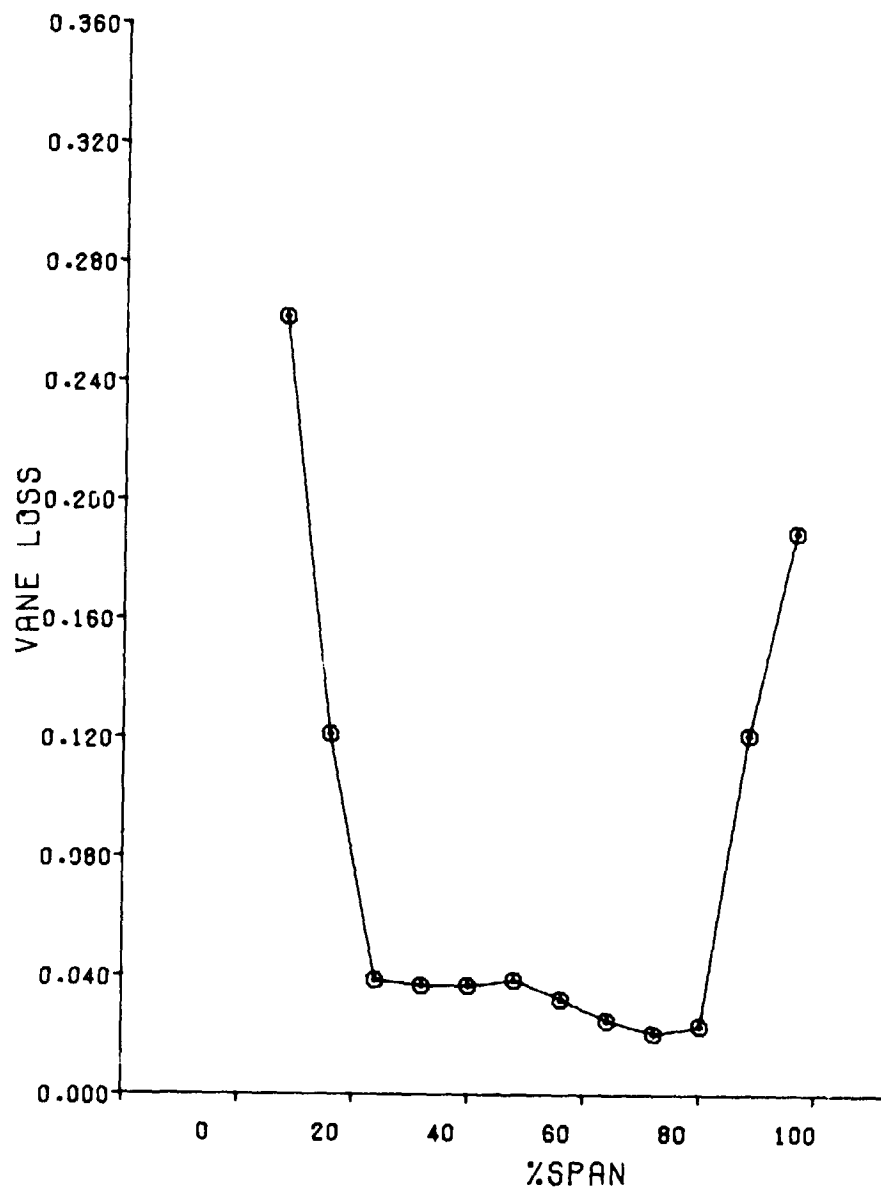


Figure B-114 Vane Loss Versus Span (Point G)

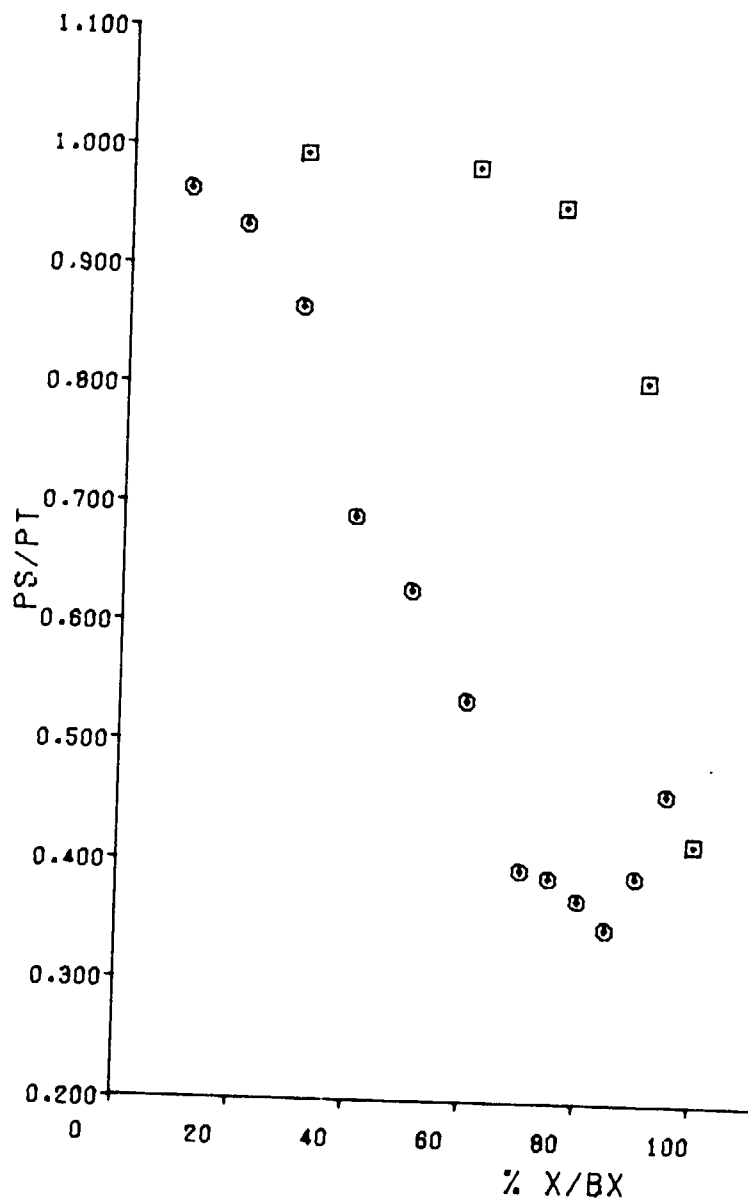


Figure B-115 Vane Pressure Distribution at 11 Percent Span (Point 6)

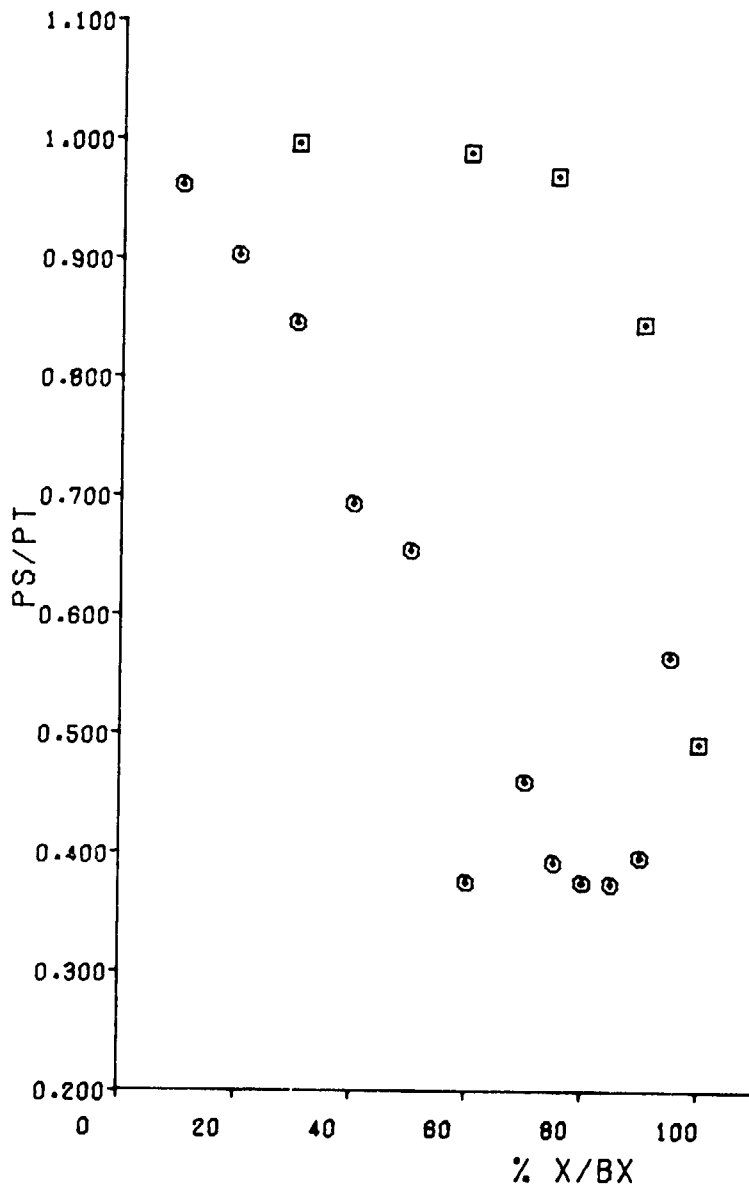


Figure B-116 Vane Pressure Distribution at 50 Percent Span (Point 6)

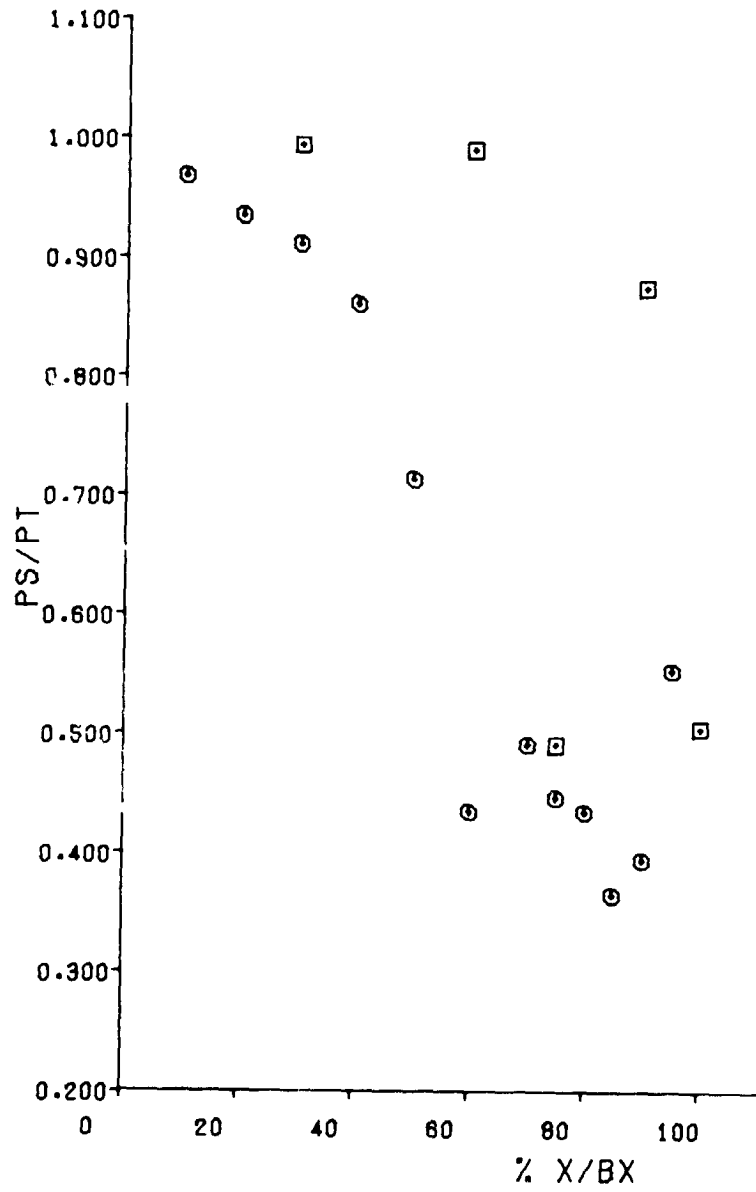


Figure B-117 Vane Pressure Distribution at 89 Percent Span (Point 6)

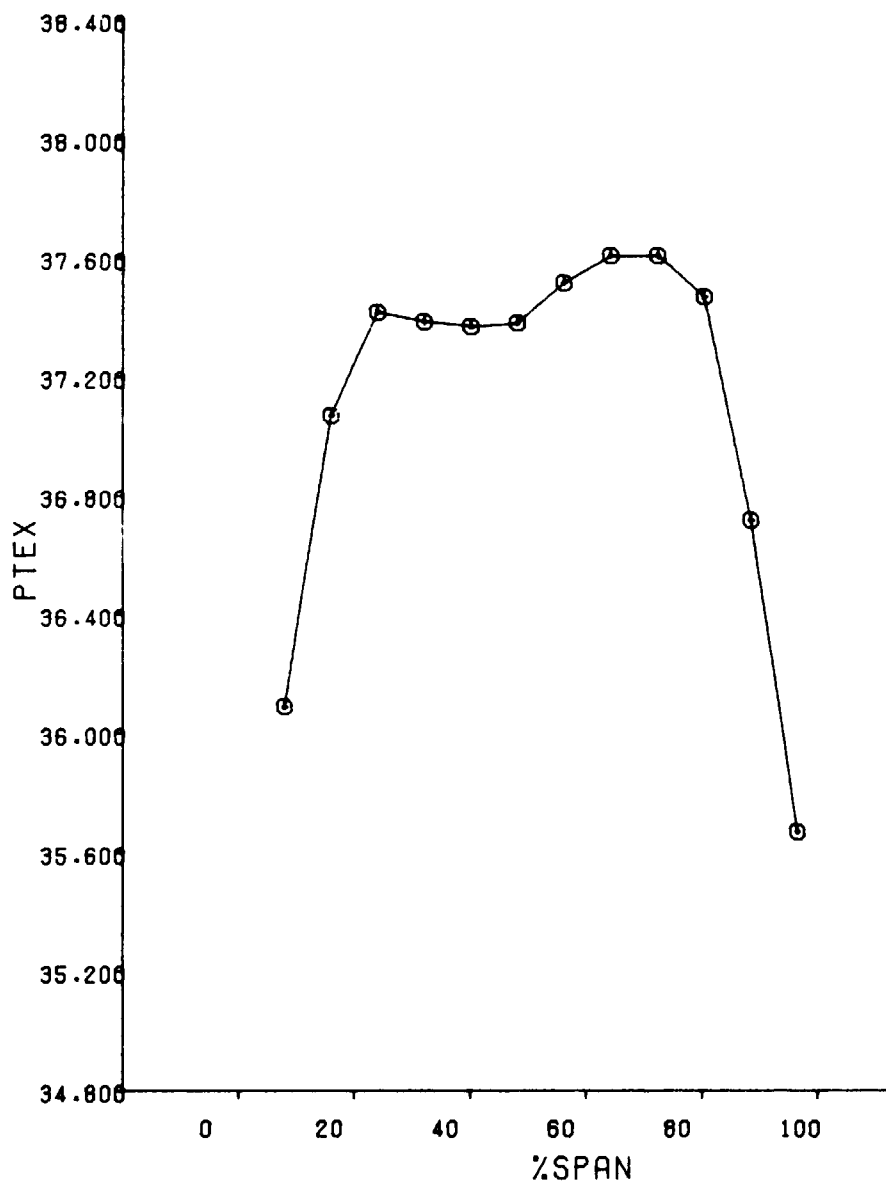


Figure B-118 Vane Average Total Pressure Versus Span (Point 7)

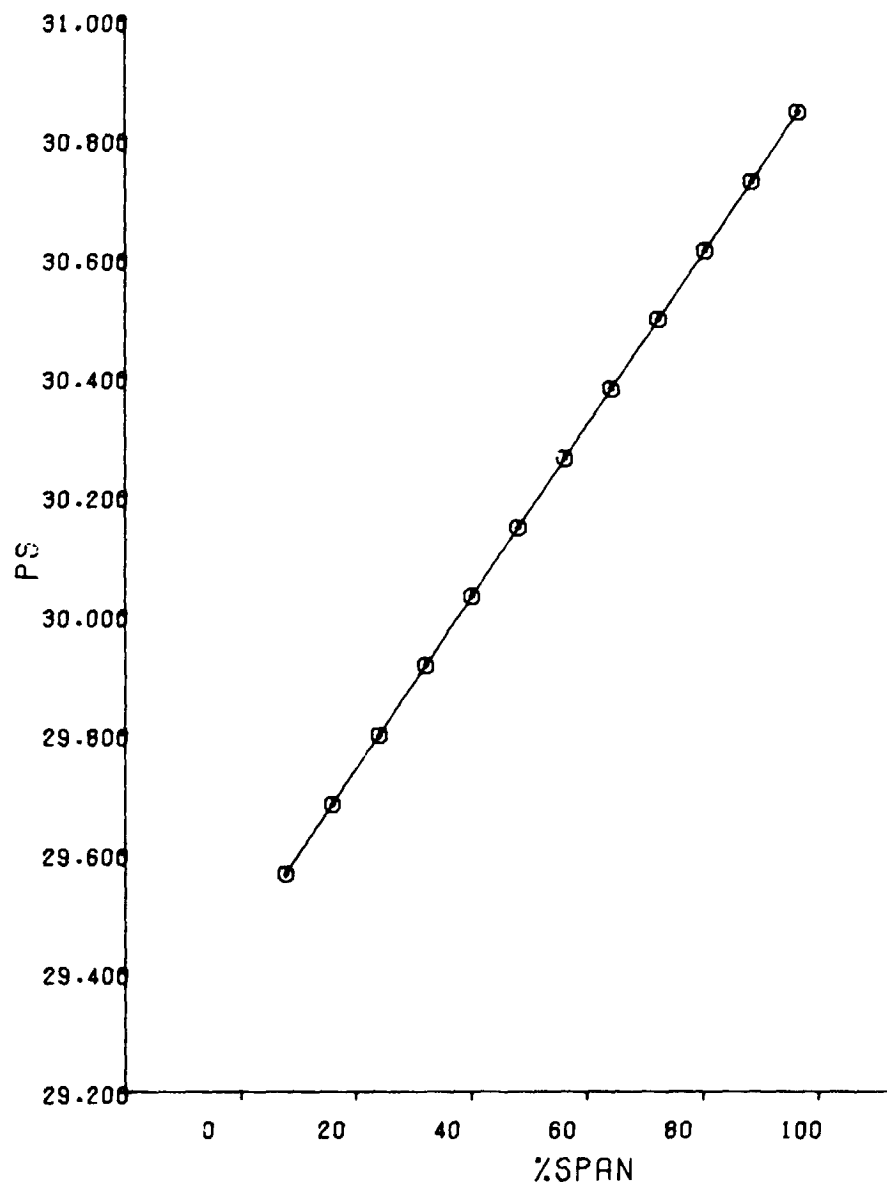


Figure B-119 Vane Average Static Pressure Versus Span (Point 7)

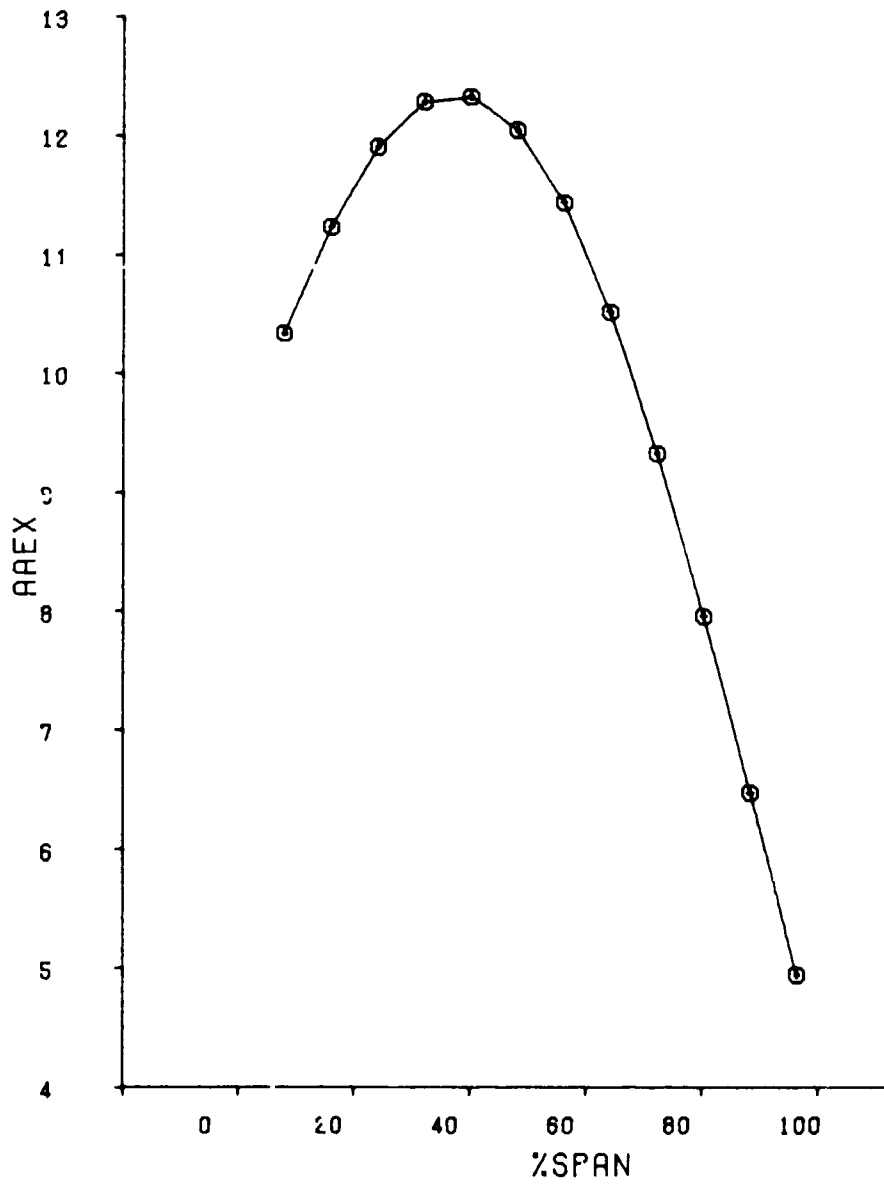


Figure B-120 Vane Average Air Angle Versus Span (Point 7)

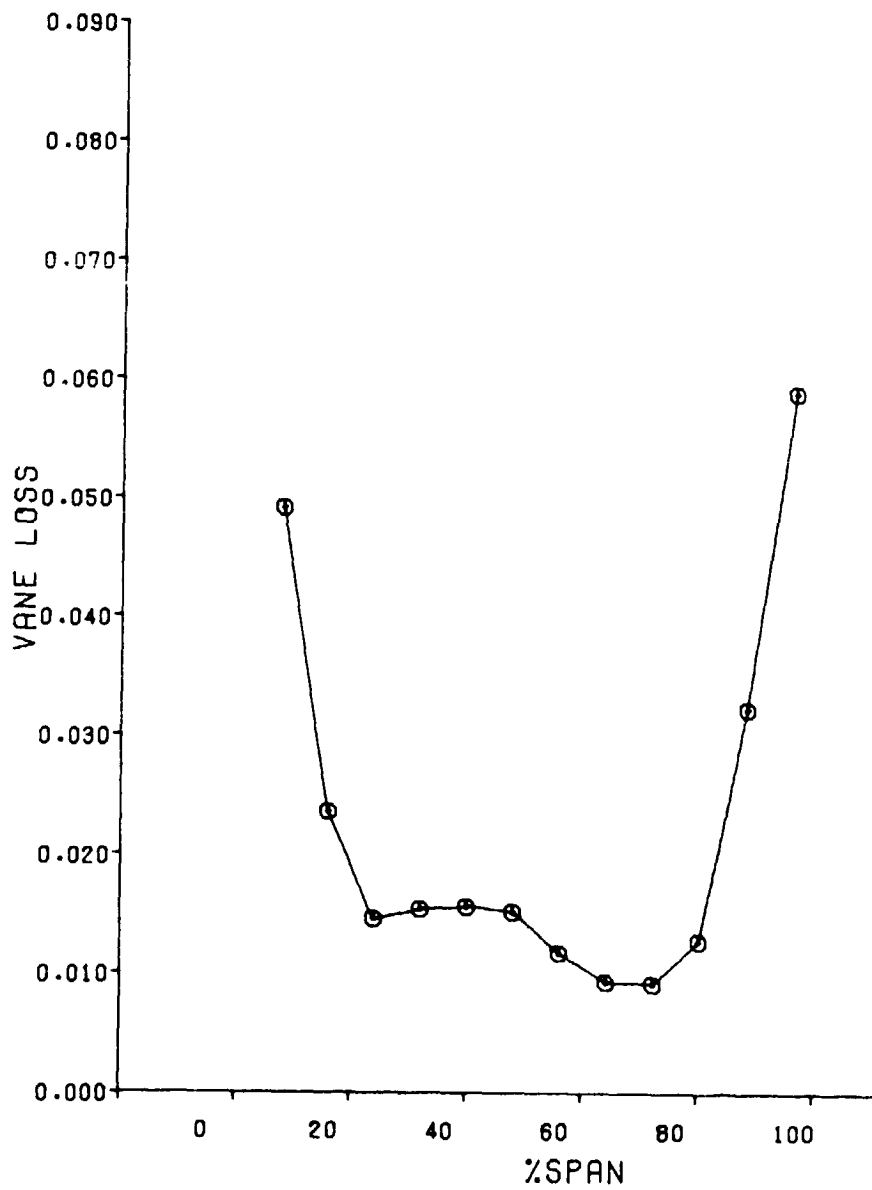


Figure B-121 Vane Loss Versus Span (Point 7)

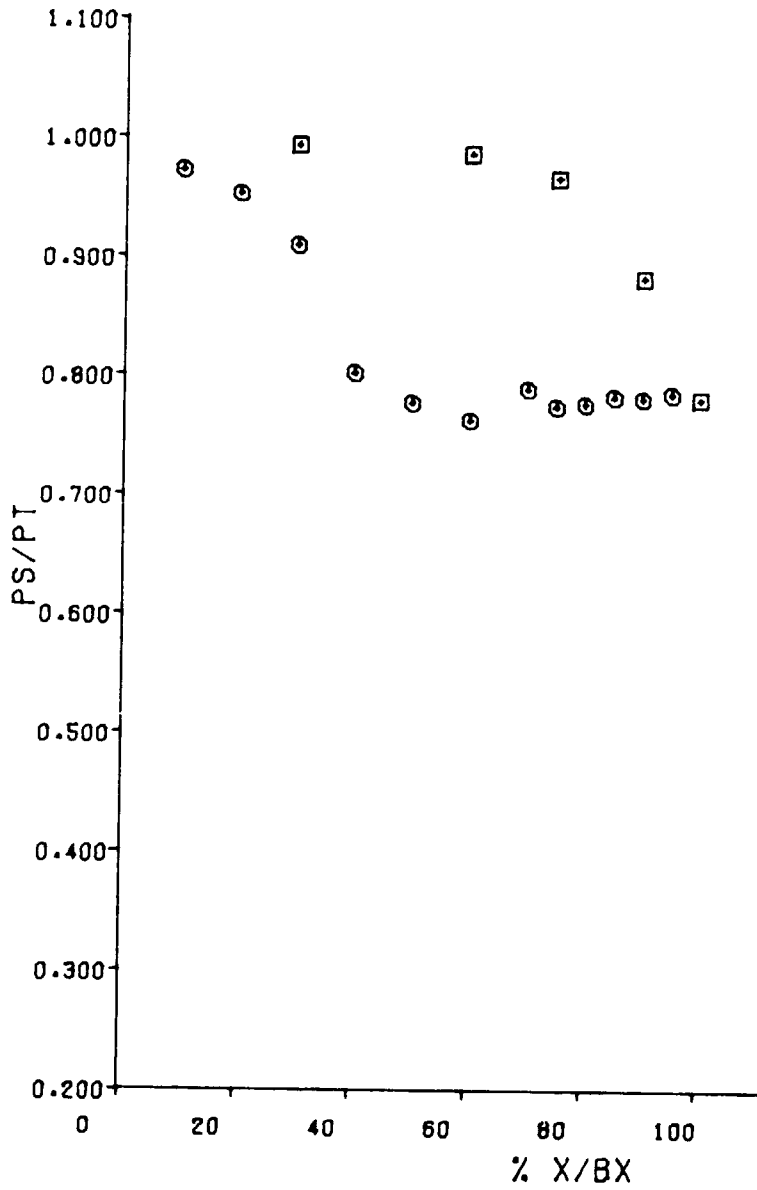


Figure B-122 Vane Pressure Distribution at 11 Percent Span (Point 7)

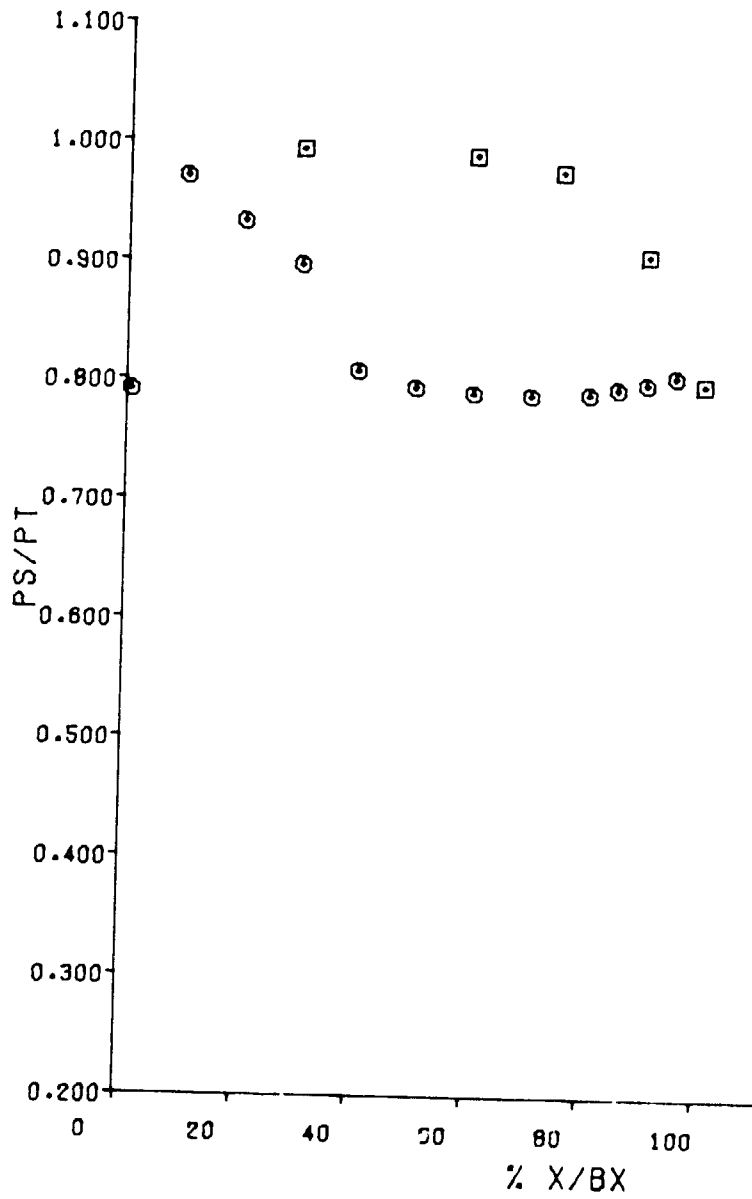


Figure B-123 Vane Pressure Distribution at 50 Percent Span (Point 7)

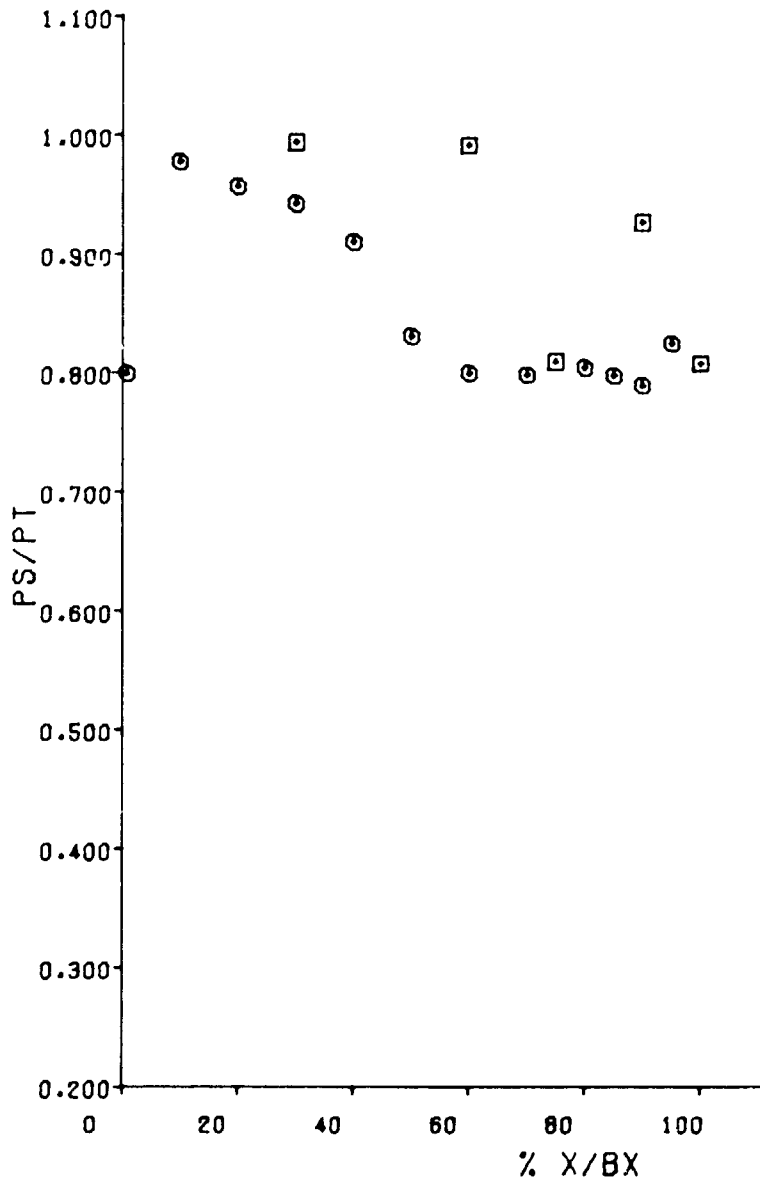


Figure B-124 Vane Pressure Distribution at 89 Percent Span (Point 7)

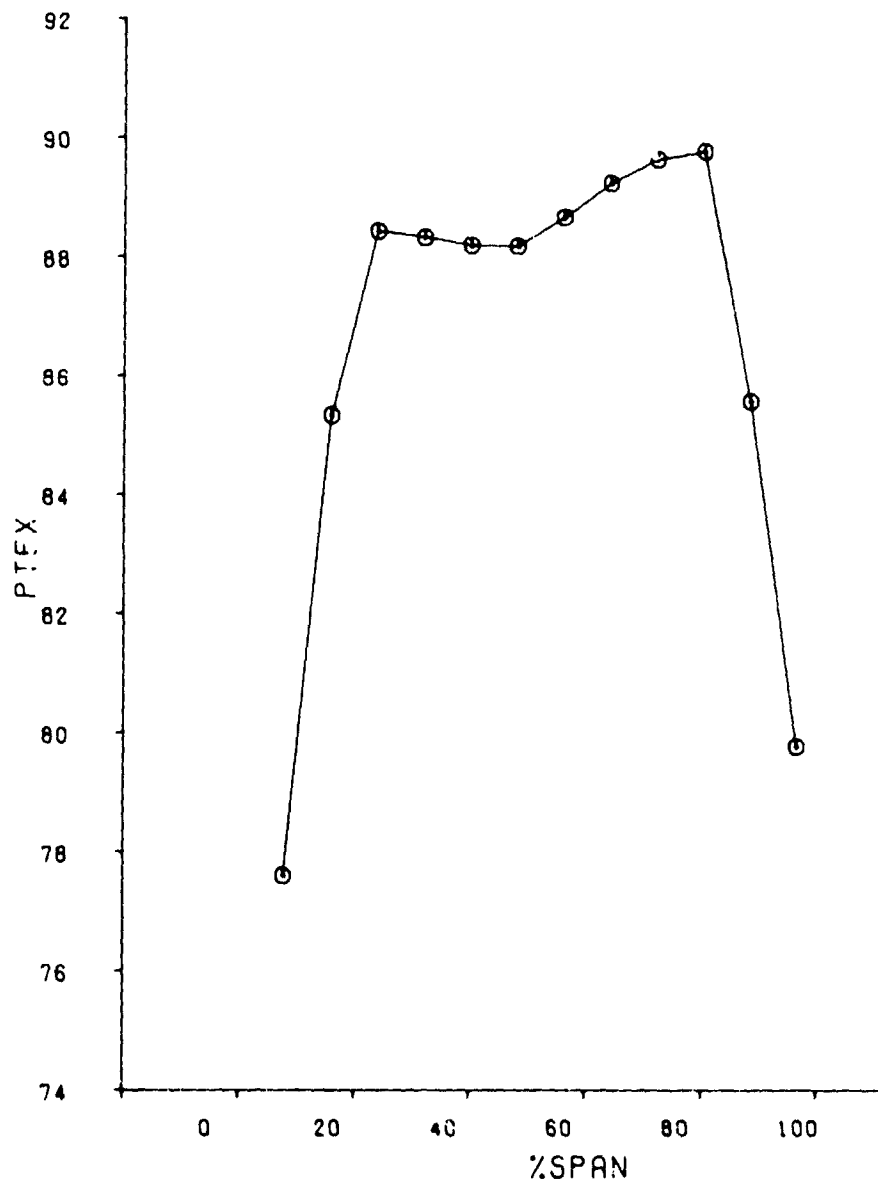


Figure B-125 Vane Average Total Pressure Versus Span (Point 8)

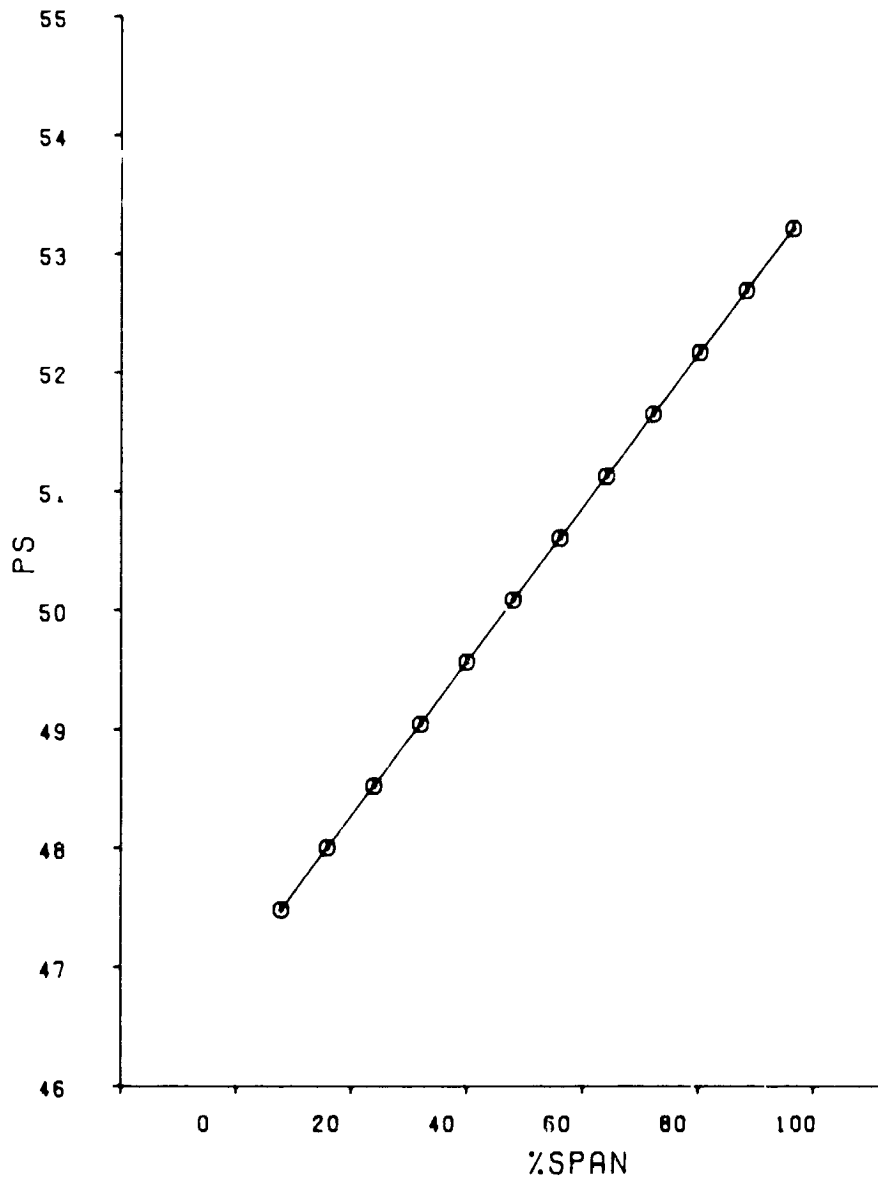


Figure B-126 Vane Average Static Pressure Versus Span (Point 8)

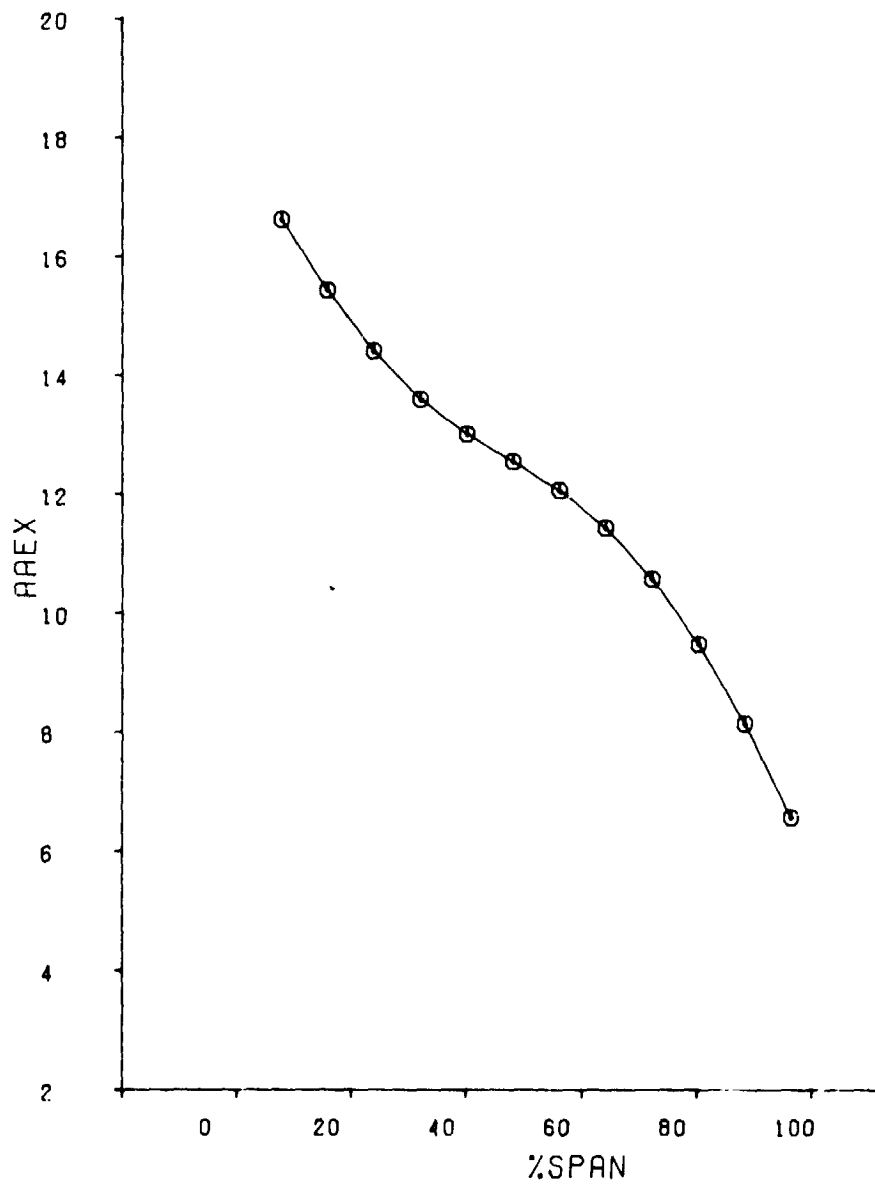


Figure B-127 Vane Average Air Angle Versus Span (Point 8)

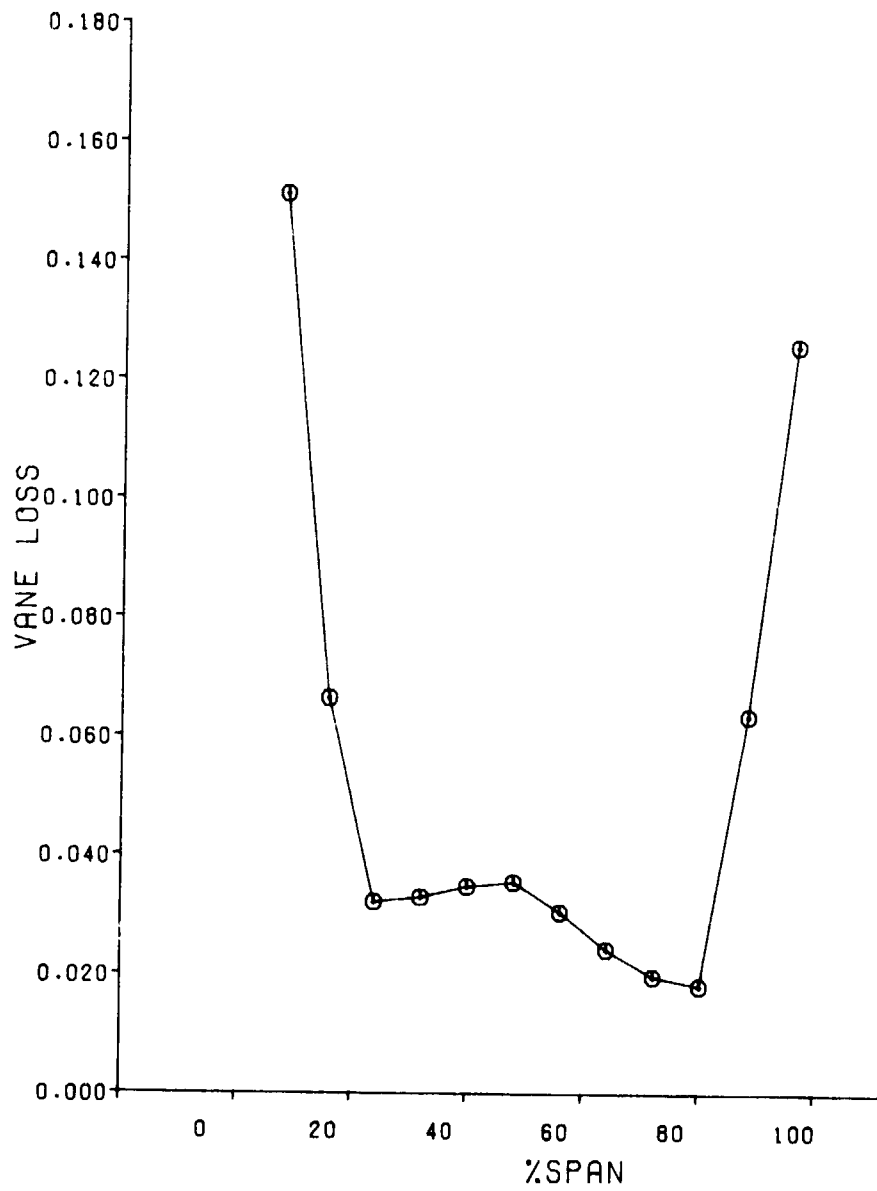


Figure B-128 Vane Loss Versus Span (Point 8)

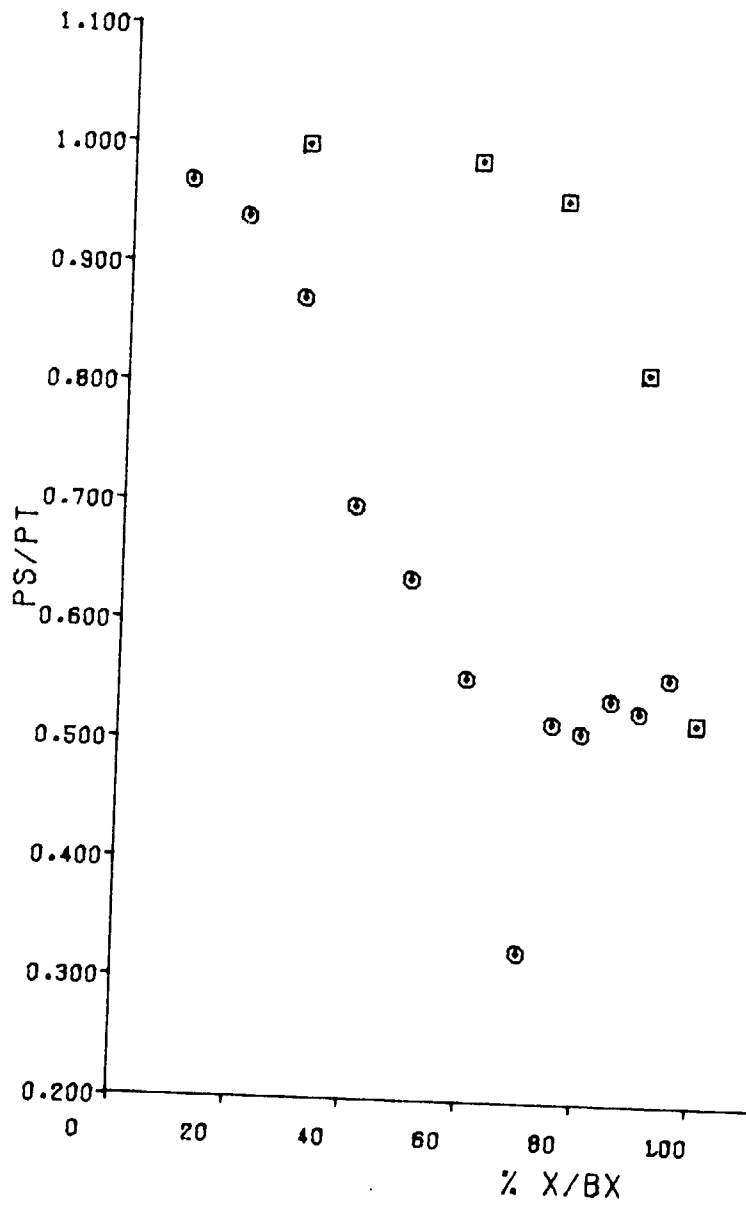


Figure B-129 Vane Pressure Distribution at 11 Percent Span (Point 8)

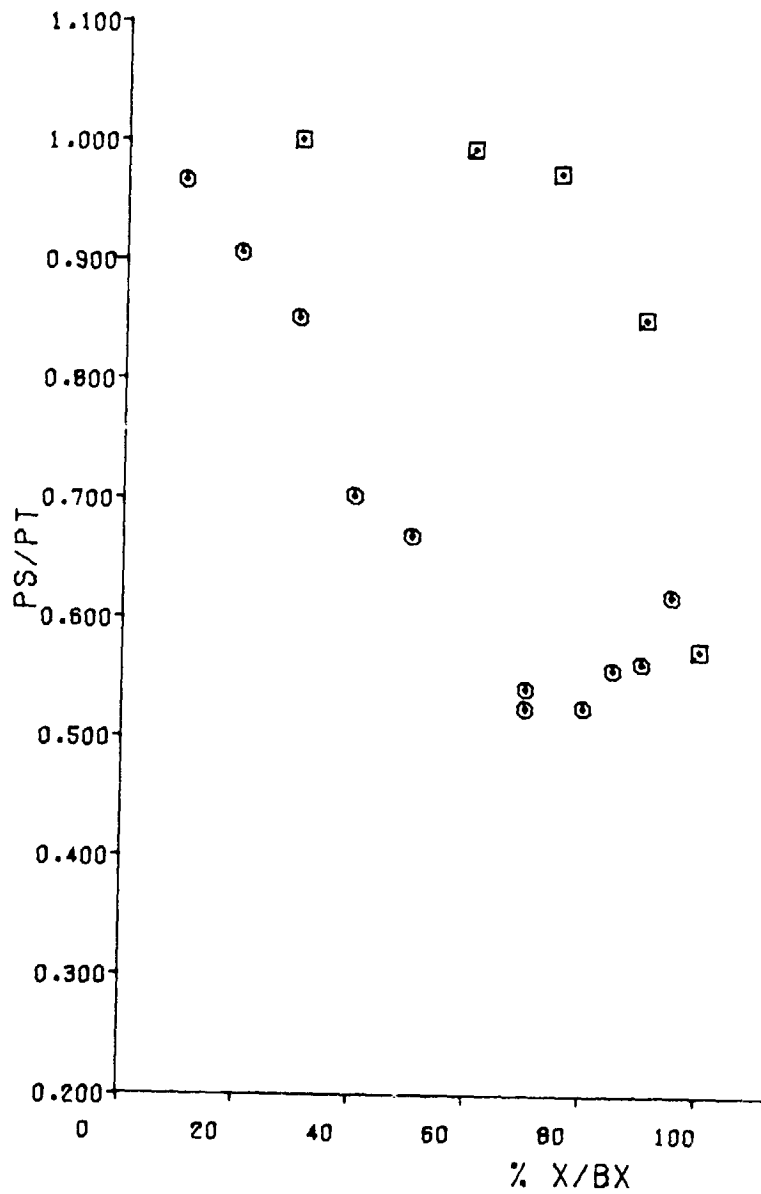


Figure B-130 Vane Pressure Distribution at 50 Percent Span (Point 8)

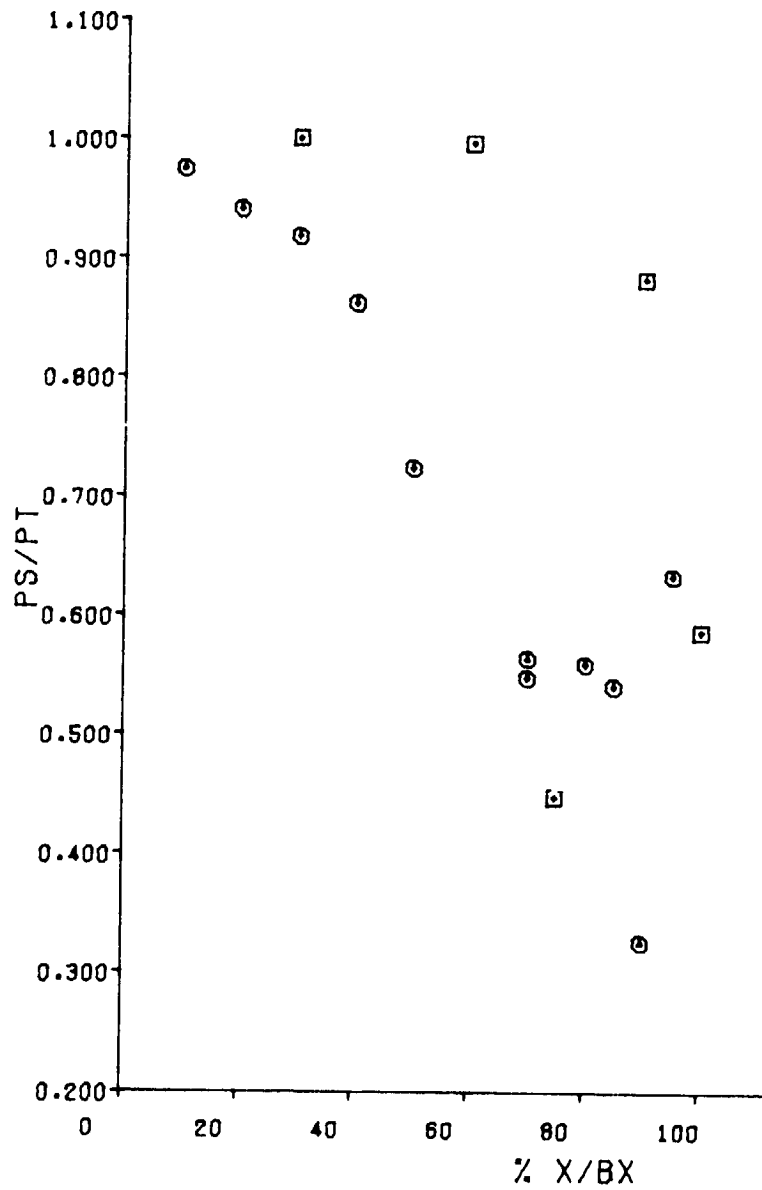


Figure B-131 Vane Pressure Distribution at 89 Percent Span (Point 8)

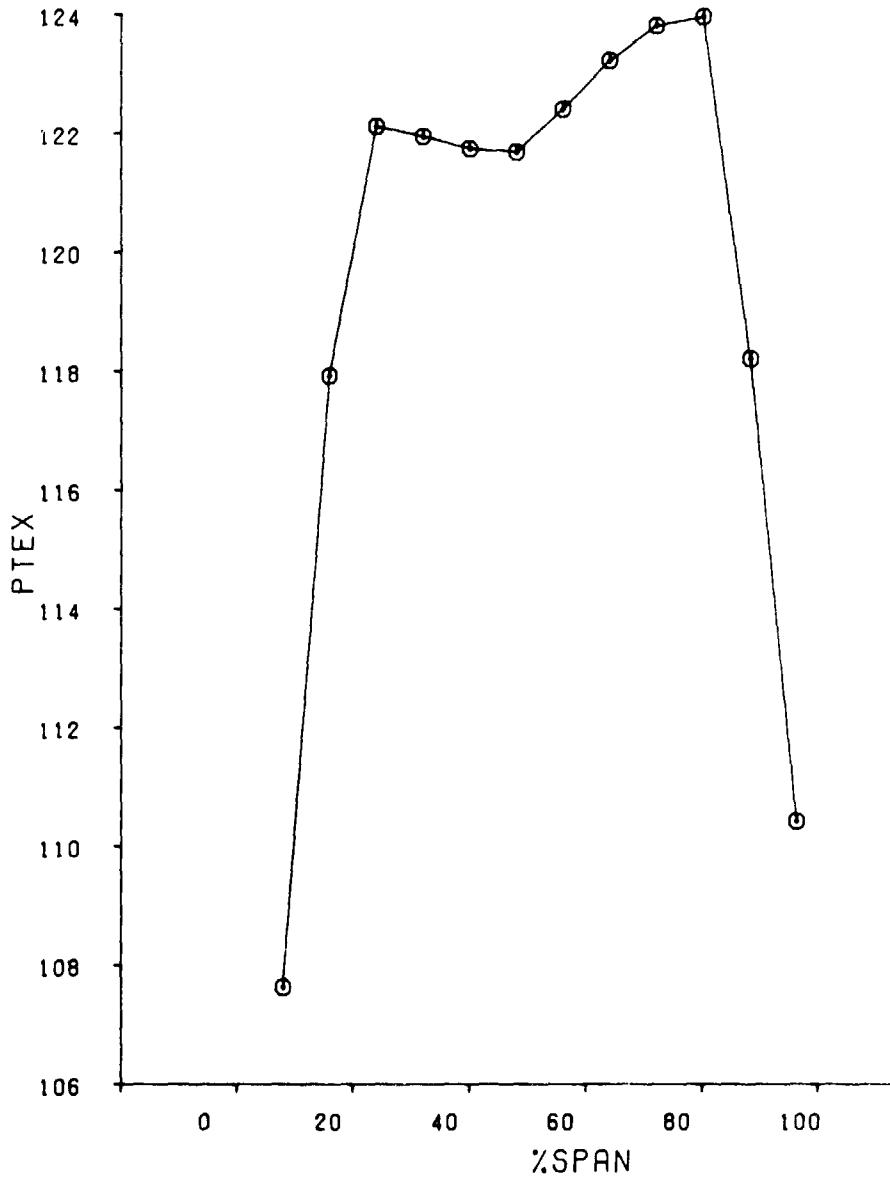


Figure B-132 Vane Average Total Pressure Versus Span (Point 9)

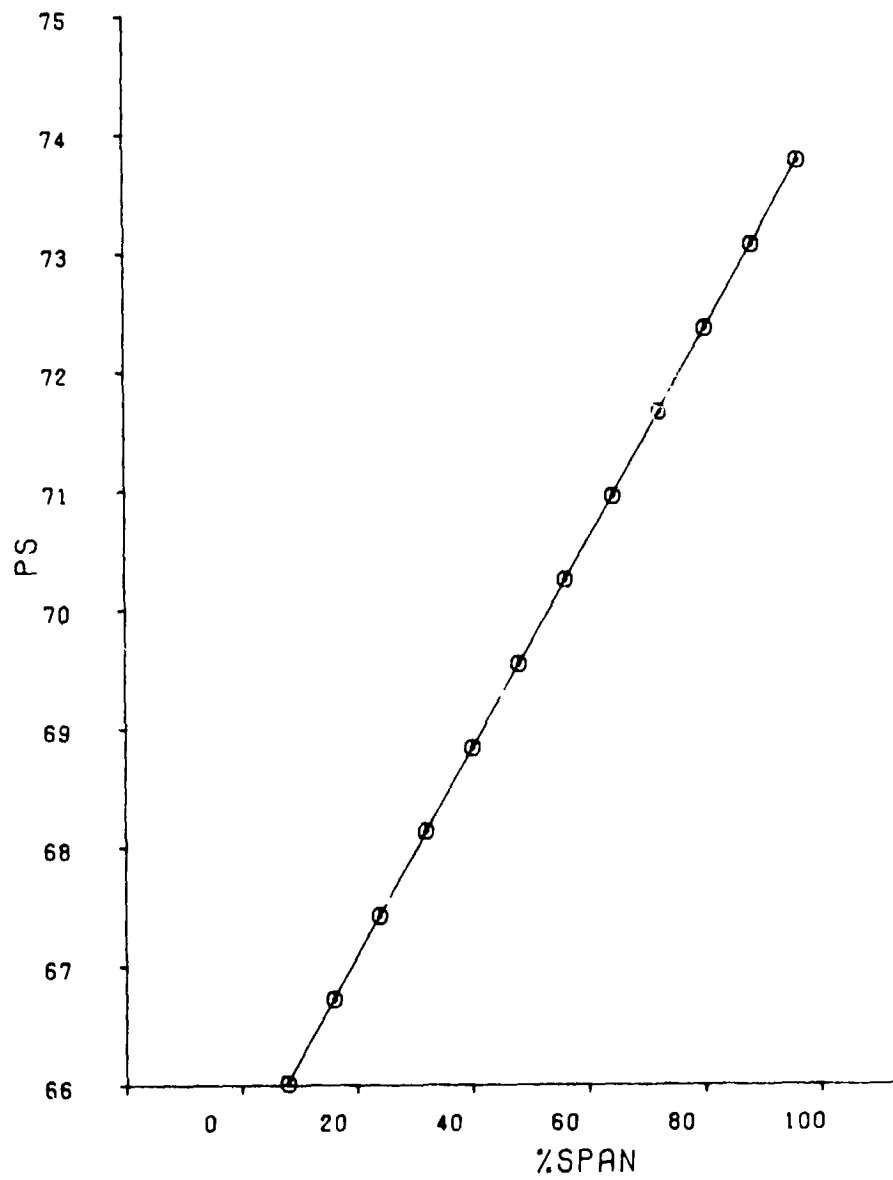


Figure B-133 Vane Average Static Pressure Versus Span (Point 9)

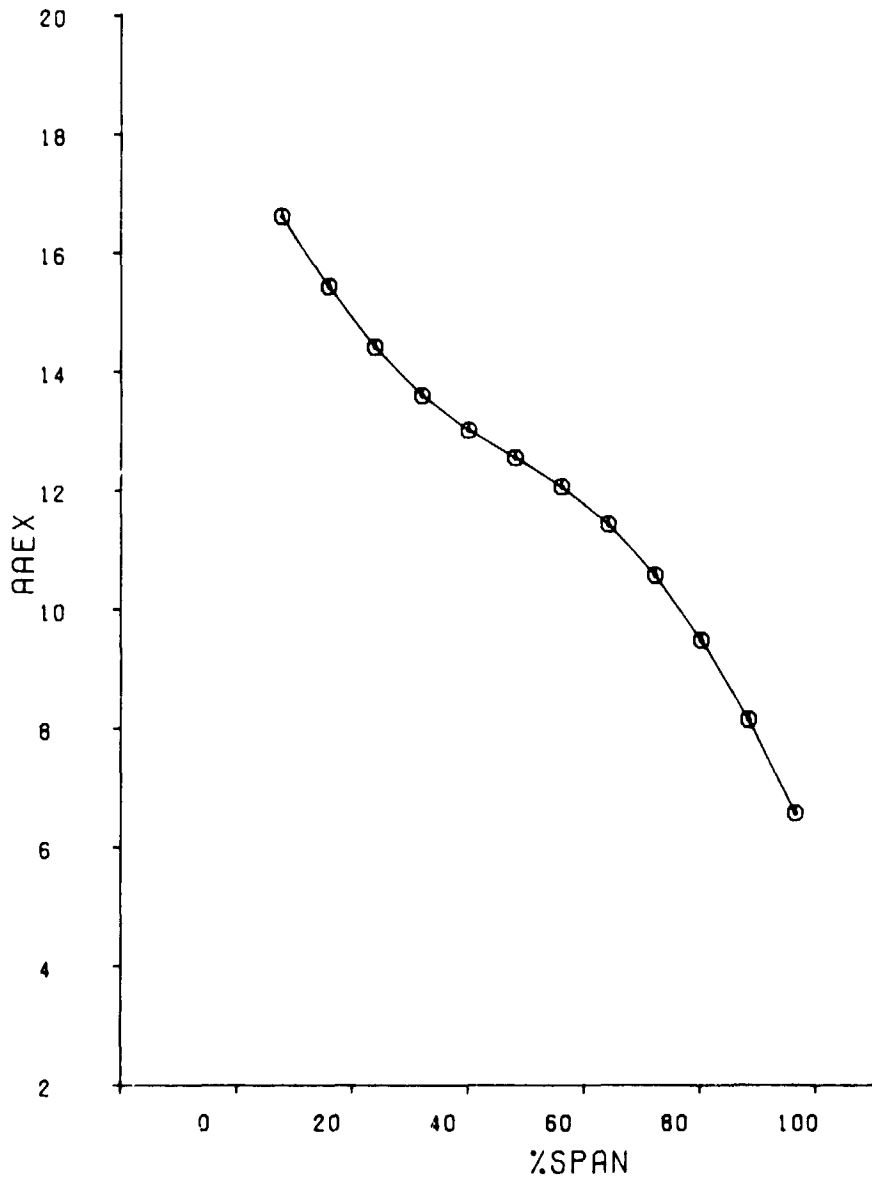


Figure B-134 Vane Average Air Angle Versus Span (Point 9)

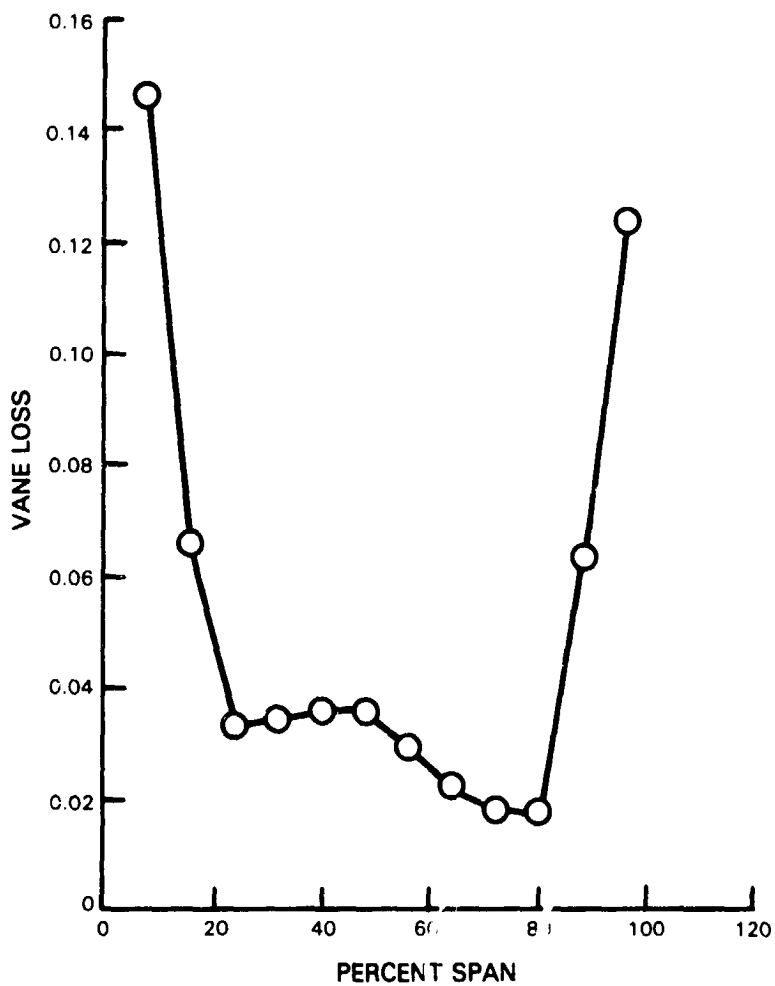


Figure B-135 Vane Loss Versus Span (Point 9)

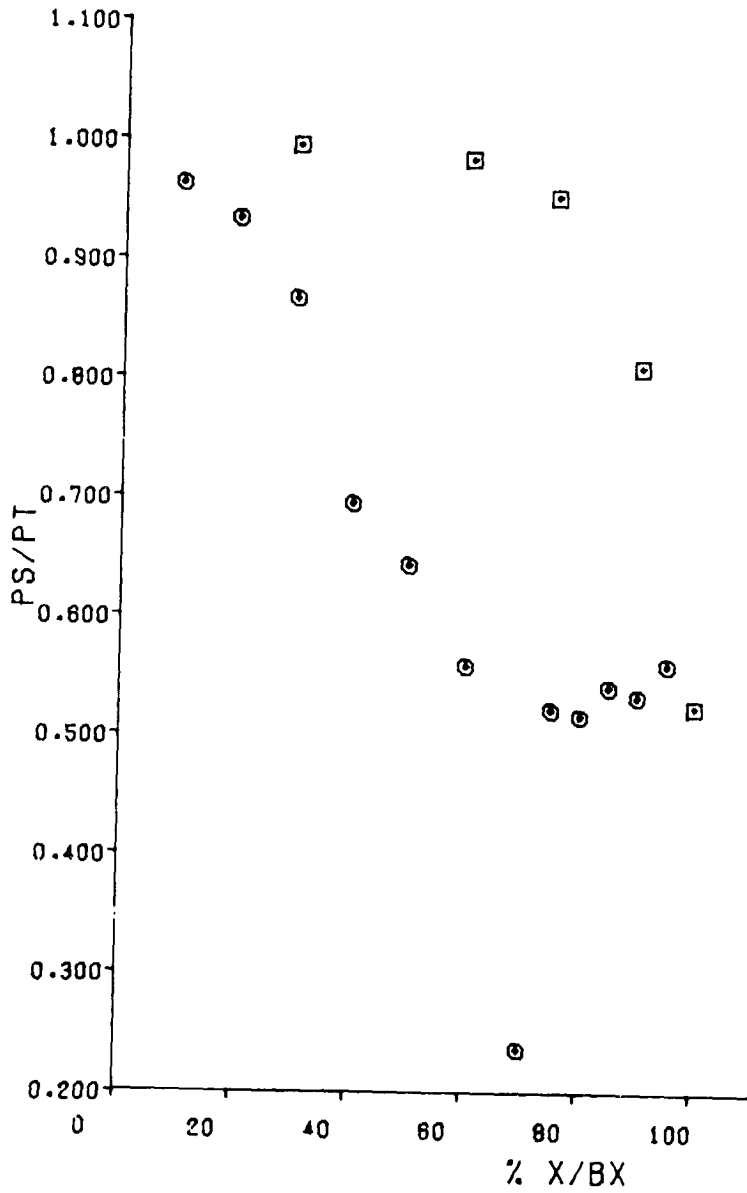


Figure 5-136 Vane Pressure Distribution at 11 Percent Span (Point 9)

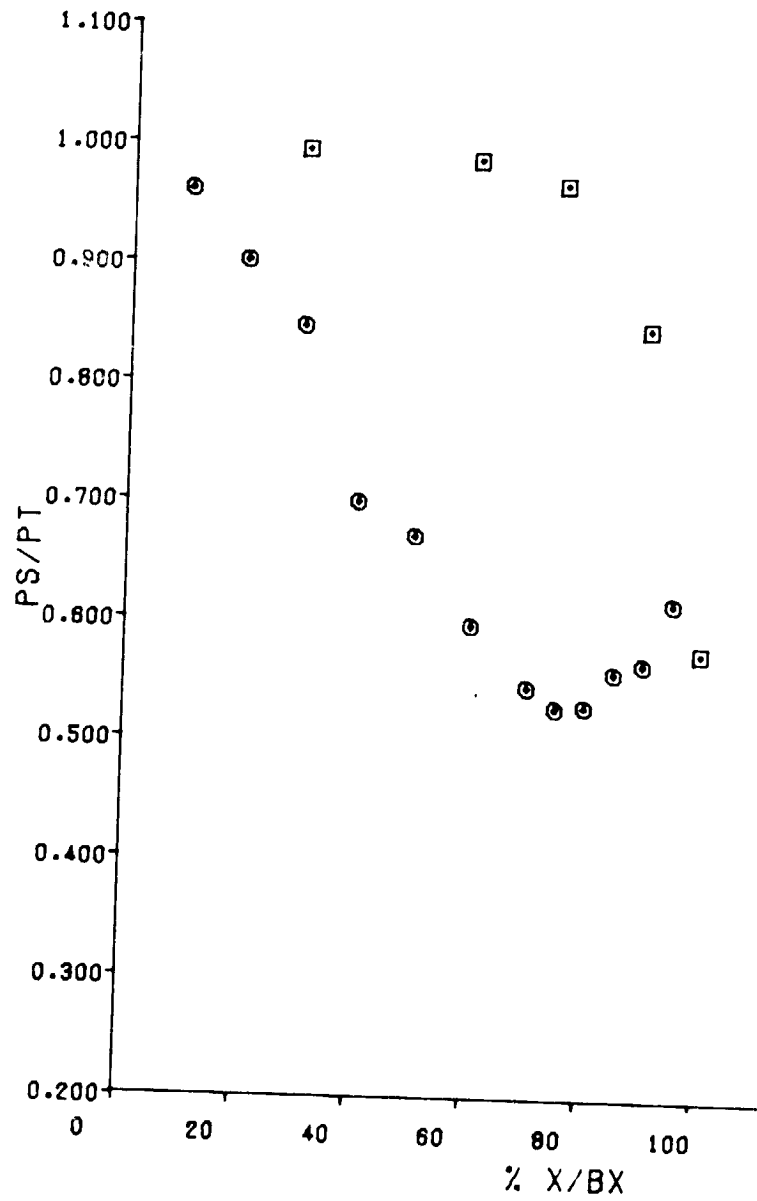


Figure B-137 Vane Pressure Distribution at 50 Percent Span (Point 9)

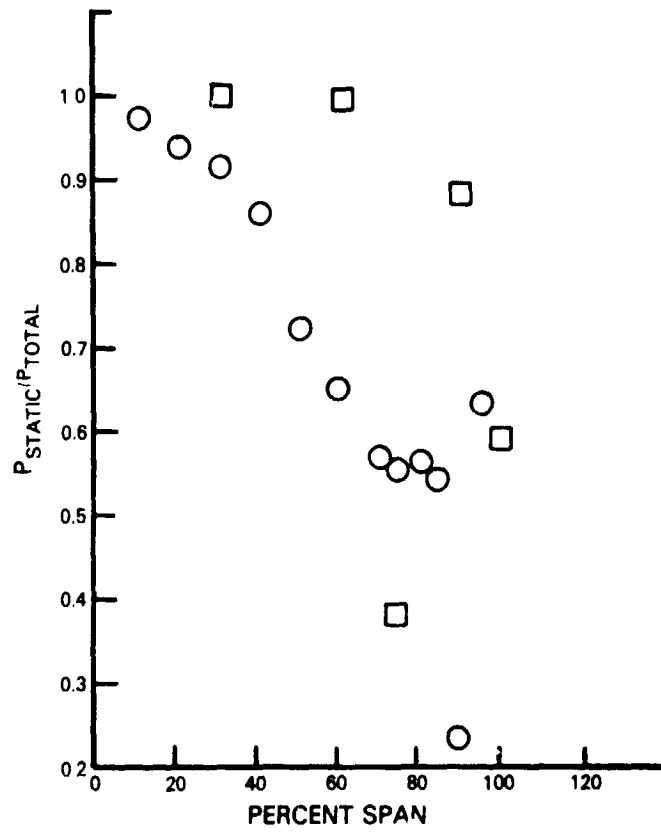


Figure B-138 Vane Pressure Distribution at 89 Percent Span (Point 9)

LIST OF SYMBOLS AND ABBREVIATIONS

A	annulus area
AA	air angle
ACC	active clearance control
B_x	axial chord
BOAS	blade outer air seal
C_x	axial flow velocity
CET	combustor exit temperature
EEE	Energy Efficient Engine
EGT	exhaust gas temperature
FP	flow parameter, $W \sqrt{T_T/P_T}$
FPS	flight propulsion system
HPT	high-pressure turbine
ICLS	integrated core/low spool
ID	inner diameter
LE	leading edge
LPT	low-pressure turbine
m	flow
M	Mach number
Mn	Mach number
N	mechanical speed, rpm
OD	outer diameter
P/PT	static to total pressure ratio
PR	total to total pressure ratio
Ps	static pressure
P_T	total pressure
R	radius
RIT	rotor inlet temperature
T_c	coolant temperature
T_f	film temperature
T_g	gas temperature
T_T	total temperature
TE	trailing edge
TEC	Tangential On Board Injection Exit Cavity
TOBI	tangential on-board injection
TR	temperature ratio
T_m	metal surface temperature
W	flow
$W_{c/a}$	total cooling air flow
W_{ae}	engine airflow
abs	absolute
U	tangential wheel speed
Θ	gas turning
α	absolute air angle
β	relative air angle
Δ	delta
η	efficiency

REFERENCES

- 1 Gardner. W. B.: "Energy Efficient Engine High-Pressure Turbine Uncooled Rig Technology Report", (CR-165149); October 1979.
- 2 Thulin, R. D., Howe. D. C., and Singer I. D. : "Energy Efficient Engine High-Pressure Turbine Detail Design Report", (CR-165608); January 1982.
- 3 Kopper. F. C. etal: "Energy Efficient Engine High-Pressure Turbine Supersonic Cascade Technology Report", (CR-165557); November 1981.